EARTH STABILISATION BY PLANT-DERIVED UREASE ENZYME FOR BUILDING APPLICATIONS

Alessia Cuccurullo

Earth stabilisation by plant-derived urease enzyme for building applications

By

Alessia Cuccurullo

A thesis submitted in fulfilment of the requirements for the degree of Doctor of Philosophy in Civil Engineering

Université de Pau et des Pays de l'Adour
Ecole Doctorale des Sciences Exactes et de leur applications

&

Durham University
Civil Engineering and Computing Science Department

Anglet. 25th October 2019

There will never be a day

when I won't think of you

and wish you were here

by my side.

(Cit. Narin Grewal)

To you, Mum

“Beat, happy stars, timing with things below,

Beat with my heart more blest than heart can tell,

Blest, but for some dark undercurrent woe

That seems to draw—but it shall not be so:

Let all be well, be well.”

(cit. Alfred Lord Tennyson)

Table of Contents

Table of Contents iv
List of Figures vii
List of Tables xvii
Acknowledgements xix
Nomenclature xx
Publications xxiii
Declaration xxv
Abstract xxvi
Résumé xxviii
1. Introduction 1
1.1. Raw earth materials 1
1.1.1. Context 1
1.1.2. Renaissance of earthen building 2
1.2. Historical overview 6
1.2.1. Evolution of earthen building 6
1.2.2. Earthen building codes and standards 9
1.3. Research objectives 11
1.4. Thesis layout 12
2. Raw earth: review of main engineering properties 14
2.1. Physical properties 14
2.1.1. Soil grading 14
2.1.2. Plasticity 18
2.1.3. Clay mineralogy 20
2.2. Mechanical behaviour 23
2.2.1. Effect of dry density 23
2.2.2. Effect of ambient humidity and temperature 31
2.3. Hygroscopic capacity 37
2.4. Sensitivity to water 43
3. Stabilisation of earth materials by carbonate precipitation: a review 51
3.1. Introduction 51
3.2. Carbonate precipitation for soil improvement 51
3.2.1. Efficiency of Microbially Induced Calcite Precipitation (MICP) 54

3.2.2. Hygro-mechanical behaviour of MICP-stabilised soil 59
3.3. Enzymatic induced calcite precipitation (EICP) 72
3.3.1. Role of urease in plant metabolism 72
3.3.2. Recent advances in enzymatic induced calcite precipitation (EICP) 73
4. Materials and methods 82
4.1. Material characterisation 82
4.1.1. Grain size distribution 82
4.1.2. Specific gravity, plasticity and clay activity 83
4.1.3. Optimisation of soil mix 84
4.2. Compaction procedures 86
4.2.1. Standard Proctor compaction 87
4.2.2. Hyper-compaction 88
4.2.2.1. Cylindrical earth samples 88
4.2.2.2. Earth bricks 92
4.3. Bio-stabilisation method 94
4.3.1. Urease enzyme from soybeans extract 94
4.3.2. Chemical reagents 95
4.3.3. Efficiency of stabilisation protocol 96
4.3.4. Urease enzyme from soybeans powder 99
5. Influence of soil grading on the hygro-mechanical and durability properties of raw earth 100
5.1. Mechanical behaviour 100
5.1.1. Unconfined compressive strength and Young's modulus 100
5.1.2. Effect of relative humidity 105
5.2. Moisture buffering capacity 121
5.3. Water durability properties 126
5.3.1. Immersion tests 127
5.3.2. Suction tests 128
5.3.3. Drip tests 130
5.3.4. Bricks classification 132
5.4. Conclusions and final remarks 134
6. Bio-stabilisation of raw earth using Enzymatic Induced Calcite Precipitation (EICP) 136
6.1. Factors affecting EICP efficiency: concentration of reagents 136
6.1.1. Test-tube experiments 137
6.1.2. X-ray Powder Diffraction (XRD) 146

6.2. Soil stabilisation 151
6.2.1. Preliminary essays 151
6.2.2. Hygro-mechanical investigation of stabilised earth 157
6.2.2.1. X-ray Powder Diffraction (XRD) on stabilised earth 160
6.2.2.2. Compressive strength and Young's modulus 164
6.2.2.3. Moisture buffering capacity 166
6.2.2.4. Water durability properties 167
6.3. Conclusions and final remarks 169
7. Conclusions 171
7.1. Materials and methods 171
7.2. Results and discussion 173
7.3. Recommendations for future work 174
References 176

List of Figures

Figure 1.1: Annual waste arising in the UK from different sources (from Dawson, 2012). 1
Figure 1.2: Embodied carbon in different masonry materials (from Morton et al., 2005). ..3
Figure 1.3: Weight of moisture adsorbed by different materials when ambient relative humidity is increased from 50 % to 80 (from Minke, 2000).....4
Figure 1.4: Model drawing of an earth block house, Çatal Höyük, Anatolia/Turkey, around 6000 BC (from Schroeder, 2016). 6
Figure 1.5: Section of the Great Wall of China built using the rammed earth technique around 2200 years ago (from Schroeder, 2016). 7
Figure 1.6: Earth block vault near Luxor/Egypt, around 1300 BC (from Schroeder, 2016). 7
Figure 1.7: Late Georgian cob town houses in Dawlish, Devon, built c. 1820 (from Keefe, 2012). 8
Figure 1.8: 150 years old rammed earth house in the South -East of France (from Bui et al., 2009). 9

Figure 2.1: Grain size distribution: upper and lower limits for compressed earth bricks according to AFNOR (2001), CRATerre-EAG (1998) and MOPT (1992) (from Bruno, 2016). 15
Figure 2.2: Recommended lower and upper proportions of clay (a), silt (b) and sand and gravel (c) in earthen materials according to various authors (from Maniatidis and Walker, 2003). 16
Figure 2.3: Drying curves for coarse earth Mix 7:1:2 and fine earth Mix 5:1:4 (after Beckett and Augarde, 2012).....18
Figure 2.4: Atterberg limits or amounts of water defining a solid, semi-solid, plastic or liquid state of the soil (after Mitchell and Soga, 2005).....19
Figure 2.5: Plasticity chart: recommendations for CEBs by AFNOR (2001), CRATerre-EAG (1998) and Houben and Guillaud (1994) (from Bruno, 2016). 20
Figure 2.6: Silica tetrahedron (a); Silica sheet (b); Alumina octahedral (c); Octahedral (gibbsite) sheet (d) (after Mitchell and Soga, 2005). 22
Figure 2.7: Diagram of the structures of kaolinite (a); illite (b); montmorillonite (c) (after Mitchell and Soga, 2005). 23
Figure 2.8: Variation of dry density and compressive strength with water content and compaction pressure from 1.2 MPa to 10 MPa (from Olivier and Mesbah, 1986). 24

Figure 2.9: Relation between energy effort and optimum water content (from Attom et al., 1997). 25
Figure 2.10: Relation between energy effort and maximum dry unit weight (from Attom et al., 1997).....25
Figure 2.11: The relation between water content and unconfined compressive strength (from Attom et al., 1997). 26
Figure 2.12: Stress-strain curve for adobe and BAP blocks and definition of the tangent E_t and equivalent E_{eq} moduli (from Kouakou and Morel, 2009).....27
Figure 2.13: Initial tangent E_t and equivalent E_{eq} moduli of BAP (from Kouakou and Morel, 2009). 27
Figure 2.14: Variation of compressive strength with dry density (from Kouakou and Morel, 2009). 28
Figure 2.15: Comparison between the Standard Proctor compaction curve and the hyper-compaction curves at 25 MPa, 50 MPa and 100 MPa (from Bruno et al., 2016).....29
Figure 2.16: Variation of Young's modulus with dry density (from Bruno et al., 2016)...30
Figure 2.17: Variation of compressive strength with dry density (from Bruno et al., 2016). 30
Figure 2.18: Variation of compressive strength with water content (from Bui et al., 2014). 32
Figure 2.19: Variation of Young's modulus with water content (from Bui et al., 2014). ..32
Figure 2.20: Variation of compressive strength with relative humidity and temperature (from Beckett and Augarde, 2012). 33
Figure 2.21: Variation of Young's modulus with total suction: unstabilised samples (from Bruno et al., 2017a).....34
Figure 2.22: Variation of compressive strength with total suction: unstabilised samples (from Bruno et al., 2017a). 35
Figure 2.23: Variation of Young's modulus with total suction: unstabilised and stabilised samples compacted at 100 MPa (from Bruno et al., 2017b). 36
Figure 2.24: Variation of compressive strength with total suction: unstabilised and stabilised samples compacted at 100 MPa (from Bruno et al., 2017b). 36
Figure 2.25: MBV measured by DTU (Technical University of Denmark), NBI (Norwegian Building Research Institute), VTT (Technical Research Centre of Finland) and LTH (Lund University of Sweden) measured on different construction materials (from Rode et al., 2005). 39

Figure 2.26: MBVs measured on unstabilised and stabilised earthen samples: comparison between different test procedures (after McGregor et al., 2014).....40
Figure 2.27: Moisture adsorption of unstabilised samples hyper-compacted at 25 MPa, 50 MPa and 100 MPa (from Bruno et al., 2016).....41
Figure 2.28: MBVs of unstabilised and stabilised compressed earth measured by McGregor et al. (2014) and unstabilised hyper-compacted earth measured by Bruno et al. (2016) (from Bruno et al., 2016).....42
Figure 2.29: Last stable cycle of unstabilised and stabilised samples (from Bruno et al., 2016).....42
Figure 2.30: Last stable MBV cycle measured on hyper-compacted earth bricks and cylindrical samples (from Bruno et al., 2016).....43
Figure 2.31: Untreated and treated adobe blocks after immersion in water for 1 hour (from Elert et al., 2015).....48
Figure 2.32: Results from suction tests on unstabilised and stabilised hyper-compacted earth bricks (from Bruno et al., 2017b).....49
Figure 2.33: Results from contact tests on unstabilised and stabilised hypercompacted earth bricks (from Bruno et al., 2017b).....50

Figure 3.1: Ureolysis-driven calcite precipitation (from De Muynck et al., 2010).....55
Figure 3.2: Scanning electron micrographs showing the effects of different calcium sources on the shape of the crystals formed: Calcium chloride (a); Calcium acetate (b); Calcium lactate (c); Calcium gluconate (d) (from Goroscope et al., 2013).....56
Figure 3.3: Bio-consolidated sand blocks made from different calcium salts: Calcium chloride (a); Calcium acetate (b); Calcium lactate (c); Control (d) (from Goroscope et al., 2013).....57
Figure 3.4: Saturated water content of control and stabilised earth blocks (a); Scanning Electron Micrograph of calcite crystals with bacterial impressions (b); X ray diffraction pattern of crystalline layer present on the surface of earth blocks treated with bacterial culture (c); Linear expansion of control and stabilised earth blocks (d). Bars mean ± SD (n = 3) (from Dhami and Mukherjee, 2015).....60
Figure 3.5: Strength of soil sample 1 stabilised with 1×10^5 cfu/ml at 0,3 and 7 days (a); 1×10^6 cfu/ml at 0,3 and 7 days (b); 1×10^7 cfu/ml at 0,3 and 7 days (c) (after Sharma and Ramkrishnan, 2016).....62

Figure 3.6: Strength of soil sample 2 with 1×10^5 cfu/ml at 0,3 and 7 days (a); 1×10^6 cfu/ml at 0,3 and 7 days (b); 1×10^7 cfu/ml at 0,3 and 7 days (c) (after Sharma and Ramkrishnan, 2016). 63
Figure 3.7: Specific urease activity, total amount of bioslurry and total urease activity for 100 mL of raw bacterial culture using varied concentrations of $CO(NH_2)_2$ and $CaCl_2$ (from Cheng and Shahin, 2016). 65
Figure 3.8: Relationship between amount of $CaCO_3$ precipitation and concentration of urea and calcium chloride in 100 mL of raw bacterial culture (from Cheng and Shahin, 2016). 65
Figure 3.9: Scanning electron microscopy (SEM) images of (a, b, c) pure bioslurry produced from 400 mmol/L $CO(NH_2)_2$ and $CaCl_2$ and (d, e, f) the same bioslurry without $CO(NH_2)_2$ and $CaCl_2$ (from Cheng and Shahin, 2016). 66
Figure 3.10: Effect of cementation solution flushes on the mechanical response of bioslurry treated sand: UCS (a) and stress–strain curves (b) (from Cheng and Shahin, 2016). 68
Figure 3.11: Particle size distribution and particle size density function of untreated and treated soils (from Morales et al., 2015). 69
Figure 3.12: Compaction curves at different energy levels for treated and untreated soils. The shaded area represents the as-compacted conditions used in the test programme (from Morales et al., 2015). 70
Figure 3.13: SEM images of treated samples before compaction: photomicrograph with calcified bacteria and calcite crystals (a); photomicrograph with calcite crystals located between grains of soil (b) (from Morales et al., 2015). 71
Figure 3.14: Shear strength envelopes for untreated and treated soils (from Morales et al., 2015). 72
Figure 3.15: Urea metabolism in plants (from Sirko and Brodzik, 2000). 73
Figure 3.16: Results of unconfined compression tests: Calcium chloride (CC) (a); Calcium hydroxide (CH) (b); Calcium nitrate (CN) (c) (from Park et al., 2014). 75
Figure 3.17: Scanning electron micrographs of EICP stabilised sand: CC-calcium chloride (a), CH-calcium hydroxide (b), CN-calcium nitrate (c) (from Park et al., 2014).....77
Figure 3.18: Result of X-ray diffraction analysis (from Park et al., 2014). 78
Figure 3.19: Relationship between calcite precipitation and amount of plant extract for specimens treated with calcium chloride, calcium hydroxide and calcium nitrate (from Park et al., 2014). 78
Figure 3.20: Test-tube experiments: relation between $CO(NH_2)_2$-$CaCl_2$ concentration and $CaCO_3$ precipitation ratio (from Carmona et al., 2016). 79

Figure 3.21: Test-tube experiments: XRD tests on precipitated material from 0.5 mol/L urea-$CaCl_2$ solution (from Carmona et al., 2016).....80
Figure 3.22: Unconfined compressive strength of soil specimens bio-stabilised with different urea-$CaCl_2$ concentrations: stress-strain curves (a); variation of strength with urea-$CaCl_2$ concentration (b) (from Carmona et al., 2016).....81

Figure 4.1: Grain size distribution of the base soil in relation to existing recommendations for the manufacture of compressed earth bricks by AFNOR (2001); CRATerre-EAG (1998) and MOPT (1992).....83
Figure 4.2: Plasticity properties of the base soil from the Bouisset brickwork factory in relation to existing recommendations for the manufacture of compressed earth bricks by AFNOR (2001); CRATerre-EAG (1998) and Houben and Guillaud (1994) (after Bruno, 2016). 84
Figure 4.3: Grain size distribution of earth mixes in relation to existing recommendations for the manufacture of compressed earth bricks by AFNOR (2001); CRATerre-EAG (1998) and MOPT (1992).....85
Figure 4.4: Grain size distribution of added sand in relation to existing recommendations for the manufacture of compressed earth bricks by AFNOR (2001); CRATerre-EAG (1998) and MOPT (1992).....86
Figure 4.5: Standard Proctor compaction curve of base soil (earth mix 1). 88
Figure 4.6: Zwick /Roell Amsler HB250 press (from Bruno, 2016).....89
Figure 4.7: Zwick /Roell Amsler HB250 compaction mould. 90
Figure 4.8: Equipment in the configuration before the start of hyper-compaction. 91
Figura 4.9: Hyper-compaction curves corresponding to the application of a static pressure of 100 MPa. 92
Figura 4.10: 3R RP 3000 TC/TH press with a load capacity of 3000 kN (from Bruno, 2016). 93
Figure 4.11: Compaction mould: disassembled (a), assembled (b) (from Bruno, 2016)....93
Figure 4.12: Procedure for obtaining the urease enzyme: soybeans are soaked in water (a), soaked soybeans are centrifugated in a blender (b), the crude urease extract is collected (c). 95
Figure 4.13: Urea powder ($CO(NH_2)_2$) and flakes of calcium chloride ($CaCl_2$).....96

Figure 4.14: Measurements of pH taken at different times after dissolution of 2 mol/L of urea in the crude soybeans extract (initial value of pH before addition of urea equal to 6). 96
Figure 4.15: Precipitation of calcium carbonate at the bottom of the beaker after addition of calcium chloride (a) and precipitated material after oven-drying (b). 97
Figure 4.16: Preliminary XRD analysis of precipitated material. 98
Figure 4.17: Thick foam at the top of the acidic soybeans extract after exposition to the laboratory atmosphere (a) and absence of precipitated calcium carbonate by using an acidic crude soybeans extract (b). 98
Figure 4.18: Sieving of the finer fraction (smaller than 0.400 mm) of the crushed soybeans powder. 99

Figure 5.1: Compressive failure mechanisms for earth mix 1 (a), earth mix 3 (b), earth mix 2 (c, d). 101
Figure 5.2: Stress-strain curves from tests performed on hyper-compacted earth mixes 1, 2 and 3. 102
Figure 5.3: Compressive strength: results of unconfined compression tests for the different earth mixes. 103
Figure 5.4: Testing set-up for measuring axial and radial displacements (Model 3542-050M-005-HT1 - Epsilon Technology Corp. and Model 3544-150M060M-ST - Epsilon Technology Corp.). 103
Figure 5.5: Cyclic test for measuring stiffness properties. 104
Figure 5.6: Young's modulus: results of unconfined loading-unloading cycles for the different earth mixes. 104
Figure 5.7: Stress-strain curve from triaxial compression tests and measurement of the Young's modulus as the slope of the tangent to the stress-strain curve. 107
Figure 5.8: Results from triaxial tests on the hyper-compacted earth mix 1 at different confining pressures and distinct humidity levels: dry (a), 25 % (b), 62 % (c), 95 % (d). .109
Figure 5.9: Results from triaxial tests on the hyper-compacted earth mix 3 at different confining pressures and distinct humidity levels: dry (a), 25 % (b), 62 % (c), 95 % (d). .111
Figure 5.10: Results from triaxial tests on the Proctor compacted earth mix 1 at different confining pressures and distinct humidity levels: dry (a), 25 % (b), 62 % (c), 95 % (d). 1133
Figure 5.11: Strength envelopes of hyper-compacted earth mix 1 at different humidity levels. 114

Figure 5.12: Stiffness envelopes of hyper-compacted earth mix 1 at different humidity levels. 115
Figure 5.13: Strength envelopes of hyper-compacted earth mix 3 at different humidity levels. 115
Figure 5.14: Stiffness envelopes of hyper-compacted earth mix 3 at different humidity levels. 116
Figure 5.15: Strength envelopes of Proctor compacted earth mix 1 at different humidity levels. 116
Figure 5.16: Stiffness envelopes of Proctor compacted earth mix 1 at different humidity levels. 117
Figure 5.17: Comparison of results from triaxial tests on hyper-compacted earth mixes 1 and 3 under dry conditions. 118
Figure 5.18: Comparison of results from triaxial tests on hyper-compacted earth mixes 1 and 3 at a relative humidity of 95 %. 119
Figure 5.19: Values of peak strength measured at different confining pressures and humidity levels on hyper-compacted earth mixes 1 and 3. 119
Figure 5.20: Comparison of results from triaxial tests on hyper-compacted and Proctor compacted samples of earth mix 1 under dry conditions. 120
Figure 5.21: Comparison of results from triaxial tests on hyper-compacted and Proctor compacted samples of earth mix 1 at a relative humidity of 95 %. 121
Figure 5.22: Values of peak strength measured at different confining pressures and humidity levels on hyper-compacted and Proctor compacted samples of earth mix 1. 121
Figure 5.23: Climatic chamber CLIMATS Type EX2221-HA. 122
Figure 5.24: MBVs during moisture uptake and release in subsequent humidity cycles. Solid markers indicate MBV uptake while hollow markers indicate MBV release. 124
Figure 5.25: Moisture adsorption curves of the hyper-compacted samples of earth mixes 1, 2 and 3. 124
Figure 5.26: Moisture adsorption curves during last stable cycle. 125
Figure5.27: Comparison of MBVs measured in the present work and in the work by McGregor et al. (2014). 126
Figure 5.28: Hyper-compacted earth mix 1 before (a) and after (b) immersion in water for ten minutes. 128
Figure 5.29: Suction test set-up. 129

Figure 5.30: Results for suction tests performed on hyper-compacted earth mixes 1, 2 and 3. 130
Figure 5.31: Drip test set-up. 131
Figure 5.32: Depth of erosion versus time for hyper-compacted bricks of earth mixes 1, 2 and 3. 132

Figure 6.1: Measurements of pH and electrical conductivity taken one hour after adding urea to the liquid soybean extract (urea concentration varying from 0.010 mol/L to 4 mol/L). 137
Figure 6.2: Measurements of pH and electrical conductivity taken 24 hours after adding urea to the crude soybeans extract (urea concentration varying from 0.010 mol/L to 4 mol/L). 139
Figure 6.3: Measurements of electrical conductivity taken 1 and 24 hours after adding urea to the crude soybeans extract (urea concentration varying from 0.010 mol/L to 4 mol/L). 139
Figure 6.4: Reduction of pH immediately after adding calcium chloride to the soybeans extract containing urea (equimolar urea and calcium chloride concentrations varying from 0.010 mol/L to 4 mol/L). 139
Figure 6.5: Visual examination of test-tubes after 72 hours from the addition of calcium chloride (equimolar urea and calcium chloride concentrations varying from 0.010 mol/L to 4 mol/L). 140
Figure 6.6: Collection of the precipitated material by using a vacuum system that facilitates percolation of the test-tubes content across the filter paper. 140
Figure 6.7: Precipitated calcium carbonate after being oven dried at 40 °C. 141
Figure 6.8: Theoretical (M^tCaCO_3) and actual (M^aCaCO_3) mass of precipitated calcite for equimolar concentrations of urea and calcium chloride from 0.010 mol/L to 4 mol/L (measured 72 hours after the addition of calcium chloride). 142
Figure 6.9: Measurements of pH and electrical conductivity taken 1 hour after adding urea to distilled water (urea concentration varying from 0.010 mol/L to 4 mol/L). 142
Figure 6.10: Increase of pH immediately after adding calcium chloride to distilled water containing urea (equimolar urea and calcium chloride concentrations varying from 0.010 mol/L to 4 mol/L). 143
Figure 6.11: Visual examination of test-tubes after 72 hours from the addition of urea and calcium chloride in distilled water (equimolar urea and calcium chloride concentrations

varying from 0.010 mol/L to 4 mol/L). No evidence of precipitation of calcium carbonate crystals.....143
Figure 6.12: Measurements of electrical conductivity taken 24 hours after adding urea to distilled water (urea concentration varying from 0.010 mol/L to 4 mol/L). 144
Figure 6.13: Measurements of electrical conductivity taken 1 and 24 hours after adding urea to distilled water plus soybeans powder (urea concentration varying from 0.010 mol/L to 4 mol/L).....145
Figure 6.14: Comparison of electrical conductivity measurements taken 1 and 24 hours after adding urea to soybeans extract and distilled water plus fine soybeans powder, respectively (urea concentration varying from 0.010 mol/L to 4 mol/L). 145
Figure 6.15: Formation of a semi-liquid paste after addition of calcium chloride to test-tubes containing distilled water, soybeans powder and urea (urea/calcium chloride concentration of 2.50 mol/L).....146
Figure 6.16: XRD analysis-Preparation of sample: sticky paste from test-tube containing distilled water, soybeans powder, urea and calcium chloride (urea/calcium chloride concentration of 2.50 mol/L) (a), distribution of the paste into the sample holder assuring a flat upper surface (b).....147
Figure 6.17: Principles of X-ray Diffraction. 148
Figure 6.18: XRD analysis performed on the material precipitated at the bottom of a test-tube containing soybeans extract, urea and calcium chloride (urea/calcium chloride concentration of 2.50 mol/L).....149
Figure 6.19: XRD analysis performed on a paste collected from a test-tube containing distilled water, soybeans powder, urea and calcium chloride (urea/calcium chloride concentration of 2.50 mol/L).....150
Figure 6.20: Hyper-compacted stabilised sample (urea/calcium chloride concentration of 2.50 mol/L) before (a) and after (b) immersion in water for 10 minutes.....152
Figure 6.21: Slurry-stabilised sample with soybean extract (urea/calcium chloride concentration of 2.50 mol/L) before (a) and after immersion (b). 153
Figure 6.22: Formation of cracks after spraying the whole amount of cementing solution (equal to 80 % LL) on the sample surface in a single application.....155
Figure 6.23: Slurry-stabilised sample with soybeans powder (urea/calcium chloride concentration of 2.50 mol/L) before (a) and during immersion at 3 minutes (b), 6 minutes (c) and 9 minutes (d). The mass loss after ten minutes of immersion in water was equal to 1% (e).....156

Figure 6.24: Growth of mould on the surface of slurry-stabilised sample with soybeans powder after exposure to moisture (a). Further mould growth was prevented by oven drying the sample at 105 °C (b).....157
Figure 6.25: Composition of cementing mixture added to the dry earth for SC, SP and SCP stabilisation methods.....159
Figure 6.26: XRD analysis on unstabilised sample.....161
Figure 6.27: XRD analysis performed on SC stabilised sample. 162
Figure 6.28: XRD analysis on SP stabilised sample.....163
Figure 6.29: Compressive strength measured from unconfined compression tests on unstabilised, SC stabilised, SP stabilised and SCP stabilised samples. 165
Figure 6.30: Young's modulus measured from unconfined compression tests on unstabilised, SC stabilised, SP stabilised and SCP stabilised samples. 165
Figure 6.31: MBVs measured during the uptake and release stages of subsequent humidity cycles on unstabilised, SC stabilised, SP stabilised and SCP stabilised samples. Solid markers indicate the MBV uptake while hollow markers indicate the MBV release. 166
Figure 6.32: Reference sample before immersion (a); unstabilised sample after immersion exhibiting a mass loss of 42% (b); SC stabilised sample after immersion exhibiting a mass loss of 13% (c); SP stabilised sample after immersion exhibiting a mass loss of 1% (d); SCP stabilised sample after immersion exhibiting a mass loss of 1% (e). 168
Figure 6.33: Digital microscope images of SC stabilised samples (a) and SP stabilised samples (b). 168

List of Tables

Table 1.1: Embodied carbon per meter cube of cement stabilised earth walls in different wall types (after Reddy and Kumar, 2010). 3

Table 2.1: Stiffness and strength of earth mixes with different clay-silt fractions (after Wu et al., 2013). 17

Table 2.2: Grain size distribution of materials tested by Bui et al. (2014) (after Bui et al., 2014). 31

Table 2.3: Ranges of Moisture Buffering Value classes (after Rode et al., 2005). 39

Table 2.4: Experimental procedures for the measurement of MBV as reproduced after McGregor et al. (2014). 40

Table 2.5: Erodability Index classification depending on the depth of pitting (after Frencham, 1982). 45

Table 2.6: Earth bricks classes according to application (after DIN 18945, 2013). 46

Table 2.7: Classification of compressed earth bricks: results from durability tests (after DIN 18945, 2013). 46

Table 2.8: Classification of earth bricks tested by Bruno et al. (2017b) in accordance to norm DIN 18945 (2013) (after Bruno et al., 2017b). 50

Table 3.1: Properties of soil samples tested as reported from Sharma and Ramkrishnan (2016). 61

Table 3.2: Summary of unconfined compression tests (after Park et al., 2014). 74

Table 4.1: Main properties of the base soil from the Bouisset brickwork factory. 83

Table 4.2: Composition of the different earth mixes. 85

Table 4.3: Urea ($CO(NH_2)_2$) and calcium chloride ($CaCl_2$) properties: molar weight (MW) in g/mol, appearance and assay in percentage. 96

Table 5.1: Total suction after equalisation at different humidity levels. 106

Table 5.2: Samples properties after equalisation……..……106

Table 5.3: Strength parameters of hyper-compacted earth mix 1 at different humidity levels. 114

Table 5.4: Strength parameters of hyper-compacted earth mix 3 at different humidity levels. 115
Table 5.5: Strength parameters of Proctor compacted earth mix 1 at different humidity levels. 116
Table 5.6: MBVs under steady state conditions. 125
Table 5.7: Percentage of mass loss during immersion tests. 128
Table 5.8: Final erosion depths of hyper-compacted bricks of earth mixes 1, 2 and 3. ...132
Table 5.9: Classes of compressed earth bricks (DIN 18945, 2013). 133
Table 5.10: Classification of the hyper-compacted bricks tested in the present work (DIN 18945, 2013). 133
Table 5.11: Erodability Index classification of the hyper-compacted bricks tested in the present work (NZS 4298, 1998). 134

Table 6.1: Composition of cementing mixture added to the dry earth for SC, SP and SCP stabilisation methods. 158
Table 6.2: MBVs of unstabilised, SC stabilised, SP stabilised and SCP stabilised samples. 167

Acknowledgements

I acknowledge the European Commission via the Marie Skłodowska-Curie Innovative Training Networks (ITN-ETN) project TERRE "Training Engineers and Researchers to Rethink geotechnical Engineering for a low carbon future" (H2020-MSCA-ITN-2015-675762) for supporting this project which was carried out in the laboratory SIAME at the Université de Pau et des Pays de l'Adour and in the laboratory of Soil Mechanics at Durham University.

I would like to express my gratitude to Pr. Domenico Gallipoli, Pr. Charles Augarde, Pr. Christian La Borderie, Dr. Paul Hughes and Dr. Agostino Walter Bruno for supervising this project and offering me their passionate and enthusiastic support. Their support and their wise guidance have been fundamental for me and this thesis. Everything I learned from them has been precious for my scientific and personal enrichment.

I would like to thank all the members and colleagues of the Laboratory (SIAME, ISA-BTP, Durham University) and all those people who have helped me during this thesis, with their wise suggestions, criticisms and comments: they all deserve my complete gratitude.

Very special thanks to my family and my closest friends. They have given me the energies to reach this wonderful milestone, supporting me in every moment and always showing me their faith in my possibilities. All my love goes to my father Michele, my brother Antonio and sister Laura that never gave up on me.

To my angel, the person who gave, give and will give me the strength to go on: I would like to dedicate this important achievement.

Finally, a special thanks to Fawzi, who unreservedly encouraged me mainly in the most difficult times, always listening to me with patience and understanding (endless calls are not your favourite but you never hang up).

Nomenclature

Abbreviations

ACC: Amorphous Calcium Carbonate

BAP: Bloques d'Adobe pressés

CC: Calcium Chloride

CEB: Compressed Earth Bricks

CH: Calcium Hydroxide

CN: Calcium Nitrate

DIC: Dissolved Inorganic Carbon

EICP: Enzymatic Induced Calcite Precipitation

EPS: Extracellular Polymeric Substances

GSD: Grain Size Distribution

MBV: Moisture Buffering Value

MICP: Microbially Induced Calcite Precipitation

MW: Molar Weight

NHL: Natural Hydraulic Lime

OD600: Optical Density (wavelength of 600 nm)

PR: Precipitation Ratio

SC: Stabilisation method using liquid soybeans extract

SCP: Stabilisation method using fine soybeans powder

SEM: Scanning Electron Microscope

SP: Stabilisation using liquid soybeans extract + fine soybeans powder

XRD: X-ray Diffraction

Symbols

A: Clay Activity

C: Percentage of clay by weight

C: Intercept of the failure envelope

c: Cohesion

d: Lattice spacing in the crystalline sample

E: Young's modulus

E_{eq}: Equivalent Moduli

E_r: Erodability Index

E_t: Initial Tangent

G_S: Specific gravity

I_P: Plasticity Index

M: Slope of the failure envelope

M: Molar mass of calcite

m_f: Final mass

m_i: Initial mass

$M^a_{CaCO_3}$: Actual mass of precipitated calcite

$M^t_{CaCO_3}$: Theoretical mass of precipitated calcite

$MBV_{practical}$: Practical Moisture Buffering Value

n: Porosity

p: Mean stress

q: Deviator stress

R: Universal gas constant

RH: Relative Humidity

S: Surface area

Sr: Degree of saturation

T: Absolute temperature

V_m: Molar volume of water

W: Mass

w_L: Liquid Limit

w_P: Plastic Limit

w_S: Shrinkage Limit

θ: Diffraction angle

λ: Wavelength of electromagnetic radiation

σ: Confining pressure

ρ_b: Bulk density

ρ_d: Dry density

φ: Friction angle

ψ: Total Suction

Chemical symbols

Al: Aluminium

Ca^{2+}: Calcium ions

$Ca(OH)_2$: Calcium hydroxide

$CaCl_2$: Calcium chloride

($CaCO_3 \cdot H_2O$): Monohydrocalcite

($CaCO_3 \cdot 6H_2O$): Hexahydrocalcite or Ikaite

$CaCO_3$: Calcium Carbonate

CO_2: Carbon dioxide

CO_3^{2-}: Carbonate ions

$CO(NH_2)_2$: Urea

H^+: Hydrogen ions

H_2CO_3: Carbonic Acid

K^+: Potassium ions

KOH: Potassium hydroxide

Mg^{2+}: Magnesium ions

NaOH: Sodium Hydroxide

NH_3: Ammonia

NH_4^+: Ammonium ions

NH_2COOH: Carbamic Acid

O: Oxygen

O^{2-}: Oxygen ions

OH^-: Hydroxide ions

Si: Silicon

Publications

Conference publications

C1) **A. Cuccurullo**, D. Gallipoli, A. W. Bruno, C. Augarde, P. Hughes, C. La Borderie (2018). The influence of the particle size distribution on the hygro-mechanical properties of hyper-compacted raw earth. Proceedings of the 10th International Masonry Conference (10thIMC), Milan (Italy), 9th-11th July 2018 - https://doi.org/ 10.15128/r2ws859f66v

C2) **A. Cuccurullo**, D. Gallipoli, A. W. Bruno, C. Augarde, P. Hughes, C. La Borderie (2018). The role of particle size distribution and suction on hyper-compacted earth material shear strength. Proceedings of the 7th International Conference on Unsaturated Soils (UNSAT2018), Hong Kong (China), 3rd-5th August 2018 - https://doi.org/ 10.15128/r29593tv142

C3) S. Muguda Viswanath, P. Hughes, C. Augarde, **A. Cuccurullo**, A.W. Bruno, C. Perlot, D. Gallipoli (2018). Advances in biologically-stabilised earthen construction materials. Proceeding of the International Symposium on Earthen Structures (ISES2018), Bengaluru (India), 22th-24th August 2018. In Earthen dwellings and structures. Singapore: Springer, pp. 191-201- https://doi.org/10.15128/r2c534fn95z

C4) **A. Cuccurullo**, D. Gallipoli, A. W. Bruno, C. Augarde, P. Hughes, C. La Borderie (2019). Soil stabilization via calcite precipitation by plant-derived enzyme. Proceedings of the 7th edition of the Italian National Congress of Geotechnical Researchers (CNRIG2019), Lecco (Italy), 3rd-5th July 2019. In National Conference of the Researchers of Geotechnical Engineering (pp. 753-762). Springer, Cham.

C5) **A. Cuccurullo**, D. Gallipoli, A. W. Bruno, C. Augarde, P. Hughes, C. La Borderie (2019). Advances in the enzymatic stabilisation of soils. Proceedings of the XVII European Conference on Soil Mechanics and Geotechnical Engineering, Reykjavik (Iceland), 1st-6th September 2019.

International journal publications

Submitted:

J1) **A. Cuccurullo**, D. Gallipoli, A. W. Bruno, C. Augarde, P. Hughes, C. La Borderie (2018). Influence of particle grading on the hygro-mechanical properties of hyper-

compacted earth. BPAR 10IMC Special Issue, Journal of Building Pathology and Rehabilitation BPAR

Declaration

The work in this thesis is based on research carried out in the Sustainable Infrastructure group, Department of Engineering, Durham University, United Kingdom and SIAME laboratory, Université de Pau et des Pays de l'Adour, France. No part of this report has been submitted elsewhere for any other degree or qualification and it all my own work unless referenced to the contrary in the text.

Abstract

The present work investigates the hygro-mechanical performance of compacted earth as an alternative to conventional energy-intensive building materials. Cement and lime have been widely employed as stabilisers to improve the strength and durability of compacted earth for building applications. Nevertheless, the use of these chemical binders partly compromises the energy efficiency of earthen materials while increasing their carbon footprint. This has recently led to the study of alternative stabilisation methods that are equally effective in improving the properties of earthen materials without however compromising their green credentials.

The present work adopts a recently proposed method for the manufacturing of earth bricks. The method is based on the application of high compaction pressures up to 100 MPa (hyper-compaction) to increase the density of the earth and hence to obtain mechanical properties that are similar to those of traditional construction materials such as fired bricks, concrete blocks and stabilised earth. A wide campaign of laboratory tests was performed on samples made of different earth mixes that were hyper-compacted at their respective optimum water contents. Stiffness and strength were measured by unconfined and triaxial compression tests while vapour adsorption/desorption was assessed by measuring moisture buffering value (MBV). Durability to water erosion was also evaluated by performing suction, immersion and drip tests according to the norms DIN 18945 (2013) and NZS 4298 (1998), respectively.

Results showed that hyper-compaction largely improves the mechanical performance of compacted earth but that a marked increase in ambient humidity can produce a considerable reduction of strength. Compacted earth is also characterised by an excellent capacity of adsorbing/releasing ambient moisture, which increases the hygro-thermal inertia of the material. Nevertheless, durability tests highlighted that the unstabilised compacted earth cannot be employed for the construction of structures exposed to natural weathering. The experiments also demonstrated the dependency of strength, stiffness, moisture buffering capacity and water durability on particle grading. In particular, it was shown that a fine and well-graded earth mix exhibits higher levels of strength, stiffness, moisture buffering capacity and durability than a coarse and poorly-graded one. This suggests that careful selection of the soil is necessary to optimise the manufacture of earth bricks.

One important challenge lies in the improvement of the earth durability against water erosion by adopting novel stabilisation techniques which exhibit small environmental impacts while preserving the advantageous properties of compacted earth in terms of mechanical and

moisture buffering behaviour. In this work, the exploitation of knowledge at the interface between physics, biology and chemistry has led to the development of an original stabilisation method based on the utilisation of plant extracts. The method is consistent with the principles of Enzymatic Induced Calcite Precipitation (EICP), which utilises the action of the urease enzyme to catalyse the hydrolysis of urea. This reaction produces carbonate ions, which then react with the calcium ions dissolved in the pore water to produce the precipitation of calcium carbonate (i.e. calcite), thus binding the soil together.

The urease enzyme is a widely occurring hexameric protein that is the product of the metabolism of microbes and is also found in the tissues of many plants. The novelty of the present work resides in the utilisation of crude plant-derived urease enzyme instead of pure reagent-grade products available from chemical suppliers, which reduces environmental and financial costs. In particular, the urease enzyme was obtained from a liquid soybeans extract, inside which the urea and calcium chloride were subsequently dissolved to induce the precipitation of calcite. A fundamental study of the relevant microbiological and biochemical processes pointed out that the concentrations of urea and calcium chloride play an important role in the activity of the urease enzyme and on the amount of precipitated calcite. Measurements of pH, electrical conductivity and precipitation ratio indicated that the optimum equimolar concentration of urea and calcium chloride (leading to the largest precipitation of calcite) is 2.5 mol/L.

An experimental campaign was finally undertaken to implement the proposed bio-stabilisation method into the manufacture of compressed earth bricks. The efficiency of the treatment was initially assessed by means of water immersion tests to quantify the improvement of the material water durability. The most promising versions of the proposed bio-stabilisation method were also the object of further investigation to assess the hygro-mechanical behaviour of the stabilised earth by means of unconfined compression and moisture buffering value tests. The findings, although preliminary, suggest that a noticeable improvement of strength and water durability can be achieved by the proposed stabilisation protocol, in spite of the difficulty in replicating exactly quantitative results. Further tests are still necessary to make the proposed treatment competitive with conventional stabilisation techniques based on the use of cement and lime.

Résumé

Cette étude se concentre sur les performances hygro-mécaniques de la terre crue compactée comme matériau de construction alternatif aux matériaux de construction classiques à forte empreinte énergétique. Pour des applications constructives, le ciment et la chaux sont couramment utilisés comme stabilisants pour améliorer la résistance mécanique et la durabilité de la terre crue. Néanmoins, l'incorporation de ces liants hydrauliques compromet partiellement la sobriété énergétique des matériaux en terre en augmentant leur empreinte carbone. Ceci a conduit à rechercher des méthodes de stabilisation alternatives permettant d'améliorer efficacement les propriétés des matériaux en terre crue sans toutefois compromettre leurs atouts écologiques.

Ce travail adopte une méthode récemment développée pour la fabrication de briques de terre crue basée sur l'application de pressions de compactage élevées (jusqu'à 100 MPa, d'où la dénomination d'hyper-compactage) pour augmenter la densité du matériau et ainsi obtenir des propriétés mécaniques similaires à celles des matériaux de construction traditionnels tels que les briques de terre cuite, les blocs de béton et la terre crue stabilisée. Une vaste campagne expérimentale a été menée sur des échantillons constitués de différents mélanges hyper-compactés de terres à leur teneur en eau optimale respective. La rigidité et la résistance mécanique ont été mesurées par des essais de compression non confinés et triaxiaux, tandis que l'adsorption/désorption de vapeur a été évaluée par la valeur de MBV (Moisture Buffering Value). La durabilité à l'érosion hydrique a également été étudiée en effectuant des tests de adsorption capillaire, d'immersion et de goutte-à-goutte conformément aux normes DIN 18945 (2013) et NZS 4298 (1998).

Les résultats confirment que l'hyper-compactage améliore largement les performances mécaniques de la terre crue compactée, mais qu'une augmentation sensible de l'humidité ambiante peut entraîner une réduction considérable de la résistance. La terre crue compactée se caractérise également par une excellente capacité d'adsorption/désorption de l'humidité ambiante, ce qui augmente l'inertie hygro-thermique du matériau. Néanmoins, les tests de durabilité révèlent que la terre compactée non stabilisée ne pouvait pas être utilisée pour la construction des parties de structures exposées aux intempéries naturelles en raison de sa sensibilité vis-à-vis de l'eau liquide. Les expériences démontrent également la dépendance de la résistance, de la rigidité, du comportement hydrique, de la sensibilité à l'eau liquide et de la durabilité à la taille des particules. En particulier, il a été observé qu'un mélange de terre à faible granulométrie et spécialement calibrées présente des caractéristiques pour les

propriétés susmentionnées supérieures à celle d'un sol à la granulométrie grossière et non maîtrisée. Cela suggère qu'une sélection minutieuse du sol est nécessaire pour optimiser la fabrication des briques de terre crue.

Un défi important demeure l'amélioration de la durabilité de la terre crue à l'érosion hydrique en adoptant de nouvelles techniques de stabilisation à faibles impacts environnementaux, tout en préservant les avantages de ce matériau en termes de résistance mécanique et de régulation de l'humidité.

Dans ce travail, l'exploitation des connaissances à l'interface de la Physique, de la Biologie et de la Chimie ont conduit à la mise au point d'une méthode originale de stabilisation basée sur l'utilisation d'extraits de plantes. Cette méthode s'apparente à la précipitation de calcite induite par voie enzymatique via l'action de l'enzyme uréase pour catalyser l'hydrolyse de l'urée. Cette réaction produit des ions carbonates, qui réagissent ensuite avec les ions calcium du sol dissouts dans l'eau interstitielle pour précipiter sous forme de carbonate de calcium (c'est-à-dire calcite), liant ainsi les particules du sol.

L'enzyme uréase est une protéine hexamère très répandue, issue du métabolisme des microbes. Elle est également présente dans les tissus de nombreuses plantes. La nouveauté de cette méthode réside dans l'utilisation de l'enzyme uréase végétale brute au lieu de réactifs synthétiques disponibles auprès de fournisseurs de produits chimiques, ce qui réduit les coûts environnementaux et financiers. Ici, l'enzyme uréase est extraite de jus de soja, auquel de l'urée et du chlorure de calcium sont ajoutés pour induire la précipitation de calcite. Une étude fondamentale des processus microbiologiques et biochimiques pertinents de ces phénomènes de précipitation établissent que les concentrations en réactifs jouent un rôle important dans l'activité de l'enzyme uréase et la quantité de calcite poduite. Les mesures de pH, de conductivité électrique et du taux de précipitation indiquent que la concentration équimolaire optimale -entraînant la plus grande précipitation de calcite- d'urée et de chlorure de calcium est de 2,5 mol/L.

Finalement, une campagne expérimentale a été menée pour appliquer cette méthode de biostabilisation à la fabrication de briques de terre crue compressée. L'efficacité du traitement a été évaluée à l'aide de tests d'immersion dans l'eau afin de quantifier l'amélioration de la durabilité du matériau. Les combinaisons les plus prometteuses de cette méthode de biostabilisation ont également fait l'objet d'investigations approfondies pour évaluer le comportement hygro-mécanique de la terre crue ainsi stabilisée au moyen d'essais de résistance en compression non confinée et de mesures du MBV. Les résultats, bien que

préliminaires, suggèrent une amélioration notable de la résistance et de la durabilité grâce au protocole de stabilisation proposé, malgré la difficulté à reproduire des résultats quantitatifs précis. Des tests supplémentaires sont requis pour rendre le traitement proposé concurrentiel par rapport aux techniques de stabilisation classiques basées sur l'utilisation de liants hydrauliques.

1. Introduction

1.1. Raw earth materials

1.1.1. Context

A "sustainable" product or technology is one that "meets the needs of the present without compromising the ability of future generations to meet their own needs" (Brundtland Commission, Our Common Future, 1987). The sustainability of the construction sector is a complex subject as the potential environmental impacts of building activities are significant. The construction sector represents one of the largest industries worldwide and is responsible for high levels of pollution which are, in great part, the result of energy consumption during extraction, processing and transportation of raw materials.

The construction sector accounts for 30 % of all carbon emissions and consumes more raw materials than any other economic activity on the planet (Pacheco-Torgal and Jalali, 2012). The cement industry alone accounts for 5 % of global carbon emissions and the production of each ton of cement generates more than one ton of carbon dioxide (CO_2) (Pacheco-Torgal and Jalali, 2012).

The construction sector is also responsible for the production of about 33 % of all waste generated in the European Union, most of which is not recyclable and is therefore disposed in landfills (EEA, 2010). As an example, Figure 1.1 illustrates the annual waste arising in the UK from different sources (Dawson, 2012), which confirms the high environmental impact of building activities.

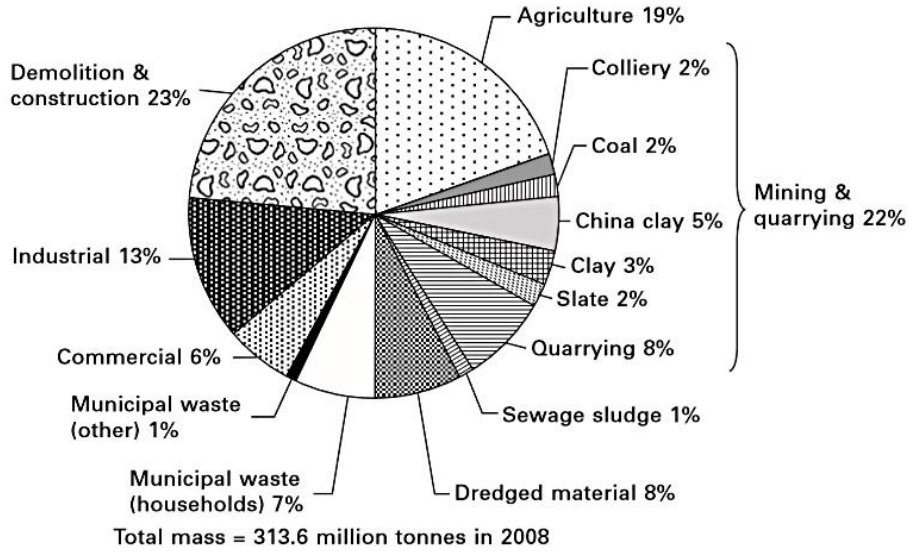

Figure 1.1: Annual waste arising in the UK from different sources (from Dawson, 2012).

In the same way, the French agency of the environment and energy management states that in France the building sector is responsible for 22 % of all greenhouse gas emissions, 44 % of all primary energy consumption and 31 % of all generated waste (ADEME, 2013).

According to Thormark (2006) an appropriate choice of building materials can reduce the overall energy consumption of the construction sector by 17 %. Similar conclusions were drawn by Gonzalez and Navarro (2006), which indicated that a suitable choice of building materials can reduce CO_2 emissions by almost 30 %.

The high environmental impact associated to both the construction and operation of dwellings has triggered a strong interest in sustainable building materials and technologies that exhibit large hygro-thermal efficiency, low carbon footprint and reduced financial costs. Modern construction standards already promote the use of materials that reduce carbon emissions and energy consumption throughout the lifetime of buildings (e.g. Arrigoni et al., 2017). In this respect, raw earth is a very promising material that can reduce energy consumption throughout the lifetime of buildings while minimising environmental impact (Gallipoli et al., 2017).

1.1.2. Renaissance of earthen building

The expression “raw earth” indicates a construction material consisting of a compacted mix of soil and water, which is put in place with the least possible transformation (Jaquin et al., 2009). Raw earth is an attractive building material because it is harmless to humans, it can be locally sourced and easily transported to the construction site. Earth is also recyclable, inexhaustible and, when properly manufactured, offers high strength, excellent hygro-thermal properties and low embodied energy at very low costs. Earthen materials can dramatically reduce exploitation of natural resources not only during construction but also during service time and up to the end of life of buildings by cutting down heating/air conditioning and limiting demolition waste. Some of these advantageous attributes of earthen materials are listed below:

Reduction of embodied energy. According to Deboucha and Hashim (2011) the extraction, transportation and manufacture of earthen materials require only 1 % of the energy that is necessary to produce cement-based materials. It has also been estimated that the manufacture of earth blocks requires no more than one third of the energy necessary to fabricate conventional fired blocks of similar dimensions, namely 440 kWh/m^3 compared to 1300 kWh/m^3 (Little and Morton, 2001). Figure 1.2 compares the CO_2 emissions associated to the production of earth blocks and other conventional masonry materials, thus demonstrating

the low environmental impact of the former with respect to the latter (e.g. Morton et al., 2005; Pacheco-Torgal and Jalali, 2012).

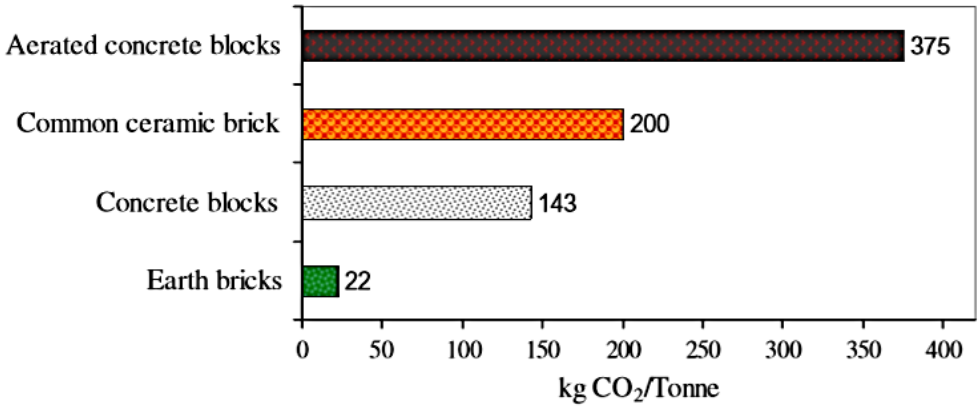

Figure 1.2: Embodied carbon in different masonry materials (from Morton et al., 2005).

Reddy and Kumar (2010) stated that the manufacture of stabilised earth blocks consumes fifteen times less energy and pollutes eight times less than the manufacture of fired bricks. Reddy and Kumar (2010) also showed that the embodied carbon of stabilised earth increases by increasing the cement content in the range of 0.4 - 0.5 GJ/m^3 for cement content in the range of 6 - 8 % (Table 1.1).

Table.1.1: Embodied carbon per meter cube of cement stabilised earth walls in different wall types (after Reddy and Kumar, 2010).

Wall type	**Kg CO_2 eqv**
Generic rammed earth	26
Rammed earth stabilised with 8 % cement	65
Rammed earth stabilised with 9 % cement	70
Brick and blockwork cavity	71

Hygro-regulator effect (reduction of operational energy). Because of its hydrophilic nature, raw earth exhibits a strong tendency to adsorb or release moisture and therefore to emit or store latent heat depending on the current levels of ambient humidity. This property helps to regulate the variation of relative humidity and temperature inside dwellings, thus contributing to the health and comfort of occupants (Wargocki et al., 1999) while increasing energy efficiency. According to Minke (2000), earth blocks are capable of adsorbing 10 times more moisture than fired bricks when relative humidity increases from 50 % to 80 % as shown in Figure 1.3.

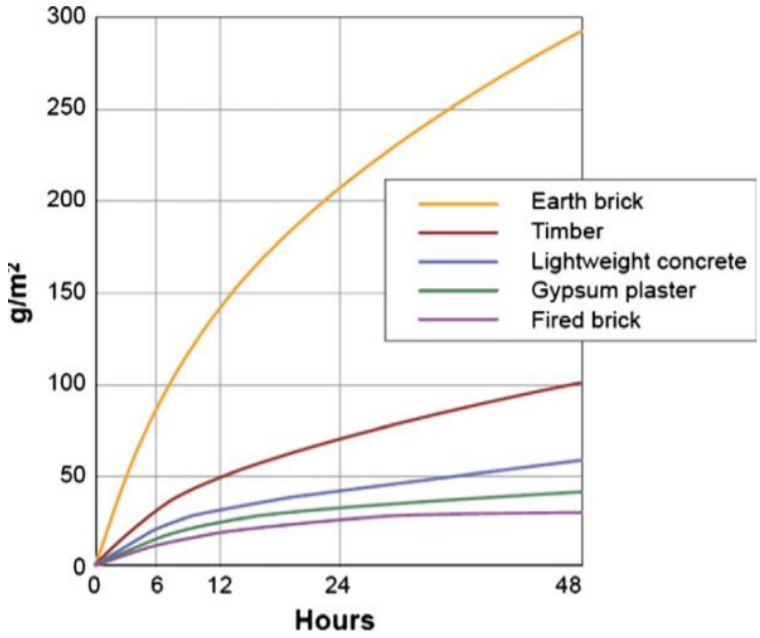

Figure.1.3: Weight of moisture adsorbed by different materials when ambient relative humidity is increased from 50 % to 80 % (after Minke, 2000).

According to Morton (2008), the elevated hygroscopicity of construction materials helps control indoor relative humidity. In this respect, earth walls are capable of keeping the relative humidity of indoor air between 40 % and 60 %, which corresponds to the comfort range for human occupation. Levels of humidity above 60 % can cause asthmatic diseases and favour the presence of mites while levels of humidity below 40 % are linked to respiratory illnesses such as tonsillitis, pharyngitis or bronchitis.

Recycling or safe disposal of demolition waste. According to Bossink and Brouwers (1996), the waste generated by the construction sector, including demolition waste, accounts for between 13 % and 30 % of all landfill storage worldwide. In this respect, the use of earthen materials may be particularly advantageous as the waste resulting from the demolition of unstabilised earth structures may be easily recycled or safely released into the environment. The potential reuse of earthen materials for further construction is the highest form of recycling and, therefore, highly desirable but, unfortunately, very little information on recycled earth building is currently available.

Despite the above eco-friendly attributes, the dissemination of earthen construction in engineering practice remains limited mainly because of the following shortcomings:

Inadequacy of local soil. In contrast to other building materials (e.g. concrete, steel, timber), the suitability of soils for building is not currently standardised, probably because of the inherent variability of such material. During the last 20 years, a number of researchers have

proposed some methods of optimising soil constituents based on the resulting strength and durability properties. Most of these studies agree that an optimum earth mix should contain 30 % clay/silt and 70 % sand/gravel, though the exact influence of soil grading on material strength and durability is unclear (Keable, 1996). Clay content strongly influences the hygro-mechanical performance of the material as the fine earth fraction is responsible for the adsorption/release of moisture and for the capillary bonding of soil grains. Many soils are generally suitable for earth building while others do not have sufficient clay content to ensure an adequate level of inter-granular bonding and therefore require the addition of stabilisers such as cement or lime. Soils may also be stabilised with locally sourced materials such as stones, organic fibres (straw, sisal, hemp) and timber.

Use of chemical stabilisers. In general, chemical stabilisers such as cement or lime have been used to improve the strength and durability of raw earth while reducing shrinkage/swelling and providing waterproofing (Walker, 2000; Jayasinghe and Kamaladasa, 2007). In general, however, the addition of chemical stabilisers lessens the "eco-friendly" characteristics of earthen materials as it increases the levels of embodied energy and reduces the possibility of recycling demolition waste. At the same time, the addition of cement or lime has been linked to a marked reduction of the hygroscopicity of earthen materials. Another aspect to consider is the financial costs of stabilisation as many stabilisers can account for more than half of the overall material price.

Sensitivity to moisture ingress. Earthen materials are very sensitive to moisture ingress as they absorb any free water which they come in contact to. Lucas (1918) and Washburn (1921) referred to the "wick effect" as the phenomena during which the moisture content of a stabilised raw earth sample exposed to free water increases linearly with the square root of time. Moisture ingress reduces the strength and stiffness of the material while also producing structural damages due to the swelling of the clay fraction.

Durability to erosion. Earthen buildings are generally vulnerable to erosion as demonstrated by the extensive damages often observed on exposed surfaces in wet rainy climates. For example, Bui et al. (2009) measured an erosion depth between 5 mm and 10 mm on the surface of 400 mm thick unstabilised earth walls exposed to a wet continental climate for twenty years. In relatively wet climates, the poor durability of earthen structures has strongly limited the diffusion of this construction technique beyond a niche market. Conversely, well-preserved earthen constructions, dating hundreds or even thousands of years, are often encountered in dry climates.

1.2. Historical overview

1.2.1. Evolution of earthen building

The first recorded cases of earthen building date back to 10000 BC according to archaeological evidence found in some relatively woodless, but clay-rich, regions of ancient Mesopotamia (between the Euphrates and Tigris rivers) and Afghanistan. The approximately 8000-year-old structures of Çatal Höyük, Anatolia, are another example of very ancient earth buildings of surprisingly high standard. The load-bearing exterior walls were constructed of earth blocks while interior wooden supports were used to carry the roof (Figure 1.4). The roof was flat, made of poles and grasses or reed with a layer of puddled earth for protection against rainwater. The dwellings were grouped together according to a honeycomb arrangement with individual houses being entered via the roof (Schroeder, 2016).

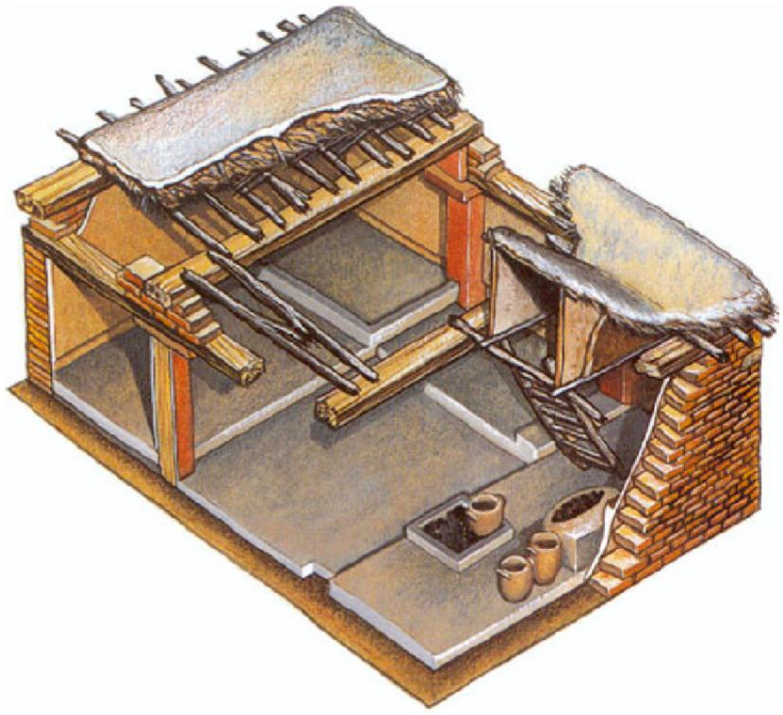

Figure 1.4: Model drawing of an earth block house, Çatal Höyük, Anatolia/Turkey, around 6000 BC (from Schroeder, 2016).

More recent earth structures, from rural habitats to impressive military citadels, are found all over the world, e.g. in France, Spain, Portugal, the Maghreb region (Morocco, Algeria), Central and South America (Mexico, Peru, Brazil) and China. There are countless cases of earth buildings erected more than 1000 years ago which are still standing. The most famous example is the Great Wall of China which was built 2000 years ago using local materials such as rammed earth, stones, baked bricks and wood (Figure 1.5).

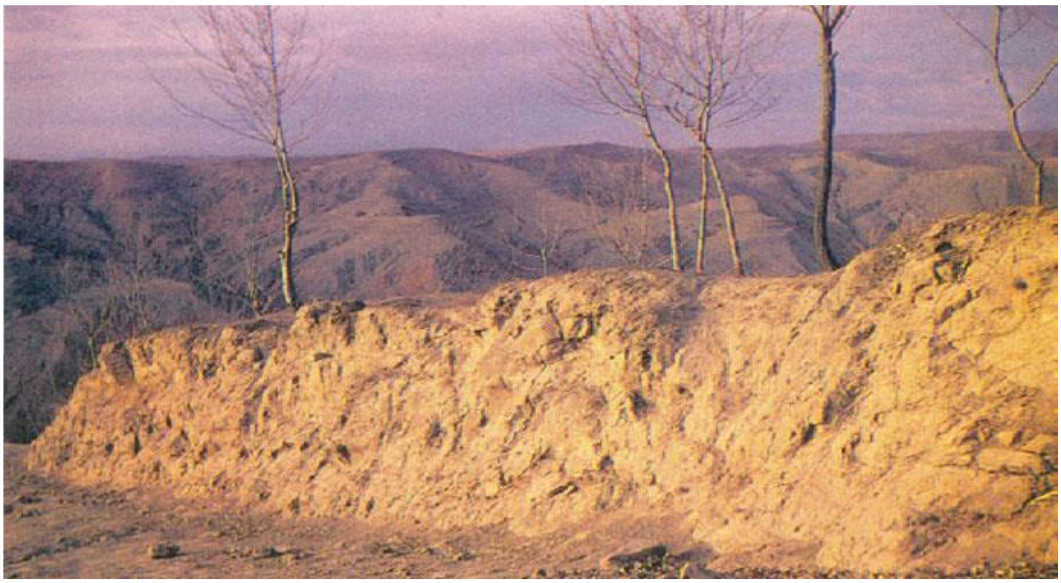

Figure 1.5: Section of the Great Wall of China built using the rammed earth technique around 2000 years ago (from Schroeder, 2016).

Archaeological remains also confirm the use of earth construction by Phoenicians across the Mediterranean region, including in Carthage, between 1500 and 300 BC. Ancient Egyptians were also familiar with various forms of raw earth building and, in particular, with the use of compressed earth blocks reinforced with straws. Figure 1.6 shows an earth block vault used as a storage room in the tomb of Ramses II from around 1300 BC.

Figure 1.6: Earth block vault near Luxor/Egypt, around 1300 BC (from Schroeder, 2016).

Advanced earth construction techniques were also developed by pre-Columbian and central America civilisations from 1000 to 1500 AC. The ruins of the city of Chanchan in Peru are among the most ancient earth-based constructions in the world (Alexandra, 2006). The oldest known existing earthwall building, the Pueblo at Taos in New Mexico, is 900 years old but requires a fresh coating of mud each year to survive.

During the late eighteenth century and throughout the nineteenth century, earthen construction experienced a strong revival. A large number of residential buildings constructed during this period are still in use and exhibit excellent performance in terms of structural stability, durability and environmental comfort despite being more than two hundred years old. Earth buildings can be found in France, Germany, United Kingdom, United States, Brazil and Australia (Figure 1.7 and 1.8). In the United States and Australia, where labour was relatively expensive, the industrialisation of the manufacture of earth blocks made this construction material particularly competitive.

Figure 1.7: Late Georgian cob town houses in Dawlish, Devon, built c. 1820 (from Keefe, 2012).

Between 1920 and 1950, thousands of raw earth dwellings were built in Germany under the instigation of the political authorities of the time. The regions of Prussia and Saxony, in particular, launched an effective programme of promotion of earthen construction between 1920 and 1921, which resulted in the realisation of nearly 20000 dwellings made of raw earth.

However, after the Second World War, post-bellic reconstruction privileged materials such as concrete and steel due to their relatively fast building techniques. In this context, raw earth became increasingly obsolete and, towards the end of the 1950s, it was virtually abandoned in the developed world.

Figure 1.8: 150 years old rammed earth house in the South-East of France (from Bui et al., 2009).

In current times, a number of important actions to promote earth constructions have been undertaken by the French laboratory CRATerre, which was founded in 1979. Similarly, universities and institutions worldwide have started to offer training programs and academic courses about earth construction. An experimental building of 72 residences, named "Domaine de la terre", was also initiated in France in 1982 by using various construction techniques, including rammed earth, soil-straw and compressed earth blocks. It is however recognised that raw earth is not suitable as a permanent building material, especially in wet climates, and unstabilised earthwall buildings over 100 years old have only survived with careful maintenance. In general the life of earthwall buildings built in the past is shorter than those using 'modern' building materials such as fired clay brick.

1.2.2. Earthen building codes and standards

The history of technical codes in the field of earth building is closely related to the development of cities in the fourteenth and fifteenth centuries in central Europe when,

because of rapid urbanisation, the availability of timber as primary building material became scarce (Schroeder, 2016). Moreover, timber structures were susceptible to fire damage and fires were responsible for wiping out entire portions of cities, either by accident or as a result of war. The German Earth Building Code (the Lehmbauordnung), was drawn up in 1944 as the first contemporary technical standard in Europe dedicated to earth as a building material. It summarises the entire technical knowledge of earthen construction available at the time. In 1944, a year before the end of the Second World War, millions of people were homeless and urgently needed new shelter. Very often earth was the only locally available building material and, for this reason, the German State Building Authority decided to regulate the use of earth for construction. However, because of post-war reorganisation, the code was put into effect only seven years later, in 1951, as DIN 18951 (1951). By the 1970s, the use of earth as a building material had all but disappeared as a result of industrialisation and, in 1971, the DIN 18951 (1951) was withdrawn and not replaced.

In present times, Australia has been one of the first countries in the world to have specific regulations on earth construction, which have been modified over the years until the publication of the Australian Earth Building Handbook in 2002. Other countries, such as Spain and New Mexico, developed state regulations for rammed earth and adobe based buildings. A number of national standards also address soil classification, soil mechanics, testing procedures, design of load-bearing earth walls and, in general, the structural design of buildings.

New Zealand has the most advanced legal regulations on earth construction, which are structured as follow:

- NZS 4297:1998 - “Engineering Design and Earth Buildings” - this document covers the stability and durability of earth wall buildings, which contain clay and silt to achieve satisfactory structural performance with or without chemical stabilisation. The scope of this document is limited to adobe, pressed bricks, poured earth and rammed earth.
- NZS 4298:1998 - “Materials and Workmanship for Earth Buildings” - this document sets out the materials and workmanship requirements for the construction of structures made of adobe, pressed earth brick, rammed earth and poured earth. It applies to buildings which are designed in accordance with NZS 4297 “Engineering Design of Earth Buildings” and NZS 4299 “Earth Buildings Not Requiring Specific Design” (see below).

- NZS 4299:1998 - “Earth Buildings Not Requiring Specific Design” - this document sets out the construction requirements for earth walls not requiring specific design. Many drawings of construction details, which have been implemented in New Zealand, are included to help builders to achieve durable and weatherproof buildings.

Technical codes have also been recently published about the conservation of historical earth buildings (Schroeder, 2016). The conservation of historic architecture constitutes a significant proportion of current earth building activities, which has led in the last few years to the development of standards by regional and national organisations.

Several groups have also undertaken surveys of technical codes in the field of earth building worldwide, with the aim of establishing a basic knowledge for the development of national standards or normative documents. Among these studies, Delgado and Guerrero (2007) focused on unstabilised earth construction, Maniatidis and Walker (2003) examined rammed earth codes and Cid et al. (2011) gave an overview of normative documents worldwide. Some handbooks on earth building, such as that by Houben and Guillaud (1994), also include chapters on the current state of the art. Finally, McHenry (1989) has provided an overview of regional earth building standards in the USA.

The development of well-accepted standards and guidelines is a necessary, though not sufficient, condition to promote dissemination of earthen materials into mainstream construction practice. Only the recognition of raw earth as a building material by practitioners worldwide can help to assure a promising future to this construction technology.

1.3. Research objectives

The aim of this thesis is to study the mechanical, hygroscopic and durability properties of hyper-compacted earth as a construction material with particular attention to the development of sustainable stabilisation methods for improving material durability against water erosion. The main objectives of the thesis can be summarised as follows:

- To manufacture an earthen material suitable for construction by means of a hyper-compaction procedure which relies on the application of very high pressures up to 100 MPa (Bruno, 2016);
- To investigate the role of grain size distribution on the hygro-mechanical properties of the material;
- To investigate the dependency of stiffness and strength on material density;

- To investigate the effect of ambient relative humidity on mechanical performance;
- To investigate the moisture buffering capacity of the material (i.e. the capacity of the material to adsorb/release water vapour from/into indoor environments);
- To investigate the durability of the material against water erosion;
- To propose an economical and sustainable bio-stabilisation method to improve the durability and the mechanical properties of the material while preserving a good moisture buffering capacity and low environmental impact;
- To investigate the key factors affecting the stabilisation of the material via the proposed method;
- To investigate the durability, mechanical performance and moisture buffering capacity of the stabilised material.

1.4. Thesis layout

Chapter 1 presents a historical overview of earthen building and analyses the advantages and limitations of raw earth as a construction material. The main objectives of the present research are also outlined.

The state of the art of the present thesis is divided for pedagogical reasons into two chapters (chapters 2 and 3) discussing two distinct and separate topics which connection is clarified by demonstrating the poor durability properties against water erosion of raw earth materials (chapters 5 and 6).

Chapter 2 discusses the basic properties of raw earth materials such as grain size distribution and plasticity. The effect of these properties on the hygro-mechanical behaviour of the material is analysed and discussed. The chapter also reviews past studies on mechanical behaviour, moisture buffering capacity and durability of earthen materials.

Chapter 3 reviews the methods of earth stabilisation based on the precipitation of calcite at inter-particle contacts. The chapter discusses the latest research on microbially/enzyme induced calcite precipitation and analyses the advantages and limitations of using one or another method of stabilisation.

Chapter 4 describes the main geotechnical properties of the material tested in this work as well as the earth compaction procedures used to manufacture both small cylindrical samples and bricks. The chapter concludes by describing the proposed method of earth stabilisation by means of enzyme induced calcite precipitation.

Chapter 5 presents the results from the hygro-mechanical tests performed in the present work to measure the adsorption capacity, the stiffness and the strength of the unstabilised earth at the scale of small cylindrical samples. The hygroscopic behaviour is investigated by exposing the samples to cyclic variations of ambient humidity. The effect of material density and ambient humidity on the mechanical behaviour of the material is studied by means of unconfined compression tests. Finally, the results from durability tests performed on both small cylindrical samples and bricks are analysed with the objective of classifying the material according to the norm DIN 18945 (2013).

Chapter 6 investigates the key factors affecting the efficiency of the proposed stabilisation method. The chapter also explores the application of the proposed stabilisation method to earth samples. The hygro-mechanical behaviour and the durability to water erosion of the stabilised earth are investigated and the results are compared with those for the unstabilised earth.

Chapter 7 draws a number of conclusions from the present research and gives some recommendations for future investigation.

2. Raw earth: review of main engineering properties

This chapter reviews the main engineering properties of raw earth as a building material and, in particular, it focuses on the grain size distribution, plasticity, hygro-mechanical behaviour and sensitivity to water. A number of manufacturing techniques have been proposed to enhance the strength, stiffness and durability of compacted earth to the levels required by modern construction. While stabilisation has attracted a large research interest, the design of the base earth mix and, in particular, the identification of the optimal plasticity and grading characteristics of the material has been overlooked. Not all soils are suitable for earth building or, at least, not all soils are suitable for all types of earth building. A clear influence of grain size distribution on the hygro-mechanical and durability characteristics of compacted earth has been highlighted in the literature.

2.1. Physical properties

Two important criteria for classifying soils are particle size distribution and plasticity. Despite most authors agree that grain size distribution and plasticity are the first properties to consider when assessing the suitability of an earthen material for construction, the ensuing recommendations for the selection of soils are rather disparate.

2.1.1. Soil grading

When considering earth as a building material, it is important to understand the significance of grain size, shape and fabric. The grain size distribution (GSD) is one of the basic and most important properties of soils. It is primarily used for classification and provides a first-order estimate of other engineering properties such as permeability, shear strength and compressibility. It also gives information on the soil's ability to pack into a dense structure.

The GSD describes the amount of the different fractions that constitute a soil such as gravel (60 mm to 2 mm), sand (fine and coarse, 2 mm to 0.06 mm), silt (0.06 mm to 0.002 mm) and clay (less than 0.002 mm) (BS1377-2, 1990). The GSD is determined by means of dry and wet sieving for the coarse fraction and sedimentation for the fine fraction. It is plotted in terms of percentage cumulative mass and depends not only on the size but also on the shape of the particles (i.e. elongated, flat, spherical) (Arasan et al, 2011: Kwan et al., 1999; Mora and Kwan, 2000). This is because particles passing through a sieve can actually have one dimension that is larger than the sieve apertures. The literature recommends the classes of suitable soils for building by specifying maximum particle size, amounts of different

fractions, nomograms for granularity and minimum clay content. The present review, in particular, highlights guidelines for the manufacture of compressed earth bricks (CEB).

Delgado and Guerrero (2007) reviewed more than 20 technical documents and national standards to define general guidelines for earthen construction. Based on this review, they recommended upper and lower limits for the grain size distribution of CEBs. Consistent with the guidelines of AFNOR (2001), CRATerre-EAG (1998) and MOPT (1992), they showed that a suitable soil should exhibit a particle size distribution inside the area defined by the nomograms of Figure 2.1.

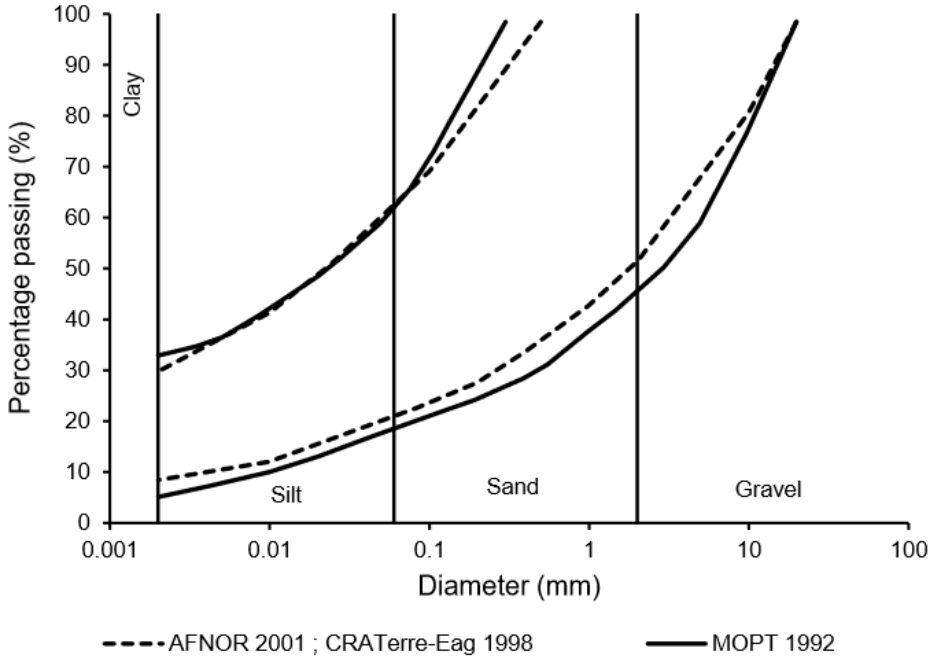

Figure 2.1: Grain size distribution: upper and lower limits for compressed earth bricks according to AFNOR (2001), CRATerre-EAG (1998) and MOPT (1992) (from Bruno, 2016).

Ideally the base soil should have a high sand/gravel content with some silt and just enough clay to act as a binder and assist soil compaction (Keable, 1996; McHenry, 1989) while any material coarser than 5 mm – 10 mm should be sieved out (Norton, 1997). Figure 2.2 presents the recommended lower and upper proportions of clay, silt, sand and gravel in earthen materials according to various authors.

Walker (2000) indicated that rammed earth mixes should contain 45 - 80 % (% by mass) of sand and gravel, 10 - 30 % of silt and 5 - 20 % of clay. Maniatidis and Walker (2003) also recommended a content of 10 - 22 % for clays (particles less than 0.002 mm) and 10 % - 25 % for silts (0.002 mm to 0.06 mm).

Other authors have suggested an optimal balance of 30 % clay/silt and 70 % sand (Bergland, 1986; Dayton, 1991; Easton, 1996). In general, the combined content of silt and clay should comprise between 20 % and 35 %. Similarly, the minimum percentage of sand should be 50 % while the maximum should be 75 %. The relatively large size of the above ranges provides further evidence of the empirical nature of rammed earth design.

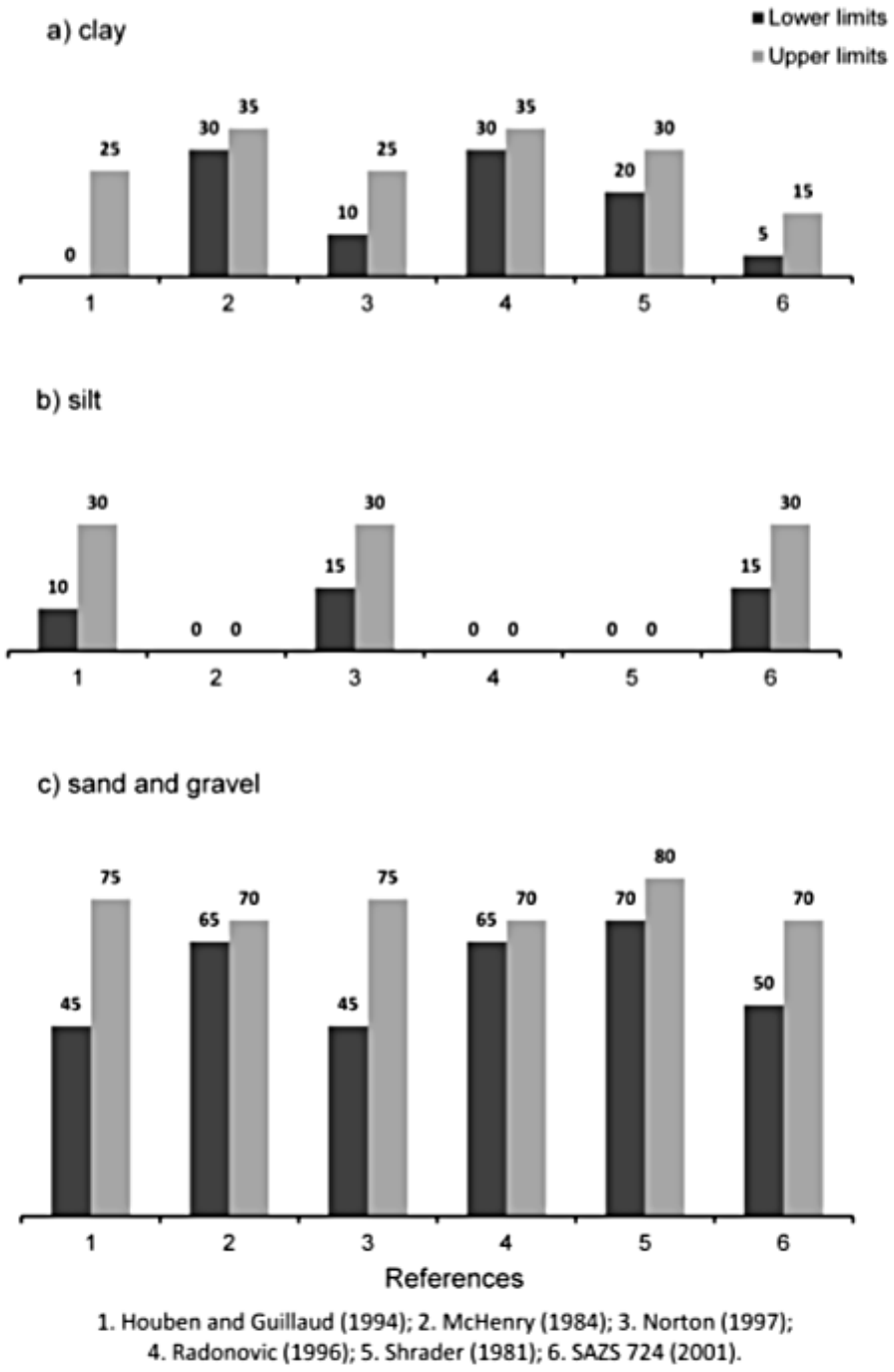

Figure 2.2: Recommended lower and upper proportions of clay (a), silt (b) and sand and gravel (c) in earthen materials according to various authors (from Maniatidis and Walker, 2003).

A direct link can be established between particle grading and compressive strength. Past studies have demonstrated that decreasing the moisture content and increasing the pressure applied during compaction process results in an increase of the dry density which corresponds to an increase of the compressive strength (Olivier and Mesbah, 1986; Attom, 1997; Kouakou and Morel, 2009; Beckett and Augarde, 2012; Bui et al., 2014; Bruno et al., 2016). However, above all, the change of the proportion of minerals in soil is the basic approach to improve the compressive properties of traditional earth bricks.

Wu et al. (2013) studied earthen materials containing a clay-silt fraction between 40 % and 55 % and a sand fraction between 45 % and 60 %. Different materials were obtained by mixing a fine soil (clay-silt 88.6 % and sand 11.4 %) with a coarse one (sand 74.7 % and gravel 25.3 %) with weight ratios of 1:0.6, 1:0.8, 1:1 and 1:1.2, respectively. Parallelepiped blocks with dimensions 200 x 90 x 50 mm^3 were lightly compacted at the optimum water content with the above ratios. After drying, the earth blocks were tested under unconfined compression to measure stiffness and strength, which both showed a strong correlation with the clay-silt content. In particular, the compressive strength and Young's modulus of the blocks varied with the clay-silt content according to a parabolic relationship within the ranges of 1.39 - 1.70 MPa and 40.61 - 42.04 MPa, respectively (Table 2.1).

Table 2.1: Stiffness and strength of earth mixes with different clay-silt fractions (after Wu et al., 2013).

Clay-Silt Content (% by weight)	**Unconfined compressive strength (MPa) Average**	**Initial tangent modulus (MPa)**
55	1.48	40.99
49	1.70	42.04
44	1.66	41.70
40	1.39	40.61

Previous research also investigated the existence of a link between suction and strength in rammed earth together with the dependency of water retention on the earth mix constituents. Beckett and Augarde (2012) selected two mixes (5-1-4 and 7-1-2) containing the maximum and minimum recommended clay contents equal to 40 % and 20 %, respectively, and the minimum recommended gravel content of 10 % according to Houben and Guillaud (1996). The aim of the study was to investigate the effects of particle size distribution on the strength and water retention properties of samples equalised at different levels of temperature (15 °C, 20 °C, 30 °C and 40 °C) and relative humidity (30 %, 50 %, 70 % and 90 %). The material was compacted in layers at the Proctor optimum water content of 12 %, which was approximately the same for both mixes. The dry density was equal to 1918 kg/m^3 for mix 5-

1-4 and 1947 kg/m^3 for mix 7-1-2. Results suggest that the use of rammed earth materials with clay contents near the minimum limit achieve higher unconfined compressive strengths that those with higher clay contents at all humidity and temperature values. This is due to the ability of finer soils to retain a larger proportion of capillary water at low suctions. Figure 2.3 indicates that the coarser 7-1-2 mix exhibits lower values of water content at the same suction compared to the finer 5-1-4 mix. Therefore, the use of lower clay content materials should be considered for rammed earth construction in order to provide sufficiently strong materials in more humid conditions.

Similar results were obtained by Jaquin et al. (2008) who showed that fine earthen materials retain more water than coarser ones at the same suction. An explanation of this result could be that the finer material is characterised by a widespread network of small sized pores than the coarser material. It is therefore likely the finer material carries more pore water in bulk state and less pore water in the pendular state compared to the coarser material. This can also be linked to the theoretical analysis of Likos and Lu (2004) showing that the soil-water retention curves for coarser materials exhibit lower water contents at a given suction compared to finer materials.

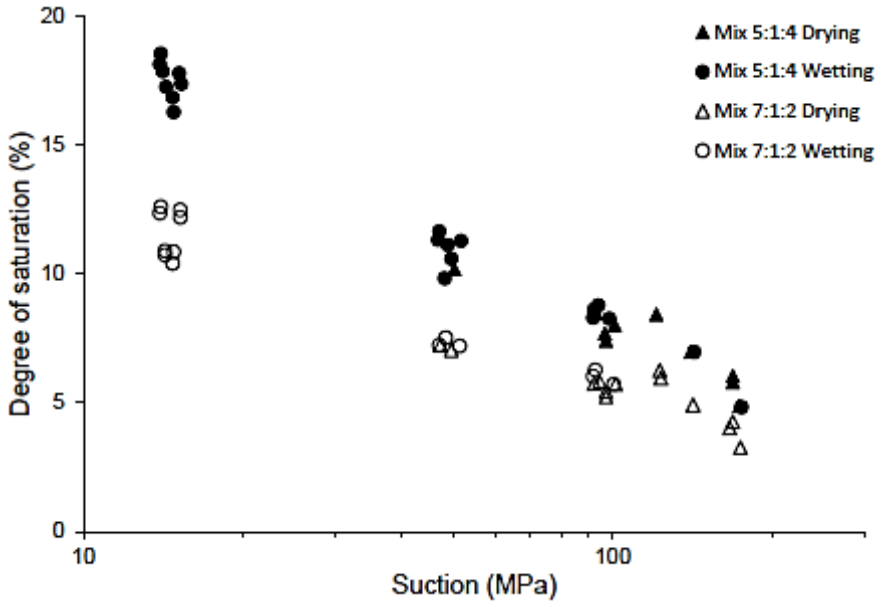

Figure 2.3: Drying curves for coarse earth Mix 7:1:2 and fine earth Mix 5:1:4 (after Beckett and Augarde, 2012).

2.1.2. Plasticity

Plasticity is an important index property of fine grained soils, and especially clays, as it represents the ability of the material to deform without breaking (ductility).

In 1911, a Swedish agriculture engineer, Albert Mauritz Atterberg, showed that a fine grained soil can exist in four states, namely, liquid, plastic, semi-solid or solid and developed a method for describing the consistency of fine-grained soils on the basis of water content. The water contents at which the soil changes from one state to other are known as the Atterberg limits (Figure 2.4).

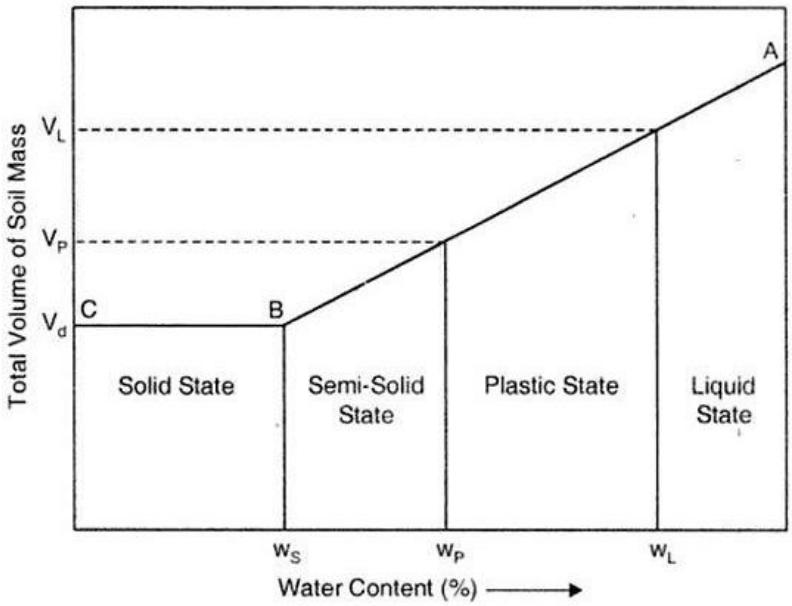

Figure 2.4: Atterberg limits or amounts of water defining a solid, semi-solid, plastic or liquid state of the soil (after Mitchell and Soga, 2005).

The liquid limit w_L is the water content, expressed as a percentage, at which the soil changes from a liquid state to a plastic state. It represents the water content at which any increase in water will cause a plastic soil to behave as a liquid. One way to define the limit is as the soil water content required to close a distance of 12.7 millimetres along the bottom of a groove after 25 blows in a device called Casagrande cup.

The plastic limit w_P is the water content at which any increase in the water content will cause a semi-solid soil to become plastic. The limit is defined as the water content at which a thread of soil crumbles when it is rolled out to a diameter of 3 mm.

The plasticity index I_P is the difference between the liquid limit and the plastic limit. It represents the range of water content over which a soil behaves plastically. Soils with high plasticity index are highly compressible. The plasticity index is also a measure of cohesiveness where high value of I_P indicates high degree of cohesion.

In particular, the thickness of the adsorbed water around a clay particle is dependent on the type of clay mineral. Thus, it can be expected that the plasticity of a given clay depends on

the nature and the amount of clay minerals. Skempton (1953) made the observation that, the plasticity index is directly proportional to the percentage of the clay size fraction smaller than 0.002 mm. He defined a parameter *A* called activity:

$$A = \frac{I_P}{C} \tag{2.1}$$

where *C* is the percentage of clay by weight. It is worth noting that the activity of soils has been widely used as an index property to determine the swelling potential of expansive clays (Seed et al., 1964).

There are not many recommendations in the literature about the optimal plasticity properties for earthen materials. In general, low plasticity inorganic clays and inorganic silts of low and medium compressibility are suitable for manufacturing CEBs. Figure 2.5 shows the admissible plasticity region, together with the Casagrande plasticity chart, for CEBs according to Houben and Guillaud (1994) and the French norm XP P13-901 (AFNOR, 2001; CRATerre-EAG, 1998) (after Delgado and Guerrero, 2007).

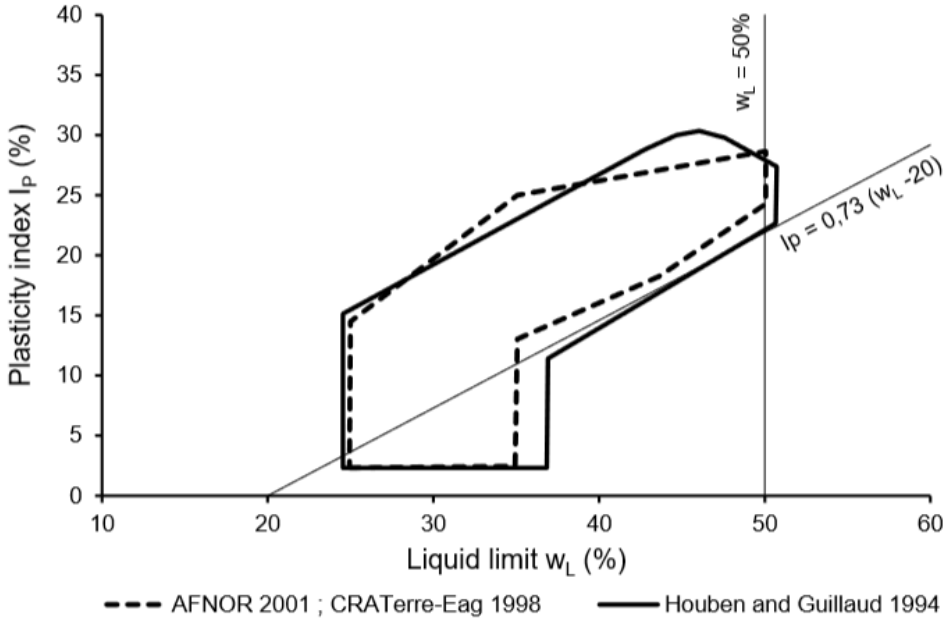

Figure 2.5: Plasticity chart: recommendations for CEBs by AFNOR (2001), CRATerre-EAG (1998) and Houben and Guillaud (1994) (from Bruno, 2016).

2.1.3. Clay mineralogy

Even though the type of earth employed during construction is often dictated by local availability, it is still important to understand the nature and properties of the clay fraction. In fact, the hydro-mechanical behaviour of fine grained soils is strongly influenced by the mineralogy of the clay particles.

A soil particle may be a mineral or a rock fragment. A mineral is a chemical compound formed in nature during a geological process, whereas a rock fragment is a combination of one or more minerals. Based on the nature of atoms, minerals are classified as silicates, aluminates, oxides, carbonates and phosphates. Out of these, silicate minerals are the most important because of their influence on the properties of clay soils. Different arrangements of atoms in the silicate minerals give rise to different silicate structures. The two basic structural units here described are the Silica tetrahedral and the Alumina octahedral.

- A Silica tetrahedral unit consists of a central Silica (*Si*) atom that is surrounded by Oxygen atoms (*O*) that, located at the corners of a tetrahedron, are strongly bonded to the Silica core atom. Silica tetrahedral sheet is symbolised with a trapezoid, of which the shorter face holds electrically unsatisfied oxygen atoms and the longer face holds electrically satisfied oxygen atoms. A combination of tetrahedrons forms a silica sheet.
- An Alumina octahedral unit consists of a central Alumina (*Al*) atom that stands at the centre of an octahedral unit surrounded by hydroxyl ions (OH^-) located at the corners of the octahedral being bonded to the Alumina core atom. An Alumina octahedral sheet is symbolised with a rectangle with top and bottom faces having the same characteristics of exposed hydroxyl ions.

Considering the valencies of the atoms forming the units, it is clear that the units are not electrically neutral and as such do not exist as single units. The basic units, in fact, combine to form sheets in which the oxygen or hydroxyl ions are shared among adjacent units. Two types of sheets are thus formed, namely Silica sheets and Octahedral (gibbsite) sheets. Figure 2.6 gives the atomic structure of the above described basic units and sheets.

The sheets then combine to form various two-layer or three-layer clay minerals, e.g. Kaolinite clay, Montomorillonite clay and Illite clay.

The main difference between these clays is the specific surface, defined as the surface area of clay per 1 gram of dry clay particles. Low specific surface means limited swelling/shrinkage upon wetting/drying and weak bonding of the coarse fraction. Conversely, high specific surface means high swelling/shrinkage upon wetting/drying and strong bonding of the coarse fraction.

- Kaolinite clay is characterised by stacking a Alumina sheet on a Silica sheet, one on top of the other, to form the mineral lattice. The units are held together by strong hydrogen bonds that do not permit water to enter the lattice (Figure 2.7a). Thus,

kaolinite minerals are stable exhibiting limited swelling/shrinkage upon wetting/drying. Kaolinite is a ‘‘two-layer’’ clay and it is characterised by a relatively low specific surface of 10 m^2/g.

- Illite clay has a basic structure that is defined by the unused OH^- face of the Alumina sheet of the structural unit of kaolinite clay attracting the unsatisfied face of another Silica sheet to make a three layer stack. However, Potassium ions (K^+) are filled between facing O^{2-} surfaces of the Silica sheets (Figure 2.7b). The characteristics of this clay are in between those of kaolinite and montmorillonite. This mineral is very stable and does not swell or shrink.
- Montmorillonite clay has the same basic structure of Illite clay but the bonding between three-layer units is assured by van der Waals forces (Figure 2.7c). This bonding is very weak and water can enter easily and the mineral can imbibe a large quantity of water causing swelling. In particular, the negatively charged surfaces of the Silica sheet attract water between two structural units and cause the expansion of the mineral during wet weather and shrinkage during dry weather. ‘‘Three-layer’’ clays are characterised by a larger specific surface, 100 times higher than the specific surface are of kaolinite.

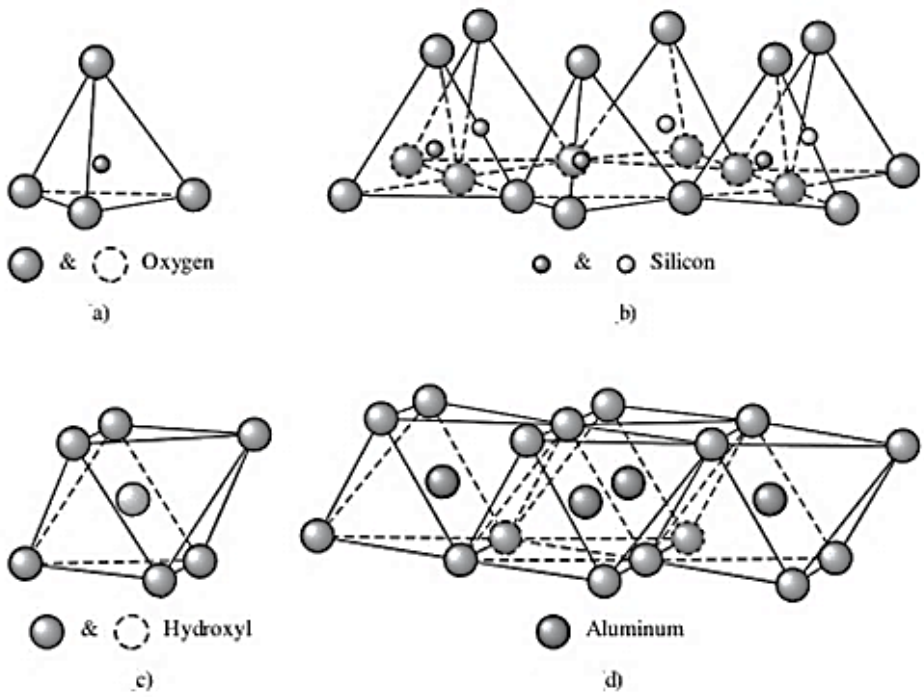

Figure 2.6: Silica tetrahedral (a); Silica sheet (b); Alumina octahedral (c); Octahedral (gibbsite) sheet (d) (after Mitchell and Soga, 2005).

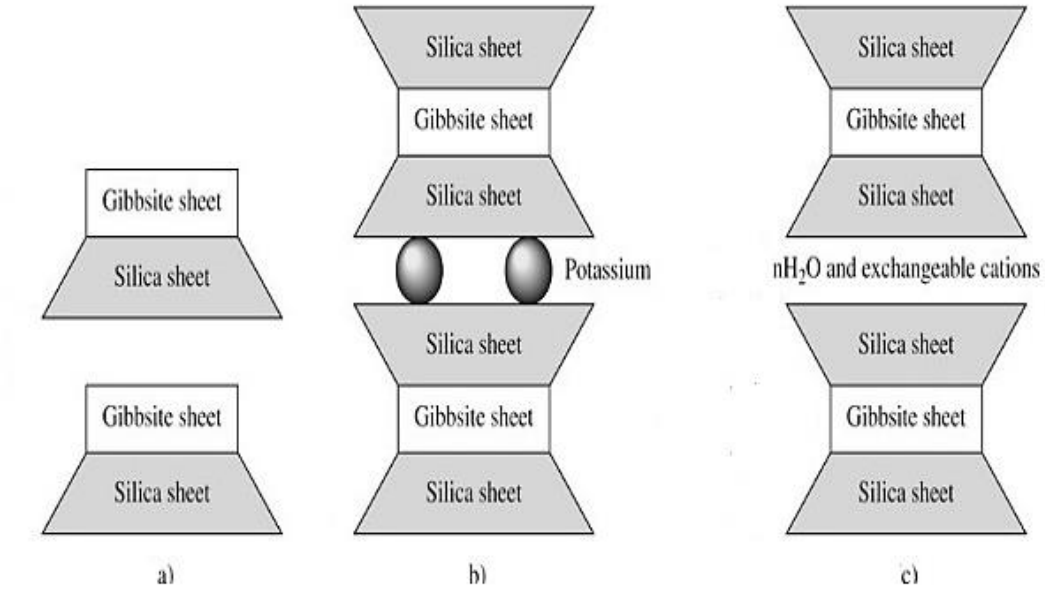

Figure 2.7: Diagram of the structures of kaolinite (a); illite (b); montmorillonite (c) (after Mitchell and Soga, 2005).

2.2. Mechanical behaviour

2.2.1. Effect of dry density

Compaction is an engineering technique to densify soil by packing particles closer together with a consequent reduction in the volume of voids. Past studies have investigated the influence of compaction effort on the dry density of earthen materials (Olivier and Mesbah, 1986; Attom, 1997; Kouakou and Morel, 2009; Bruno et al., 2016; Bruno et al., 2017a). All authors agree that a higher compaction effort increases the dry density and, consequently, the stiffness and strength of the material.

Olivier and Mesbah (1986) investigated the effect of compaction pressure on the mechanical properties of an earth mix composed of 50 % sand, 33 % silt and 17 % kaolinitic clay. Cylindrical samples were prepared by means of static double compaction at different pressure levels from 1.2 MPa to 10 MPa and at different water contents. Olivier and Mesbah (1986) observed that compaction curves shift towards lower values of water content and higher values of dry density as the compaction stress increases (Figure 2.8). After compaction, samples were equalised at constant temperature (27 °C) and relative humidity (60 %) before being tested under unconfined compression until failure. Results demonstrated that an increase of the compaction stress corresponds to an increase of both dry density and compressive strength.

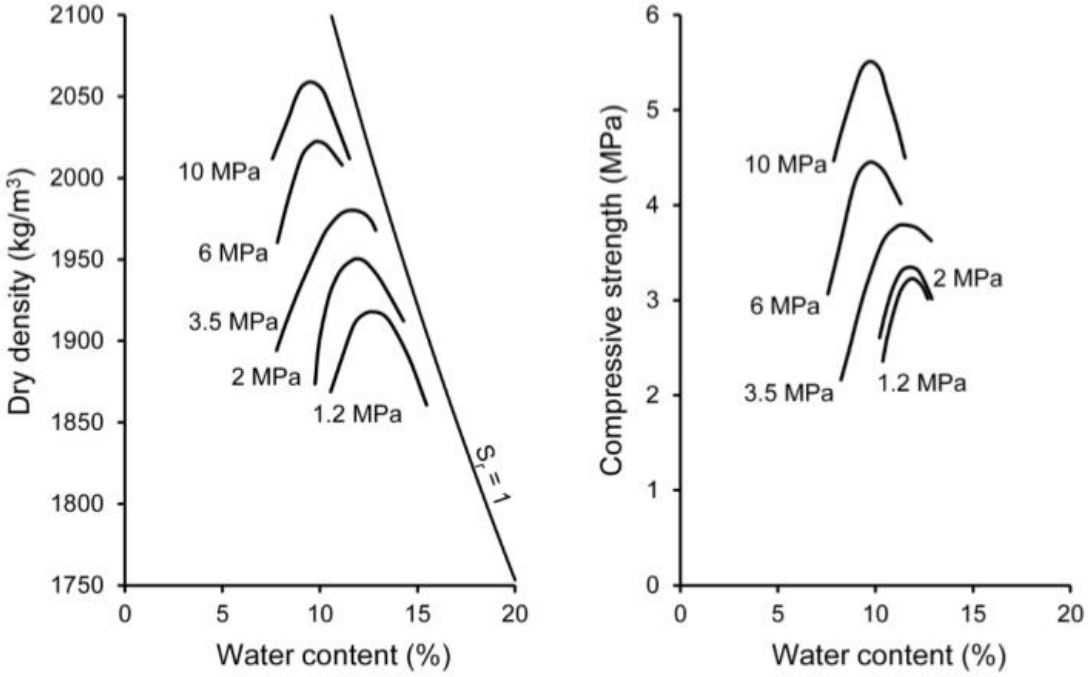

Figure 2.8: Variation of dry density and compressive strength with water content and compaction pressure from 1.2 MPa to 10 MPa (from Olivier and Mesbah, 1986).

Another study by Attom (1997) investigated the effect of compaction energy on the unconfined compressive strength of a cohesive soil. A natural disturbed clayey soil composed of 74 % clay, 18 % silt and 8 % sand, whose mineralogy was an abundance of kaolinite, was tested. The study was based on the application of ten different compaction energy levels on the selected soil by using Standard Proctor and AASHTO hammers. Moreover, for each compaction energy level three different levels of water contents were considered, i.e. dry of optimum, optimum and wet of optimum. Afterwards, the specimens were tested to determine the unconfined compressive strength under a constant displacement rate of 1.5 mm/min.

Figures 2.9 and 2.10 show the effect of the compaction energy per unit volume on the optimum water content and the maximum dry unit weight, respectively. Results indicate that the increase of the compaction energy corresponds to a decrease of the optimum water content and an increase of maximum dry density. An explanation of this behaviour could be that, when water is added to the soil, the inter-granular capillary bonds tend to reduce, and the soil particles can slide to a denser state. This also means that a larger compaction energy requires a lower water content to reach the same maximum dry density.

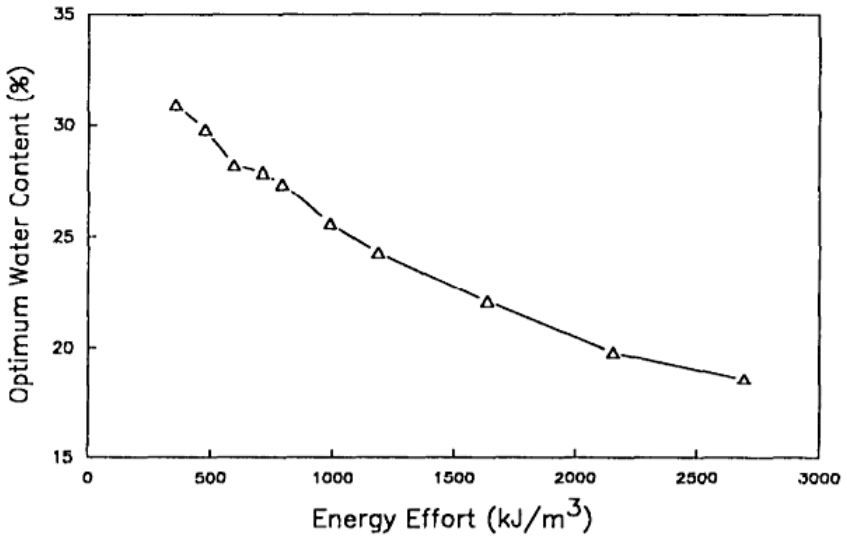

Figure 2.9: Relation between energy effort and optimum water content (from Attom, 1997).

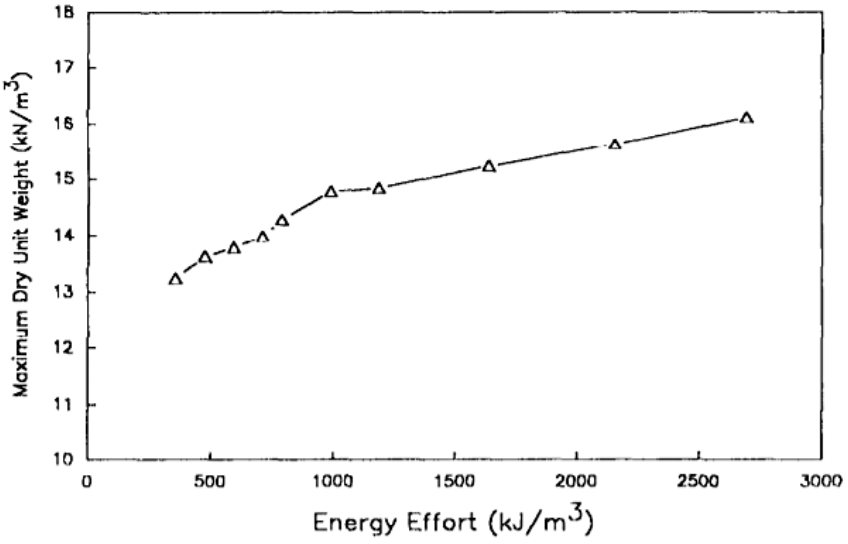

Figure 2.10: Relation between energy effort and maximum dry unit weight (from Attom, 1997).

The effect of both water content and compaction energy on the unconfined compressive strength is shown in Figure 2.11 where E1 - E10 are different levels of the compaction energy varying from 355.6 kJ/m^3 to 2693.8 kJ/m^3, respectively. Attom (1997) found that, for the same energy effort, the unconfined compressive strength increases with increasing water content up to the optimum. Once the water content exceeds the optimum value, the unconfined compressive strength starts to decrease. According to Attom (1997), this behaviour can be explained by Lambe's edge-to-face theory. When the water content increases on the dry side of the optimum, the compaction energy causes the flocculated particles to come closer to each other in a denser position resulting in increasing shear strength. The increase of the compaction energy on the wet side of the optimum, results in a

slight increase or decrease in the unconfined compression strength of the soil. This can be explained, when the compaction energy increases this will cause the clay particles which are in a dispersive condition to slide over each other causing, in general, reduction of the shear strength. This result indicates that increasing the compaction energy for any water content higher than the optimum (on the wet side of the optimum) does not influence the unconfined compressive strength very much.

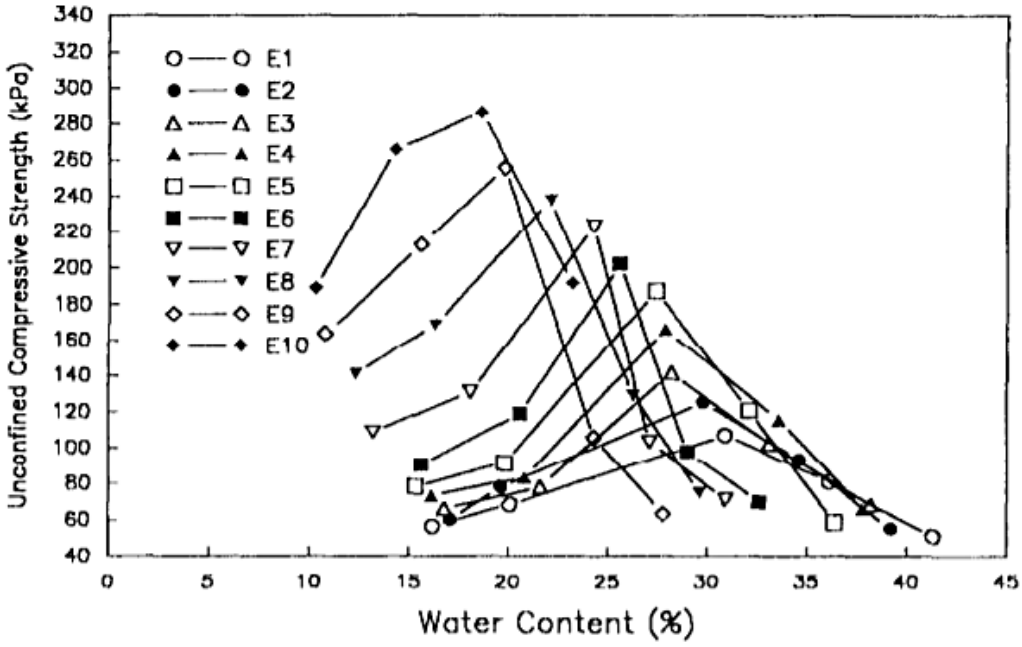

Figure 2.11: The relation between water content and unconfined compressive strength (from Attom, 1997).

Kouakou and Morel (2009) investigated the compressive strength of both traditional adobe blocks and pressed adobe blocks (BAP - "Bloques d'Adobe pressés"), whose base earth was composed of 44.5 % sand, 30 % silt and 25.5 % clay with a liquid limit of 38 % and a plasticity index of 18 %. Traditional adobe blocks were manufactured by pouring the earth mix at high water contents inside wooden moulds and subsequently drying the demoulded blocks in the sun. Pressed adobe blocks were instead manufactured at much lower water contents and compressed to 2 MPa to increase dry density. Specimens were tested under unconfined loading-unloading cycles to measure deformations. Results showed that the material behaviour was not elastic and they defined two different stiffness moduli. These were obtained by subdividing the stress-strain curves into an initial adjustment phase (initial tangent E_t), when the press plates and the sample bed into contact, and a subsequent phase until failure (equivalent E_{eq} moduli). The definition of the initial tangent E_t and equivalent E_{eq} moduli is described in Figure 2.12 with the residual strain ε_r at the end of the load and unload cycle.

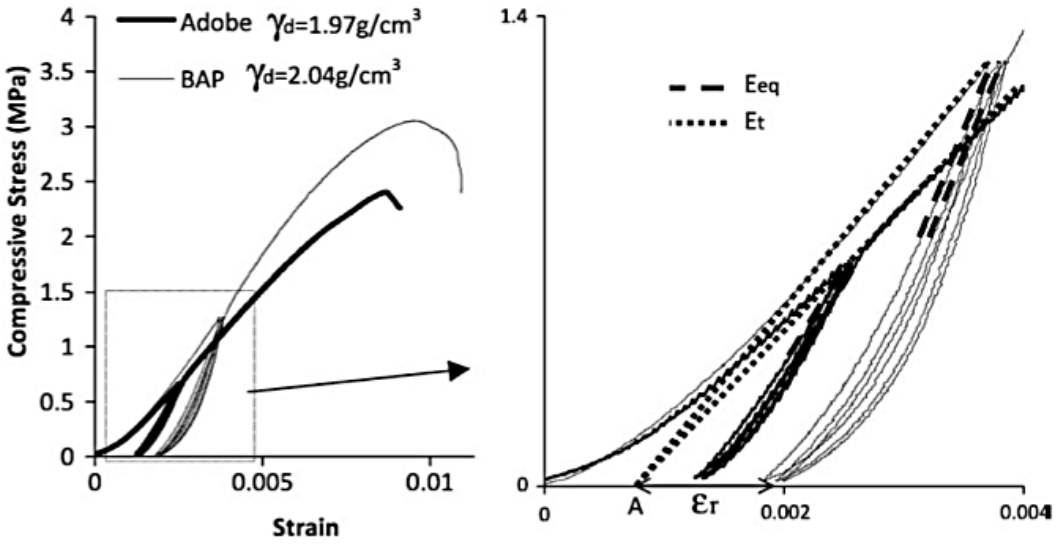

Figure 2.12: Stress-strain curve for adobe and BAP blocks and definition of the tangent E_t and equivalent E_{eq} moduli (from Kouakou and Morel, 2009).

Kouakou and Morel (2009) surprisingly observed that both the initial tangent E_t and the equivalent E_{eq} moduli do not vary significantly with the dry density of the BAP (Figure 2.13). This result partly contradicts previous observations that have shown that an increase of dry density produces an increase of stiffness.

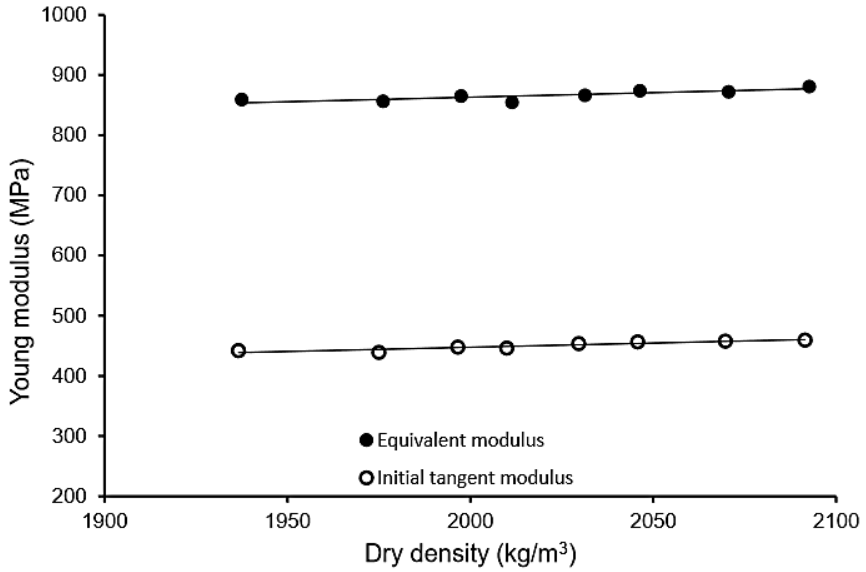

Figure 2.13: Initial tangent E_t and equivalent E_{eq} moduli of BAP (from Kouakou and Morel, 2009).

Kouakou and Morel (2009) also demonstrated that unconfined compressive strength increases with increasing dry density for both BAP and traditional adobe (Figure 2.14), which implies that gain in dry density leads to gain in strength.

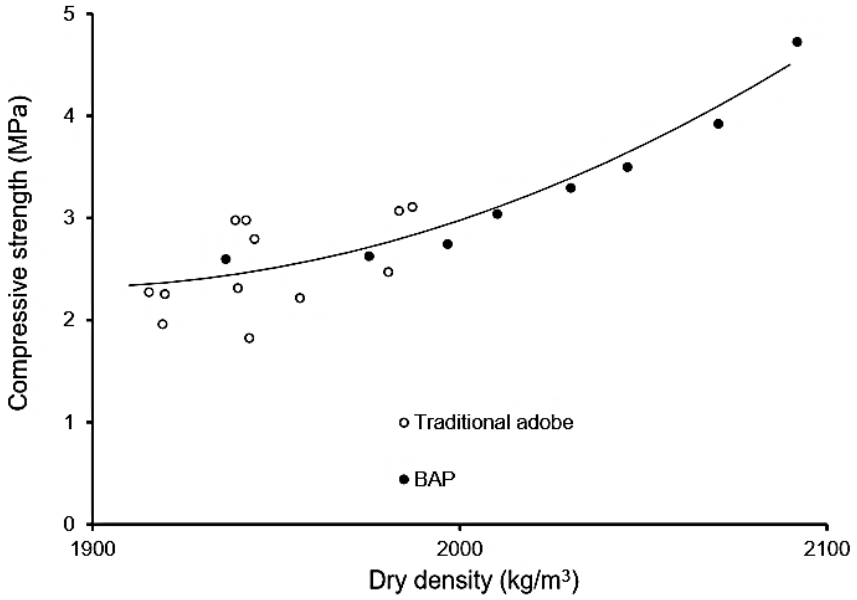

Figure 2.14: Variation of compressive strength with dry density (from Kouakou and Morel, 2009).

Bruno et al. (2016) devised an innovative hyper-compaction technique, also adopted in the present work (see Chapter 4) to increase the dry density of an earthen material and hence improve the mechanical performance.

In this study, hyper-compacted samples were statically compressed at pressure levels of 25 MPa, 50 MPa and 100 MPa. The lowest pressure level of 25 MPa is comparable to that of the most powerful presses available on the market for the manufacture of compressed earth blocks. For ease of comparison, Standard Proctor samples were also manufactured. For each compaction level, the experimental values of dry density against the corresponding water contents are plotted in Figure 2.15. Similar to Olivier and Mesbah (1986), the results from Bruno et al. (2016) show that the compaction curve shifts towards higher values of dry density and lower values of water content, as the compressive energy increases from Proctor standard to static compaction at 25 MPa, 50 MPa and 100 MPa. Also, the highest value of dry density increases less than linearly with compaction pressure, i.e. the increase in dry density from 25 MPa to 50 MPa is greater than the increase in dry density from 50 MPa to 100 MPa. Bruno et al. (2016) therefore remarked that it would be necessary to apply an unfeasibly high pressure to attain the theoretical "no porosity" point, in which the dry density of the earth becomes equal to the density of the soil particles and all porosity is erased.

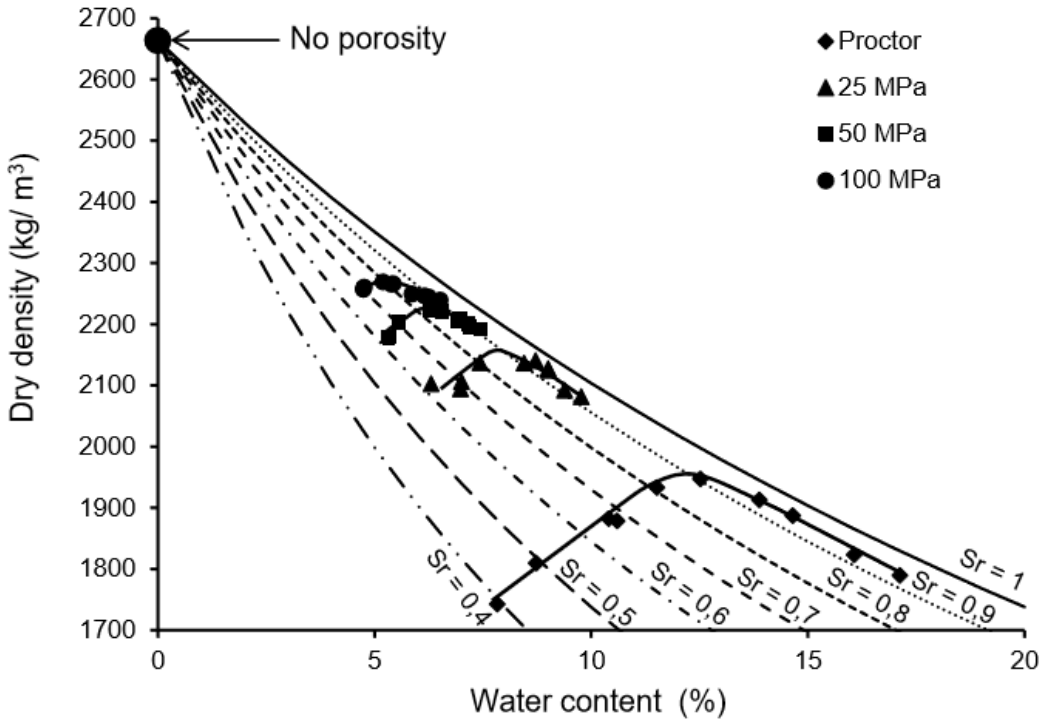

Figure 2.15: Comparison between the Standard Proctor compaction curve and the hyper-compaction curves at 25 MPa, 50 MPa and 100 MPa (from Bruno et al., 2016).

After compaction, all samples were equalised at a temperature of 25 °C and a relative humidity of 62 % for a minimum time of two weeks. After equalisation, the samples were subjected to unconfined loading-unloading cycles, at a loading rate of 0.005 MPa/s, between one ninth and one third of their compressive strength. The Young's modulus was determined as the average slope of the unloading branches of the five unconfined loading-unloading cycles on the assumption that material behaviour is elasto-plastic during loading but essentially elastic during unloading (see Chapter 5 for additional details). Figure 2.16 shows the Young's modulus plotted against the corresponding values of dry density (measured after equalisation and hence before testing) for all specimens. Bruno et al. (2016) demonstrated that the Young's modulus increases more than linearly with increasing dry density. Any small increase of dry density beyond the measured maximum value of 2280 kg/m^3 would therefore produce a significant augmentation of the Young's modulus.

Bruno et al. (2016) confirmed the potential inadequacy of the Proctor compaction method to manufacture earthen materials with sufficient stiffness to be used in masonry construction. In particular, they observed a variation of one order of magnitude between the values of the Young's modulus for the specimens compacted according to the Proctor Standard and those compacted at 100 MPa.

The same specimens were subsequently loaded to failure to measure their unconfined compressive strength under a constant displacement rate of 0.001 mm/s. This rate was the slowest rate that could be applied by the available equipment and the rate suggested by Bruno (2016) himself to obtain a regular stress-strain curve without instabilities. Figure 2.17 shows the variation of the measured peak strength with dry density and indicates that the compressive strength again increases more than linearly with increasing dry density. Remarkably, samples compacted at 100 MPa show a compressive strength that is about ten times higher than that of the Proctor samples and comparable with that of conventional masonry materials.

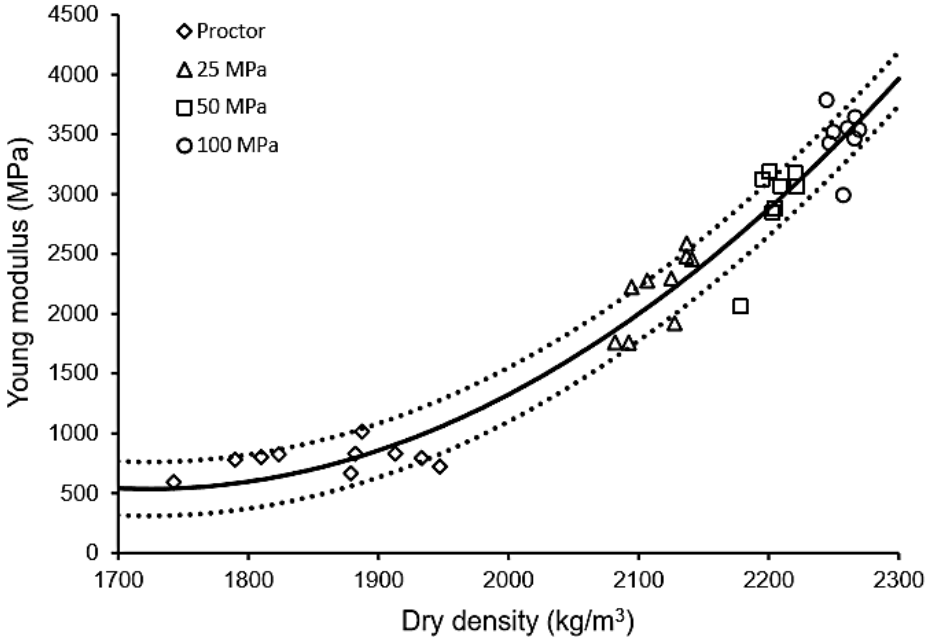

Figure 2.16: Variation of Young's modulus with dry density (from Bruno et al., 2016).

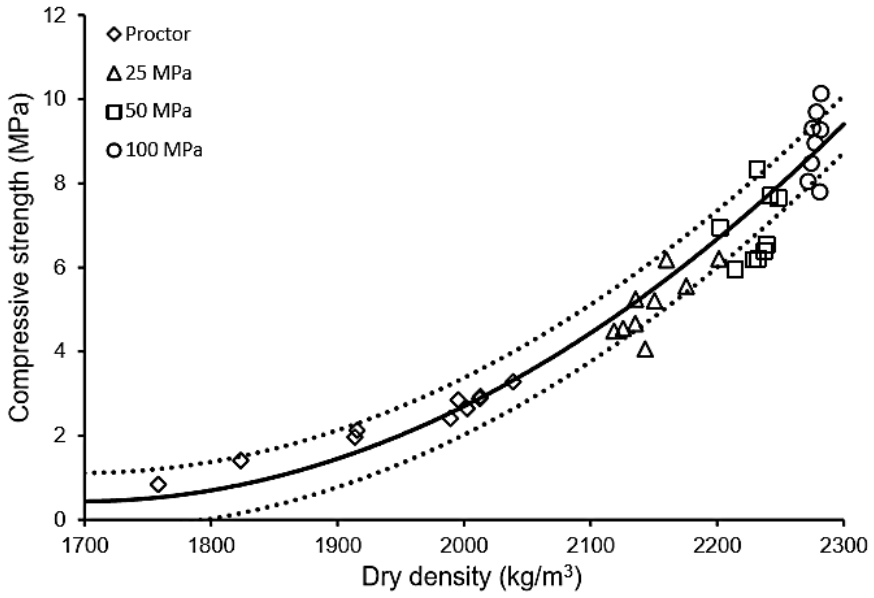

Figure 2.17: Variation of compressive strength with dry density (from Bruno et al., 2016).

2.2.2. Effect of ambient humidity and temperature

The external and internal surfaces of a building envelope are generally exposed to very different ambient conditions, which may lead to gradients of temperature, humidity and suction across earthen walls affecting the mechanical performance of earthen structures. This is one of the reasons why a number of investigations have been recently devoted to the effect of humidity and temperature on the strength and stiffness of earthen materials. Jaquin et al. (2009) studied the influence of suction on mechanical characteristics of rammed-earth material. They found that suction was the main source of strength in unstabilised rammed-earth, and that the strength increased as moisture content reduced and, hence, suction increased. However, in the study of Jaquin et al. (2009), the water content varied between 5.5 % and 10.2 % (by mass), while in normal conditions in earthen materials, water content varies from 1 % to 2 % (Bui et al., 2009). In addition, in that study, only one soil was tested and the mechanical strengths obtained were relatively low compared to other studies (Walker et al., 2005).

Bui et al. (2014) studied the role played by suction and the effect of moisture on the mechanical performance of different types of rammed earth materials from the wet state after manufacturing (water contents between 1 % and 13 %) to the "dry" state under atmospheric conditions (water contents between 1 % and 2 %). The physical composition of the different types of earth investigated by Bui et al. (2014) is reported in Table 2.2. The samples were tested under unconfined compression at different water contents, which correspond to different suction levels.

Table 2.2: Grain size distribution of materials tested by Bui et al. (2014) (after Bui et al., 2014).

	Clay	**Silt**	**Sand**	**Gravel**
Earth A	5 %	30 %	49 %	16 %
Earth B + 2 % NHL	4 %	35 %	59 %	2 %
Earth C	9 %	38 %	50 %	3 %

Figure 2.18 presents the variation of compressive strength with water content for the different earth types tested by Bui et al. (2014). Inspection of Figure 2.18 indicates that, in all three cases, the compressive strength remains approximately constant for water contents below 4 % and progressively decreases for wetter states. Bui et al. (2014) also noted that stabilisation by natural hydraulic lime (NHL) can decrease the sensitivity of rammed earth to water, though it does not always produces an increase in compressive strength.

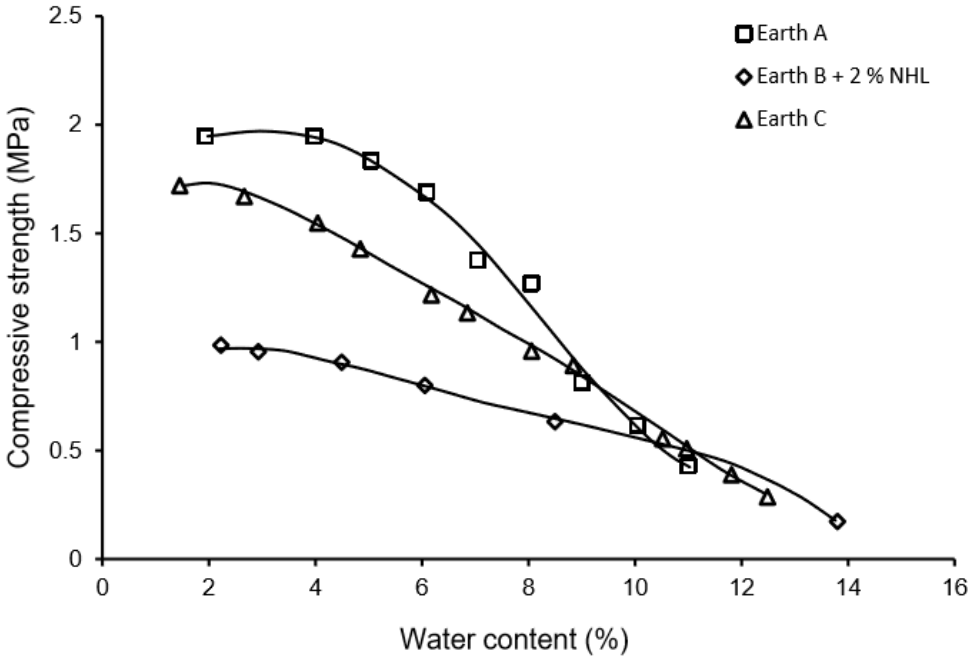

Figure 2.18: Variation of compressive strength with water content (from Bui et al., 2014).

In a similar way, Figure 2.19 shows that, for a sandy soil (Earth A) and a stabilised soil (Earth B + 2 % NHL), the Young's modulus changes little as the water content increases up to 5 %. Instead, for a clayey soil (Earth C), the Young's modulus appears relatively sensitive to variations of water content even at low moisture levels.

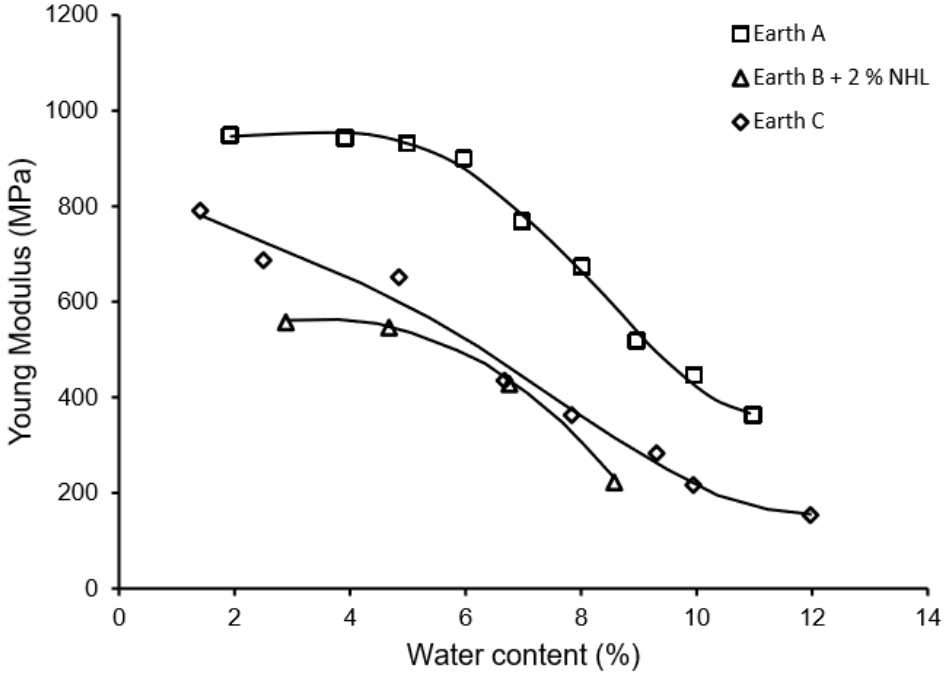

Figure 2.19: Variation of Young's modulus with water content (from Bui et al., 2014).

The above results confirm that suction plays an important role in the mechanical performance and that this water sensitivity of earth materials can be an important weakness.

Similar results were obtained by Beckett and Augarde (2012), who investigated the unconfined compressive strength of raw earth samples equalised at different levels of temperature (15 °C, 20 °C, 30 °C and 40 °C) and relative humidity (30 %, 50 %, 70 % and 90 %). The tests were performed on the same two earth mixes, i.e. mix 5:1:4 and mix 7:1:2, described in Section 2.1.1. Figure 2.20 indicates that strength is always larger for the earth mix with lower clay content and increases with decreasing humidity and increasing temperature.

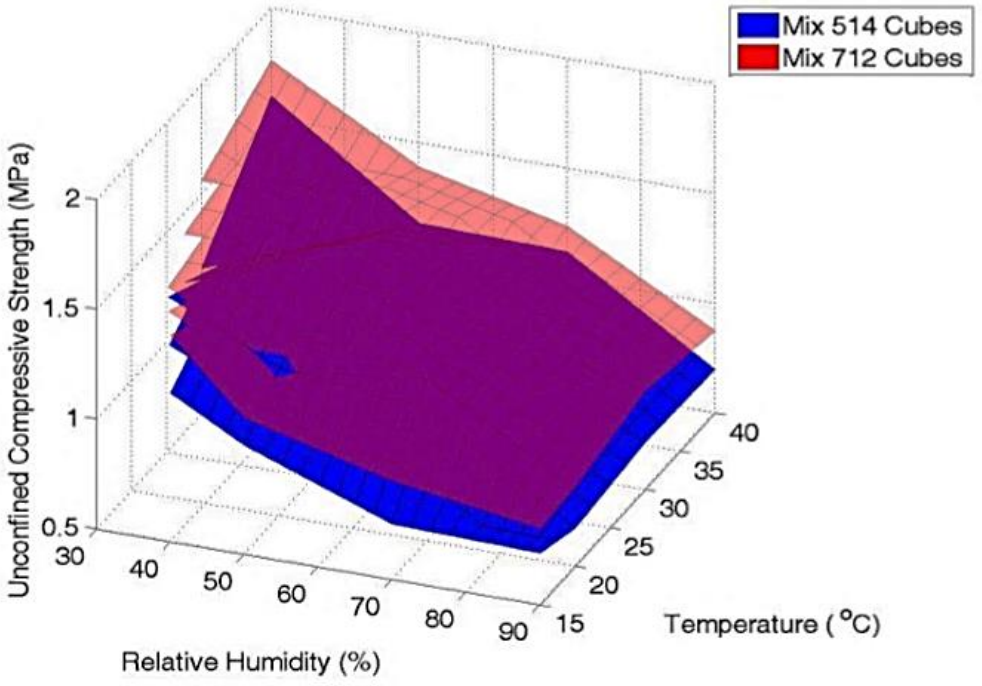

Figure 2.20: Variation of compressive strength with relative humidity and temperature (from Beckett and Augarde, 2012).

Bruno et al. (2017a) also performed mechanical tests on both unstabilised samples that were hyper-compacted at the three pressure levels of 25 MPa, 50 MPa and 100 MPa and on stabilised samples hyper-compacted at 100 MPa. In all cases, the samples were hyper-compacted to their respective optimum water contents. Stabilisation was achieved by replacing the optimum water content with one of the following three liquid additives, namely a silane-siloxane emulsion, a sodium hydroxide (NaOH) solution at 2 mol/L concentration and a blend of the previous two additives.

After compaction, each set of samples was equalised inside a climatic chamber at different relative humidities of 95 %, 77 %, 62 %, 44 % and 25 % under a constant temperature of 25

°C. After equalisation, samples were tested to determine the Young's modulus and the unconfined compressive strength by using the same experimental procedure described in Section 2.2.1. Both stiffness and strength were related to the total suction ψ inside the sample, which was calculated from the imposed values of temperature T and relative humidity RH using the Kelvin equation:

$$\psi = -\frac{RT}{V_m}\ln(RH) \tag{2.2}$$

where R is the universal gas constant and V_m is the molar volume of water.

Figure 2.21 shows the variation of Young's modulus with total suction for the unstabilised samples compacted at the three different pressures. In general, it can be observed that stiffness increases as suction increases from 7 MPa to 112 MPa but then tends to level off as suction increases above 112 MPa. For the samples compacted at 25 MPa and 50 MPa, the value of stiffness increases by a factor of about 2.5 as suction grows from the lowest value of 7 MPa to the highest value of 190 MPa. Instead, for the samples compacted at 100 MPa, the stiffness increases by a factor of about 3.1 over the same suction range.

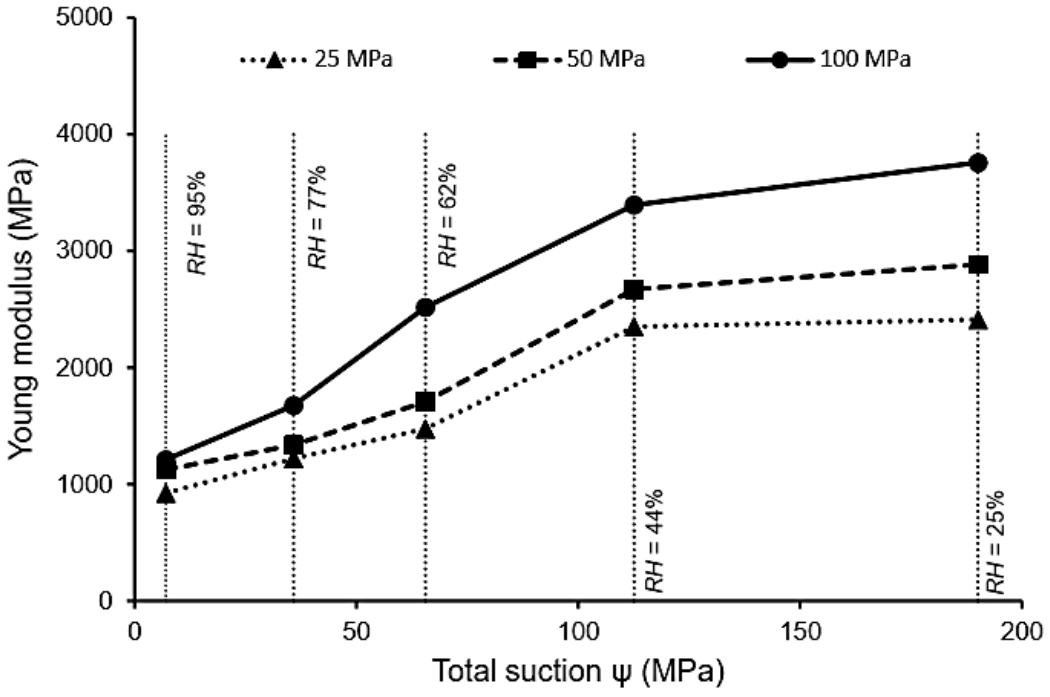

Figure 2.21: Variation of Young's modulus with total suction: unstabilised samples (from Bruno et al., 2017a).

Figure 2.22 shows that the peak compressive strength grows as suction increases from 7 MPa to 112 MPa but then tends to stabilise as suction increases further. This progressively smaller increase of both Young's modulus and compressive strength with growing suction is

consistent with the Fisher (1926) idealised capillarity model where the stabilising effect produced by a water meniscus at the contact between two identical spheres grows with suction but tends towards a constant asymptote.

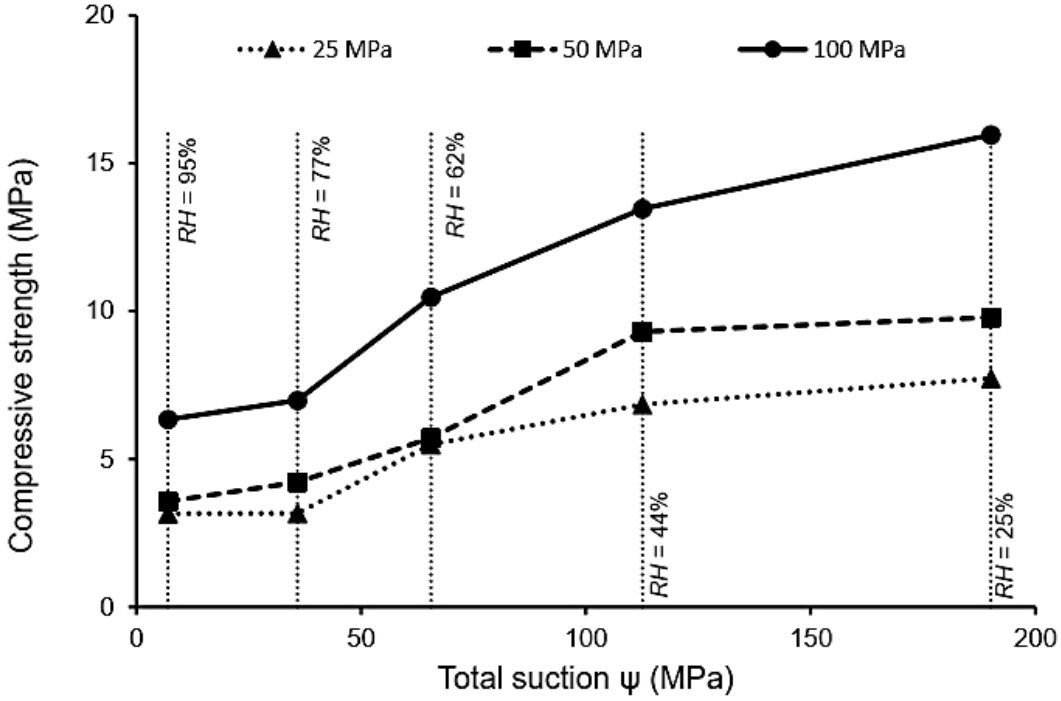

Figure 2.22: Variation of compressive strength with total suction: unstabilised samples (from Bruno et al., 2017a).

Figure 2.23 shows that the growth of Young's modulus with increasing suction is smaller for stabilised samples than for unstabilised samples. This is probably because the inter-particle bonding produced by capillarity is overridden by that produced by chemical stabilisation. Samples stabilised with the silane-siloxane emulsion and with a mix of NaOH solution and silane-siloxane emulsion exhibit lower stiffness than unstabilised samples at all suction levels. The stiffness of the samples stabilised with the NaOH solution is higher than that of unstabilised samples but only at low suction levels.

Figure 2.24 shows that the peak compressive strength of both unstabilised and stabilised samples increases with increasing suction. Stabilised samples exhibit, however, lower values of compressive strength than unstabilised samples with the only exception of the samples stabilised with NaOH solution at low suction levels. Bruno et al. (2017b) observed that the smaller growth of stiffness and strength of stabilised samples with increasing suction also means that the mechanical properties of stabilised samples are less sensitive to variations of ambient humidity compared to unstabilised samples.

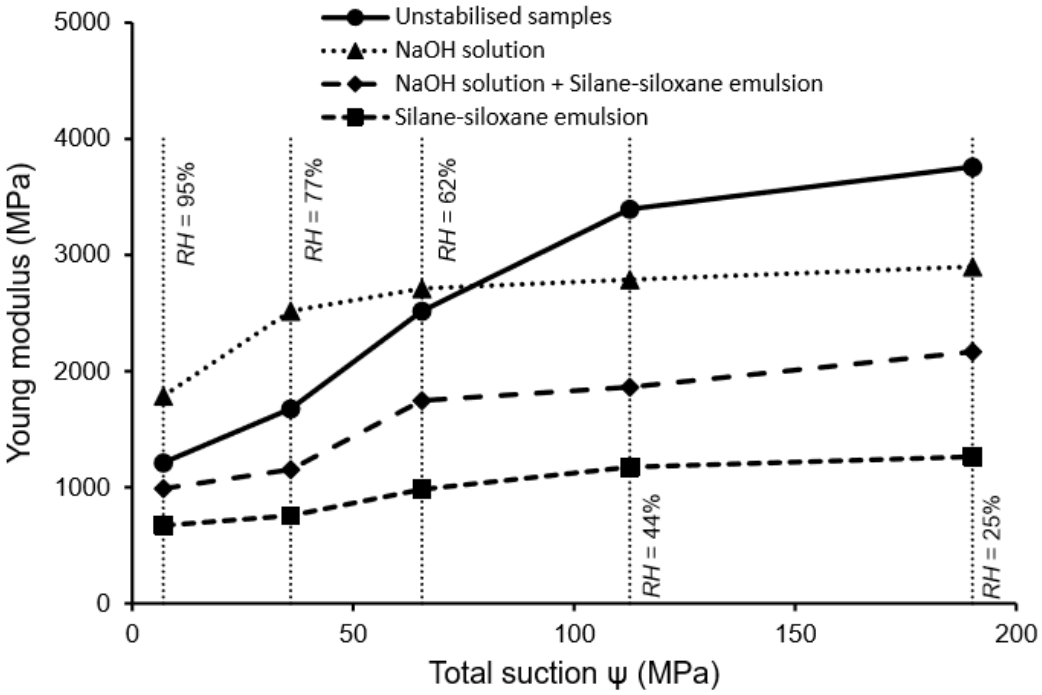

Figure 2.23: Variation of Young's modulus with total suction: unstabilised and stabilised samples compacted at 100 MPa (from Bruno et al., 2017b).

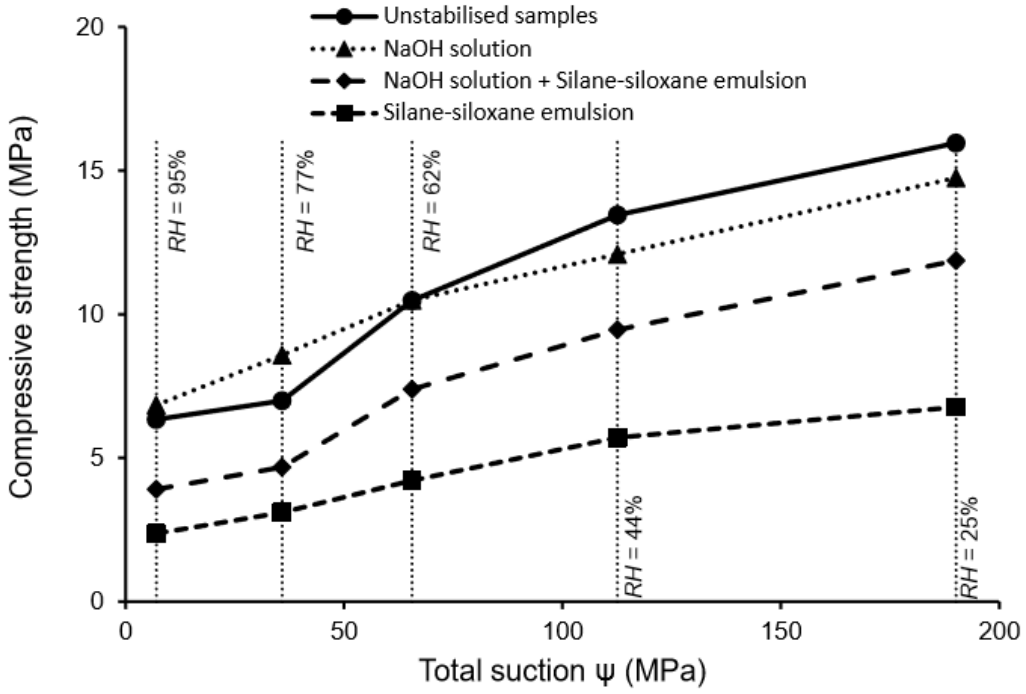

Figure 2.24: Variation of compressive strength with total suction: unstabilised and stabilised samples compacted at 100 MPa (from Bruno et al., 2017b).

In summary, chemical stabilisation appears to have a negative impact on the mechanical properties of hyper-compacted earth. Despite this counterintuitive conclusion, it is consistent with the observations made by Bui et al. (2014) for conventional earth blocks. An explanation may be that chemical stabilisers inhibit inter-particle bonding due to water capillarity, thus limiting the improvement of mechanical properties with growing suction. The detrimental effect of stabilisation on stiffness and strength is even more evident in the two cases where the additive includes the silane-siloxane emulsion. As suggested by Bruno et al. (2017b), this is probably due to the hydrophobic nature of this emulsion, which modifies the wettability of the solid grains thus disrupting the formation of stabilising capillary lenses at inter-particle contacts. This conclusion however applies to the stabilisation methods described above and cannot be extended to all types of chemical stabilisations.

2.3. Hygroscopic capacity

The hygroscopicity of raw earth is defined as the capacity of the material to store or release moisture to achieve equilibrium with the vapour pressure in the surrounding environment. The amount of vapour pressure in the environment is often described by the relative humidity *RH* which is the ratio between the actual vapour pressure and the saturation vapour pressure. In indoor environments raw earth can act as a passive buffering material, which smooths peaks of vapour pressure and stabilises relative humidity levels. According to Arundel et al. (1986), indoor air quality is strongly affected by relative humidity, which has an important effect on the health and well-being of the occupants. For this reason, an increasing research interest is focusing on the moisture buffering properties of adsorbent, porous materials. Earth building materials are widely perceived to be excellent passive humidity regulators and are more sustainable than artificial ventilation systems and dehumidifiers. Due to their extended network of very fine pores (of the order of nanometers), earthen materials can absorb vapour from humid environments and release it into dry ones. An earth wall can therefore help to regulate hygroscopic conditions inside buildings by absorbing, storing and releasing moisture as necessary.

The hygroscopic capacity of a material can be synthetically described by its Moisture Buffering Value (MBV). Rode et al. (2005) stated that "*the practical Moisture Buffer Value ($MBV_{practical}$) indicates the amount of water that is transported in or out of a material per open surface area, during a certain period of time, when it is subjected to variations in relative humidity of the surrounding air. When the moisture exchange during the period is*

reported per open surface area and per % RH variation, the result is the $MBV_{practical}$. The unit for $MBV_{practical}$ is kg/(m^2 %RH)".

The $MBV_{practical}$ or, in short, the MBV of a material is measured by subjecting samples to cyclic variations of relative humidity at constant temperature, which simulate the daily changes of indoor atmosphere. The MBV is then calculated as:

$$MBV_{pratical} = \frac{\Delta m}{S\ \Delta\%RH} \tag{2.3}$$

where Δm is the variation of sample mass due to the change in relative humidity, S is the exposed surface and $\Delta\%RH$ is the difference between the high and low imposed levels of relative humidity. Several testing procedures have been proposed to determine the MBV, which mainly differ for the imposed humidity levels applied and the duration over which these humidity levels are maintained.

In order to characterise the moisture buffering capacity of materials Rode et al. (2005), in the context of the NORDTEST project, proposed the definition of a protocol which expresses how materials should be tested. According to the NORDTEST protocol, the MBV is determined by exposing the sample to cyclic step-changes of relative humidity between one high and one low value for 8 and 16 hours, respectively. The normal case consists in a periodical exposure of 8 hours at 75 % *RH* and 16 hours at 33 % *RH*. These relative humidity cycles are also performed at a constant temperature, which is usually equal to 23 °C.

The NORDTEST procedure leads to rather repeatable results as shown by a benchmarking exercise performed by different research institutions to determine the MBV of distinct building materials (Figure 2.25) (Rode et al., 2005).

The project NORDTEST also proposed a classification of building materials based on their MBVs. In particular, five different categories were defined by Rode et al. (2005) and are reported in Table 2.3.

Besides the NORDTEST protocol, different authors have suggested alternative procedures to measure the moisture buffering capacity of building materials. These procedures mainly differ for the choice of the relative humidity levels and the time of exposure, which can strongly affect the measured MBV. For example, it has been demonstrated that a larger interval of relative humidity corresponds to a larger variation of moisture content inside the material (McGregor et al., 2014).

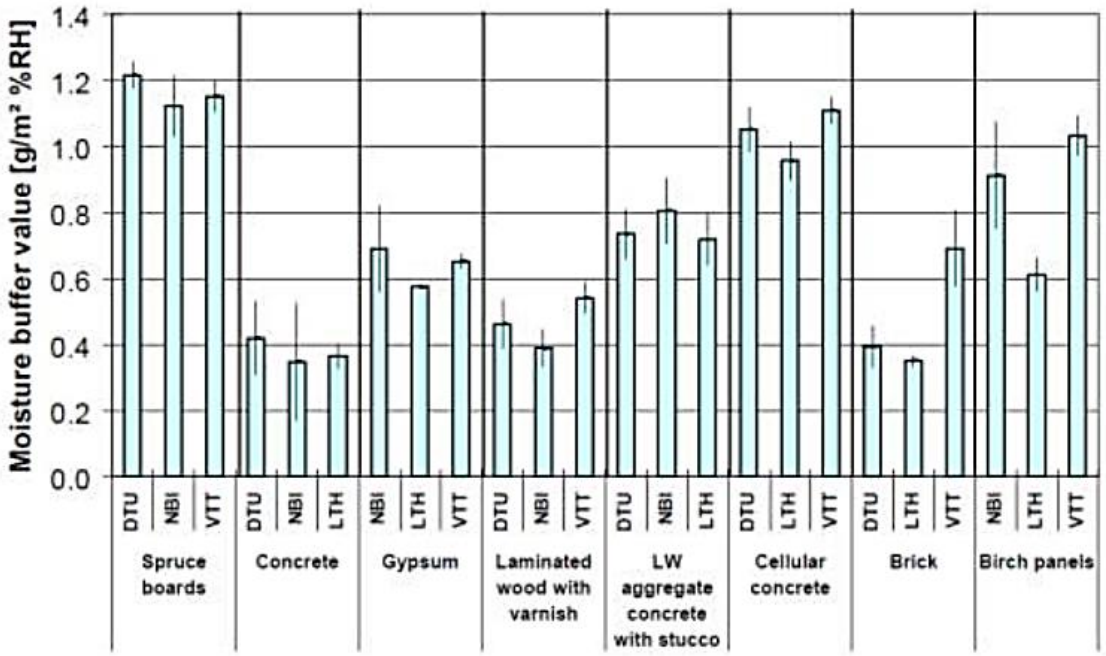

Figure 2.25: MBV measured by DTU (Technical University of Denmark), NBI (Norwegian Building Research Institute), VTT (Technical Research Centre of Finland) and LTH (Lund University of Sweden) measured on different construction materials (from Rode et al., 2005).

Table 2.3: Ranges of Moisture Buffering Value classes (after Rode et al., 2005).

Moisture buffering capacity	**MBV_{MIN}**	**MBV_{MAX}**
Negligible	0	0.2
Limited	0.2	0.5
Moderate	0.5	1.0
Good	1.0	2.0
Excellent	2.0	…

McGregor et al. (2014) measured the moisture buffering capacity of unstabilised and stabilised compressed earth blocks. Stabilisation was achieved by adding Portland cement CEM I, air lime CL90 or dissolved NaOH to the soil mix. Samples were statically compacted by using a press with a capacity of 50 kN inside a Standard Proctor mould. McGregor et al. (2014) determined the MBV of unstabilised and stabilised earth sample by performing cycles of relative humidity which are variations of the test procedures proposed by the NORDTEST project, the norm ISO 24353 (2008) and the Japanese Industrial Standard (2002) as summarised in Table 2.4.

Figure 2.26 shows that, regardless of chosen testing procedure, unstabilised earthen materials exhibited the highest MBVs. The effect on the recorded MBV was very similar for cement and lime stabilisation while NaOH stabilisation induced the largest reduction of moisture buffering capacity. Moreover, the lowest MBV was obtained for the cycle where the relative humidity of 75 % is kept for only 8 hours.

Table 2.4: Experimental procedures for the measurement of MBV as reproduced after McGregor et al. (2014).

RH [%]	Time step [h]
85/50	8/16
75/53	8/16
75/53	12/12

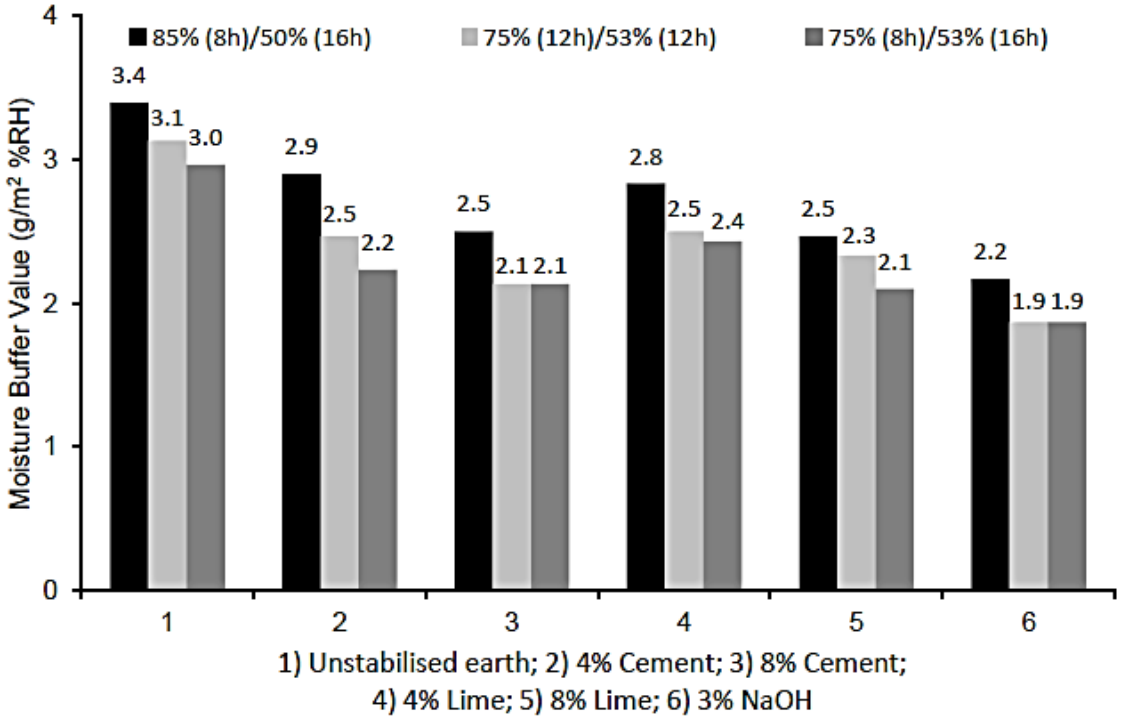

Figure 2.26: MBVs measured on unstabilised and stabilised earthen samples: comparison between different test procedures (after McGregor et al., 2014).

Bruno (2016) investigated the moisture buffering capacity of unstabilised hyper-compacted earth according to the norm ISO 24353 (2008). Cyclic variations of relative humidity were performed on unstabilised cylindrical earth samples compacted at the three pressure levels of 25 MPa, 50 MPa and 100 MPa. These tests aimed to determine the effect of the compaction pressure on hygroscopic behaviour and, in particular, on the measured MBV. All unstabilised samples showed identical hygroscopic behaviour, regardless of the compaction level (Figure 2.27). This is because, according to the Kelvin and Washburn

equations, under the imposed conditions of temperature and relative humidity the exchanges of water vapour take place prevalently within pores with diameters from 3 nm to 7 nm, which were not affected by mechanical compaction.

It is also remarkable that the unstabilised material tested by Bruno (2016) exhibits a moisture buffering capacity that is considerably higher than that of both unstabilised and stabilised materials tested by McGregor et al. (2014) (Figure 2.28). The higher moisture buffering capacity of the former may be due to the larger fine fraction compared to the material tested by McGregor et al. (2014). A finer soil is capable of retaining more water than a coarser soil when submitted to the same hygro-thermal conditions as observed by Jaquin et al. (2008) and by Beckett and Augarde (2012).

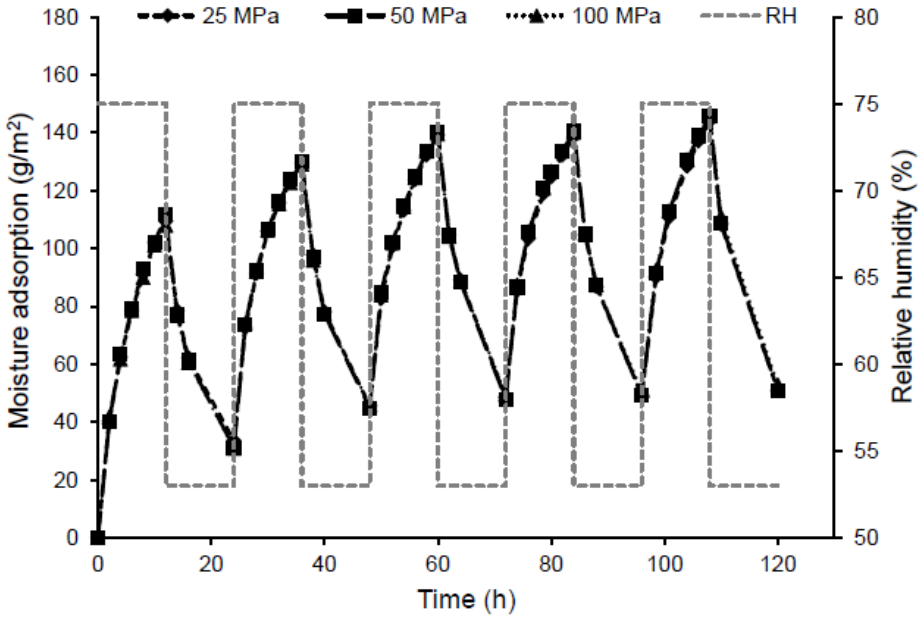

Figure 2.27: Moisture adsorption of unstabilised samples hyper-compacted at 25 MPa, 50 MPa and 100 MPa (from Bruno, 2016).

Bruno (2016) also investigated the effect of stabilisation on the moisture buffering capacity of earth samples hyper-compacted under a pressure of 100 MPa at the optimum water content. As suggested by previous studies (Kebao and Kagi, 2012; McGregor et al., 2014; Elert et al. 2015), alkaline solutions and silane-siloxane emulsions were employed to stabilise the base soil. In particular, stabilisation was achieved by replacing the optimum water content with one of the following three liquid additives, namely a silane-siloxane emulsion, a NaOH solution at 2 mol/L concentration and a blend of the previous two additives.

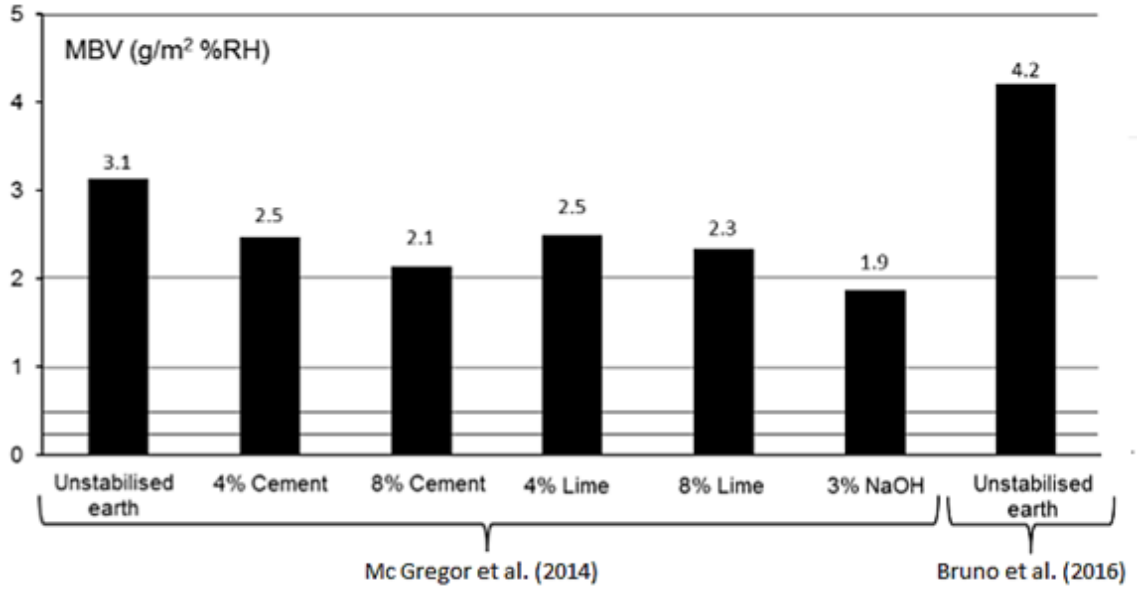

Figure 2.28: MBVs of unstabilised and stabilised compressed earth measured by McGregor et al. (2014) and unstabilised hyper-compacted earth measured by Bruno (2016) (from Bruno, 2016).

Figure 2.29 shows that stabilisation reduces the moisture buffering capacity of the material and this reduction depends on the type of stabiliser. The samples stabilised with the NaOH solution maintained an excellent capacity to buffer ambient humidity according to the classification of Rode et al. (2005). The samples stabilised with the silane-siloxane emulsion and with a mix of silane-siloxane emulsion and NaOH solution showed instead a good moisture buffering capacity according to the classification of Rode et al. (2005).

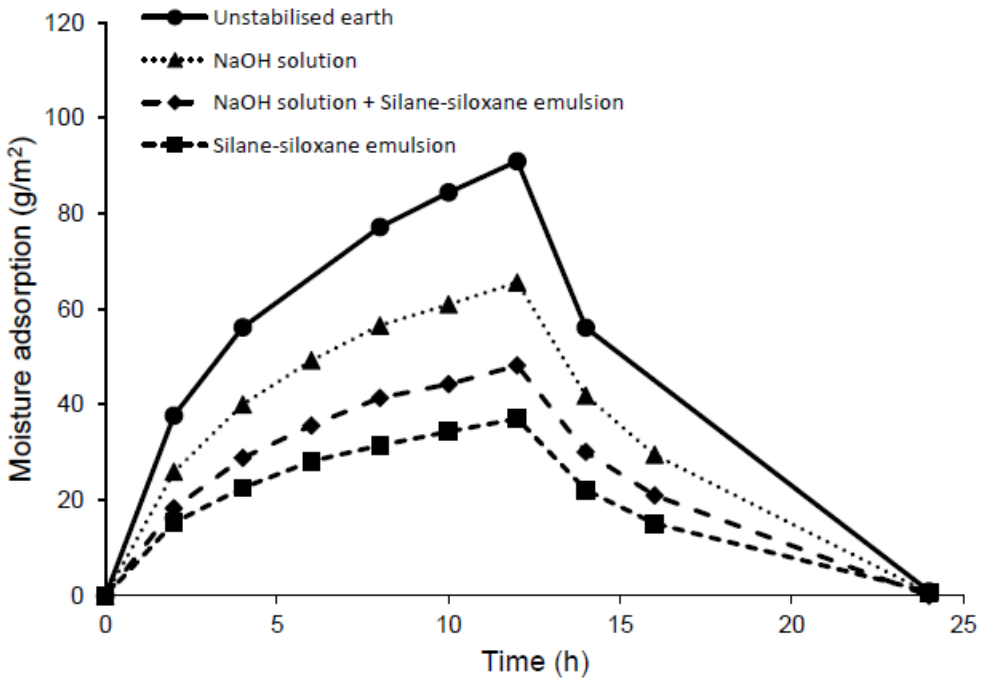

Figure 2.29: Last stable cycle of unstabilised and stabilised samples (from Bruno et al., 2017b).

Bruno (2016) also investigated the effect of the vapour flow direction on the measured MBV by comparing the case of unidirectional flow for bricks with the case of multidirectional flow for cylindrical samples. In the case of bricks, only one of the two largest surfaces was exposed to the humidity cycles while all other surfaces were sealed. In the case of cylindrical samples, instead, only the top and lateral surfaces of the samples were directly exposed to the ambient humidity of the climatic chamber. Bricks and cylindrical samples showed very similar hygroscopic responses, thus suggesting that the measured MBV is independent of the direction of vapour flow (Figure 2.30).

The above brief review indicates that earthen materials exhibit a significantly higher moisture buffering capacity compared to conventional building materials. This offers a range of potential benefits for construction from the reduction of embodied and operational energy of buildings to an improvement of the health and well-being of occupants. Furthermore, it has been demonstrated that stabilisation reduces the moisture buffering capacity of the material in a way that depends on the type of stabiliser.

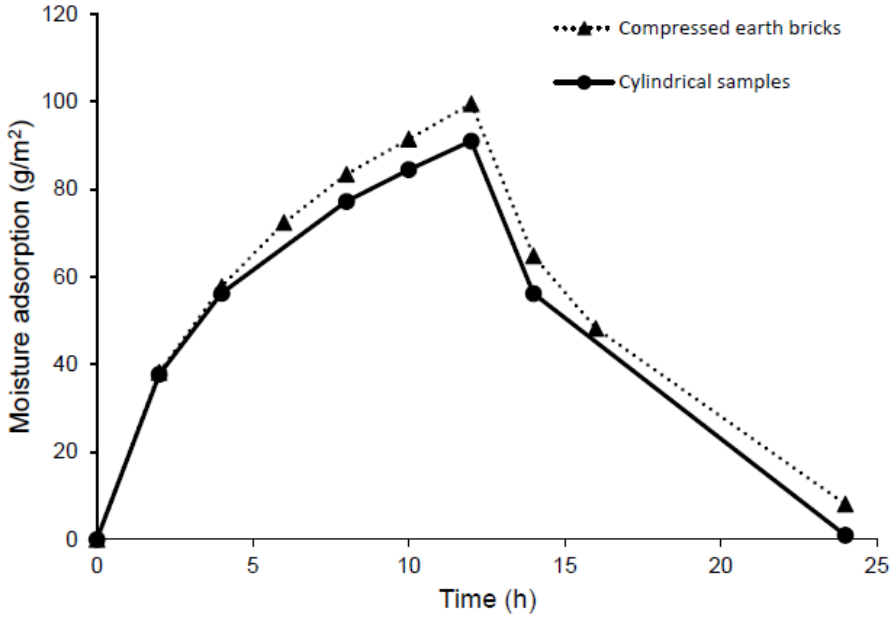

Figure 2.30: Last stable MBV cycle measured on hyper-compacted earth bricks and cylindrical samples (from Bruno, 2016).

2.4. Sensitivity to water

In addition to the mechanical properties, the durability of earthen materials is one of the main aspects to consider when characterising their suitability for buildings construction. The affinity of raw earth for water is one of the main factors that have so far hindered the dissemination of earth construction technologies. The hydrophilic nature of earth is partly

beneficial, as it increases moisture buffering capacity, and partly detrimental as it undermines mechanical properties and durability (Houben and Guillaud, 1994; Walker et al., 2005; Morel et al., 2007). Stabilisation appears therefore as an inevitable requirement for the manufacture of earthen materials that are less sensitive to water and capable of fulfilling minimum durability requirements especially in wet environments. At the same time, researchers have attempted to devise stabilisation methods that do not compromise the ability of earthen materials to buffer moisture and, hence, to smooth variations of ambient humidity inside dwellings. Another important factor causing the erosion of earth walls is the release of kinetic energy from the rain drops impacting on the material surface. Therefore, a number of durability tests were also developed to assess inter-particle bonding under the action of a simulated rainfall. The most common water durability tests are described below together with the corresponding criteria to assess the performance of the material (Heathcote, 1995).

- Wearing test (ASTM D559-03, 2012). In this test, earthen blocks are placed in water for 2 minutes, removed and then oven dried at 105 °C for 24 hours. Twelve cycles of wetting and drying are performed before that the samples are finally dried, the dried final weight is calculated and the wearing performance of the earthen block is determined. Between each cycle, the blocks are brushed with wire brush strokes (corresponding to a force of about 13 N) on all sides to remove the loosened material.
- Spray erosion test (NZS 4298, 1998). In this test, the surface of an earth specimen is sprayed with a jet of water for a period of one hour. The jet of water is delivered at constant pressure of 0.05 MPa through a nozzle at a distance of 0.47 m from the sample. The exposed area of the specimen corresponds to a circle with a diameter of 150 mm. After exposure to the water jet, the maximum depth of erosion is measured and the specimen is visually checked to determine the extent of moisture penetration. If the maximum depth of erosion exceeds 60 mm or water penetrates to the back of the block, the tests is considered failed. The test is an empirical one and there appears to be no field correlation to justify its use. Furthermore, distinct spray tests were separately developed in different countries, thus there is not a unique protocol to follow. Procedures may vary for the duration of the test, the pressure of the water jet, the distance of spraying, the exposed area and the erosion tolerance criteria. Qualitative evidence has, however, suggested that samples that are suitable according to the New Zealand standard NZS 4298 (1998) are also adequate for service.

Regardless of the adopted procedure, specimens are then classified in different classes depending on the erosion depth.

- Drip test (NZS 4298, 1998). This test consists in releasing 100 ml of water in drops via a cloth wick placed 400 mm above a sample that is inclined at an angle of 27° respect to the horizontal. This action is meant to simulate the regular fall of rain droplets on an exposed earth surface. The suitability of the material for construction is then evaluated according to the recorded depth of pitting. In particular, if erosion is not deeper than 10 mm, the material is considered suitable for construction. Frencham (1982) developed the approach further and related the depth of pitting to an Erodability Index (E_r) as shown in Table 2.5.

Table 2.5: Erodability Index (E_r) classification depending on the depth of pitting (after Frencham, 1982).

Erodability Index (E_r)	**Depth of pitting (mm)**	**Rating**
1	0	Non-erosive
2	>0 and <5	Slightly erosive
3	>5 and <10	Erosive
4	>10	Very erosive

Frencham (1982) also concluded that the drip test provides an efficient and cheap method of testing bricks in areas where the rainfall is around 500 mm per annum, though the application to areas of higher rainfall has yet to be confirmed. Cid-Falceto et al. (2012) concluded instead that the criteria for the evaluation of the drip test should be modified and related, for example, to the loss of sample weight.

The German norm DIN 18945 (2013) also suggests that the water durability of earthen bricks can be classified by performing the following tests:

- Immersion test. The test consists in dipping specimens, previously equalised to the atmosphere until a constant mass is reached, in water for ten minutes. Afterwards, the specimens are dried at 40 °C for 24 hours, equalised again to atmosphere and finally weighed. The ratio between the material lost during the test and the initial mass of the sample is then calculated, which allows a first qualitative assessment of the material durability.
- Contact test. This test reproduces the application of a mortar joint or coating on the surface of earthen bricks. An absorbent cellulose cloth is dipped in water and then placed on the exposed face of the brick, which corresponds to the application of an amount of water per surface area equal to 0.5 g/cm^2. Samples are then stored for 24

hours in a sealed container on a rack placed above water. The absorbent cloth is subsequently removed and the bricks are exposed to atmospheric conditions for 2 days. After this, a visual examination of the bricks is performed to detect cracks and/or permanent deformations owed to swelling.

- Suction test. The aim of this test is the investigation of the performance of earthen bricks when exposed to a temporary excess supply of water. First, earth brick are equalised under standard hygro-thermal conditions (T = 23 ± 2 °C; RH = 50 ± 5 %) until a constant mass is reached. Meanwhile, conventional fired bricks are placed at the bottom of a pan filled with water up to 1 mm - 5 mm below the upper edge of the fired bricks, which are then covered with an adsorbent cloth. Next, the earthen bricks are placed on the adsorbent cloth, thus starting the suction test. During the test, water is progressively adsorbed by the earthen bricks and extra water must therefore be added to the pan in order to keep the same level. Samples are visually assessed at 30 min, 3h and 24h after the beginning of the test to detect cracks and permanent deformations owed to swelling.

The German norm DIN 18945 (2013) also proposes a categorisation of earthen bricks into four different classes depending on the results from the previous three tests (Tables 2.6 and 2.7).

Table 2.6: Earth bricks classes according to application (after DIN 18945, 2013).

Application	**Class**
External wall exposed to natural weathering	Ia
Coated external wall exposed to natural weathering	Ib
External wall not exposed to natural weathering – Internal wall	II
Dry applications	III

Table 2.7: Classification of compressed earth bricks: results from durability tests (after DIN 18945, 2013).

Class	**Immersion test** **Mass loss (%)**	**Contact test**	**Suction test**
Ia	≤5 %	No cracks and no permanent swelling deformations	≥ 24 h
Ib	≤5 %		≥ 3 h
II	≤15 %		≥ 0.5 h
III	No requirement	No requirement	No requirement

The sensitivity of earthen materials to water is also partly due to presence of clays (especially expansive clays) that act as a binder for sand and silt particles but also swell/shrink due to changes of moisture, thus causing structural damage.

Conventional stabilisation treatments based on the use of synthetic polymers or alkoxysilanes have so far had only limited success as their application is limited to a superficial material layer, which typically detaches and falls off. Apart from limited penetration, stabilisation treatments do generally not tackle the expansion and contraction of clay minerals, but rather only diminish the symptoms of such processes, thus being ineffective in the long-term (Price et al., 2011). There is therefore an urgent need of alternative methods that allows in-situ stabilisation of earthen architecture by reducing the swelling capacity of clays.

Alkaline activation is an innovative method for stabilising earthen materials relying on the use of alkaline activators that have the potential of dissolving and transforming clay minerals into non-expandable binding materials with cementing capacity. The most common alkaline activators are calcium hydroxide ($Ca(OH)_2$), sodium hydroxide (NaOH) and potassium hydroxide (KOH).

Elert et al. (2015) investigated the suitability of alkaline activation to consolidate existing earthen buildings. They compacted adobe earthen blocks with a soil/water mass ratio of 3:1 which were afterwards impregnated for 20 minutes in three different alkaline solutions of 0.025 mol/L $Ca(OH)_2$, 5 mol/L NaOH and 5 mol/L KOH. After impregnation, samples were stored for 50 days in plastic bags to simulate an in-situ consolidation treatment. Plastic bags were then opened and the samples were left to equalise to the atmosphere ($T \approx 20$ °C; RH ≈ 45 %) until a constant mass was reached. The interaction of these highly concentrated alkaline solutions with the clay minerals are manifold and may include: a) the exchange of cations in the clay minerals for the dominant cation in the alkaline solution (Fernandez et al., 2006; Gaucher and Blanc, 2006); b) flocculation which results in decreased osmotic and intracrystalline swelling of clays depending on the electrolyte concentration (Karnland et al., 2007); c) clay mineral dissolution and transformation (Elert et al., 2008). Adobe blocks treated with different alkaline solutions were subsequently immersed in water over prolonged periods of time to assess their durability. The $Ca(OH)_2$ treatment did not improve water resistance as the stabilised samples experienced severe material loss and a complete disintegration after 2.5 hours. Samples treated with NaOH and especially those treated with KOH showed instead an improved durability by withstanding the action of water for almost

48 hours. Figure 2.31 shows untreated and treated adobe blocks after immersion in water for 1 hour.

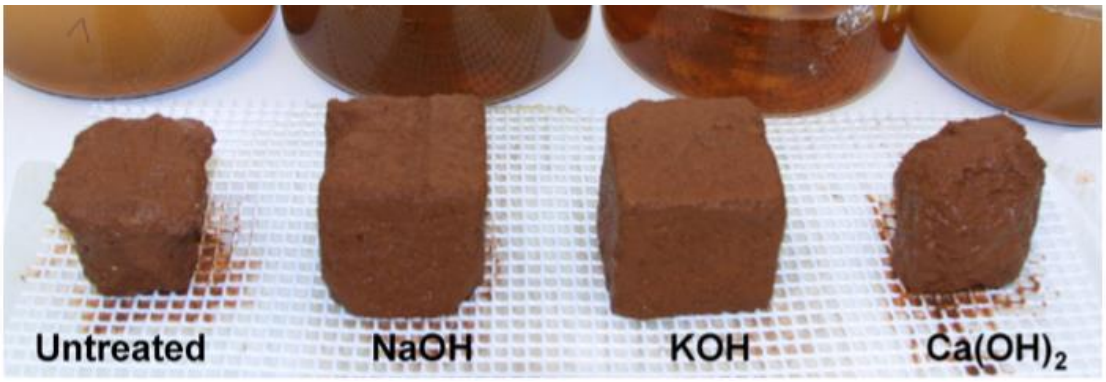

Figure 2.31: Untreated and treated adobe blocks after immersion in water for 1 hour (from Elert et al., 2015).

In conclusion, Elert et al. (2015) demonstrated that the application of alkaline solutions for the consolidation of earthen structures is a valuable alternative to conventional consolidation treatments. The authors also remarked that the use of a KOH solution is preferable because potassium carbonates, which form during alkaline activation, are generally found to have a lower damage potential than sodium carbonates.

Bruno et al. (2017b) investigated the effect of different stabilisation methods on the water resistance of hyper-compacted bricks to water erosion. Both unstabilised and stabilised earth bricks were compacted at a pressure of 100 MPa as described in Chapter 4. The unstabilised samples were manufactured at the optimum water content (see Paragraph 2.2.1.) while, in the case of stabilised samples, the optimum water content was replaced with an equal amount of a stabilising liquid additives. Three stabilising liquid additives were considered, namely a silane-siloxane emulsion, a NaOH solution at 2 mol/L concentration and a blend of the previous two additives.

Earth bricks were subjected to suction and contact tests performed according to the German norm DIN 18945 (2013) as described previously. Figure 2.32 shows some observations made at different times during suction tests on unstabilised and stabilised bricks. As expected, the unstabilised bricks exhibited cracks and irreversible deformations after only 30 minutes from the beginning of the test. Earth bricks stabilised with the NaOH solution + silane-siloxane emulsion exhibited better durability as cracks started to appear after 3 hours from the beginning of the test. The best results were, however, obtained for the earth bricks stabilised with NaOH solution or with the silane siloxane emulsion. These bricks showed the appearance of cracks only at the last visual examination after 24 hours from the beginning of the test.

The observations at the end of the contact tests are instead presented in Figure 2.33, which shows that all bricks experienced cracking and permanent deformations at the end of the test. Note that Bruno et al. (2017b) also performed immersion tests on small cylindrical samples, whose results have not been presented here in the sake of brevity. Table 2.8 shows a classification of the different materials tested by Bruno et al. (2017b) according to the norm DIN 18945 (2013) (Table 2.6).

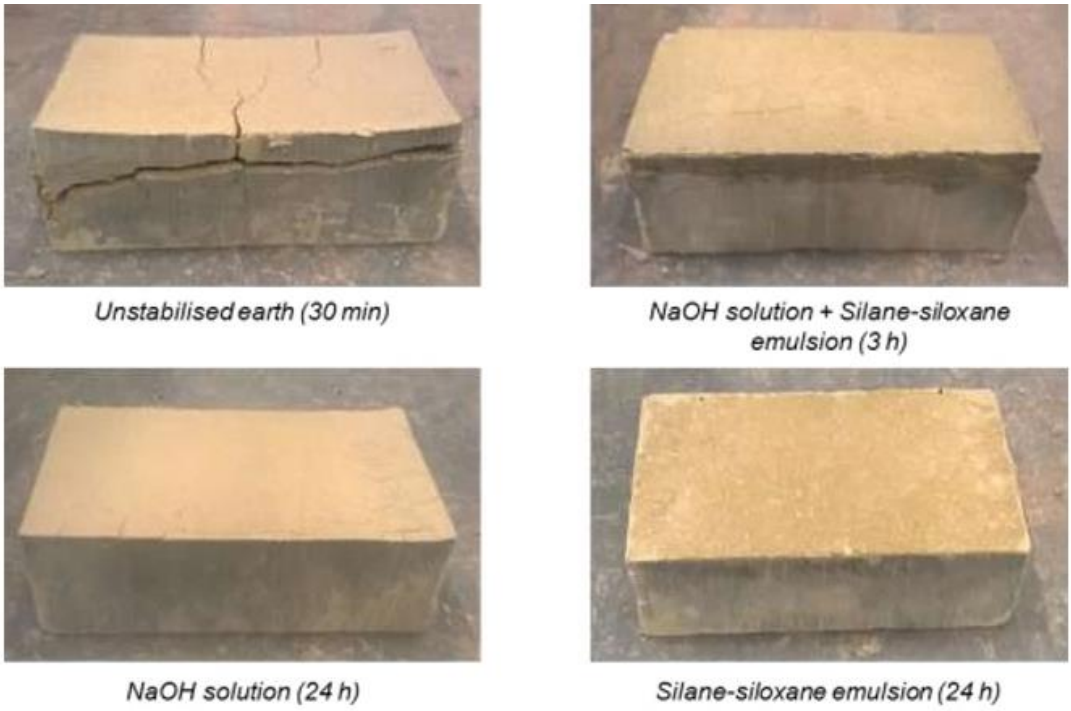

Figure 2.32: Results from suction tests on unstabilised and stabilised hyper-compacted earth bricks (from Bruno et al., 2017b).

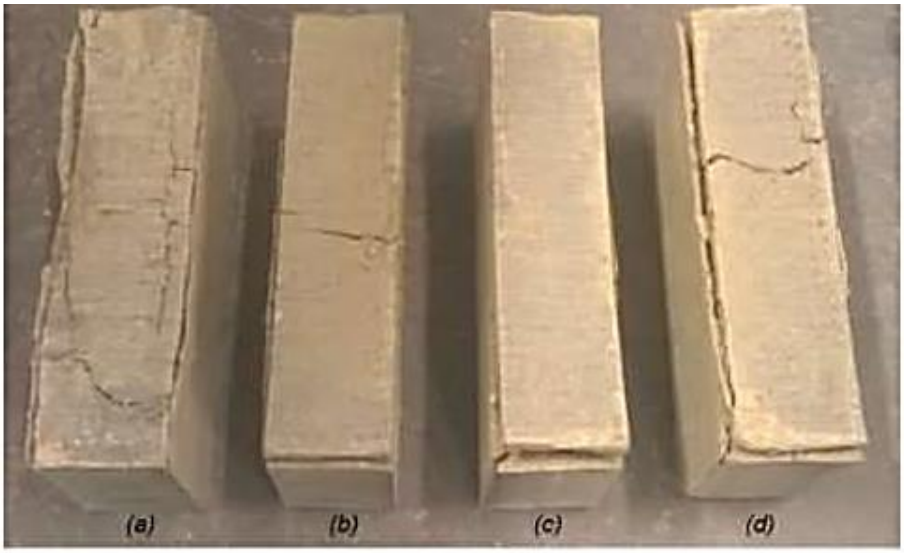

Figure 2.33: Results from contact tests on unstabilised and stabilised hypercompacted earth bricks (from Bruno et al., 2017b).

Table 2.8: Classification of earth bricks tested by Bruno et al. (2017b) in accordance to norm DIN 18945 (2013) (after Bruno et al., 2017b).

Type of stabilisation	**Immersion test**	**Suction test**	**Contact test**
Unstabilised	III	III	III
Silane-siloxane emulsion	I	Ib	III
NaOH solution	II	Ib	III
NaOH solution + silane-siloxane emulsion	I	II	III

Inspection of Table 2.8 indicates that the unstabilised earth bricks exhibit the worst classification and can only be employed in dry applications where they are protected from natural weathering. Inspection of Table 2.8 also shows that the contact test provides the most severe assessment of material durability among all tests prescribed by the norm DIN 18945 (2013). This is also confirmed by the fact that all stabilised bricks were classified as I or II class according to immersion and suction tests but not according to the contact test.

Bruno et al. (2017b) concluded that the durability of earthen materials against water erosion can be improved by the use of alkaline solutions such as in particular, silane-siloxane emulsion. However, silane-siloxane stabilisation resulted in a considerable deterioration of the mechanical and moisture buffering properties of the material as shown in the previous sections.

3. Stabilisation of earth materials by carbonate precipitation: a review

3.1. Introduction

Current soil stabilisation techniques in geotechnical engineering are either invasive (e.g., jet grouting) or energy intensive (e.g., compaction, vibration, heating) or require environmentally unfriendly hazardous binders (e.g., cement or lime). Alternative, nature-inspired, stabilisation methods have therefore been recently proposed to avoid the use of costly and carbon inefficient materials. Mitchell and Santamarina (2005) published a seminal article outlining the main biological stabilisation techniques for soils. Since then, research has proceeded at pace with the role of microbial processes in geotechnical engineering capturing the attention of many scientists across the world. A comprehensive report of different bio-geotechnical processes can be found in De Jong et al. (2006).

This review presents some of the most promising bio-mediated processes for improving the hydraulic and mechanical properties of soils with possible application to earth building. Indeed, researchers have started to develop processes that eliminate the need to fire earth bricks by exploiting biologically controlled cementation processes. An important part of bio-mediated stabilisation methods rely on the catalysis of urea hydrolysis to enhance soil properties through the precipitation of minerals such as calcium carbonate (Stocks-Fischer et al., 1999; Barkay and Schaefer, 2001; DeJong et al., 2006; Whiffin et al., 2007; De Muynck et al., 2010; Dilrukshi and Kawasaki, 2016). This is similar to hydroponics-whereby block units mixed with the microorganism are fed an aqueous solution to harden the bricks to specification. These stabilisation methods need however further refinements to improve material performance and reduce production costs.

3.2. Carbonate precipitation for soil improvement

The precipitation of calcium carbonate ($CaCO_3$) can occur via different mechanisms such as photosynthesis (Thompson and Ferris, 1990; McConnaughey et al., 1997), sulfate reduction (Castanier et al., 1999; Warthmann et al., 2000; Hammes et al., 2003), anaerobic sulfide oxidation (Warthmann et al., 2000), biofilm and extracellular polymeric substances (Kawaguchi and Decho, 2002; Arias and Fernandez, 2008). However, among all these mechanisms, the most popular and relevant to this study is urea hydrolysis (Stocks-Fischer et al., 1999; Hammes and Verstraete, 2002; De Muynck et al., 2010; DeJong et al., 2010; Dhami et al., 2013a). Large masses of $CaCO_3$ can precipitate in short times via urea

hydrolysis due to the high solubility of the substrates in solution (urea and calcium chloride) (Van Paassen et al., 2010).

The mechanism through which urea hydrolysis leads to the precipitation of $CaCO_3$ is described by the following chemical equations:

$$CO\ (NH_2)_2 + \ H_2O \rightarrow NH_2COOH + NH_3 \quad (3.1)$$

$$NH_2COOH + \ H_2O \rightarrow NH_3 + H_2CO_3 \quad (3.2)$$

$$2NH_3 + 2H_2O \rightarrow 2NH_4^+ + 2OH^- \quad (3.3)$$

$$2OH^- + H_2CO_3 \rightarrow CO_3^{2-} + 2H_2O \quad (3.4)$$

$$CO\ (NH_2)_2 + \ 2H_2O \rightarrow 2NH_4^+ + CO_3^{2-} \quad (3.5)$$

$$Ca^{2+} + CO_3^{2-} \rightarrow CaCO_3 \quad (3.6)$$

Equation 3.1 shows that the hydrolysis of one mole of urea ($CO(NH_2)_2$) generates one mole of ammonia (NH_3) and one mole of carbamic acid (NH_2COOH) (Dilrukshi et Kawasaki, 2016). Hydrolysis of $CO(NH_2)_2$ takes places spontaneously in water but at a very slow pace. The urease enzyme can however act as a catalyst and accelerate considerably the kinetics of the reaction. Equation 3.2 indicates that one mole of NH_2COOH is hydrolysed into another mole of NH_3 plus one mole of carbonic acid (H_2CO_3). Equations 3.3 and 3.4 then show that the two moles of NH_3 and one mole of H_2CO_3, obtained from the above reactions, equilibrate in water to form one mole of carbonate ions (CO_3^{2-}) and two moles of ammonium ions (NH_4^+). This also produces hydroxide ions (OH^-) and therefore leads to an increase of alkalinity. Equation 3.5 summarises the above four reactions (Equations 3.1 – 3.4) and indicates that the overall result of the hydrolysis of one mole of $CO(NH_2)_2$ is the production of two moles of NH_4^+ and one mole of CO_3^{2-}. Finally, Equation 3.6 shows that, in the presence of calcium ions (Ca^{2+}), one mole CO_3^{2-} precipitates to form one mole of $CaCO_3$ (e.g., calcite) once supersaturation is attained.

In particular, it has been found that some types of bacteria are able to produce large amounts of urease and hence induce calcium carbonate precipitation. Most studies in the domain of bio-geotechnics have focused on a method of stabilisation called microbially induced carbonate precipitation (MICP). The MICP method mostly relies on passive precipitation of $CaCO_3$ which bonds the soil grains togheter thus increasing stiffness and strength. In particular, the urea hydrolysis, result of bacterial activity, leads to the production of CO_3^{2-} and then the precipitation of $CaCO_3$ in the presence of Ca^{2+}.

The most widely known ureolytic bacteria is the Sporosarcina pasteurii, which is used for multiple applications such as heavy metals and radionuclides remediation, crack reparation in concrete and soil improvement (Whiffin et al., 2007; Sarada et al., 2009; Gorospe et al., 2013; Lauchnor et al., 2013; Li et al., 2013). Achal et al. (2009) developed a mutant strain of Sporosarcina pasteurii capable of greater urease activity and $CaCO_3$ precipitation than the wild strain of Sporosarcina pasteurii MTCC 1761. Bacillus species are known for their ubiquity in nature and their high resistance to chemical and physical agents, which facilitates field applications (Al Qabany and Soga, 2013).

Interestingly, Bacteria exist in sub-soils in surprisingly high concentrations (around 10^{14} bacteria/kilogram) and their biological activity can be harnessed when nutrient additives such as animal blood, eggs and molasses are mixed with the soil (De Jong et al., 2010). The bacterial cells also act as nucleation sites and create micro niche conditions favouring precipitation of minerals. The presence of microbes within the soil can also reduce inter-granular friction, thus easing compaction (Martirena et al., 2014) while $CaCO_3$ precipitation can increase compressive strength and reduce moisture adsorption (Dhami et al., 2013c). MICP can be therefore implemented either by supplying nutrients to stimulate resident bacteria in the soil (bio-stimulation) or by adding new bacterial species to the soil (bio-augmentation). Bio-stimulation requires an in-depth analysis of resident bacterial colonies and their fitness to ensure appropriate carbonate precipitation. Bio-augmentation has, however, a higher success rate as only proven bacterial strains are introduced to the soil.

Researchers have also investigated the potential use of MICP for reducing erosion by creating a $CaCO_3$ layer at the soil surface that is more resistant to the shear stresses imposed by wind or water. Both Gomez et al. (2015) and Hamdan and Kavazanjian (2016) investigated carbonate precipitation via urea hydrolysis as a means of suppressing dust generated by wind erosion. Gomez et al. (2015) utilised S. pasteurii whereas Hamdan and Kavazanjian (2016) used jack bean urease enzyme. In both cases, the treated soils exhibited enhanced erosion resistance measured via jet-impingement tests (Gomez et al., 2015) or wind tunnel tests (Hamdan and Kavazanjian, 2016). In particular, the wind speed required to initiate erosion in treated soils exceeded that of control samples. Studies have also demonstrated the efficiency of MICP in reducing the water-induced erosion of embankments and slopes in riverine and coastal/estuarine environments or to mitigate scour around bridge piers (Amin et al., 2017; Bao et al., 2017; Salifu et al., 2016).

3.2.1. Efficiency of Microbially Induced Calcite Precipitation (MICP)

Two distinct MICP mechanisms are reported in the literature (Stock-Fischer et al., 1999; DeJong et al., 2006).

In the first mechanism, known as active precipitation, the bacterial cells act as nucleation sites for $CaCO_3$ precipitation. The bacterial cells have negatively charged groups that act as scavengers for divalent cations (e.g. calcium Ca^{2+} and magnesium Mg^{2+} ions) by binding them onto their surfaces at neutral pH, which make ideal nucleation sites for calcite deposition (Ferris et al. 1996; Stocks-Fischer et al. 1999; Ramachandran et al., 2001). The bound cation (metal ions) subsequently reacts with anions (carbonate) to form $CaCO_3$ in an insoluble form (Figure 3.1).

The second mechanism, known as passive precipitation, operates by producing CO_3^{2-} and bicarbonate ions that lead to the precipitation of $CaCO_3$. Two metabolic cycles can be involved: the nitrogen cycle and the sulphur cycle. In the nitrogen cycle, passive bacterial precipitation follows three different pathways: ammonification of amino acids, dissimilatory reduction of nitrate and degradation of urea or uric acid. These three pathways produce carbonate and bicarbonate and, as a metabolic end-product, ammonia which raises the pH around the cells. When the H^+ concentration decreases, the carbonate-bicarbonate equilibria are shifted towards the production of carbonate ions CO_3^{2-}. If calcium ions are present, calcium carbonate precipitation occurs.

The precipitation of calcium carbonate is a rather straightforward chemical process governed by the following main key factors: the concentrations of $CO(NH_2)_2$ and Ca^{2+} (Hammes and Verstraete, 2002; Ng et al., 2012), the concentration of the dissolved inorganic carbon (DIC), the pH, the temperature and the availability of nucleation sites (Kile et al., 2000; Castanier et al., 1999). The first three factors influence the concentration of CO_3^{2-} (i.e., saturation state), while the last parameter (i.e., availability of nucleation sites) is very important for a stable and continuous formation of calcium carbonate (Phillips et al., 2013).

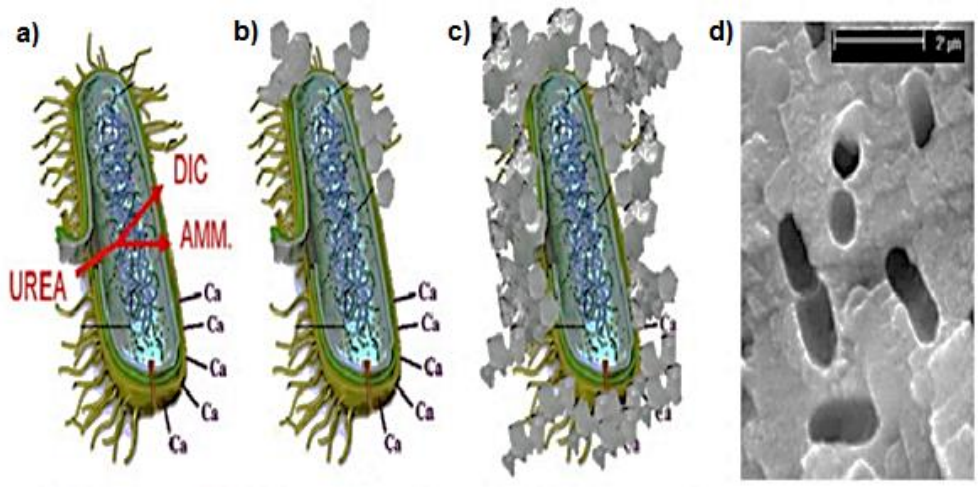

Figure 3.1: Ureolysis-driven calcite precipitation (from De Muynck et al., 2010).

- Ca^{2+} source

In general, bio-mineralisation can lead to the precipitation of different phases of $CaCO_3$ including anhydrous polymorphs phases, such as calcite, aragonite and vaterite as well as hydrated crystalline phases such as monohydrocalcite ($CaCO_3 \cdot H_2O$) and hexahydrocalcite or ikaite ($CaCO_3 \cdot 6H_2O$) and amorphous calcium carbonate (ACC) (Hammes et al., 2003; Wei et al., 2003; Ben Chekroun et al., 2004; Xu et al., 2006; Chen et al., 2009; Sanchez-Navas et al., 2009; Gebauer et al., 2010; Dhami et al., 2013b). Among these phases, calcite and vaterite are the most common polymorphs (Dhami et al., 2013b).

Vaterite is a metastable transitional phase during calcite formation (Tourney and Ngwenya, 2009). Calcite is instead the most stable polymorph of $CaCO_3$ and the primary product of $CaCO_3$ in many MICP processes (Spanos and Koutsoukos, 1998; Stocks-Fischer et al., 1999; Okwadha and Li, 2010; Ganendra et al., 2014).

The precipitation of $CaCO_3$ by mixing concentrated Ca^{2+} and CO_3^{2-} solutions usually involves the following three subsequent steps: a) formation of amorphous $CaCO_3$ characterised by low stability and high solubility, b) transformation of amorphous $CaCO_3$ into vaterite, and c) transformation of thermodynamically unstable vaterite into stable calcite (Wei et al., 2003; Shen et al., 2006; Hua et al., 2007).

Different calcium sources induce precipitation of $CaCO_3$ crystals with different shapes (Figure 3.2). The rhombohedral shape induced by calcium chloride is characteristic of the most stable form of $CaCO_3$ (calcite) (De Yoreo and Vekilov, 2003; Favre et al., 2009; Gorospe et al., 2013). Calcium acetate induces a lettuce like or lamellar shape composed of vaterite (a metastable form of $CaCO_3$), while calcium lactate and calcium gluconate induce

a more complex form and a growth of vaterite with a spherical shape (Tai and Chen, 1998). Examination by electron microscopy reveals the shape of calcium crystals according to the specific Ca^{2+} source (Figure 3.2).

The morphological crystal differences may also be bacterial strain-specific, owing to differences in urease activity (Hammes et al., 2003; Park et al., 2010). These differences could reflect the specific extracellular polymeric substances (EPS) produced by different bacteria controlling calcite or aragonite polymorph selection (Kawaguchi and Decho, 2002). This is because EPS proteins may specifically bind Ca^{2+} and promote carbonate precipitation (Dhami et al. 2013b). The composition of the medium or culture may also affect crystal morphology because different bacterial species are able to precipitate different amounts, shapes and types of carbonate crystals from the same synthetic medium (Ferrer et al., 1988; Hammes and Verstraete, 2002; Dhami et al., 2013b).

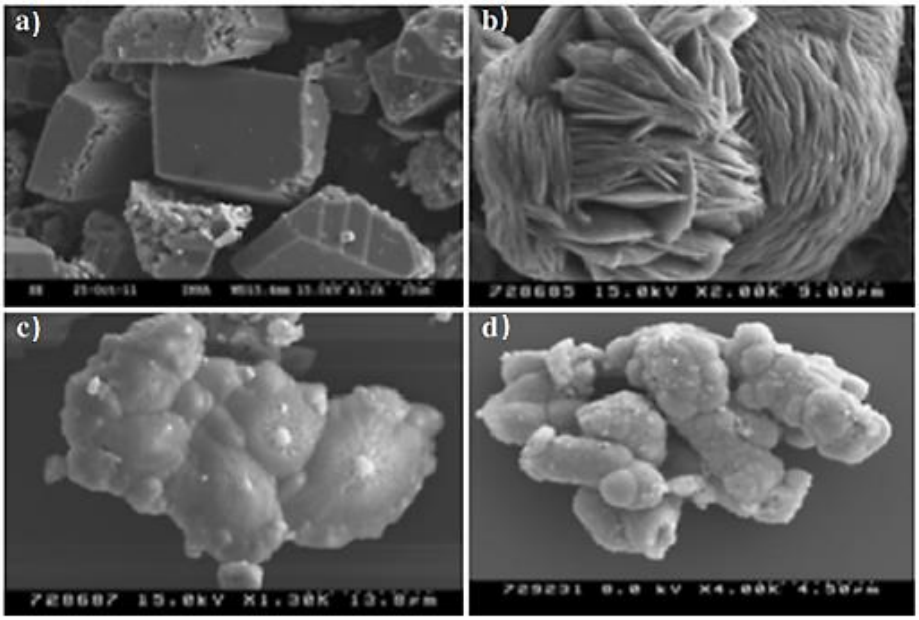

Figure 3.2: Scanning electron micrographs showing the effects of different calcium sources on the shape of the crystals formed: Calcium chloride (a); Calcium acetate (b); Calcium lactate (c); Calcium gluconate (d) (from Goroscope et al., 2013).

Achal and Pan (2014) studied the $CaCO_3$ precipitation induced by Bacillus sp. CR2 when different calcium sources were added to a nutrient broth containing urea. They showed that calcium chloride is best for the production of calcite as well as for higher urease activity.

Goroscope et al. (2013) investigated the role of calcium salts on $CaCO_3$ precipitation by making sand blocks bio-cemented with various calcium sources (Figure 3.3). The blocks treated with $CaCl_2$ showed the best mechanical performance whereas the control blocks incorporating dead cells collapsed after demoulding from the Petri dish.

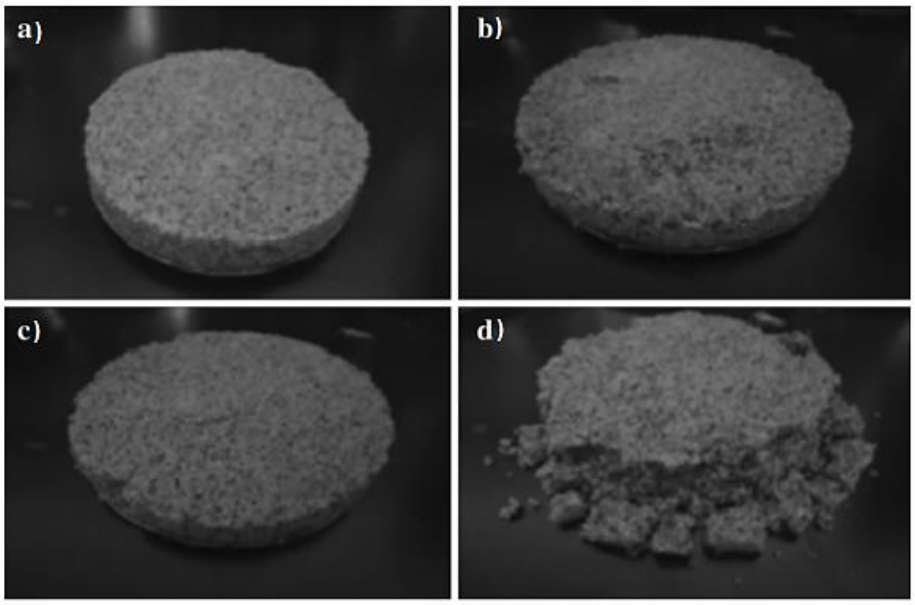

Figure 3.3: Bio-consolidated sand blocks made from different calcium salts: Calcium chloride (a); Calcium acetate (b); Calcium lactate (c); Control (d) (from Goroscope et al., 2013).

- $CO(NH_2)_2$ and Ca^{2+} concentrations

$CO(NH_2)_2$ and Ca^{2+} concentrations have a strong influence on the efficiency of $CaCO_3$ precipitation. Even though many researchers have used different calcium sources for inducing $CaCO_3$ precipitation, calcium chloride ($CaCl_2$) appears to be the best source (Achal and Pan, 2014). Okwadha and Li (2010) noticed that high concentrations of $CO(NH_2)_2$ and $CaCl_2$ (above 0.5 M) decrease the efficiency of precipitation while the greatest efficiency was observed at low concentrations (0.05 M - 0.25 M). De Muynck et al. (2010) reported that the best $CO(NH_2)_2$ and $CaCl_2$ concentrations for calcite precipitation are between 0.5 M and 0.25 M, respectively. Ca^{2+} are not likely utilized by metabolic processes, but accumulate outside the cell, where they are readily available for $CaCO_3$ precipitation (Silver et al., 1975). Okwadha and Li (2010) reported that the amount of $CaCO_3$ precipitation depends more on Ca^{2+} than $CO(NH_2)_2$ concentration. However, increasing the concentration of Ca^{2+} in solution shifts the saturation state of the system (and can increase the pH if an adjustment is not made), so an higher concentration of Ca^{2+} than the $CO(NH_2)_2$ concentration may lead to more rapid precipitation. Nemati et al. (2005) found that increasing $CaCl_2$ alone from 0.045 M to 0.27 M resulted in increasing amounts of $CaCO_3$. Al Qabany and Soga (2013) found that, as equimolar concentration increased to 0.5 M, slightly more $CaCO_3$ precipitation was required to achieve the same strength in stabilised samples with the samples treated with 1 M of $CO(NH_2)_2$ and $CaCl_2$ frequently failing before tests. This was attributed to larger $CaCO_3$ crystals forming in the pore space at high concentrations of $CO(NH_2)_2$ and $CaCl_2$

and a poor spatial distribution of $CaCO_3$. Hammes et al. (2003) found that the urease enzyme activity increased by tenfold in the presence of Ca^{2+}.

- pH

The bio-mineralisation of $CaCO_3$ is strongly influenced by the pH of the precipitation medium. In particular, an alkaline environment is essential for the $CaCO_3$ precipitation to prevent the dissolution rather than the precipitation of the carbonates (Loewenthal and Marais, 1978). Authors have found that calcite precipitation occurs preferably under pH values from 8.7 to 9.5 (Stocks-Fischer et al., 1999; Ferris et al., 2003; Dupraz et al., 2009). Although a rise in pH is necessary, an instantaneous increase may not be desirable in field applications as it can lead to clogging the soil matrix near the injection point due to the rapid precipitation of $CaCO_3$. This, in turn, restricts the extent of soil improvement to a region around the inject point. Equally, a prolonged delay in precipitation might result in excess volumes of treatment fluids being injected into the soil matrix leading to increased costs as well as potentially negative impacts on adjacent locations where the treatment is not mandated. Therefore, controlling the time required for precipitation by regulating the pH with a buffer, which does not interfere with the activity of the cells or the reaction process, may be necessary.

- Temperature

Like other enzymatic reactions, the catalysis of urea by urease is temperature dependent. The optimum temperature for most ureases ranges from 20 °C to 37 °C (Mitchell and Ferris, 2005; Okwadha and Li, 2010). Mitchel and Ferris (2005) reported that the urease activity increased by about 5 times when the temperature increased from 15 to 20 °C and 10 times when the temperature increased from 10 °C to 20 °C. Dhami et al. (2014) found that urease was completely stable at 35 °C but activity decreased by almost 47 % when the temperature increased to 55 °C.

- Bacterial cells concentration

High concentrations of bacterial cells (from 106 to 108 cells) increase the amount of calcite precipitation by increasing urease concentration (Okwadha and Li, 2010). Therefore, urea hydrolysis has a direct relationship with bacterial cell concentrations (Ng et al., 2012). Stocks-Fischer et al. (1999) reported that bacterial cells also serve as nucleation sites for $CaCO_3$ precipitation, which is very important for accelerating the formation of calcite (Ng et al., 2012). Stocks-Fischer et al. (1999) compared the efficiency of MICP with chemically induced precipitation at pH of 9. They confirmed that 98 % of the initial Ca^{2+} concentration

was precipitated microbially, but only 35 % and 54 % was precipitated chemically in water and culture medium, respectively. This is because bacterial cells provide nucleation sites for $CaCO_3$ precipitation and create an alkaline environment to promote the growth of calcite (Stocks-Fischer et al., 1999).

- Urease activity

The rate of urea hydrolysis is governed by the urease activity, which is determined by the amount of enzyme present in the solution, and is measured in mM urea hydrolyzed/min. Given that bacteria are the source of the enzyme, this is often expressed as specific urease activity Kurea (mM urea/min/OD600). OD600 indicates the absorbance, or optical density, of a sample measured at a wavelength of 600 nm and it is a common method for estimating the concentration of bacterial or other cells in a liquid. Kurea is commonly measured using the change in electrical conductivity over a period of 5 min, based on the premise that non-ionic urea is hydrolysed into ionic ammonium. The calibration relationship was developed by Whiffin (2004), where urea hydrolysed in mM is equal to 11.11 multiplied by the change on conductivity in mS/cm. Urease activity varies in the range 0.5 mM - 60 mM urea hydrolysed/min while specific urease activity varies in the range 0.8 mM - 29 mM urea hydrolysed/min/OD (Harkes et al., 2010; Minto et al., 2016; Terzis and Laloui, 2017; van Paassen et al., 2010).

3.2.2. Hygro-mechanical behaviour of MICP-stabilised soil

Dhami and Mukherjee (2015) incorporated MICP technology in rammed earth to alleviate problems such as moisture adsorption, swelling and cracking. A 10 % bacterially inoculated nutrient broth media supplemented with 2 % urea and 25 mM $CaCl_2$ was used to make stabilised earth blocks. In particular, a bacterial culture of sp. Bacillus megaterium SS3 with density 10^8 cells/ml was used while the block density was set at 1800 kg/m^3. For control blocks, a 10% uninoculated media was used. The effect of MICP on water absorption, compressive strength, linear expansion and porosity was subsequently measured. The authors noticed that the saturated water content of the bacterially inoculated blocks was 40 % lower than that of control ones (Figure 3.4a). A scanning electron microscopy analysis of the stabilised material revealed the presence of calcite crystals with imprint of bacteria (Figure 3.4b). Finally, Figure 3.4c highlights a reduction of the linear expansion of stabilised samples compared to control ones, which reduces the risk of cracking. Dhami and Mukherjee (2015) concluded that MICP was a promising stabilisation method for rammed earth construction as it made the earth material stronger and more durable.

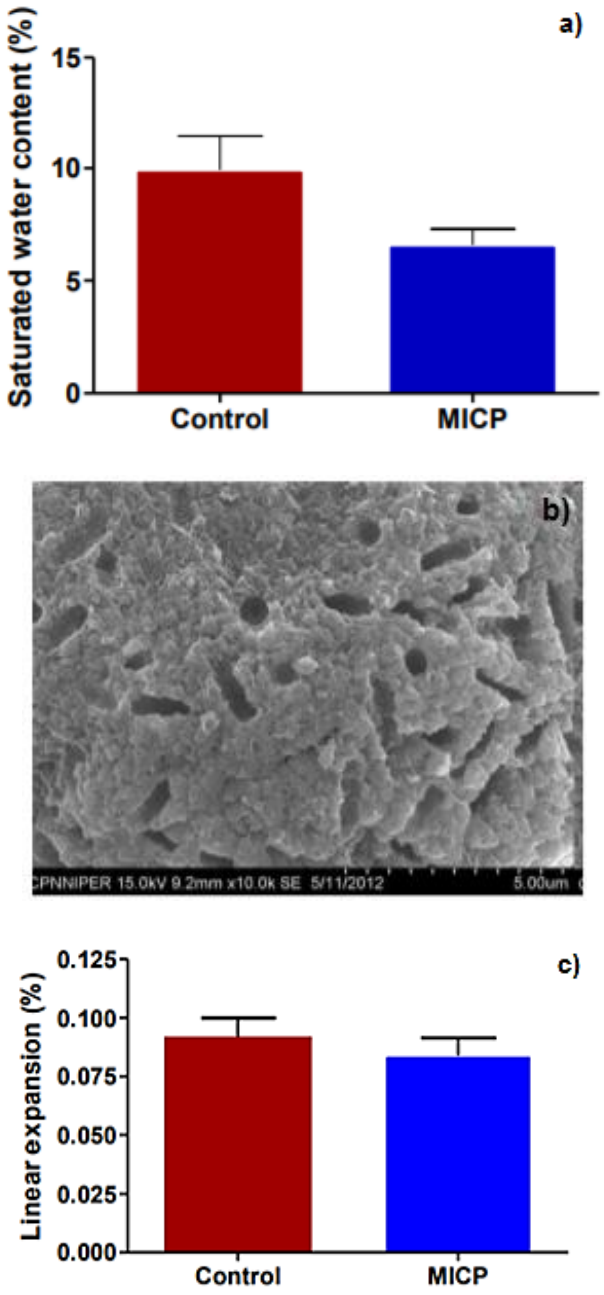

Figure 3.4: Saturated water content of control and stabilised earth blocks (a); Scanning Electron Micrograph of calcite crystals with bacterial impressions (b); Linear expansion of control and stabilised earth blocks (c). Bars mean ± SD (n = 3) (from Dhami and Mukherjee, 2015).

A study by Sharma and Ramkrishnan (2016) investigated the effect of MICP on the strength of fine grained soils by performing unconfined compressive tests. Samples were manufactured with two types of soils, whose main properties are shown in Table 3.1.

Table 3.1: Properties of soil samples tested as reported from Sharma and Ramkrishnan (2016).

Description	Symbol	Soil sample 1	Soil sample 2
Gravel	G	0.3%	0.24%
Sand	S	47.1%	17.48%
(Silt + clay)	M + C	53.6%	82.28%
Liquid limit	w_L	45.4%	61.38%
Plastic limit	w_P	16.8%	28.2%
Plasticity index	I_P	28.5%	33.2%
Shrinkage limit	w_S	8.2%	7.6%
Specific gravity	G_S	2.5	2.7
Soil classification		CI	CH
Optimum moisture content	OMC	16.8%	19.7%
Maximum dry density	$\gamma_{d\ max}$	1.86 g/cc	1.64 g/ cc
Unconfined compressive strength	q_u	0.99 kg/cm^2	1.28 kg/cm^2

The soils were mixed with solutions of the cementation reagents and B. pasteurii. The chosen concentrations of B. pasteurii were 1×10^5 cfu/ml, 1×10^6 cfu/ml and 1×10^7 cfu/ml according to previous studies by Ng et al. (2012). The cementation solutions were composed by equimolar concentrations of urea and calcium chloride equal to 0.25 M, 0.5 M, 0.75 M and 1.0 M with a fixed amount of nutrient, i.e. 3 mg/L, for the growth of the bacterial culture. Bacteria were added to the soil and mixed properly before the addition of the cementation reagents. After preparation, soil samples were cured for 0, 3 and 7 days under a temperature of 20 °C - 30 °C. Results from unconfined compressive tests on stabilised samples 1 and 2 are presented in Figures 3.5 and 3.6, respectively.

Results show that MICP stabilisation more than doubled the unconfined compressive strength of soil sample 1. A bacterial concentration of 1×10^7 cfu/ml and a cementation reagent concentration of 0.5 M gave the optimum results with the unconfined compressive strength increasing from 0.99 kg/cm^2 to 2.44 kg/cm^2 when the soil was cured for 7 days. MICP was found to increase considerably the unconfined compressive strength also for soil sample 2. A maximum strength of 3.72 kg/cm^2 was observed when the soil was cured for 7 days with a bacterial concentration of 1×10^7 cfu/ml and a cementation reagent concentration of 0.5 M. The effect of MICP on unconfined compressive strength was more evident for sample 2 than sample 1 while the strength generally increased with curing time. Additional reasons for the higher strength of sample 1 can be the closer arrangement of the granular matrix and the formation of stronger bonds due to the larger specific surface area.

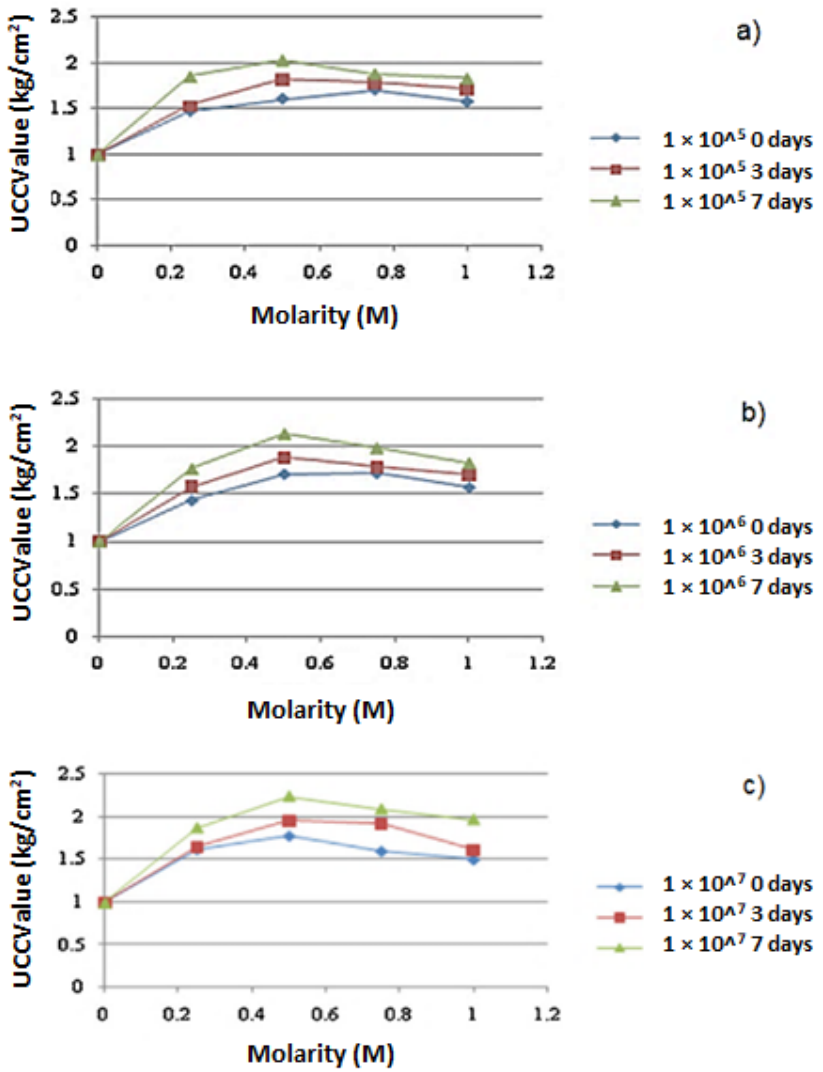

Figure 3.5: Strength of soil sample 1 stabilised with 1×10^5 cfu/ml at 0,3 and 7 days (a); 1×10^6 cfu/ml at 0,3 and 7 days (b); 1×10^7 cfu/ml at 0,3 and 7 days (c) (after Sharma and Ramkrishnan, 2016).

Many researchers have also related $CaCO_3$ content to unconfined compression strength under different experimental conditions (Al Qabany and Soga, 2013; Cheng et al., 2013; Cheng et al., 2014; Choi et al., 2016; Rowshanbakht et al., 2016 ; Terzis and Laloui, 2018; van Paassen et al., 2010). Despite differences in the experimental procedure to measure the unconfined compressive strength, it can be concluded that it exists a general trend in which the parameters causing a slow ureolysis rate (low temperature, low urea concentration) or $CaCO_3$ precipitation (low $CaCl_2$ concentration) results in marginally greater unconfined compressive strength for a given $CaCO_3$ content. This may be due to the influence of the rate of ureolysis on the amount, size and distribution of crystals. For example, van Paassen et al. (2009) demonstrated that high rates of ureolysis (> 0.3 mM urea hydrolysed/min) resulted in the formation of large spherical crystals whereas intermediate rates resulted in smaller calcite crystals and very low rates in a small number of very large calcite crystals.

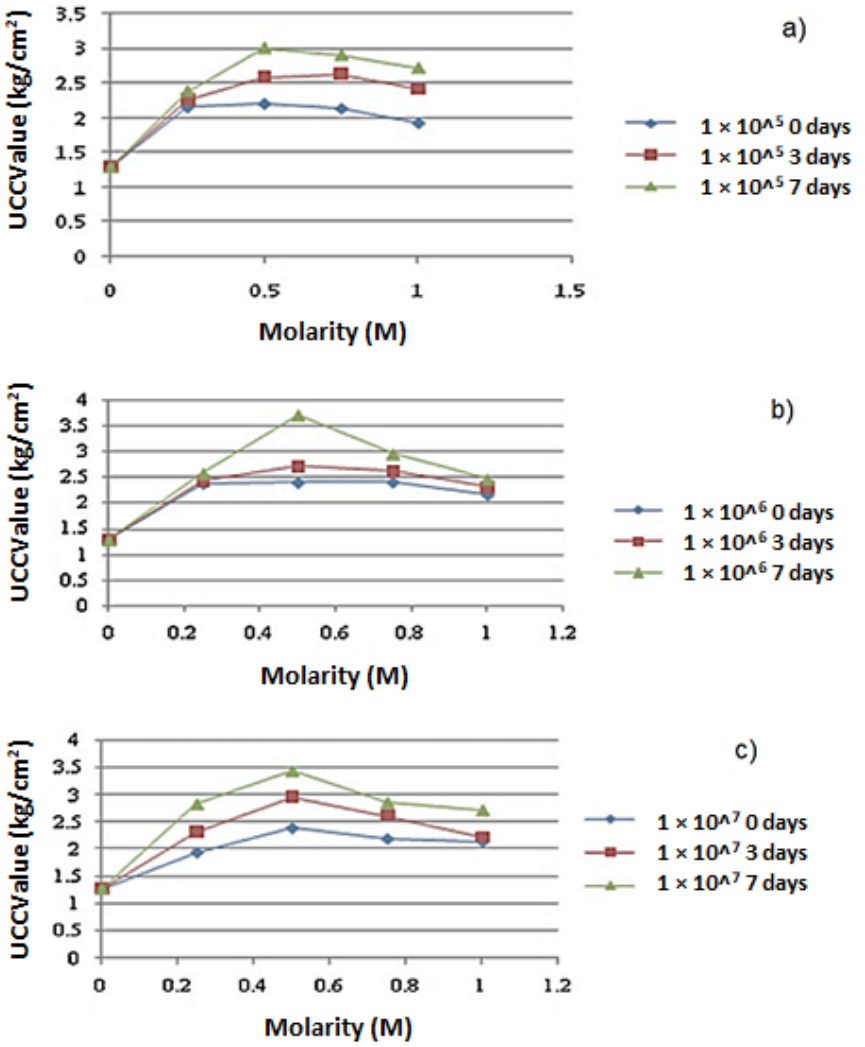

Figure 3.6: Strength of soil sample 2 with 1×10^5 cfu/ml at 0,3 and 7 days (a); 1×10^6 cfu/ml at 0,3 and 7 days (b); 1×10^7 cfu/ml at 0,3 and 7 days (c) (after Sharma and Ramkrishnan, 2016).

Some studies have also reported increased rates of ureolysis and precipitation after initial calcite deposition, suggesting that bacteria preferentially attach to these surfaces rather than silica, glass or polycarbonate (El Mountassir et al., 2014; Schultz et al., 2011; Tobler et al., 2012). Furthermore, the activation energy required for nucleation is typically greater than that required for crystal growth (e.g., Rodriguez-Blanco et al., 2011). This means that $CaCO_3$ precipitation proceeds more rapidly once calcium carbonate is already present in the system.

Cheng and Shahin (2016) presented a MICP stabilisation method using a "bioslurry". The bioslurry was prepared by adding equal moles of $CO(NH_2)_2$ and $CaCl_2$ into a Bacillus sp. culture. The resulting solution was stirred at a speed of 600 rpm for about 12 h. Because of the presence of $CO(NH_2)_2$ and Ca^{2+}, $CaCO_3$ crystals were formed due to urea hydrolysis catalysed by the bacteria. The bioslurry was then mixed with a pure silica sand (> 0.425 mm (0.53 %); 0.3 mm - 0.425 mm (50.78 %); 0.15 mm - 0.3 mm (45.96 %); and < 0.15 mm

(2.73 %)) resulting in more than 95 % of the bioslurry being retained in the soil matrix due to mechanical trapping. This stabilisation led to a high resistance during flushing with a low-salinity solution. To find the optimum conditions for bioslurry production, various concentrations of $CO(NH_2)_2$ and $CaCl_2$ were used corresponding to 50 mmol/L, 100 mmol/L, 200 mmol/L, 400 mmol/L, 600 mmol/L and 800 mmol/L. Figure 3.7 shows the linear relationship between the total amount of the bioslurry and the concentration of $CO(NH_2)_2$ and $CaCl_2$. For example, for the 800 mmol/L concentration about 8 g of bioslurry (dry weight) was produced from 100 mL bacterial culture, which was 16 times higher than the mass produced using a 50 mmol/L concentration. The bioslurries produced using different concentrations of $CO(NH_2)_2$ and $CaCl_2$ showed remarkably different specific urease activity (defined as the urease activity per dry weight of bioslurry). In particular, the specific urease activity decreased significantly with the increase in concentration of $CO(NH_2)_2$ and $CaCl_2$. The maximum specific urease activity was about 1050 U/g (where 1 U corresponds to the amount of enzyme which hydrolyses 1 Pmol $CO(NH_2)_2$ per minute at a pH of 7.0 and a temperature of 25 ºC) and was observed for a 50 mmol/L concentration. This value was about 15 times higher than that of the bioslurry produced using a concentration of 800 mmol/L. Higher concentration of $CO(NH_2)_2$ and $CaCl_2$ caused larger crystal precipitation, with the possible formation of a thick calcite layer around the bacterial cells. This thick crystal layer would reduce the $CO(NH_2)_2$ diffusion rate towards the bacteria. As suggested by Cuthbert et al. (2012), the growth of crystals on the surface of bacterial cells leads to a reduction of the ureolysis rate. It should be noted that, although the highest specific urease activity was obtained for a concentration of 50 mmol/L, the maximum total urease activity was instead obtained with a 400 mmol/L concentration. This is due to an optimal combination of bioslurry yield and specific urease activity. Note, however, that the optimum concentration of $CO(NH_2)_2$ and $CaCl_2$ obtained in this study may not be applicable to other bacterial cultures with different urease activity and biomass concentration.

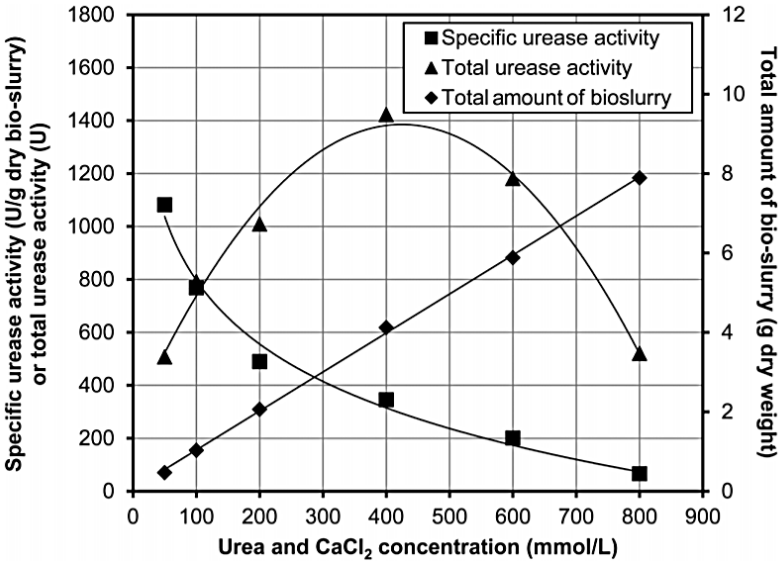

Figure 3.7: Specific urease activity, total amount of bioslurry and total urease activity for 100 mL of raw bacterial culture using varied concentrations of $CO(NH_2)_2$ and $CaCl_2$ (from Cheng and Shahin, 2016).

Figure 3.8 shows that the maximum $CaCO_3$ precipitation (21.9 g) was obtained with a 400 mmol/L concentration, which is also the concentration generating the maximum urease activity (Figure 3.7).

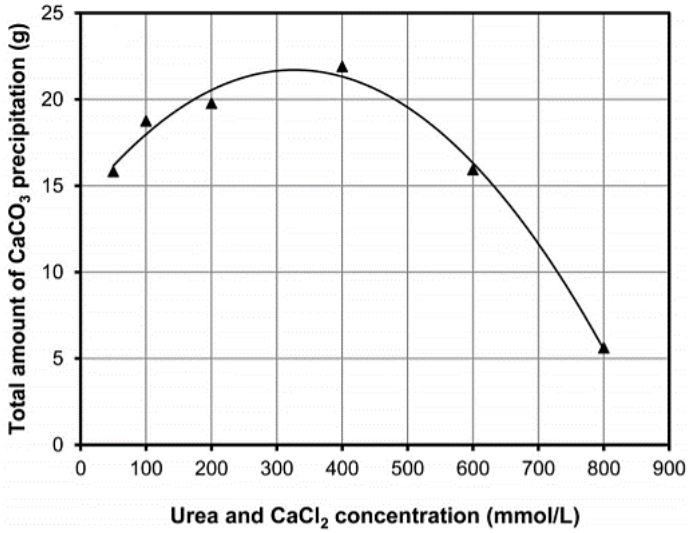

Figure 3.8: Relationship between amount of $CaCO_3$ precipitation and concentration of urea and calcium chloride in 100 mL of raw bacterial culture (from Cheng and Shahin, 2016).

Cheng and Shahin (2016) also conducted a microscopy analysis of dried bioslurry and cemented soil samples. Results revealed the localisation of large rhombohedral $CaCO_3$ crystals around the bioslurry spherical fine crystals (Figure 3.9d,e,f). These rhombohedral crystals were not observed in the pure bioslurry sample without $CO(NH_2)_2$ and $CaCl_2$ (Figure 3.9a,b,c).

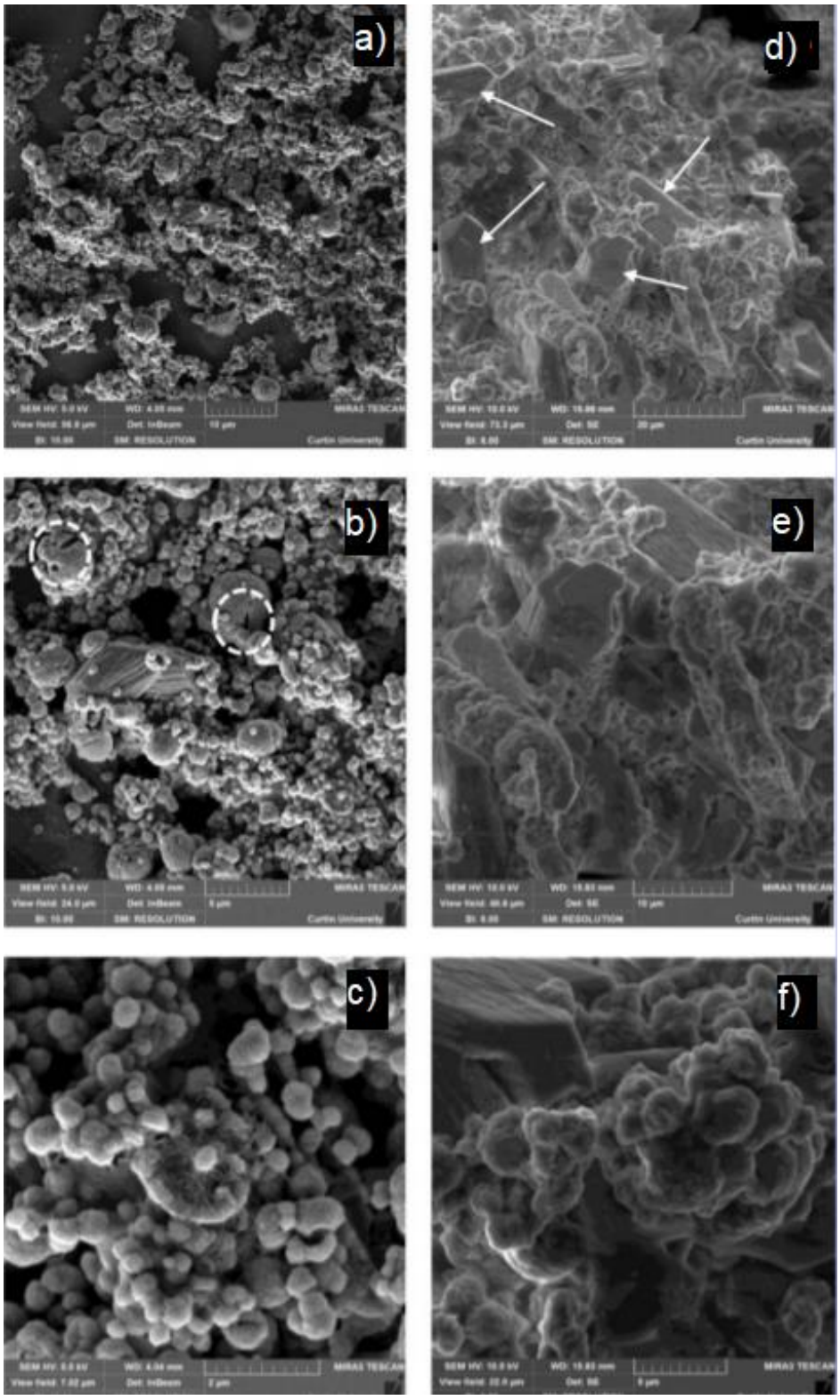

Figure 3.9: Scanning electron microscopy (SEM) images of pure bioslurry produced from 400 mmol/L $CO(NH_2)_2$ and $CaCl_2$ (d., e, f) and the same bioslurry without $CO(NH_2)_2$ and $CaCl_2$ (a, b, c) (from Cheng and Shahin, 2016).

The absence of the imprints of bacterial cells on the rhombohedral surface suggests that a pure chemical reaction might have occurred during precipitation of this type of crystal. This in turn suggests a diffusion mechanism of CO_3^{2-} ions from the inside of the bacterial cells

(where urea hydrolysis occurs) towards the surrounding solution where precipitation of rhombohedral crystals occurs once supersaturation of Ca^{2+} and CO_3^{2-} is achieved (Al-Thawadi and Cord-Ruwisch, 2012). The rhombohedral crystals of cubic faces are a typical form of calcite (De Yoreo and Vekilov, 2003). No stabilisation was obtained when the pure bioslurry was mixed with sand without addition of cementation solution containing $CO(NH_2)_2$ and $CaCl_2$ (data not shown).

In conclusion, Cheng and Shahin (2016) suggested that the bioslurry itself without $CO(NH_2)_2$ and $CaCl_2$ could not provide a bonding force between sand grains. On the contrary (similarly to the calcite crystals which precipitation is induced by ureolytic bacteria) the crystals precipitated by using the bioslurry and the cementation solution were able to adhere to the sand particle surface, connecting them together and improving soil strength improvement. A number of bioslurry treated sand specimens, with an aspect ratio between 1:1.5 and 1:2, were produced for mechanical testing. Prior to the test, the samples were flushed with at least five void volumes of tap water to wash away any excess soluble salts and subsequently dried at 105 °C for at least 24 hours. The specimens were then axially loaded at a constant rate of 1.0 mm/min to measure unconfined compressive strength (ASTM D2166, 2013). Multiple tests were performed on soil specimens treated with different flushes of cementation solution.

Cheng and Shahin (2016) found that the unconfined compressive strength increased with the number of flushes (Figure 3.10a). However, the rate of strength improvement decreased with the number of flushes, probably due to the lower chemical efficiency in each subsequent flush (Figure 3.10a) and the decreased urease activity because of the encapsulation of bacterial cells inside a layer of $CaCO_3$. Figure 3.10b shows the stress–strain curves of the bioslurry treated soils. It can be seen that a fewer numbers of flushes produce a more ductile behaviour compared to the samples treated with a higher number of flushes. It was also found that the tangent Young's modulus increased with the number of flushes from 7 MPa (one flush) to 190 MPa (eight flushes). Cheng and Shahin (2016) emphasised the potential of the proposed bioslurry approach, as an alternative to the injection of a bacteria-cementation solution, by highlighting the significant improvement of mechanical strength with number of flushes.

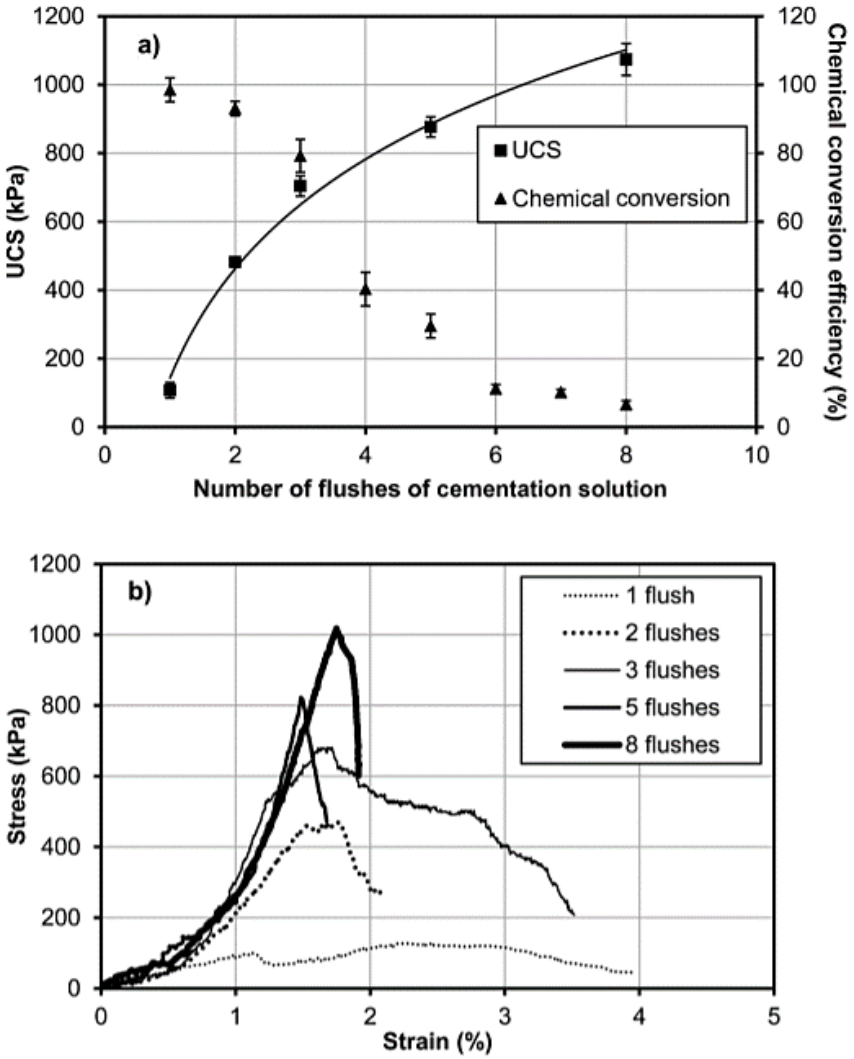

Figure 3.10: Effect of cementation solution flushes on the mechanical response of bioslurry treated sand: UCS (a) and stress–strain curves (b) (from Cheng and Shahin, 2016).

An experimental study was undertaken by Morales et al. (2015) to investigate the possibility of stabilising compacted soils by means of soft bio-mediated treatment. This bio-mediated treatment consisted in the addition of microorganisms to the compaction water content while relying on the natural presence of urea and calcium ions in superficial soils. This research presents a valuable contribution to the biological treatments of compacted soils, which is a rather neglected research area in the existing literature. Morales et al. (2015) opted for a silty clayey sand from South-East Spain, which is widely used in earthwork construction. Microorganisms of the Bacillaceae family were added to the compaction water content, without sterilising the soil prior to inoculation. The soil was then compacted at water contents between 0.13 and 0.15, and was allowed to age at a relative humidity higher than 97 % for a minimum of 7 days. The bacterial activity was then stopped by increasing temperature so that it did not interfere with the following tests.

Figure 3.11 shows the grain size distributions of both untreated and treated soils indicating that the biological treatment tends to aggregate soil particles, thus resulting in a coarser material. In particular, the grain size distribution of the untreated soil is characterised by a dominant grain size around 10 mm, which increases to 20 mm in the treated material.

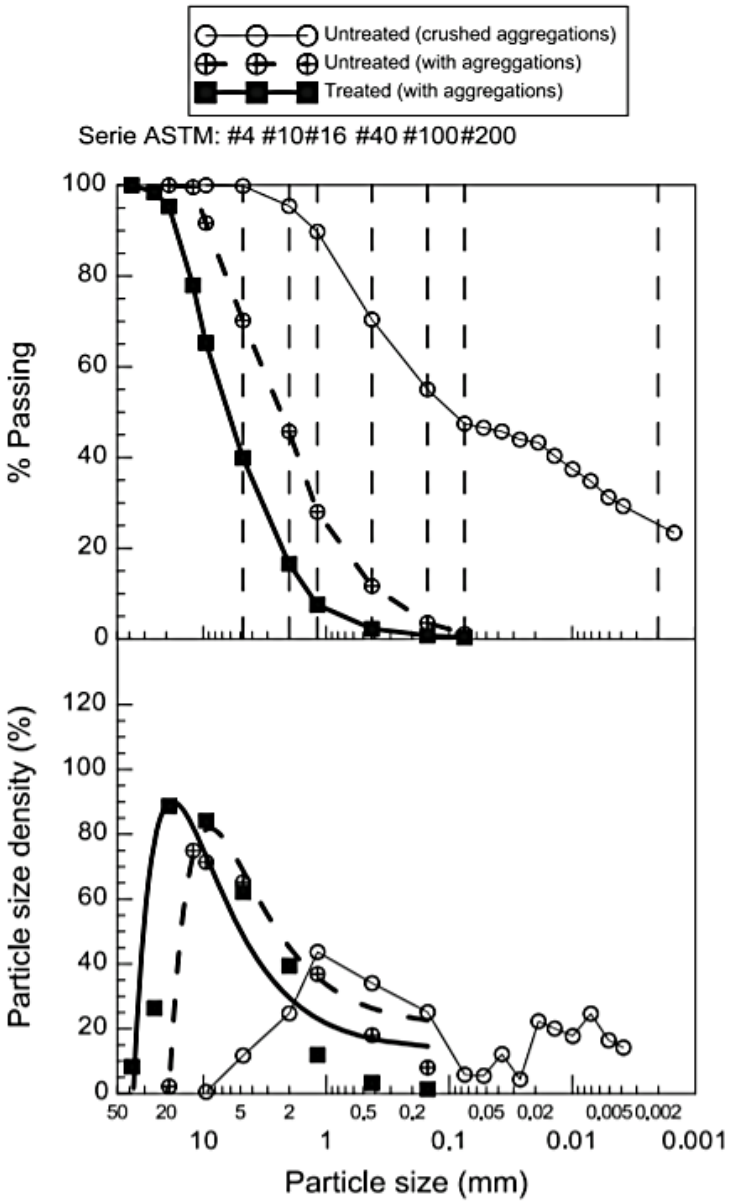

Figure 3.11: Grain size distribution and grain size density function of untreated and treated soils (from Morales et al., 2015).

Figure 3.12 compares the compaction curves of the untreated soil at four energy levels of ½ Standard Proctor (1/2 SP at 0.3 MJ/m^3), Standard Proctor (SP at 0.6 MJ/m^3), 2 Standard Proctor (2SP at 1.2 MJ/m^3) and Modified Proctor (MP at 2.7 MJ/m^3). The treated soil was also dynamically compacted after ageing at a Standard Proctor energy level to isolate the effect of bio-mediated treatment from that of compaction energy.

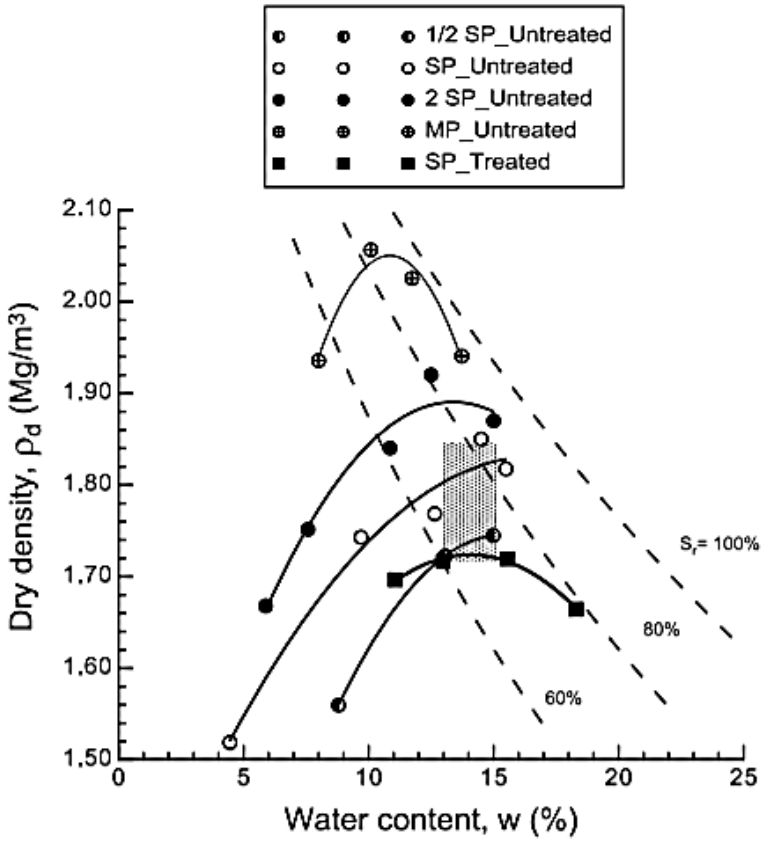

Figure 3.12: Compaction curves at different energy levels for treated and untreated soils. The shaded area represents the as-compacted conditions used in the test programme (from Morales et al., 2015).

Inspection of Figure 3.12 indicates that the aggregates formed during ageing limit the efficiency of compaction in reducing the void ratio because part of the energy is dissipated by breaking the coarser aggregates and the organogenic bonds. The compacted treated soils has a higher void ratio compared to the untreated soil. In particular, for the treated material, a dry density of 1.72 Mg/m^3 is reached at the optimum water content of 0.15 corresponding to the bottom of the shaded area in the Figure 3.12. This approximately coincides with the dry density obtained using 1/2 Standard Proctor energy on the untreated material.

The microstructural features of both untreated and treated soils were also studied by scanning electron microscopy (SEM). Different structures can be identified in Figure 3.13, namely calcified bacteria and calcite crystals (Figure 3.13a). In particular, Figure 3.13b shows carbonate crystals filling the large inter-grain pores (bio-filling) and bonding soil grains (bio-cementation). Morales et al. (2015) demonstrated that bio-filling takes place within pores with sizes from 3 to 50 µm. This is compatible with the vital space required by bacteria, which have a size of around 1 µm.

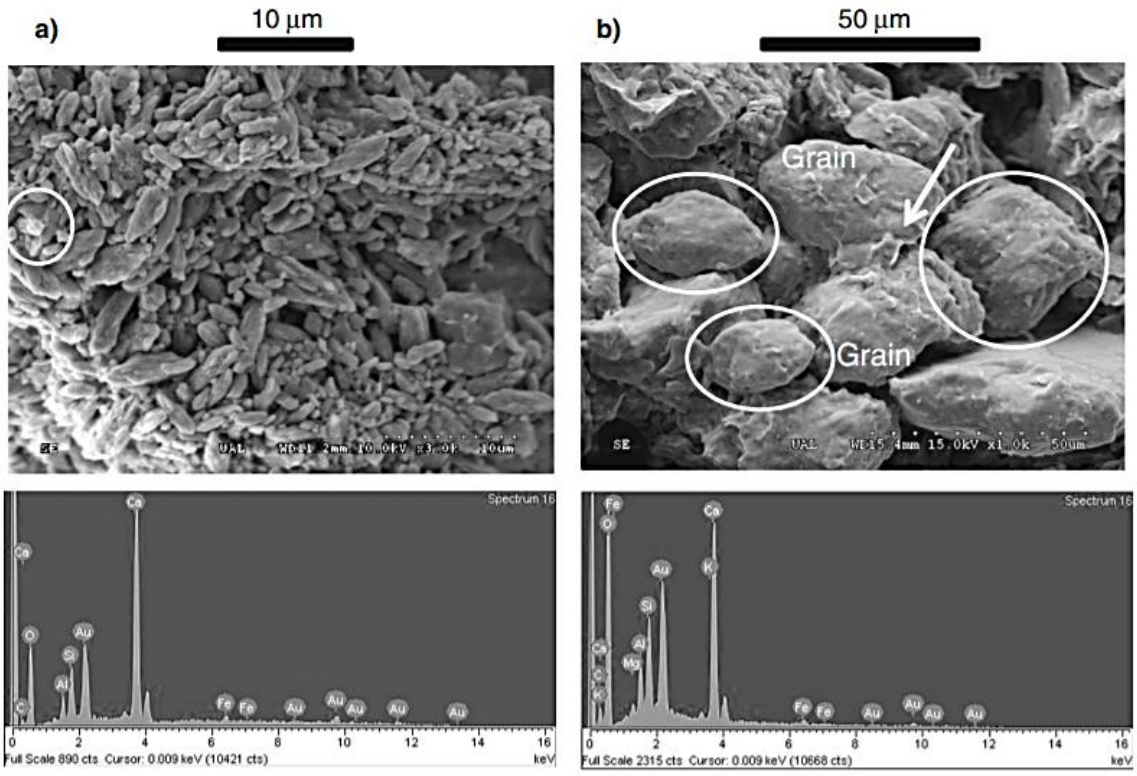

Figure 3.13: SEM images of treated samples before compaction: photomicrograph with calcified bacteria and calcite crystals (a); photomicrograph with calcite crystals located between grains of soil (b) (from Morales et al., 2015).

Direct shear tests were performed on both untreated and treated samples (compacted after treatment) to analyse the strength of the soil. The tests were performed on saturated samples to mimic the condition in the field during water infiltration. The initial void ratio was 0.47 for the untreated soil and 0.59 for the treated soil. Shearing was performed at a controlled displacement rate of 0.005 mm/min, which ensured drained conditions. All samples contracted on shearing but the treated soil displayed slightly higher shear strength (Figure 3.14). This is reflected in a friction angle of about 40 ° for the treated soil compared to about 38° for the untreated soil. Note that, although the treated samples were compacted at a lower density, they still exhibit higher shear strength than the denser untreated samples. This is because the intermediate pore classes between 3 µm and 50 µm, corresponding to inter-grain or inter-aggregate porosity, are partially filled with calcite crystals thus increasing the friction angle.

Morales et al. (2015) highlighted that the shear strength envelopes of both treated and untreated soils samples pass through the origin (Figure 3.14). This suggests that the treatment does not provide any cohesion but just an increase of friction angle.

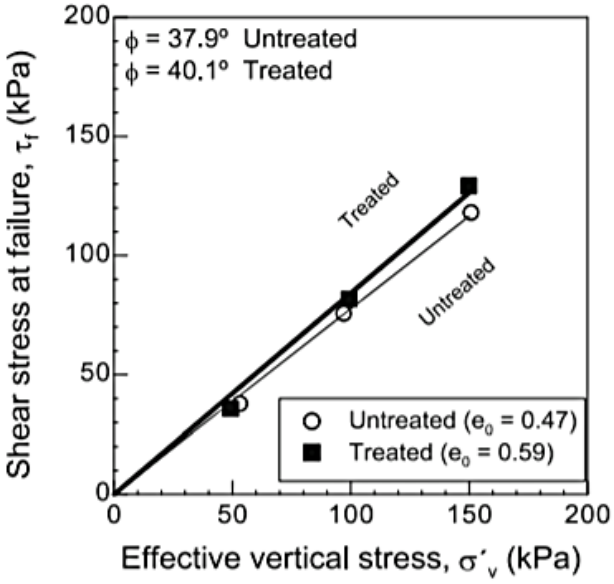

Figure 3.14: Shear strength envelopes for untreated and treated soils (from Morales et al., 2015).

3.3. Enzymatic induced calcite precipitation (EICP)

Most studies about microbially induced calcite precipitation (MICP) focus on coarse-grained materials (i.e., sands) due to the physical limitations associated to the migration of micro-organisms through the pores of fine-grained materials (i.e., clays and silts). For example, the S.pasteurii bacteria has a size of few microns, which tends to be larger than most pores in fine-grained soils. The direct use of the urease enzyme has therefore been recently proposed as an alternative to the cultivation of bacteria in the soil (Nam et al., 2015), which has led to a new stabilisation method referred to as enzyme induced calcite precipitation (EICP). Note that the molecule of the urease enzyme has a size of around 12 nm and therefore fits well in small pores. Several families of plants are very rich in urease, including some varieties of beans (jack beans and soybeans) or seeds (melon, pumpkin and pineapple). The urease enzyme can also be purchased from chemical suppliers as a synthesised product, which tends however to be very expensive. Furthermore, the urease enzyme has a relatively short life span with an activity that naturally degrades with time (Pettit et al., 1976) whereas microbial colonies remain alive inside the soil long after the stabilisation reactions have occurred with potential negative impacts on the ecosystem.

3.3.1. Role of urease in plant metabolism

Nitrogen is a crucial element in plant nutrition and enzymes play an essential role in the metabolism of all organisms. In particular, an efficient recycling of reduced nitrogen in the form of urea is essential for plant growth (Polacco and Holland, 1993). There are at least

three key enzymes involved in urea metabolism in plants, namely the arginase, urease and glutamine synthetase. Sirko and Brodzik (2000) described the urea metabolism in plants as a process by which the nitrogen from proteins and other compounds is constantly recycled (Figure 3.15).

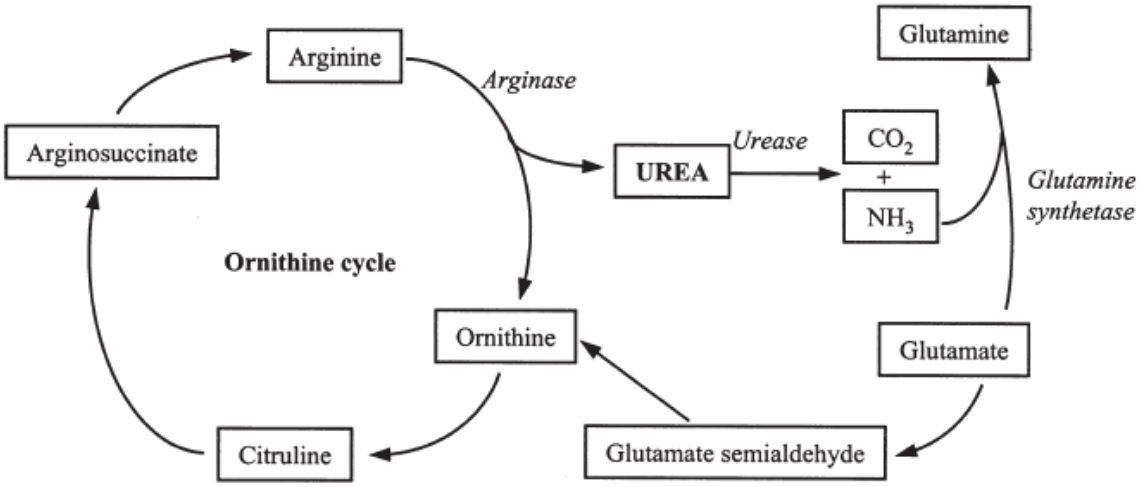

Figure 3.15: Urea metabolism in plants (from Sirko and Brodzik, 2000).

Urease allows the plant to use external and internally generated urea as a nitrogen source (Mobley and Hausinger, 1989; Mobley et al., 1995). In fact, the nitrogen present in the urea produced from arginine or the degradation of purines and ureides (Polacco and Holland, 1993) is not usable by plants unless hydrolysed by urease. The ammonia, which is the result of the urease activity, is finally incorporated into organic compounds by glutamine synthetase thus controlling the nitrogen metabolism in plants and plant growth itself (Stitt, 1999; Von Wirén et al., 2000). Urease is also the only nickel-containing metalloenzyme yet identified in plants according to Polacco and Holland (1993). Successive studies by Gerendas et al. (1998) have demonstrated the importance of nickel for urease activity by observing that urea-grown nickel-deprived rice plants (Oriza sativa) reduced in growth and accumulated larger amounts of urea due to reduced urease activity. Urease from jack beans (Canavalia ensiformis) was the first enzyme ever purified and crystallised in 1926, an achievement of James B. Summer (Nobel Prize in Chemistry in 1946).

3.3.2. Recent advances in enzymatic induced calcite precipitation (EICP)

Park et al. (2014) explored the efficiency of urease enzyme from jack beans to precipitate calcite within a sand from the Nakdong River. Ten grams of a calcium salt, such as calcium chloride (CC), calcium hydroxide (CH) and calcium nitrate (CN), were dissolved into a

solution of urea containing plant derived urease before mixing it with the sand. Three different amounts of jack bean extract and urea were considered in this investigation as presented in Table 3.2. The mixed sand was then compacted into cylindrical specimens, which were cured for 3 days at room temperature. Control specimens without the urease extract were also prepared for comparison (Table 3.2). Results from unconfined compression tests are shown in Figure 3.16, which demonstrates that the unconfined compressive strength (UCS) of the treated sand augments, up to 317 kPa, as the amount of urea increases. Specimens CC-0, CH-0, and CN-0 were prepared without jack bean extract so that no calcite precipitation occurred within the sand matrix in this case. Specimens CC-0, CH-0, and CN-0, which were prepared without jack bean extract so that no calcite precipitation occurred, exhibited the lowest unconfined compressive strength. Moreover, the specimens containing calcium chloride experienced higher compressive strength compared to the specimens containing calcium hydroxide or calcium nitrate (Figure 3.16). This may be due to the relatively low solubility of calcium hydroxide and calcium nitrate resulting in a lower concentration of calcium ions and a consequent reduction of calcite precipitation. Park et al., 2014 suggested that the increase of strength achieved through bio-cementation was similar to that obtained with 4% of high-early strength Portland cement.

Table 3.2: Summary of unconfined compression tests (after Park et al., 2014).

Test ID	**Calcium source**	**Urea/Water [g/mL]**	**Jack bean extract [mL]**	**Unconfined compressive strength [kPa]**	**Precipitated calcite [%]**
CC-0	Calcium chloride	25/50	0	30	0
CC-1		5/50	5	90	2.34
CC-2		10/50	10	160	6.37
CC-3		25/50	25	317	6.58
CH-0	Calcium hydroxide	25/50	0	89	0
CH-1		5/50	5	129	3.44
CH-2		10/50	10	197	4.02
CH-3		25/50	25	244	4.52
CN-0	Calcium nitrate	25/50	0	68	0
CN-1		5/50	5	104	2.91
CN-2		10/50	10	209	3.50
CN-3		25/50	25	253	4.72

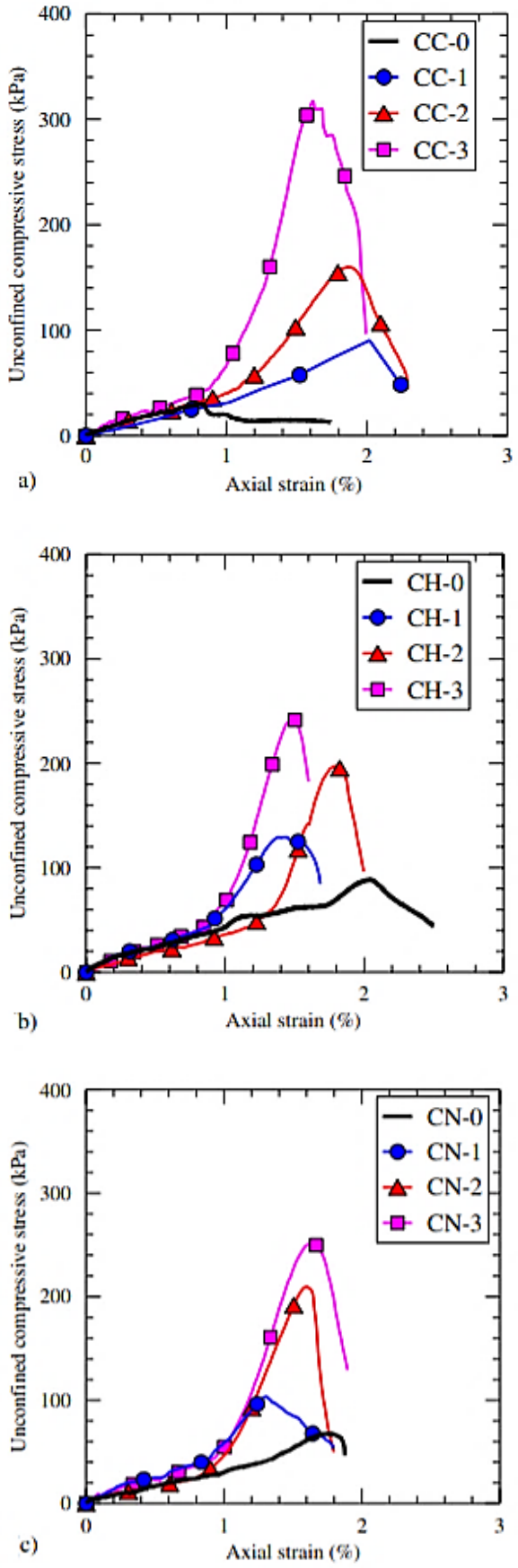

Figure 3.16: Results of unconfined compression tests: Calcium chloride (CC) (a); Calcium hydroxide (CH) (b); Calcium nitrate (CN) (c) (from Park et al., 2014).

Scanning electron microscope (SEM) images were obtained to evaluate the degree of cementation corresponding to different amounts of jack bean extract and urea. Figure 3.17 shows images with a magnification of 100 times indicating the precipitation of larger amounts of calcite when larger amounts of jack bean extract and urea were used, regardless of the calcium source.

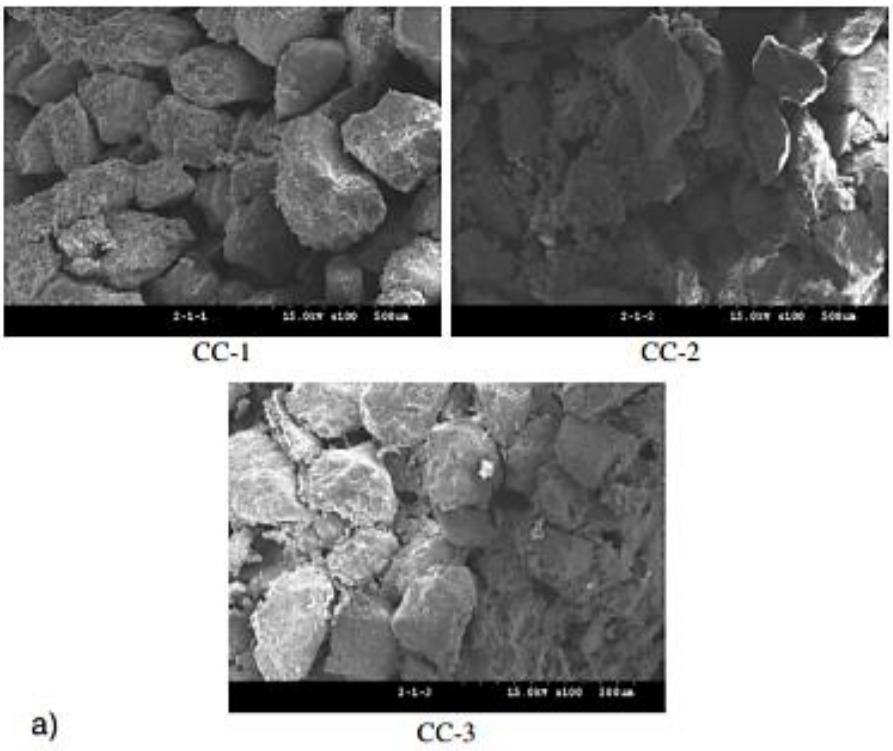

CC-1 CC-2

CC-3

a)

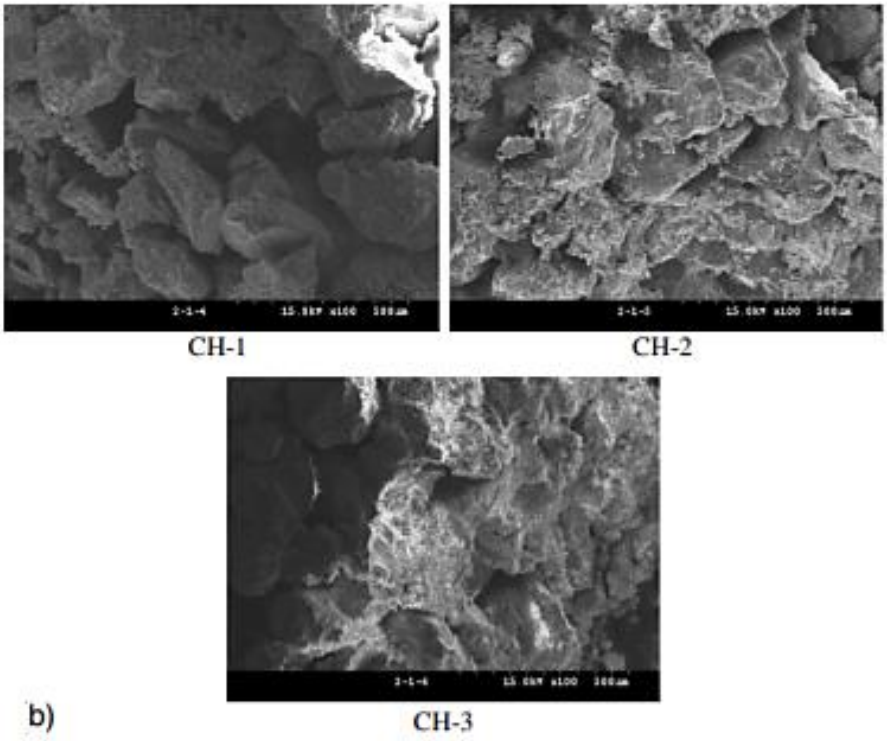

CH-1 CH-2

CH-3

b)

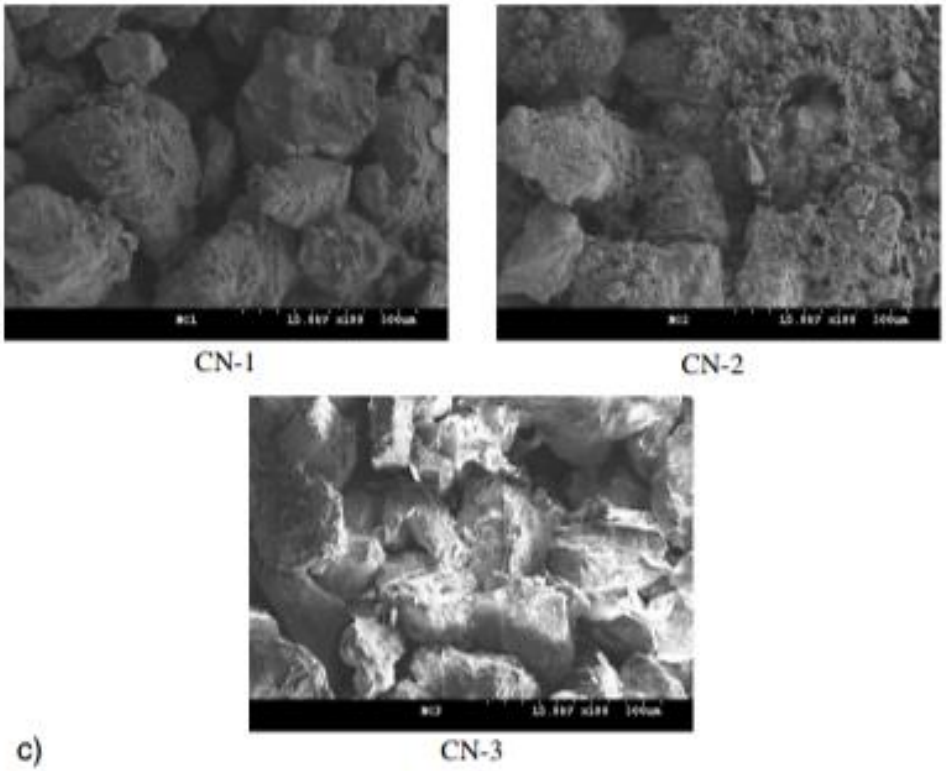

Figure 3.17: Scanning electron micrographs of EICP stabilised sand: CC-calcium chloride (a), CH-calcium hydroxide (b), CN-calcium nitrate (c) (from Park et al., 2014).

The precipitation of calcite was qualitatively analysed by XRD analysis (Figure 3.18). As the amount of urea and jack bean extract increased, the amount of precipitated calcite gradually increased, regardless of the calcium source. The amount of precipitated calcite within the sand matrix was between 2.34 % and 6.58 % depending on the amount of jack bean extract and urea (Figure 3.19). The unconfined compressive strength was also directly correlated with the precipitated amount of calcite. This is also consistent with other studies (Whiffin et al., 2007; Van Paassen et al., 2010), which showed that strength and stiffness increase with growing amounts of precipitated calcite, with at least 4 % of calcite being required for a substantial increase of strength.

Carmona et al. (2016) analysed the effect of urea and calcium chloride amounts on the precipitation induced by the urease enzyme. The enzyme was purchased from Sigma Aldrich Company Ltd. in powder form and presented an activity of 34.310 U/g. The soil was an inorganic sandy soil with a uniform grain size distribution (gravel = 15.5 %, sand = 78.7 %; silt = 3.5 %; clay = 2.3 %) and was classified as poorly graded sand (ASTM D2487, 2000). A cementing grout was produced by mixing the urease enzyme with urea ($CO(NH_2)_2$) and calcium chloride ($CaCl_2$) with purity levels of 99.5 % and 95 %, respectively. The bio-calcification process was initially studied in test-tube experiments to verify the existence of

$CaCO_3$ through XRD analysis and evaluate the amount of precipitation. Afterwards, unconfined compression tests were run to examine the strengthening effects of the bio-treament. Bio-treated samples were compacted with an energy corresponding to Standard Proctor and left 14 days for curing inside a room with controlled humidity (60 ± 5 %) and temperature (20 ± 2 ºC).

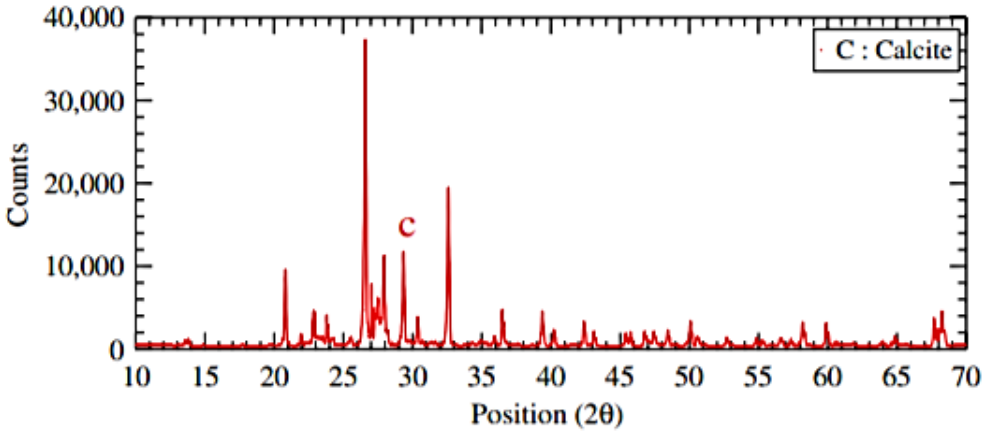

Figure 3.18: Result of X-ray diffraction analysis (from Park et al., 2014).

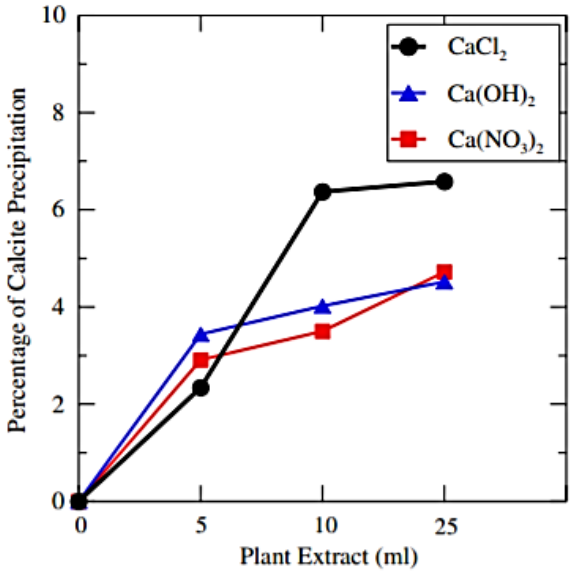

Figure 3.19: Relationship between calcite precipitation and amount of plant extract for specimens treated with calcium chloride, calcium hydroxide and calcium nitrate (from Park et al., 2014).

Water solutions of urea-$CaCl_2$, with equimolar concentrations of 0.25 mol/L, 0.5 mol/L, 0.75 mol/L, 1.0 mol/L and 1.25 mol/L were prepared to examine the rate of urea hydrolysis. The amount of urease used in all the tests was instead constant and equal to 4 kU/L. The different solutes were thoroughly mixed with water to guarantee complete dissolution. After 14 days, the amount of precipitated material was evaluated as follows: (i) the solution was filtered through filter paper; (ii) the filter paper and the test-tube were dried and the amount of the

deposited particles was evaluated; (iii) the total amount of $CaCO_3$ was calculated from the addition of the material deposited on the filter paper and in the test tube. The precipitation ratio (PR) was defined as the ratio between the actual mass of precipitated calcite $M^a_{CaCO_3}$ measured as described above and the theoretical mass of precipitated calcite $M^t_{CaCO_3}$ calculated from the chemical reactions of Equations 3.1 – 3.6. The precipitation ratio was therefore defined by the following expression:

$$PR(\%) = \frac{M^t_{CaCO_3}}{M^a_{CaCO_3}} \times 100 = \frac{C \times V \times M}{M^a_{CaCO_3}} \times 100 \qquad (3.7)$$

where C is the concentration of the solution in mol/L, V is the solution volume in liters, and M is the molar mass of calcite (100.087 g/mol). Figure 3.20 illustrates the effect of the equimolar concentration of the urea-$CaCl_2$ solution on the precipitation ratio. The results show that the precipitation ratio is about 95 % for the lowest concentration of urea-$CaCl_2$ (0.25 mol/L), which means that in this case almost all the urea is hydrolised. An increase of urea-$CaCl_2$ concentration induces a reduction of efficiency, i.e. the precipitation ratio decreases, which means that a large part of urea is not hydrolysed. This may be due to an insufficient quantity of urease enzyme and/or due to a negative effect of high urea-$CaCl_2$ concentrations, which tend to inhibit the urease activity, thus making catalysation less effective.

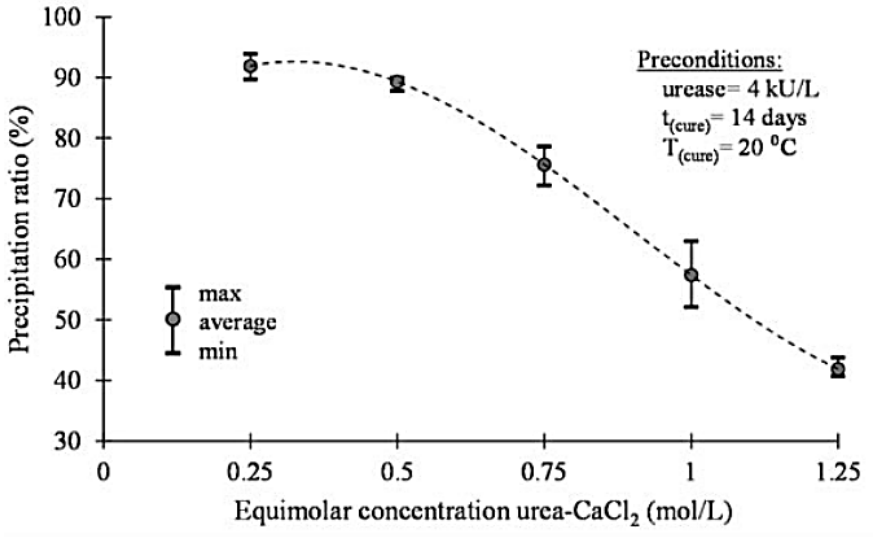

Figure 3.20: Test-tube experiments: relation between urea-$CaCl_2$ concentration and $CaCO_3$ precipitation ratio (from Carmona et al., 2016).

A XRD test was also performed on the precipitated material for the solution with 0.5 mol/L of urea-$CaCl_2$ (Figure 3.21). This test showed that the precipitated material mainly consisted

of calcite, i.e. $CaCO_3$, thus confirming the occurrence of the reactions described in Equations 3.1 - 3.3.

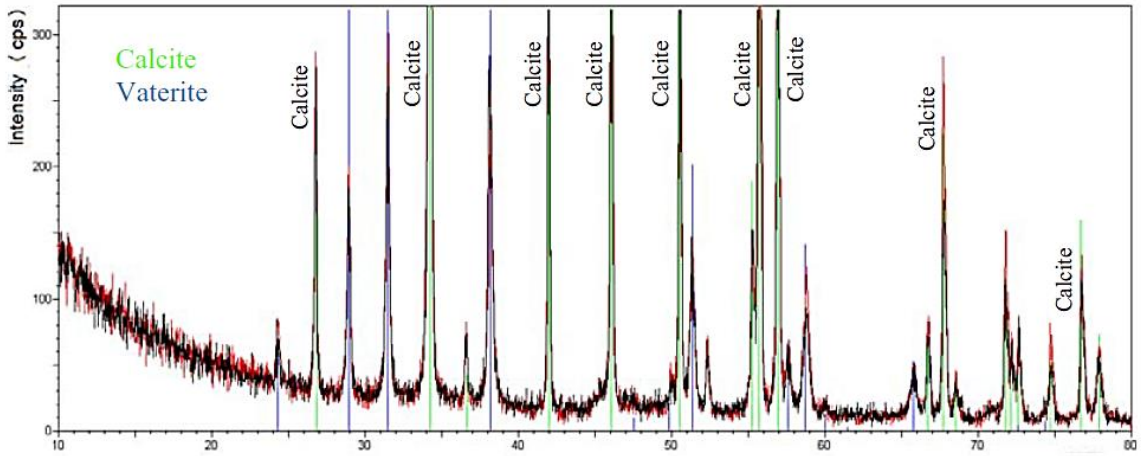

Figure 3.21: Test-tube experiments: XRD tests on precipitated material from 0.5 mol/L urea-$CaCl_2$ solution (from Carmona et al., 2016).

Figure 3.22 shows the results from unconfined compression tests (ASTM D2166, 2013) on soil specimens stabilised with a constant urease concentration (4 kU/L) and different urea-$CaCl_2$ concentrations (0.25 mol/L - 1.25 mol/L). The stress-strain curves in Figure 3.22a confirm the effectiveness of the bio-treatment that leads to an increase of unconfined compressive strength up to a maximum value of about 140 kPa, In particular, the results show a quasi-linear decrease of q_u with the increment of the urea-$CaCl_2$ concentration from about 140 kPa to 50 kPa, for a variation of urea-$CaCl_2$ concentration from 0.25 mol/L to 1.25 mol/L. The stress-strain curves also highlight that specimens treated with lowest concentration of urea-$CaCl_2$ are stiffer due to the presence of calcite minerals in the void spaces and/or around soil particles. Figure 3.22b shows that the unconfined compressive strength tends to be higher for small concentrations of $CO(NH_2)_2$-$CaCl_2$ decreasing almost linearly with growing $CO(NH_2)_2$-$CaCl_2$ concentration from about 140 kPa to 50 kPa for a variation of $CO(NH_2)_2$-$CaCl_2$ concentration from 0.25 mol/L to 1.25 mol/L. This result is consistent with the test-tube experiments as a decrease of $CaCO_3$ precipitation causes a reduction of the bonds between particles. In conclusion, the best urea-$CaCl_2$ concentration was 0.25 mol/L, at least for the chosen urease concentration of 4 kU/L, while higher concentrations of urea-$CaCl_2$ inhibited the activity of the enzyme, leading to a decrease in calcite precipitation and hence a weaker material.

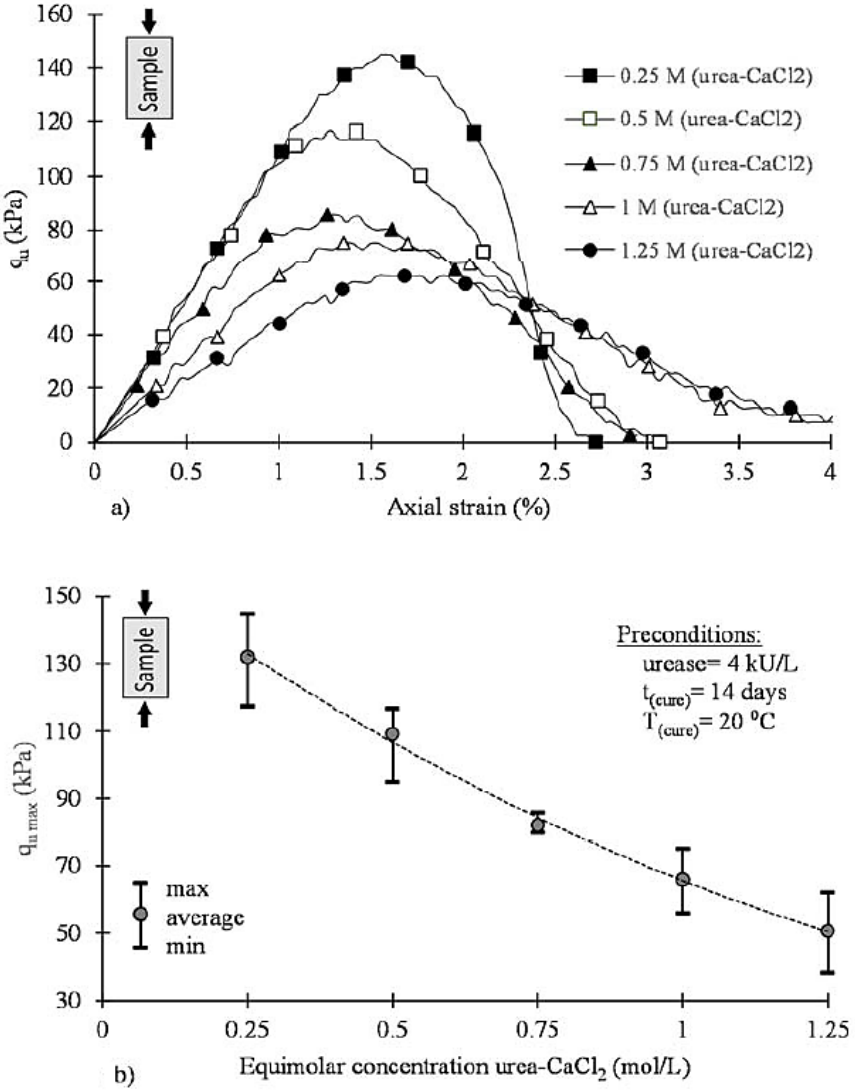

Figure 3.22: Unconfined compressive strength of soil specimens bio-stabilised with different urea-$CaCl_2$ concentrations: stress-strain curves (a); variation of strength with urea-$CaCl_2$ concentration (b) (from Carmona et al., 2016).

4. Materials and methods

This chapter describes some of the properties of the earth tested in the present work as well as the compaction procedures to manufacture both cylindrical samples and bricks. The chapter also presents the experimental methods for the preparation and the characterisation of the soybeans extract, which has been used as a source of the urease enzyme for the stabilisation of the earth material.

4.1. Material characterisation

The base soil used in the present work has been provided by the brickwork factory Bouisset from the region of Toulouse (France). The Bouisset soil was chosen among five different soils from five distinct brickwork factories in France (Barthe, Bouisset, Capelle, Nagen, Saves), which were tested in a separate project (TERCRUSO, 2013). In fact, the Bouisset soil exhibited comparable hygro-mechanical performance and the best durability properties against water erosion of all five materials (TERCRUSO, 2013), which is the reason why it was selected in the present work as a base soil.

4.1.1. Grain size distribution

The grain size distribution of the base soil was determined by means of wet sieving and sedimentation tests in compliance with the norms XP P94-041 (AFNOR, 1995) and NF P 94-057 (AFNOR, 1992). Figure 4.1 shows the grain size distribution of the base soil obtained as the average of three independent tests. Figure 4.1 presents also the lower and upper limits of the particle size distribution as recommended by different guidelines for the manufacture of compressed earth bricks (AFNOR, 2001; CRATerre-EAG, 1998; MOPT, 1992). Inspection of Figure 4.1 indicates that the base soil exhibits a well graded grain size distribution that lies marginally outside the recommended region. In particular, the soil appears to be slightly finer than the limit prescribed by the recommendations. This small violation of current recommendations is however considered to be acceptable for the purposes of the present work.

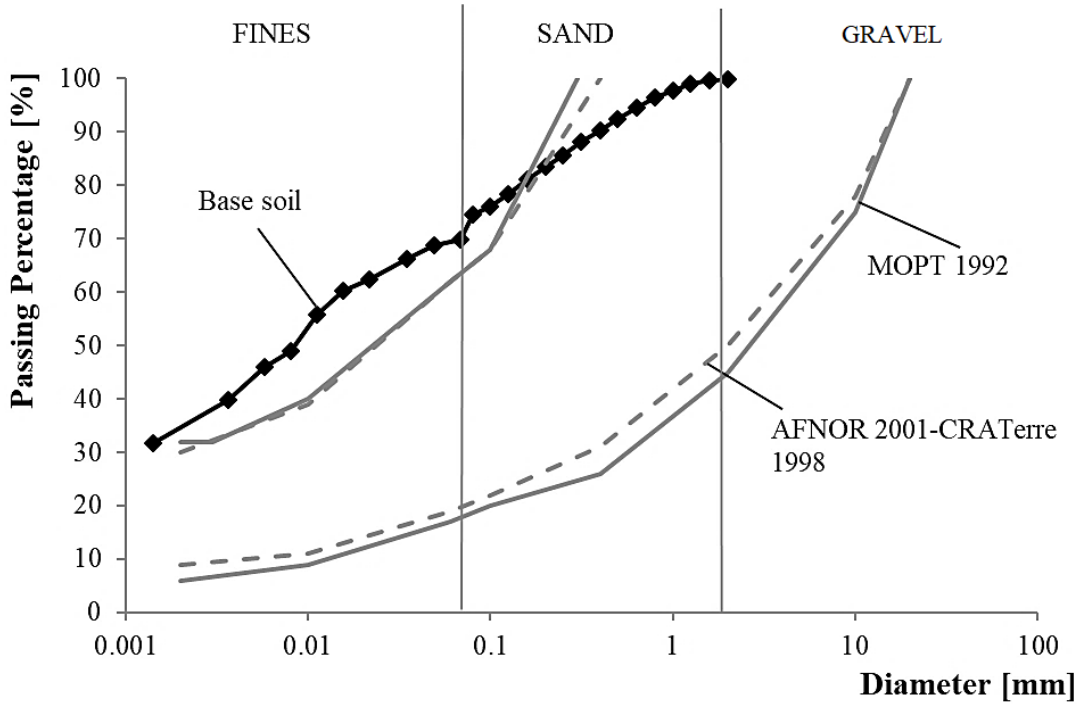

Figure 4.1: Grain size distribution of the base soil in relation to existing recommendations for the manufacture of compressed earth bricks by AFNOR (2001); CRATerre-EAG (1998) and MOPT (1992).

4.1.2. Specific gravity, plasticity and clay activity

The specific gravity of the solid particles G_s was measured by means of pycnometer tests, according to the French norm NF P 94-054 (AFNOR, 1991), as the average of four independent measurements and the result is given in Table 4.1.

The plasticity properties of the fine fraction (i.e. the fraction smaller than 0.400 mm) of the base soil were instead measured according to the French norm NF P94-051 (AFNOR, 1993). In particular, the Atterberg limits, i.e. the liquid limit w_L, plastic limit w_P and plasticity index I_P, were all determined as the average of four independent measurements and are also given in Table 4.1.

Table 4.1: Main properties of the base soil from the Bouisset brickwork factory.

Grain size distribution	
Gravel content (> 2 mm, %)	0
Sand content (≤ 2 mm, %)	31
Silt content (≤ 63 μm, %)	35
Clay content (≤ 2 μm, %)	34
Specific gravity G_s	2.65
Atterberg limits	
Plastic limit w_P (%)	18.7
Liquid limit w_L (%)	29.0
Plasticity index I_P(%)	10.3
Clay activity A	0.30

Figure 4.2 shows the plasticity characteristics of the base soil with reference to the Casagrande chart, which indicates that the material can be classified as low plasticity clay. Note also that the base soil fits inside the recommended plasticity regions for the manufacture of compressed bricks according to Houben and Guillaud (1994) and AFNOR (2001); CRATerre–EAG (1998), respectively.

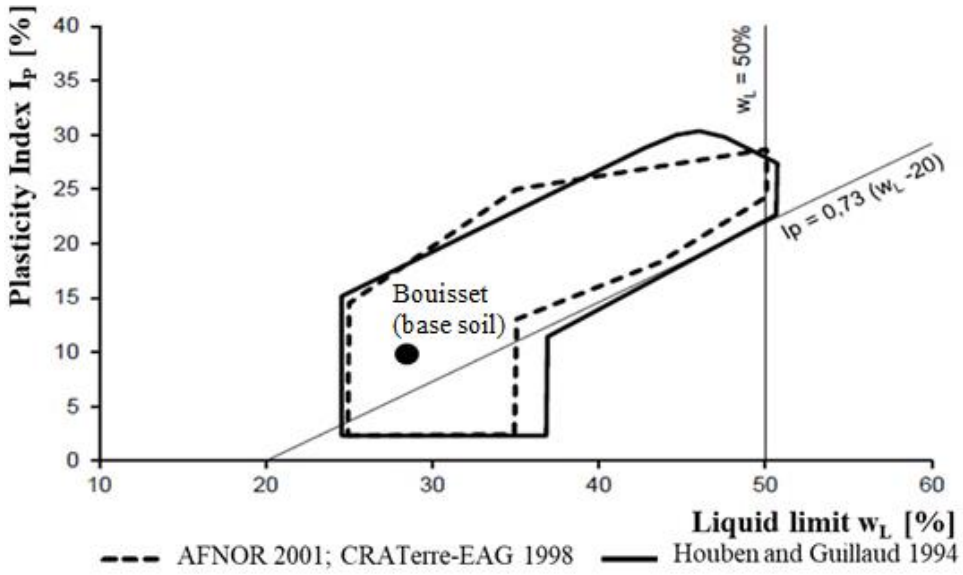

Figure 4.2: Plasticity properties of the base soil from the Bouisset brickwork factory in relation to existing recommendations for the manufacture of compressed earth bricks by AFNOR (2001); CRATerre-EAG (1998) and Houben and Guillaud (1994) (after Bruno, 2016).

The hydro-mechanical behaviour of earth materials is significantly influenced by the nature of the clay fraction, which is therefore an important characteristic to be considered during selection of the base soil. Previous mineralogical studies of the Bouisset soil (TERCRUSO, 2013) have indicated a predominantly kaolinitic clay fraction, which makes the material suitable for construction with small swelling/shrinkage upon wetting/drying cycles. Another measure of the soil sensitivity to water is the clay activity *A*, which is defined as the ratio between the plasticity index and the percentage clay fraction (i.e. the percentage fraction of the soil that is smaller than 0.002 mm). For the Bouisset soil used in the present work, the clay activity has been established to be 0.30, which classifies the clay fraction as low active (Skempton, 1953).

The grain size distribution and index properties of the base soil are all summarised in Table 4.1, which indicates that the soil can be classified as a well graded silty clay.

4.1.3. Optimisation of soil mix

The base soil was blended with different proportions of a silica sand to obtain three distinct

earth mixes with different clay contents spanning the entire range of the recommended region. Table 4.2 shows the percentages of the base soil and added sand together with the corresponding clay content (i.e. the fraction of particles with sizes smaller than 0.002 mm) for each earth mix. Earth mix 1 contains only the base soil and therefore coincides with the original material provided by the Bouisset brickwork factory. Earth mixes 2 and 3 however, contain about 1/3 and 2/3 of sand by mass, respectively (note that the fractions refer to the overall mass of the dry soil), which produces an increasingly coarser material as reflected by the decreasing clay content in Table 4.2.

Table 4.2: Composition of the different earth mixes.

Material	Base soil percentage [%]	Added sand percentage [%]	Clay content [%]
Earth mix 1 (base soil)	100	0	≈32
Earth mix 2	66	34	≈20
Earth mix 3	32	68	≈10

Figure 4.3 shows the particle size distributions of the three earth mixes together with the recommended upper and lower limits suggested by AFNOR (2001); CRATerre-EAG (1998) and MOPT (1992) for compressed earth bricks. Figure 4.4 shows the grain size distribution of the added sand, whose grading is rather monodisperse with most particles having a size comprised between 0.06 and 2 mm.

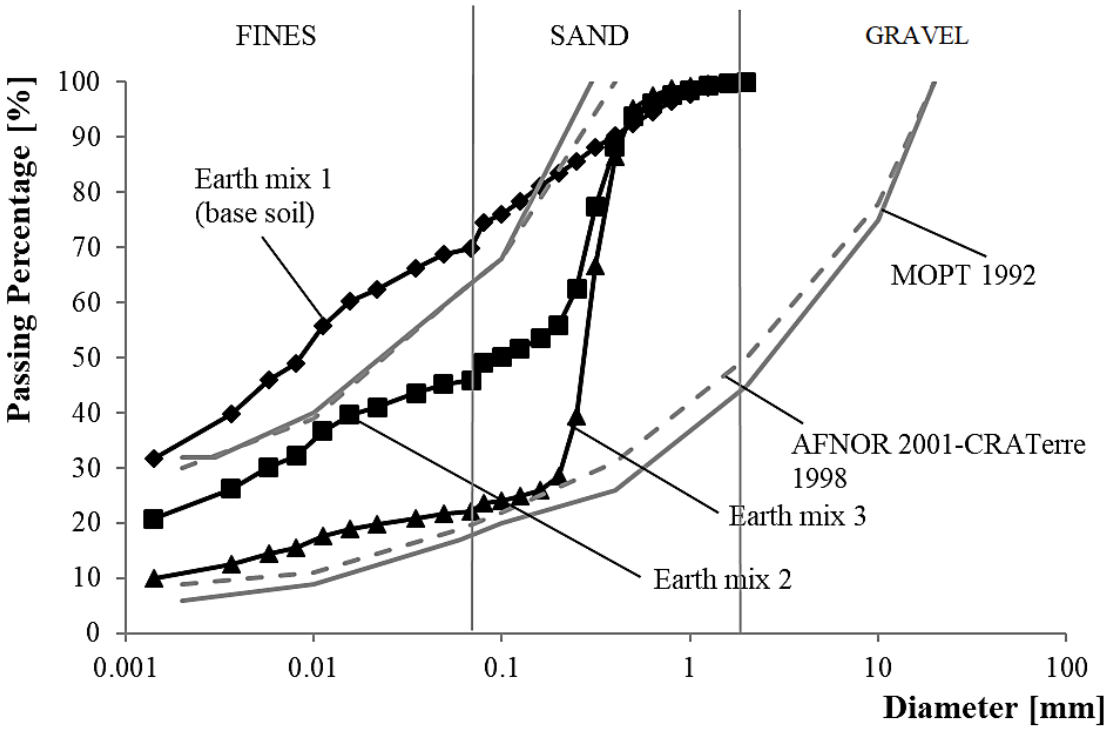

Figure 4.3: Grain size distribution of earth mixes in relation to existing recommendations for the manufacture of compressed earth bricks by AFNOR (2001); CRATerre-EAG (1998) and MOPT (1992).

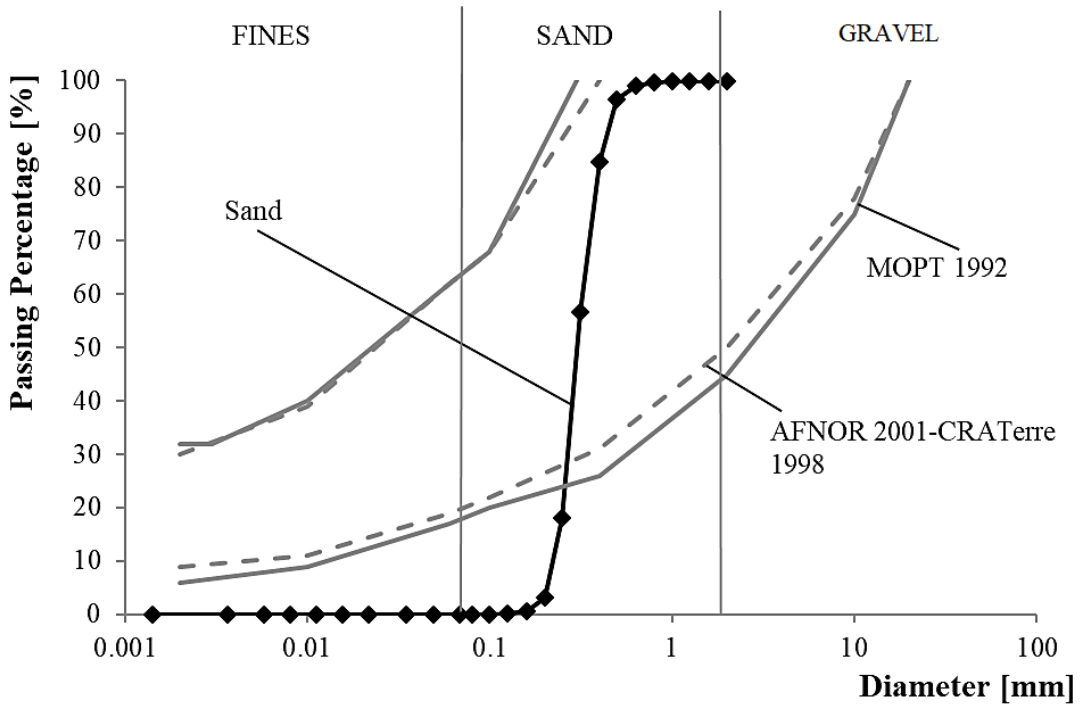

Figure 4.4: Grain size distribution of added sand in relation to existing recommendations for the manufacture of compressed earth bricks by AFNOR (2001); CRATerre-EAG (1998) and MOPT (1992).

Earth mix 2 presents an intermediate clay content compared to the recommended range, with a reasonably well graded particle size distribution, which is located in the middle of the recommended band. Finally, earth mix 3 exhibits a clay content close to the lowest limit of the recommendations with a poorly graded particle size distribution, which cuts across the entire admissible band from the upper limit down to the lower limit. Importantly, despite these differences, all earth mixes are consistent with existing guidelines (only earth mix 1 lies slightly outside the admissible band but the difference is not very significant).

4.2. Compaction procedures

This section describes the compaction procedures adopted in the present work for the manufacture of cylindrical earth samples and earth bricks. As explained in Chapter 2, an increase of dry density generally produces an increase of strength and stiffness of any soil including an earthen construction material. The hyper-compaction procedure involving the application of a large static compaction effort of 100 MPa, proposed by Bruno (2016), was adopted in the present work to manufacture very dense samples. Additional less dense samples were manufactured by standard Proctor compaction for comparison.

4.2.1. Standard Proctor compaction

Standard Proctor samples were manufactured in compliance with the French norm NF P 94-093 (AFNOR, 1999). The standard Proctor dynamic compaction procedure was used to determine the optimum water content corresponding to the maximum dry density of the material. A fixed mass of 2250 grams of dry soil was mixed with the desired amount of water and then left to equalise for at least one day in three plastic bags to prevent evaporation, so that moisture could redistribute prior to compaction. The moist soil was then compacted into a standard Proctor mould with an internal diameter of 102 mm and a height of 116 mm in three layers by 25 blows of a 2490 kg hammer falling from a fixed height of 305 mm. After compaction, the compacted soil, along with the Proctor mould and base plate, were weighed. The weight of the soil sample was then divided by the standard volume of the mould for the determination of the bulk density. The sample was subsequently extracted from the mould for the determination of the moisture content. In particular, three samples of about 50 grams each were collected at the top, middle and bottom parts of the Proctor sample and dried at 105 °C until their mass became constant (AFNOR, 1995) by using a weight-scale with an accuracy of 0.01 grams. The water content was then determined as the average of these three independent measurements and was used to calculate the dry density of the compacted material. The above procedure was repeated to obtain the values of dry density at all different compaction water contents. The relationship between the dry density and the water content was then plotted to establish the standard Proctor compaction curve.

For example, Figure 4.5 shows the standard Proctor compaction curve for the base soil of the present work (earth mix 1). The maximum dry density, corresponding to the peak of the compaction curve, corresponds to the optimum value of the water content. The samples compacted at the optimum water content exhibit the largest dry density while wetter and drier samples show smaller values of dry density. To facilitate the interpretation of results, Figure 4.5 also shows equisaturation lines, which converge towards the theoretical ‘‘no porosity’’ point defined by a zero water content and a dry density equal to the density of the solid particles. In conclusion, for the base soil, the standard Proctor optimum water contents is equal to 12.4%, while the dry density is equal to 1.97 g/cm^3.

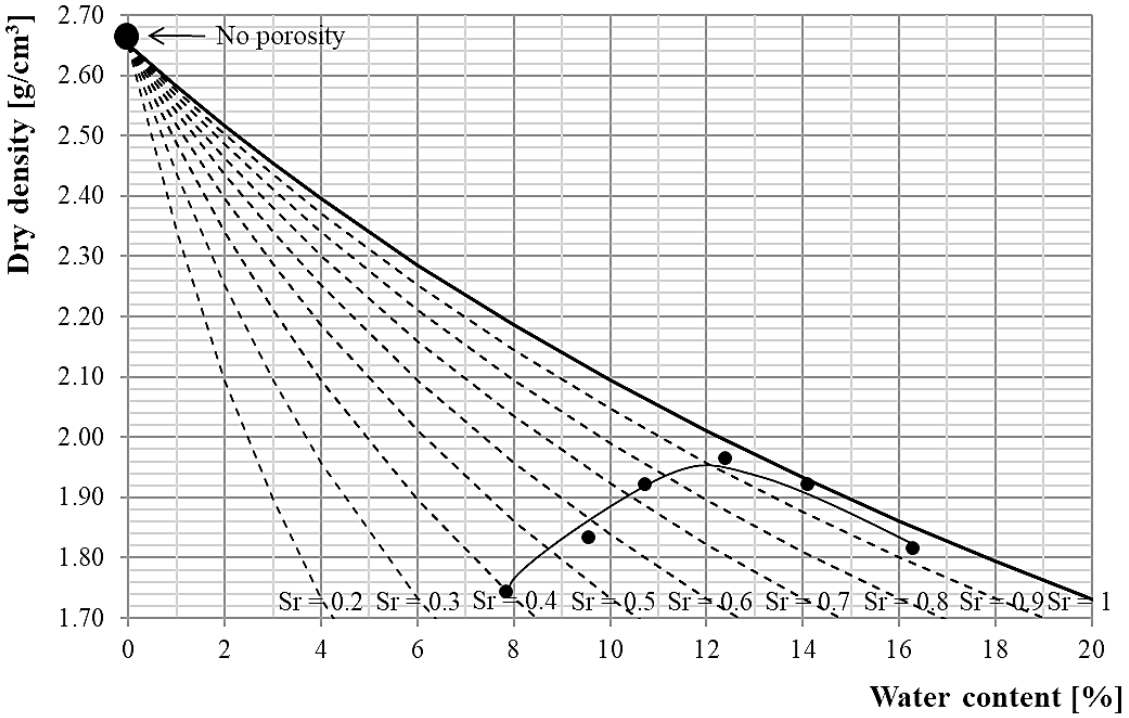

Figure 4.5: Standard Proctor compaction curve of base soil (earth mix 1).

4.2.2. Hyper-compaction

In order to increase the dry density and hence to enhance the stiffness and strength of the material, an alternative hyper-compaction technique was employed as described by Bruno (2016). As discussed in Chapter 2, the hyper-compaction technique can produce earth bricks exhibiting a mechanical performance that is comparable to that of conventional building materials. In this case, the earth mix was statically compacted to a very large pressure of 100 MPa, which is significantly higher than the compaction effort applied during the production of ordinary earth bricks which typically does not exceed 10 MPa. In the following, the application of the hyper-compaction procedure for the manufacture of both earth cylindrical samples and bricks is described. The mechanical tests of the present work were performed on cylindrical samples rather than bricks. This is because cylindrical samples do not incorporate sharp corners, which may result in stress concentrations during compaction and therefore undermine the representativeness of material behaviour.

4.2.2.1. Cylindrical earth samples

Prior to compaction, the dry soil was mixed with the desired amount of water and placed inside three plastic bags to prevent evaporation. The moist soil was then left to equalise for at least one day so that moisture could redistribute prior to compaction. The soil was then placed inside a stiff cylindrical steel mould with a diameter of 50 mm and vertically

compacted by using a load-controlled Zwick/Roell Amsler HB250 press with a capacity of 250 kN (Figure 4.6). The samples to be tested mechanically were manufactured with a height of 100 mm to obtain a suitably large aspect ratio for the accurate measurement of strength and stiffness.

Figure 4.6: Zwick /Roell Amsler HB250 press (from Bruno, 2016).

Bruno (2016) designed a special mould for the hyper-compaction of cylindrical samples (Figure 4.7). The mould consists of a hollow stainless steel cylinder with an external diameter of 170 mm, an internal diameter of 50 mm and a height of 200 mm. This relatively large thickness of the mould wall is necessary to safely withstand the lateral pressures exerted by the soil during one-dimensional hyper-compaction. The pressure is applied by two cylindrical aluminum pistons acting on the top and bottom extremities of the cylindrical

sample. This double compression reduces the negative impact of the friction between the mould and the soil, thus increasing the uniformity of the compaction stress inside the sample. Eight longitudinal fine grooves are also machined on the outer surface of the pistons to facilitate the possible drainage of pore water during compaction.

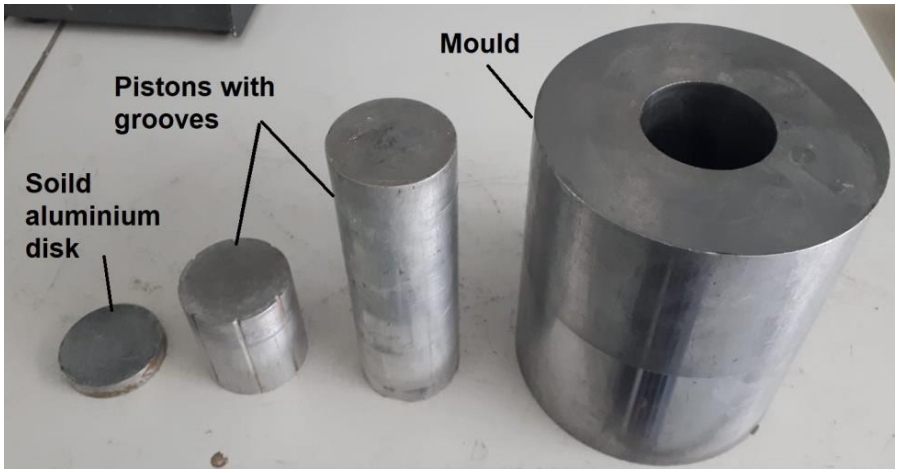

Figure 4.7: Zwick /Roell Amsler HB250 compaction mould.

The moist soil was compacted in three layers, with each layer equal to one third of the total mass of the sample. A small compaction stress of about 5 MPa is applied to each layer before adding the next amount of soil. The upper surface of the last compacted layer was scarified before adding the next amount of soil in order to ensure a good adherence between layers. With soil in place (three layers), only 80 % of the target compaction pressure was applied for few seconds in order to make sure that the sample sticked to the inner surface of the mould. In particular, the mould could be subsequently lifted without causing the soil to fall out thanks to the friction between the soil and the mould. Figure 4.8 shows the equipment in the initial configuration just before the start of the double compaction at 100 MPa.

The compaction pressure was gradually applied to the soil with a constant rate of 5 MPa/s until the target value of 100 MPa was attained. After achieving the pressure of 100 MPa, the load was kept constant for 20 minutes to allow the consolidation of the soil. Additional details about the hyper-compaction of cylindrical samples are available in Bruno (2016).

After extruding the sample from the mould, three diameter measurements were taken at different heights and three height measurements were taken at different angles. The volume of the sample V was then calculated from the average values of diameter and height. The mass W was also measured by means of a scale with an accuracy of 0.01 grams, which allowed to calculate the bulk density ρ_b of the sample. Finally, the water content w was measured on three small pieces (of about 50 grams) of soil taken from the top, middle and

bottom parts of the sample, which were oven-dried at 105 °C until the mass became constant as specified by the norm NF P 94-050 (AFNOR, 1995). The water content *w* was then calculated as the average of these three measurements (in general very similar values of water content were measured at different heights suggesting that moisture was uniform across the entire sample). The dry density ρ_d was then calculated from the previously measured values of bulk density ρ_b and water content *w* according to the following equations:

$$\rho_b = \frac{W}{V} \tag{4.1}$$

$$\rho_d = \frac{\rho_b}{(1+w)} \tag{4.2}$$

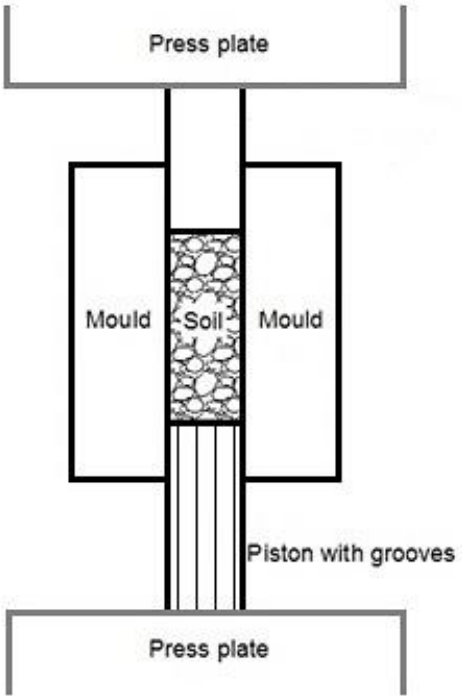

Figure 4.8: Equipment in the configuration before the start of hyper-compaction.

Figure 4.9 presents the values of dry density measured on different samples compacted at different water contents for each earth mix. Inspection of Figure 4.9 shows that the better graded and finer earth mixes 1 and 2 exhibit almost identical compaction curves with higher dry densities compared to the poorer graded and coarser earth mix 3. Accordingly, earth mixes 1 and 2 present almost identical values of the optimum water content (i.e. the water content corresponding to the highest dry density), which are also markedly lower than the optimum water content of earth mix 3. In particular, the optimum water content for earth mixes 1, 2 and 3 is equal to 4.88 %, 4.73 % and 6.50 % respectively while their dry density is equal to 2.31 g/cm^3, 2.28 g/cm^3 and 2.12 g/cm^3 respectively.

Comparison of Figures 4.5 and 4.6 also indicates that the hyper-compaction procedure results in significantly higher values of dry density with considerably lower values of the optimum water content with respect to the case of standard Proctor compaction.

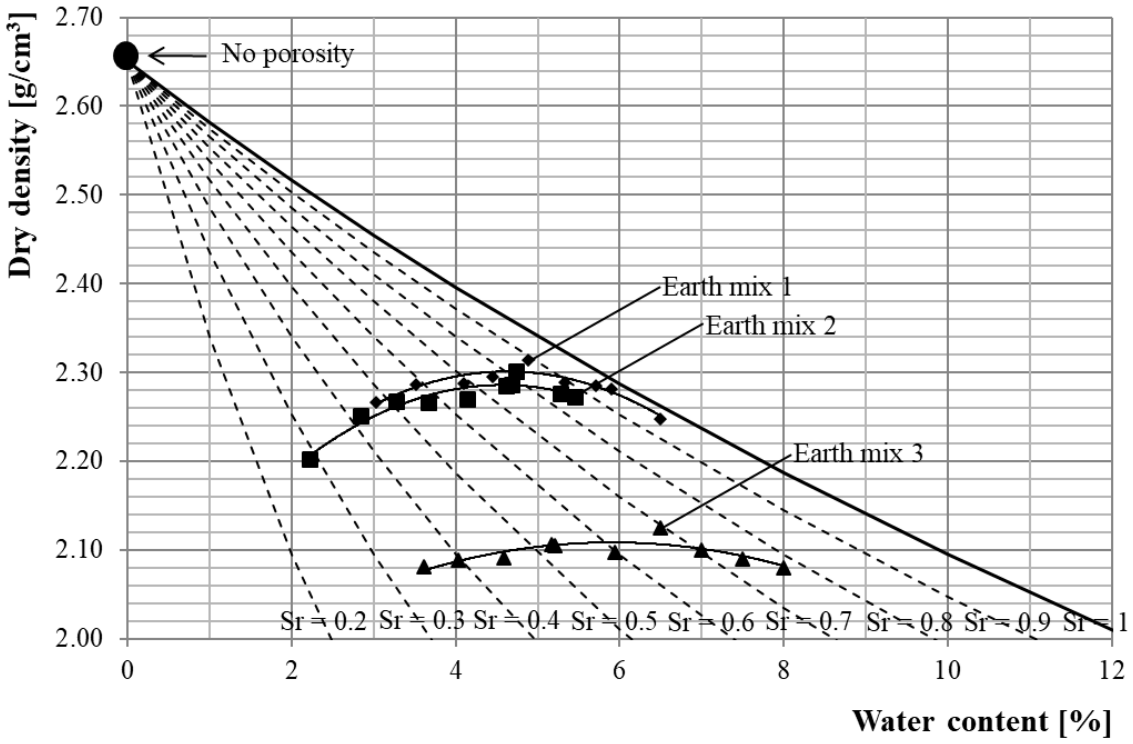

Figure 4.9: Hyper-compaction curves corresponding to the application of a static pressure of 100 MPa.

4.2.2.2. Earth bricks

Hyper-compacted earth bricks were manufactured with dimensions 200 × 100 × 50 mm^3, which are comparable to the dimensions of standard fired clay bricks (i.e. 215 × 102.5 × 65 mm^3 according to BS 3921, 1985). Bricks were one-dimensionally compacted by applying a pressure of 100 MPa on their largest face, whose area is about ten times bigger than that of the cylindrical samples. It was therefore necessary to apply a much larger load than in the case of cylindrical samples to attain the same compaction stress. For this reason, the hyper-compacted bricks were manufactured by using a higher capacity press (i.e. a 3R RP 3000 TC/TH press) that can apply a maximum load of 3000 kN (Figure 4.10).

Prior to compaction, 2300 grams of dry soil were mixed with an amount of water equal to the optimum water content of the corresponding cylindrical samples compacted at 100 MPa (Figure 4.9). After mixing, the moist soil was sealed inside three plastic bags for at least 24 hours to ensure the homogenous distribution of moisture before being placed inside the mould to be compacted. The mould for the hyper-compaction of bricks was designed by Bruno (2016) in collaboration with the company 3R Recherches & Realisations Remy S.A.S.

(Figure 4.11).

Figure 4.10: 3R RP 3000 TC/TH press with a load capacity of 3000 kN (from Bruno, 2016).

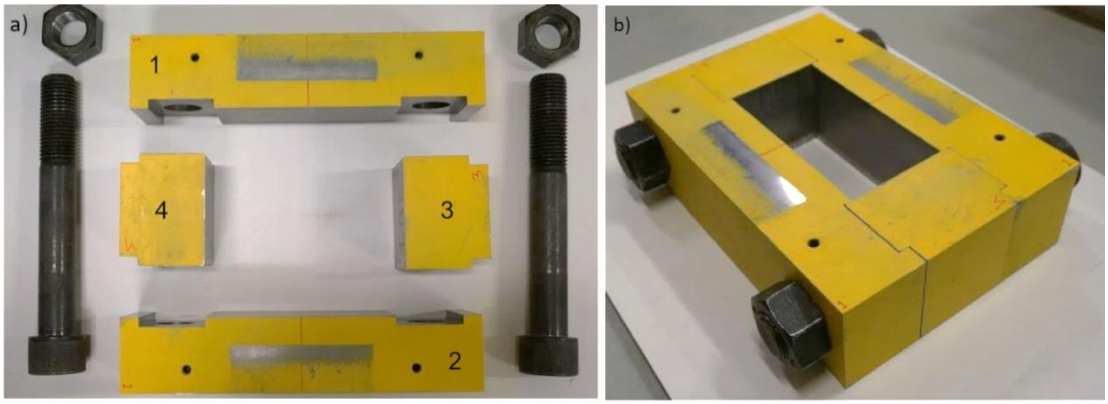

Figure 4.11: Compaction mould: disassembled (a), assembled (b) (from Bruno, 2016).

Similar to the cylindrical samples, the earth was one-dimensionally compacted inside the mould by means of two rectangular aluminium pistons acting at the top and bottom extremities of the brick. This double compaction mechanism reduces the negative impact of friction on the lateral surface of the brick and therefore increases the uniformity of stresses inside the material. Unlike the cylindrical case, the two rectangular pistons did not include

any groove to facilitate water drainage during compaction. This is because the soil was compacted at the optimum water content, which is not wet enough to cause the saturation of the soil and hence the expulsion of water during compaction. Further details about the procedure for assembling the mould, compacting the soil and demoulding the brick are presented in Bruno (2016).

4.3. Bio-stabilisation method

This section describes the Enzymatic Induced Calcite Precipitation (EICP) method that has been adopted in the present work to induce the precipitation of calcium carbonate inside the soil for stabilising the material. EICP is a bio-stabilisation method that has already been described in Chapter 3. It requires the presence of the urease enzyme, which acts on the urea substrate leading to the precipitation of calcium carbonate in aqueous solution. The occurrence of calcium carbonate precipitation requires the presence of calcium ions, which typically originate from the dissolution of calcium containing salts. This bio-stabilisation method therefore requires three ingredients that are the urease enzyme, the urea and a calcium salt. The following sections also present the results from some preliminary experiments to assess the efficiency of the EICP stabilisation protocol that has been adopted in the present work.

4.3.1. Urease enzyme from soybeans extract

The urease enzyme was the first nickel metalloenzyme ever purified and crystallised from jack beans (canavalia ensiformis). This important achievement yielded the Nobel Prize in Chemistry to James B. Summer in 1946. Since then, different types of nickel dependent ureases have been isolated from bacteria, fungi and plants. Chemical suppliers commercialise pure reagent-grade urease enzyme, which is very effective for catalysing the hydrolysis of urea but it is also very expensive. These high financial costs make the pure reagent-grade urease enzyme not eligible for construction purposes. The present research proposes instead an effective and economical procedure for obtaining the urease enzyme from the centrifugation of soybeans, which is one of the many naturally occurring plants that contain such enzyme. The present work made use of soybeans that were bought from an Asian food supermarket in the city of Anglet (France).

The procedure consisted of the following three steps (Figure 4.12):

- the soybeans were soaked for 24 hours in 10 ml of distilled water for each gram of dry beans;

-the moist soybeans were then centrifuged in a blender together with the water they were soaked in;

- the semi-transparent grey-yellow juice produced by centrifugation was collected and kept as a crude urease extract.

Figure 4.12: Procedure for obtaining the urease enzyme: soybeans are soaked in water (a), soaked soybeans are centrifugated in a blender (b), the crude urease extract is collected (c).

4.3.2. Chemical reagents

The two chemical reagents that have used in the proposed EICP stabilisation method are urea ($CO(NH_2)_2$) and calcium chloride ($CaCl_2$).

Urea is a colourless and odourless organic material that serves an important role in the metabolism of nitrogen compounds and is also the main nitrogen containing substance of the urine of mammals. Urea is highly soluble in water and practically non-toxic. Importantly, the hydrolysis of urea exhibits a high calcite conversion rate compared to other calcium carbonate precipitation processes (Whiffin et al., 2007; Harkes et al., 2010).

The calcium chloride salt has been used in this work as a source of calcium ions because of its relatively high hygroscopicity and solubility in water. The solubility of calcium chloride at room temperature is up to 100 times greater than that of other salts such as calcium hydroxide or calcium nitrate, which makes calcium chloride a very effective reagent to generate high concentrations of calcium ions. This is an important aspect to consider during EICP stabilisation because a large concentration of calcium ions contributes to a high rate of calcium carbonate precipitation (Park et al., 2014).

The urea and calcium chloride used in the present work (Figure 4.13) were supplied by Labbox and their properties are synthetically described in Table 4.3.

Figure 4.13: Urea powder ($CO(NH_2)_2$) and flakes of calcium chloride ($CaCl_2$).

Table 4.3: Urea ($CO(NH_2)_2$) and calcium chloride ($CaCl_2$) properties: molar weight (MW) in g/mol, appearance and assay in percentage.

	Chemical formula	**Labbox reference**	**MW (g/mol)**	**Appearance**	**Assay (%)**
Urea	$CO(NH_2)_2$	UREA-00P-1K0	60.06	White/crystal, powder	>99.6 %
Calcium chloride	$CaCl_2$	CACH-A0P-1K0	110.98	White pearls	>94 %

4.3.3. Efficiency of stabilisation protocol

A number of preliminary tests were carried out on the soybeans extract to confirm the occurrence of the ureolytic reaction and the consequent precipitation of calcium carbonate. As previously described, the urease enzyme was obtained from the centrifugation of soaked soybeans, which yielded a juice with a pH of about 6. The dissolution of two moles of urea in one litre of this crude soybeans extract resulted in an immediate rise in pH to about 9 (Figure 4.14). This marked increase of alkalinity indicates the occurrence of the hydrolysis of urea and confirms the activity of the enzyme in the extract. Note that the same increase of alkalinity was not observed when the urea was dissolved in distilled water.

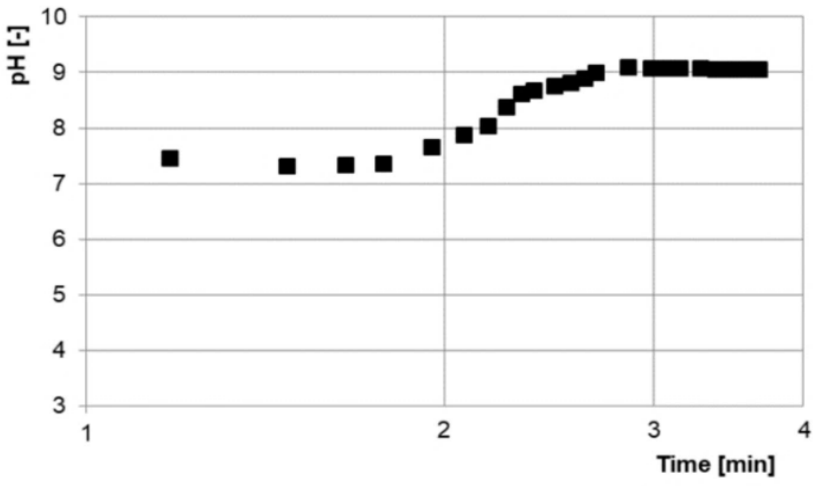

Figure 4.14: Measurements of pH taken at different times after dissolution of 2 mol/L of urea in the crude soybeans extract (initial value of pH before addition of urea equal to 6).

The alkaline environment, produced by the hydrolysis of urea inside the soybeans extract, is the result of the production of ammonia and the consequent release of carbon dioxide during the hydrolysis reaction and it is necessary condition for the precipitation of calcium carbonate (Castanier et al., 1999). Note that the experimental values of pH shown in Figure 4.14 are the average of three tests, which confirmed the repeatability of results. Inspection of Figure 4.14 also indicates that the alkaline environment remains stable, i.e. with a constant pH of about 9, after dissolution of urea and the consequent occurrence of the ureolytic reaction. Calcium chloride was then added to the solution with an equimolar concentration of 2 mol/L, which produced a sudden drop of pH to about 6 due to the precipitation of calcium carbonate. This reduction of alkalinity happens because of the dissolution of calcium chloride, which causes the formation of calcium hydroxide and the release of hydrogen ions making the solution more acidic. Figure 4.15a shows the precipitated material collected at the bottom of the beaker while Figure 4.15b shows the precipitated material after oven-drying at a temperature of 40 °C.

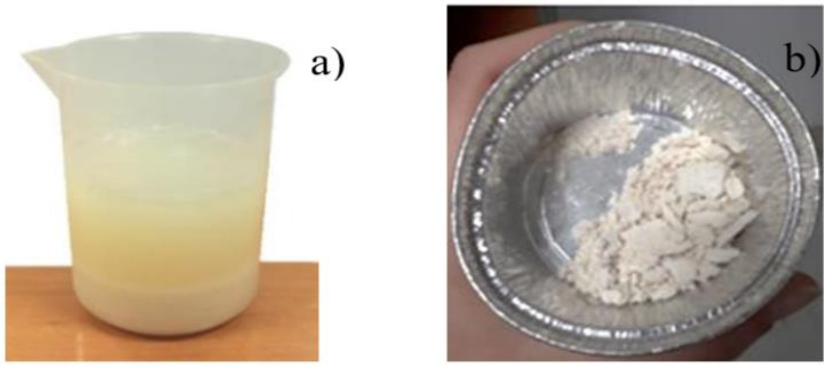

Figure 4.15: Precipitation of calcium carbonate at the bottom of the beaker after addition of calcium chloride (a) and precipitated material after oven-drying (b).

The subsequent performance of XRD tests confirmed that the mineralogy of the precipitated material comprises calcium carbonate in the form of calcite minerals (Figure 4.16), which provides further evidence of the occurrence of the reactions described in Equations 1 - 6 (Chapter 3).

A number of samples of the crude soybeans extract were also exposed to the laboratory atmosphere, i.e. at a temperature of 20 ± 5 °C and a relative humidity of 40 ± 5 %, for 72 hours. Measurements taken over this period of time indicated that the extract becomes acidic after only few hours of exposure to the laboratory atmosphere attaining a pH of about 4.5. At this point, the pH stops reducing and the acidity level of the extract remains constant over time.

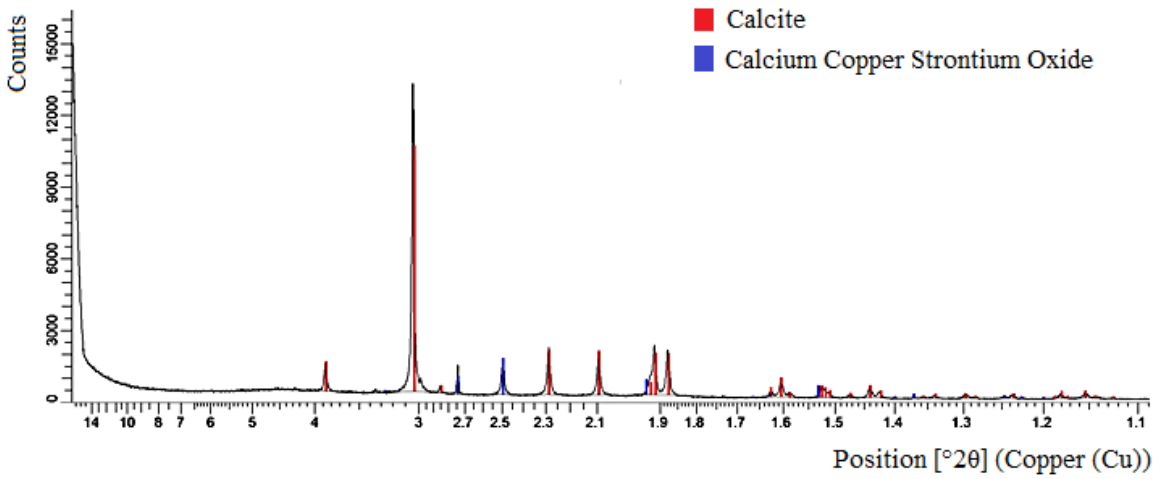

Figure 4.16: Preliminary XRD analysis of precipitated material.

A thick foam also develops at the top of the acidic soybeans extract during the time it is exposed to the laboratory atmosphere (Figure 4.17a). Note that, unlike the case of the fresh extract, the addition of 2 mol/L of urea to this aged extract did not produce any increase of pH, which suggests that no hydrolytic reaction takes place in the aged extract. The absence of a hydrolytic reaction may be a consequence of the inhibition of the urease enzyme in an acidic environment (Stocks-Fischer et al., 1999). Equally, the subsequent addition of calcium chloride with a concentration of 2 mol/L to the solution of aged extract and urea did not produce any precipitation of calcium carbonate (Figure 4.17b). This was, however, an expected result because the dissolution of calcium ions cannot cause the precipitation of calcite in the absence of the carbonate ions produced by the hydrolysis of urea.

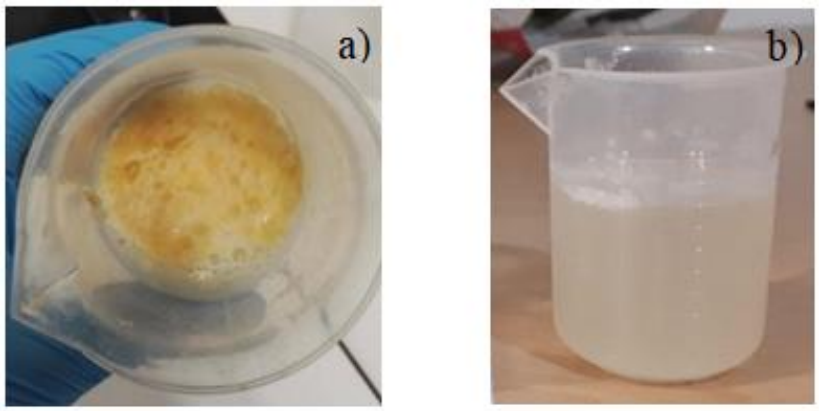

Figure 4.17: Thick foam at the top of the acidic soybeans extract after exposition to the laboratory atmosphere (a) and absence of precipitated calcium carbonate by using an acidic crude soybeans extract (b).

The above experiment indicates that only a fresh soybeans extract can catalyse the hydrolysis of urea and hence the precipitation of calcite crystals. It is therefore important to use the extract as soon as possible after centrifugation to ensure that the pH does not decrease before

the addition of urea. Further investigation is being undertaken to assess whether the activity of the enzyme can be preserved for a longer time by sealing and/or freezing the extract prior to use.

4.3.4. Urease enzyme from soybeans powder

The present work explored an alternative, albeit similar, EICP stabilisation procedure that relied on the direct addition of soybeans as fine powder into the soil. The urease enzyme is contained in the shell of the soybeans and the direct use of a fine soybeans powder mixed to the soil might therefore enhance the activity of the enzyme and the precipitation of calcium carbonate. To this end, the soybeans were crushed into a powder by using a coffee grinder machine and passed through a sieve to collect only the finest particles with dimension smaller than 0.400 mm (Figure 4.13). This cut-off size was chosen to boost the finer fraction of the earth mix and to avoid imperfections during manufacture of the samples due large inclusions, which may improve durability against water erosion. The fine soybeans powder was then mixed with distilled water and equimolar concentrations of urea ($CO(NH_2)_2$) and calcium chloride ($CaCl_2$), thus resulting in a sticky glue that adhered well to the soil particles.

Figure 4.18: Sieving of the finer fraction (smaller than 0.400 mm) of the crushed soybeans powder.

5. Influence of soil grading on the hygro-mechanical and durability properties of raw earth

This chapter addresses the link between the particle size distribution and the engineering performance of raw earth materials. A wide experimental campaign was undertaken including compression tests to measure stiffness and strength, hygroscopic tests to measure water vapour storage capacity and immersion/suction/drip tests to measure durability against water erosion. The main objective was to determine the influence of particle size distribution and density on the hygro-mechanical and the durability characteristics of hyper-compacted unstabilised earth at the scale of small cylindrical samples. However, durability tests such as suction and drip tests were performed at the brick scale in accordance with the norms DIN 18945 (2013) and norm NZS 4298 (1998).

5.1. Mechanical behaviour

5.1.1. Unconfined compressive strength and Young's modulus

Unconfined compression tests were performed on cylindrical samples with a diameter of 50 mm and a height of 100 mm. Mechanical tests were performed on cylinders rather than bricks to avoid samples with sharp corners that could induce stress concentration during fabrication and testing. In particular, cylinders with an aspect ratio of two were manufactured to limit the radial confinement caused by friction between the sample extremities and the press plates during axial compression. Samples were manufactured in accordance with the description in Section 4.1.3 and 4.2.2 and hyper-compacted at their respective optimum water contents of 4.88 %, 4.73 % and 6.50 % in reference to earth mix 1, 2 and 3 respectively. Before testing, all samples were equalised inside a climatic chamber at a temperature of 25 °C and a relative humidity of 62 %. This was necessary to avoid the influence of potentially different ambient conditions on the measured values of strength and stiffness. During this equalisation phase, the samples were weighted every day until their mass changed less than 0.1 % over at least one week, which took generally 15 days.

A first series of unconfined compression tests was performed to measure the strength of the hyper-compacted samples. The samples were compressed under a constant axial displacement rate of 0.001 mm/s, which allowed recording the post-peak part of the stress-strain curve. This displacement rate was the slowest that could be applied by the press and was chosen to obtain a regular stress-strain curve without instabilities (Bruno, 2016). Two

samples were tested for each earth mix and the final peak strength was then calculated as the average of the two measurements.

In general, earth mix 1 exhibited a localised shearing failure along a plane cutting across the top and bottom surfaces of the sample. This was consistent with the assumption that the friction between the earth material and the press plates was negligible and did not affect the failure mechanism. Conversely, earth mix 3 showed diffused fracturing and failed by breaking down into small pieces. Finally, earth mix 2 exhibited an intermediate failure mechanism with the formation of a double shearing plane or axial splitting. The different failure mechanisms of the three earth mixes are illustrated in Figure 5.1.

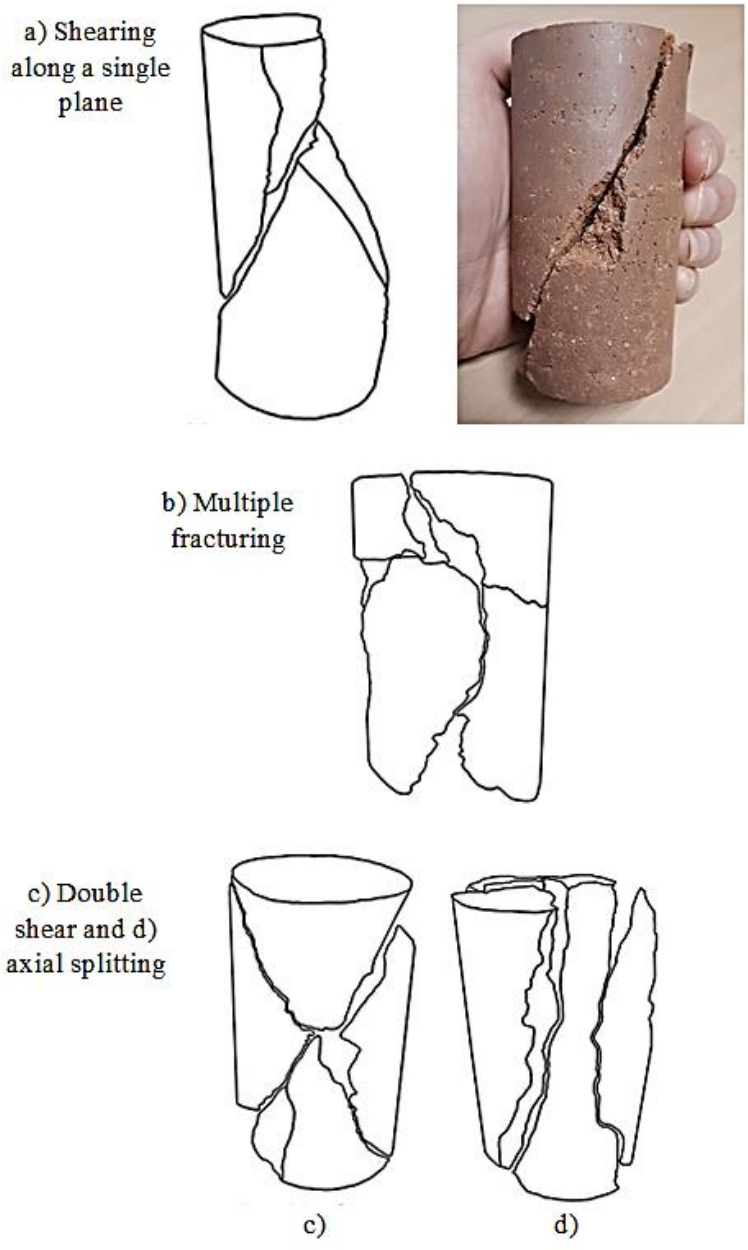

Figure 5.1: Compressive failure mechanisms for earth mix 1 (a), earth mix 3 (b), earth mix 2 (c, d).

Figure 5.2 presents results obtained from unconfined compression tests performed on each of the three mixes in terms of stress-strain curves.

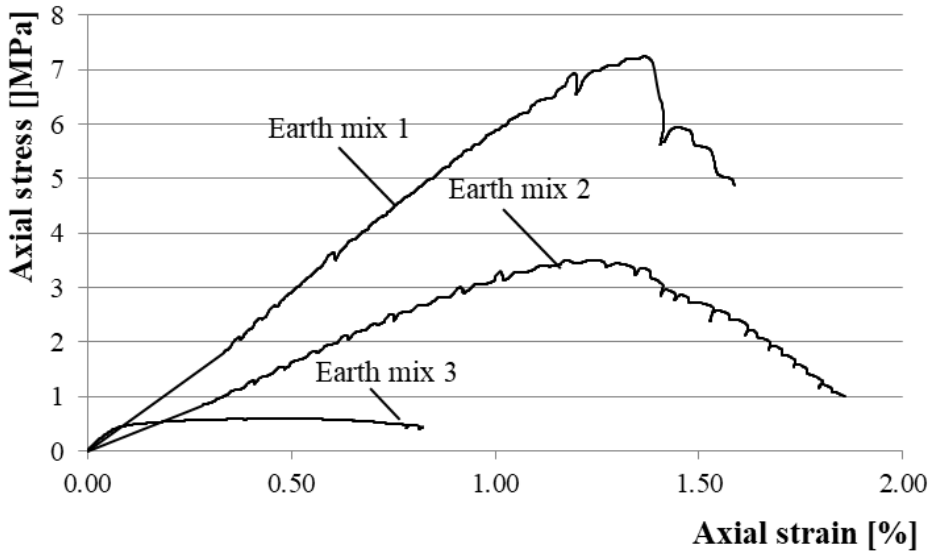

Figure 5.2: Stress-strain curves from unconfined compression tests performed on hyper-compacted earth mixes 1, 2 and 3.

Figure 5.3 shows the average peak value of compressive strength measured from the two tests for each earth mix while the inset graph shows the same values of compressive strength but plotted against dry density. Inspection of Figure 5.3 indicates that, as expected, the compressive strength increases with growing density.

A second series of unconfined compression tests was undertaken to determine the stiffness of the three hyper-compacted earth mixes. In particular, the Young's modulus was measured by performing five axial loading-unloading cycles with a constant loading rate of 0.005 MPa/s between one ninth and one third of the peak strength measured from the previous tests. The axial strain was measured between two points at a distance of 50 mm by means of two extensometers (Model 3542-050M-005-HT1 - Epsilon Technology Corp.), which were symmetrically located on the diametrically opposite sides of the sample (Figure 5.4). Radial displacements were also measured by means of a chain fitted around the sample at middle height, which was connected to a displacement transducer (Model 3544-150M060M-ST - Epsilon Technology Corp.) as shown in Figure 5.4. Measurements of radial displacements are however not reported in the present work.

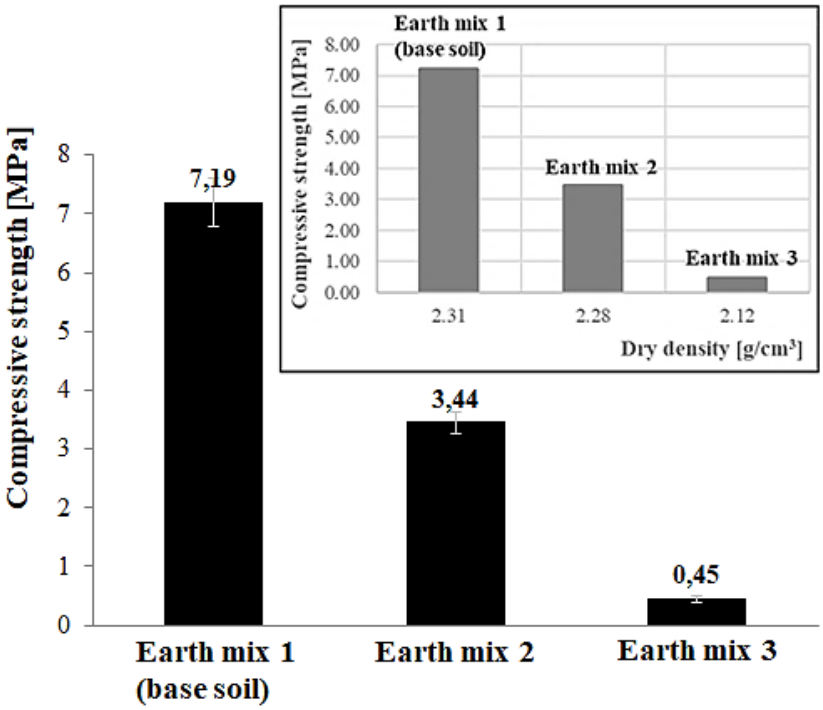

Figure 5.3: Compressive strength: results of unconfined compression tests for the different earth mixes.

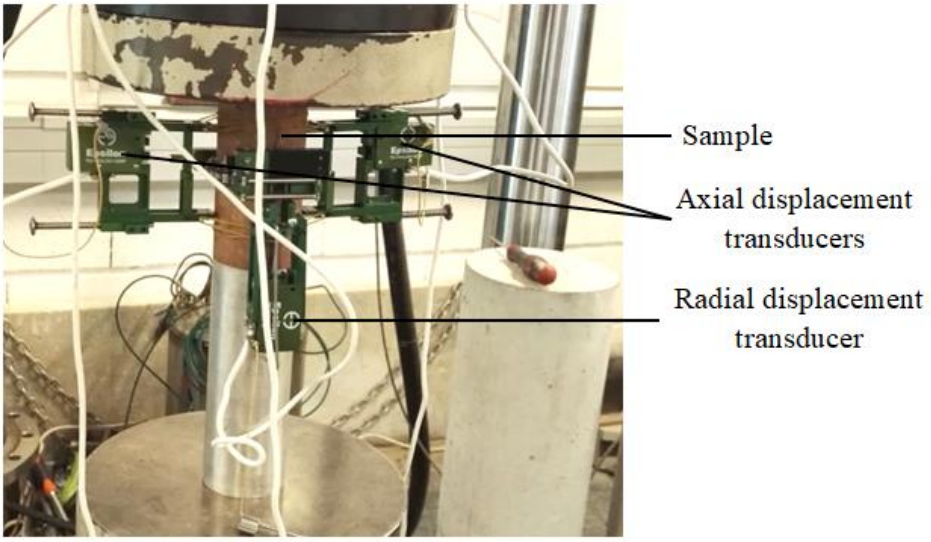

Figure 5.4: Testing set-up for measuring axial and radial displacements (Model 3542-050M-005-HT1 - Epsilon Technology Corp. and Model 3544-150M060M-ST - Epsilon Technology Corp.).

Figure 5.5 shows the cyclic test for measuring stiffness properties performing five axial loading-unloading cycles. Based on the assumption that material behaviour is elasto-plastic during loading but essentially elastic during unloading, the Young's modulus was determined from the slope of the lines best fitting the unloading branches in the stress-strain plane. More specifically, the Young's modulus was determined as the average slope of the five lines fitting the different five unloading branches.

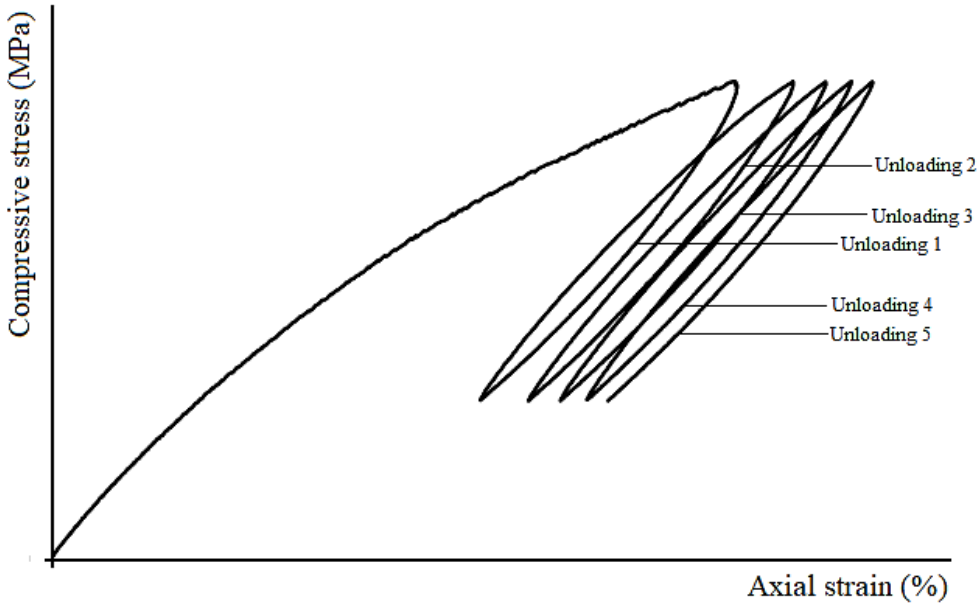

Figure 5.5: Cyclic test for measuring stiffness properties.

Two tests were performed for each earth mix and the average of these measurements are shown in Figure 5.6. The inset graph shows instead the average Young's modulus plotted against the dry density of each earth mix. Similarly to compressive strength, the Young's modulus increases for denser materials, even though this increase is not linear because of the influence of earth grading (and not only dry density) on the material stiffness.

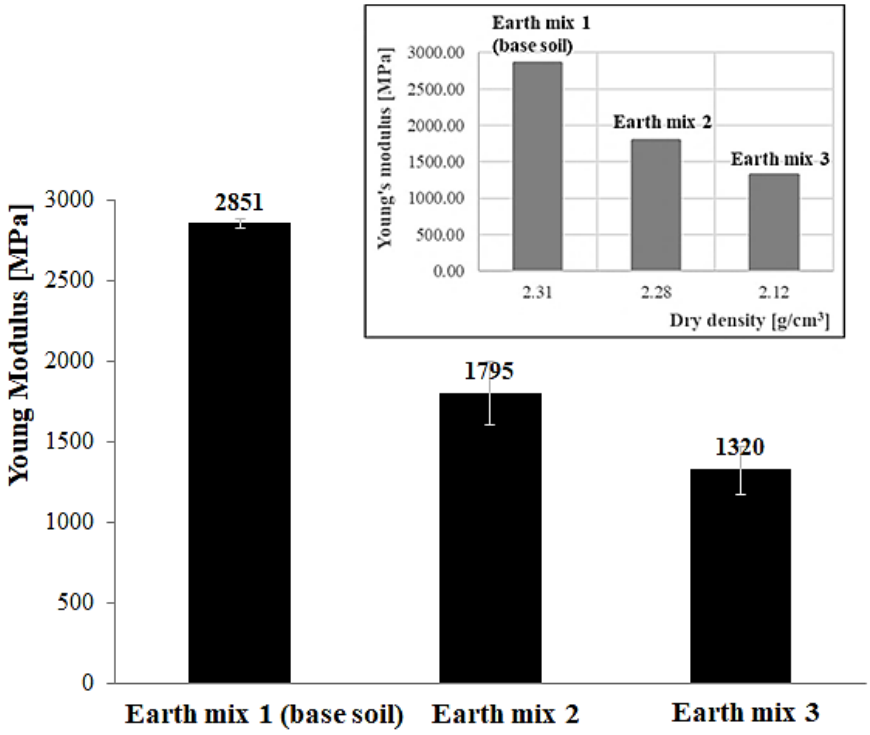

Figure 5.6: Young's modulus: results of unconfined loading-unloading cycles for the different earth mixes.

Inspection of Figures 5.3 and 5.6 indicates significant differences of stiffness and strength between earth mixes 1 and 2 despite an almost identical value of dry density. An explanation of this result might be found in the different physical composition of the two materials. Earth mix 2 is a blend of a silty clay and a sand with a bimodal, gap-graded, particle size distribution while earth mix 1 is a well-graded silty clay (see Figure 4.3 in Section 4.1.3). This indicates that density cannot be considered as the only factor governing mechanical behaviour and that particle grading plays an equally important role. The results from the above tests indicate that two different particle gradings, which are both compatible with current recommendations for earth building (see Figure 4.3 in Section 4.1.3), can result in significantly different mechanical properties even when compacted to similar dry densities.

5.1.2. Effect of relative humidity

This section investigates the variation of the mechanical properties of the previous hyper-compacted earth mixes when exposed to fluctuations of ambient humidity. A variation of ambient humidity produces a corresponding change of moisture content inside the earth, which affects the inter-particle bonding that is generated by capillary water. This in turns influences the measured values of strength and stiffness as discussed in Section 2.2.2. In particular, stiffness and strength were measured with a geotechnical perspective by means of triaxial tests under different levels of radial stress to explore the effect of material confinement inside thick earthen walls.

Due to the limited time available, the investigation was limited to earth mixes 1 and 3 because the clay contents of these two mixes are respectively equal to the upper and lower limits recommended for compressed earth bricks by AFNOR (2001); CRATerre-EAG (1998) and MOPT (1992). Earth mixes 1 and 3 therefore correspond to the two extremes of the range of admissible materials while earth mix 2, which lies in the middle of this range, is likely to be characterised by an intermediate behaviour. Cylindrical samples for earth mixes 1 and 3 were hyper-compacted at the corresponding optimum water contents of 4.88 % and 6.50 %. Additional samples made of Bouisset base soil were also compacted at the Proctor optimum water content of 12.31 % by applying a static pressure that produced the same optimum dry density of standard Proctor compaction equal to 1.97 g/cm^3.

All samples were then equalised inside a climatic chamber at a constant temperature of 25 °C and at different levels of relative humidity, namely 25 %, 62 %, 95 %, hence, exhibiting different degrees of saturation. Samples were weighted every day and equalisation was assumed to be complete when the mass of the sample changed less than 0.1 % over at least

one week, which took generally 15 days. Once the sample attained equilibrium, the total suction, ψ inside the material was calculated from the imposed values of temperature, *T* and relative humidity, *RH* according to Kelvin's law as:

$$\psi = -\frac{R\,T}{V_m}\ln(RH) \tag{5.1}$$

where *R* is the constant of perfect gases and V_m is the molar volume of water. The values of total suction calculated through Equation 5.1 are shown in Table 5.1.

An additional set of samples was placed inside an oven for three days at a temperature of 105 °C to test the mechanical behaviour of the material when dried.

For each specimen, the dimensions (i.e. diameter and height) and mass were measured after equalisation and just prior to mechanical testing. After the end of the test, a small fragment of material, corresponding to about 50 grams, was taken from the failed specimen to determine the water content in agreement with the French norm NF P 94-050 (AFNOR, 1995). By using the measured values of diameter, height, mass, water content and specific gravity, it was then possible to calculate the bulk density ρ_b, the dry density ρ_d, the porosity *n* and the degree of saturation *Sr* of the tested samples (assuming that the moisture content of the sample did not change during the test). Table 5.2 summarises the average values of bulk density ρ_b, water content *w*, dry density ρ_d, degree of saturation *Sr* and porosity *n* measured after equalisation for all samples.

Table 5.1: Total suction after equalisation at different humidity levels.

Relative humidity [%]	**Total suction[MPa]**
RH = 25 %	190.1
RH = 62 %	65.5
RH = 95 %	7.03

Table 5.2: Samples properties after equalisation.

Relative humidity [%]	**ρ_b [g/cm^3]**	**w [%]**	**ρ_d [g/cm^3]**	**Sr [%]**	**n [%]**
	Earth mix 1 – 100 MPa				
Dry	2.28	0	2.28	0	14.1
RH = 25 %	2.31	0.683	2.29	11.7	13.4
RH = 62 %	2.33	2.24	2.28	36.7	13.9
RH = 95 %	2.38	4.61	2.28	74.9	14.0
	Earth mix 3 – 100 MPa				

Dry	2.12	-	-	-	-
RH = 25 %	2.12	-	-	-	-
RH = 62 %	2.15	-	-	-	-
RH = 95 %	2.13	-	-	-	-
	Earth mix 1 – Proctor				
Dry	1.95	0	1.95	0	26.3
RH = 25 %	1.99	0.88	1.97	6.76	25.6
RH = 62 %	1.98	2.43	1.93	17.3	27.1
RH = 95 %	2.09	4.91	1.99	39.3	24.9

After equalisation all samples were subjected to triaxial compression under three different levels of radial stress equal to 0 kPa, 300 kPa and 600 kPa. All tests were performed inside a conventional triaxial cell with a constant axial displacement rate of 0.06 mm/min while the back pressure line was open to atmosphere. During compression, the exchange of moisture between the sample and the atmosphere, through the back pressure line, was considered negligible and the sample water content was assumed constant. Shearing was continued until failure, which generally took between 23 and 35 minutes depending on the test.

The results from triaxial tests were subsequently processed to determine the variation of both stiffness and peak strength with confining pressure at each humidity level. Unlike the previous series of unconfined compression tests (Figure 5.3 and Figure 5.6), no stress-strain cycles were performed during triaxial tests. The Young's modulus was therefore simply measured as the slope of the tangent to the stress-strain curves over the stress range where the material response is reasonably linear (Figure 5.7).

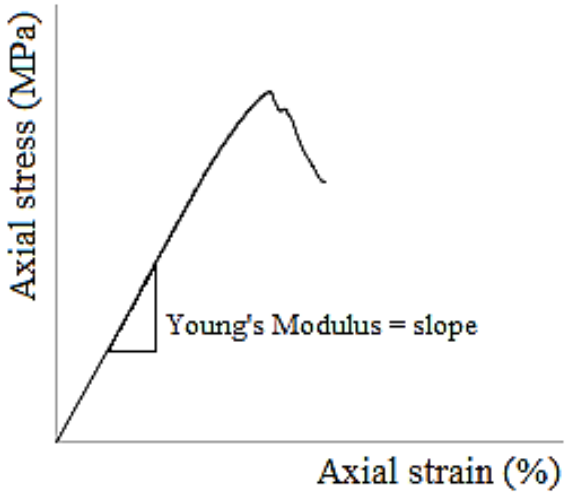

Figure 5.7: Stress-strain curve from triaxial compression tests and measurement of the Young's modulus as the slope of the tangent to the stress-strain curve.

Figure 5.8 shows the stress-strain curves measured during the triaxial tests performed at different confining pressures on the hyper-compacted samples of earth mix 1 equalised at different humidity levels. Inspection of Figure 5.8 indicates that, as expected, the peak strength increases as the confining pressure increases at each given humidity level. Moreover, the peak stresses at a given confining pressure increase as the relative humidity decreases, which provides further evidence of the link between the material water content and strength. This result corroborates the assumption that, in unsaturated conditions, capillary menisci at inter-granular contacts bond particles together, thus improving the mechanical characteristics of the material (Beckett and Augarde, 2012). It might therefore be surprising that the highest values of strength were measured on dry samples, for which the peak stress attained values greater than 20 MPa. If the samples were indeed dry, no capillary menisci should be present and the strength should be the lowest one and similar to that measured under saturated conditions. A dry material is in fact conceptually no different from a saturated one, for which the principle of effective stresses applies. The explanation of this apparent contradiction might be that the oven-dried samples are in fact not completely dry and a small quantity of adsorbed or capillary water still exists under very high levels of tension, thus continuing to bond particles together.

Inspection of Figure 5.8 also indicates that the mechanical behaviour changes from fragile to ductile as humidity increases. Therefore, an increase of ambient humidity reduces the shear strength but also improves the ability of the material to undergo significant plastic deformation before failure.

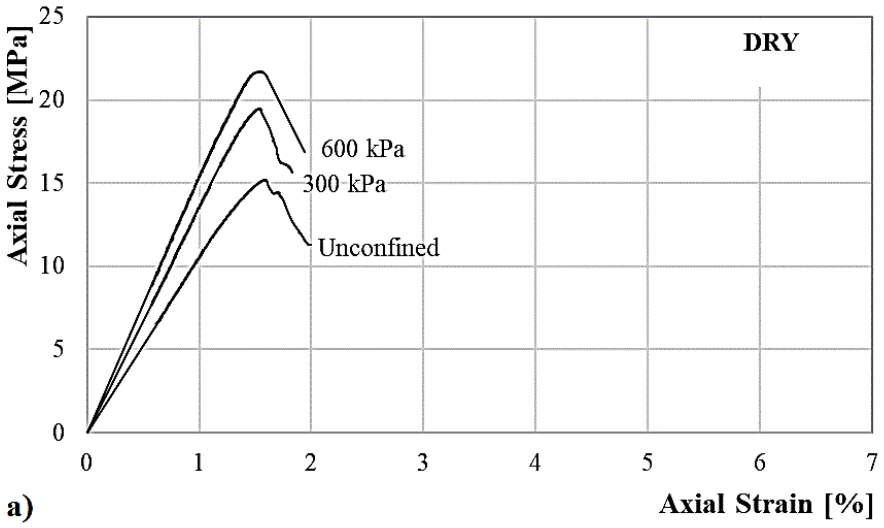

a)

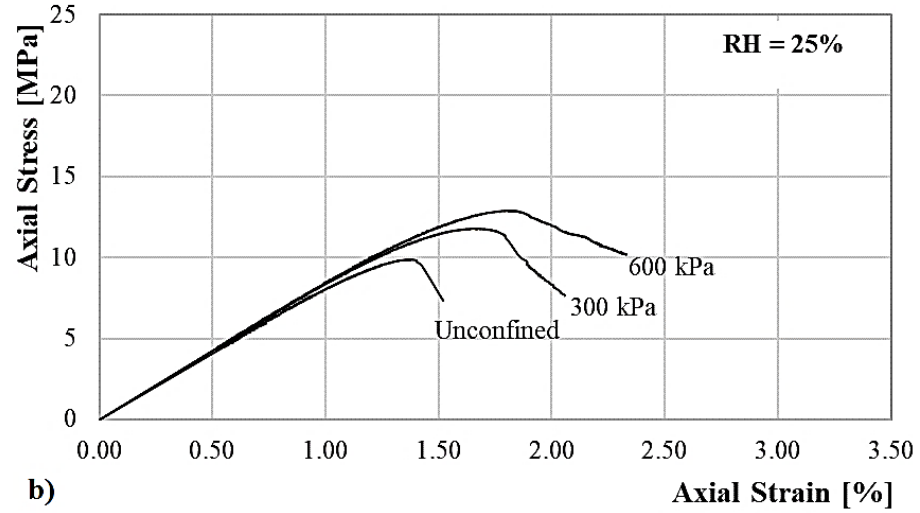

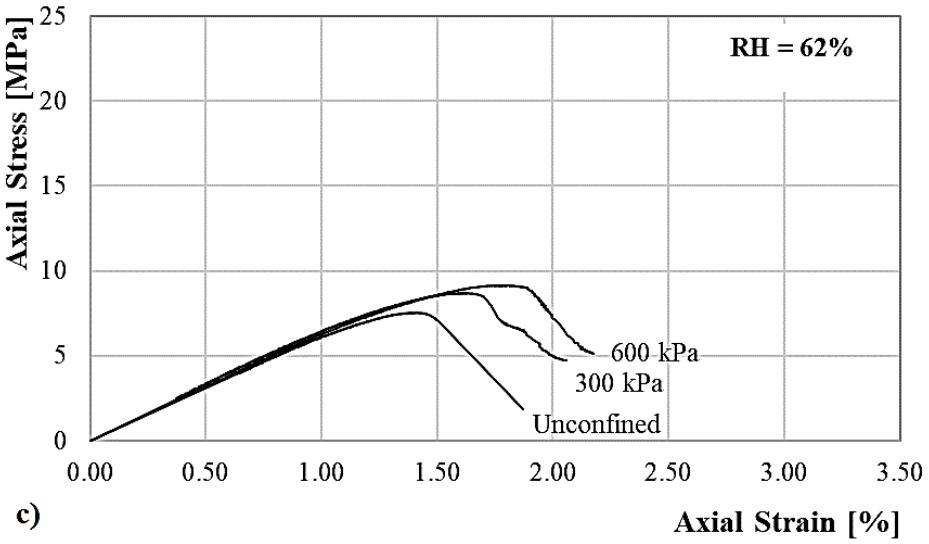

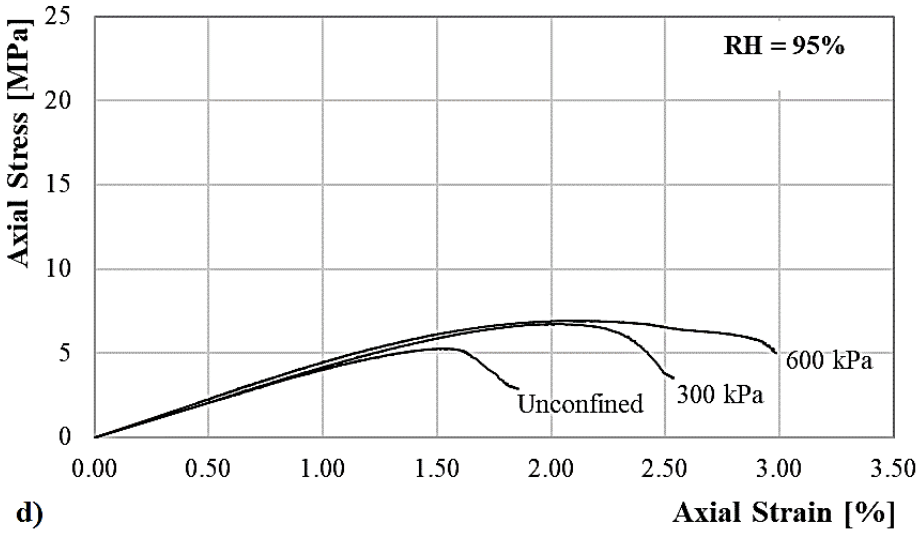

Figure 5.8: Results from triaxial tests on the hyper-compacted earth mix 1 at different confining pressures and distinct humidity levels: dry (a), 25 % (b), 62 % (c), 95 % (d).

Figure 5.9 presents the stress-strain curves measured from the tests on the hyper-compacted samples of earth mix 3. As expected, also in this case the peak stress increases as the relative humidity decreases regardless of confining pressure, which provides further evidence of the link between degree of saturation and strength. The highest values of strength were measured on dry samples with a maximum of about 6 MPa, which is however significantly lower than the level measured on earth mix 1. Inspection of Figure 5.9 confirms, once again, the change in mechanical behaviour from fragile to ductile as humidity increases thus improving the ability of the material to deform plastically before failure.

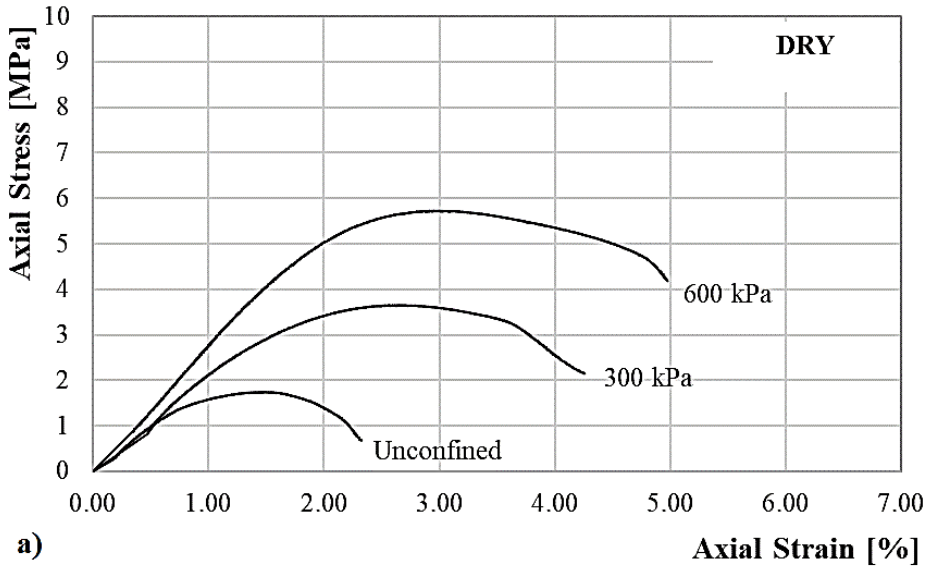

a)

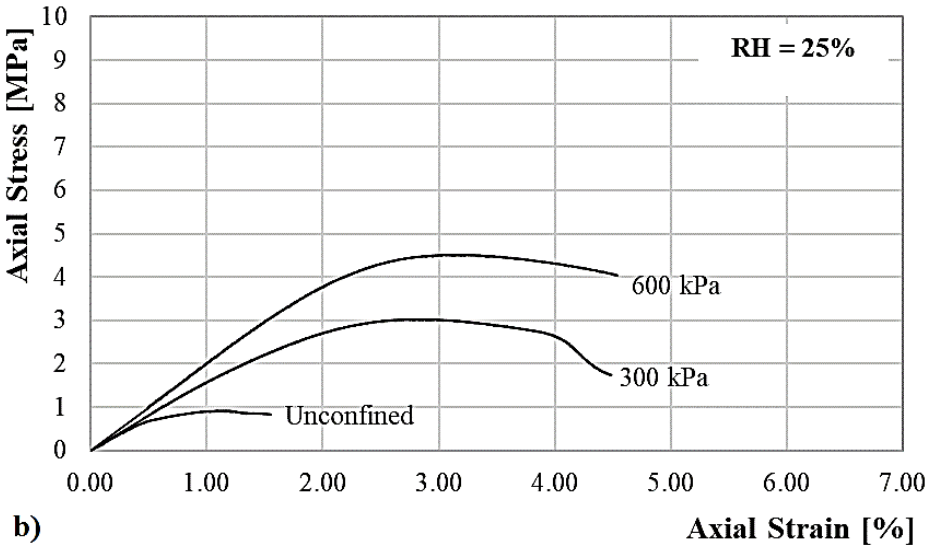

b)

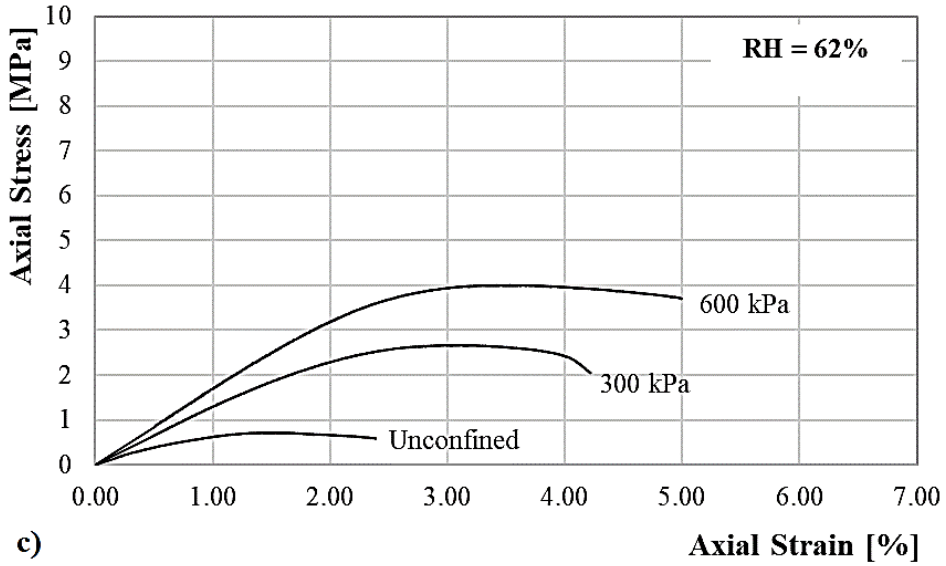

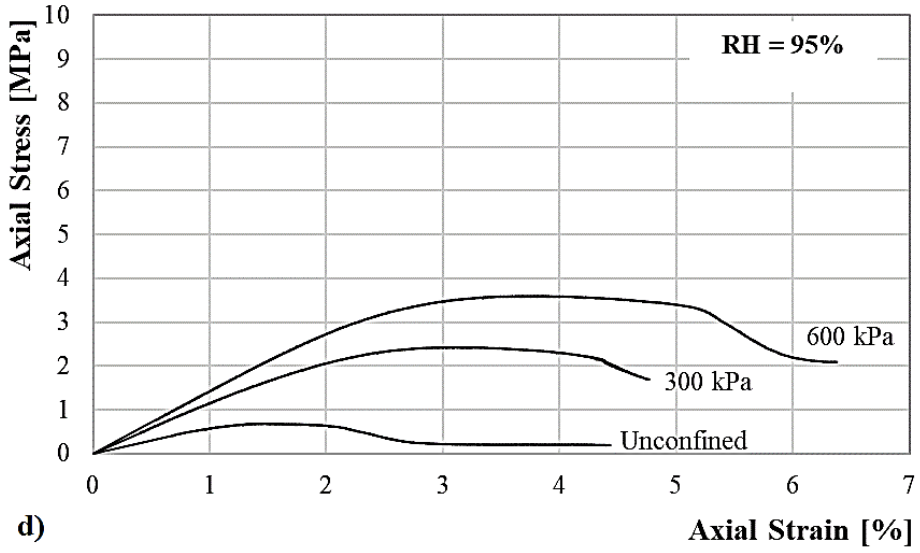

Figure 5.9: Results from triaxial tests on the hyper-compacted earth mix 3 at different confining pressures and distinct humidity levels: dry (a), 25 % (b), 62 % (c), 95 % (d).

Figure 5.10 shows the stress-strain curves measured from the triaxial tests on the samples of earth mix 1 compacted at the Proctor optimum as previously described. Similar observations to those already made in relation to the hyper-compacted samples of earth mixes 1 and 3 can be made.

For the Proctor samples, the highest values of strength were measured on the dry samples attaining a maximum of about 7 MPa. Interestingly, this level of strength is higher than that recorded on the hyper-compacted samples of earth mix 3 despite the Proctor samples of earth mix 1 exhibit a markedly lower density than the hyper-compacted ones. This confirms, once again, the importance of particle grading in defining the mechanical properties of earth materials.

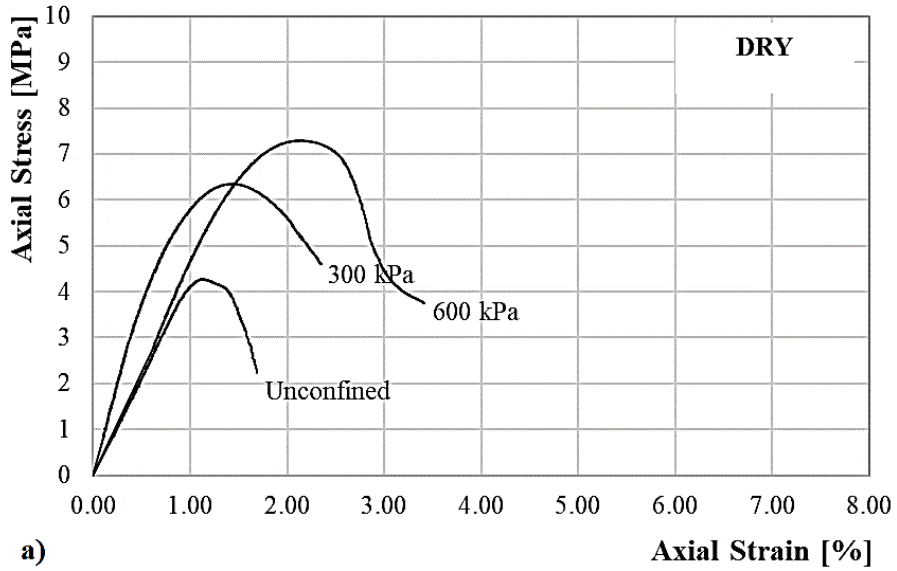
DRY
Axial Stress [MPa]
10
9
8
7
6
5
4
3
2
1
0
300 kPa
600 kPa
Unconfined
0.00
1.00
2.00
3.00
4.00
5.00
6.00
7.00
8.00
Axial Strain [%]

a)

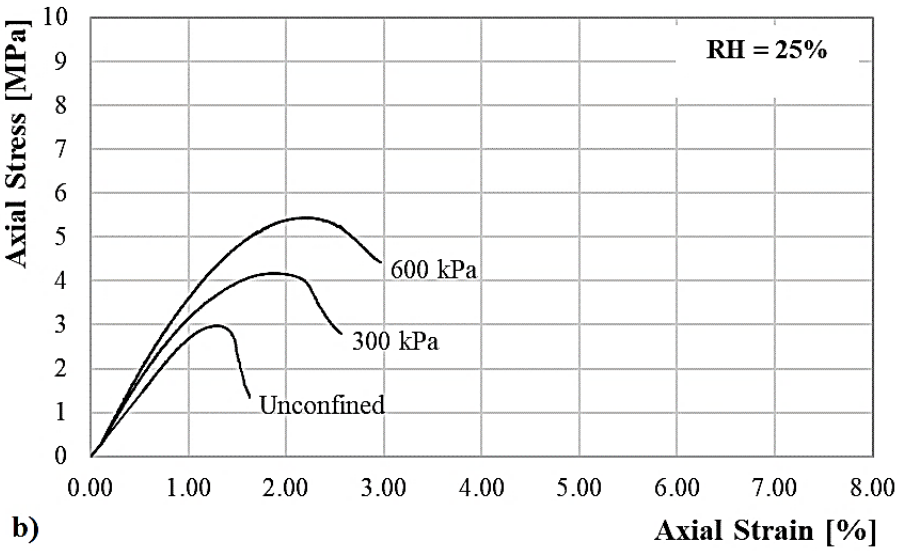
RH = 25%
Axial Stress [MPa]
10
9
8
7
6
5
4
3
2
1
0
600 kPa
300 kPa
Unconfined
0.00
1.00
2.00
3.00
4.00
5.00
6.00
7.00
8.00
Axial Strain [%]

b)

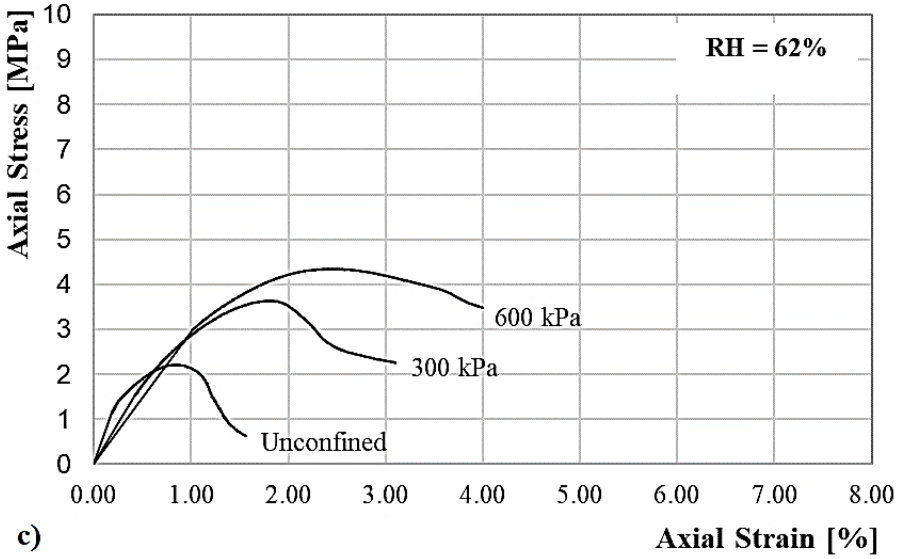
RH = 62%
Axial Stress [MPa]
10
9
8
7
6
5
4
3
2
1
0
600 kPa
300 kPa
Unconfined
0.00
1.00
2.00
3.00
4.00
5.00
6.00
7.00
8.00
Axial Strain [%]

c)

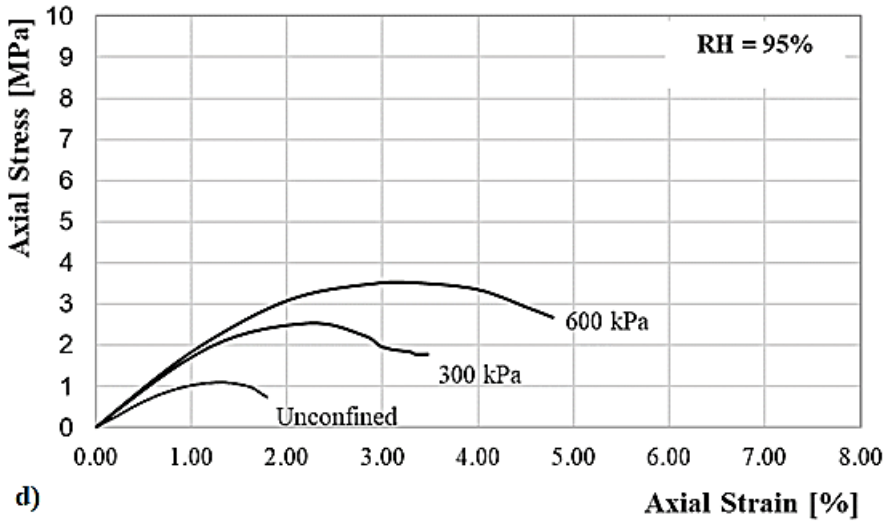

Figure 5.10: Results from triaxial tests on the Proctor compacted earth mix 1 at different confining pressures and distinct humidity levels: dry (a), 25 % (b), 62 % (c), 95 % (d).

The effect of humidity on strength and stiffness was described by defining both the strength envelope in the *q:p* plane (where *q* is the deviator stress and *p* is the mean stress) and the stiffness envelope in the *E:σ* plane (where *E* is the Young's modulus and σ the confining pressure) at each humidity level.

In particular, for each humidity level, the peak values of deviator stress *q* measured at the three different confining pressures were plotted against the corresponding values of mean stress *p*. Four interpolating lines were then defined according to the following general equation:

$$q = C + (M\ p) \tag{5.2}$$

where the coefficients *C* and *M* are respectively the intercept and slope of the failure envelope at the relevant humidity level. The above coefficients can also be converted into the corresponding values of cohesion *c* and friction angle *φ* by means of the following equations:

$$M = \frac{6 \sin \varphi}{3 - \sin \varphi} \tag{5.3}$$

$$\sin \varphi = \frac{3\ M}{6 + M} \tag{5.4}$$

$$C = \frac{6\ c \cos \varphi}{3 - \sin \varphi} \tag{5.5}$$

$$c = \frac{(3 - \sin \varphi)\ C}{6 \cos \varphi} \tag{5.6}$$

Figure 5.11 shows the variation of the strength envelope with humidity levels for the hyper-compacted earth mix 1 while Table 5.3 summarises the strength parameters at the different humidities. Inspection of Table 5.3 indicates that the cohesion remains approximately constant regardless of the humidity level while the friction angle tends to increase considerably as the material is exposed to a drier atmosphere, and hence the degree of saturation decreases. A slight deviation from this trend is noticed for the samples equalised at the highest humidity of 95 %, which is probably due to the greater scatter of these tests.

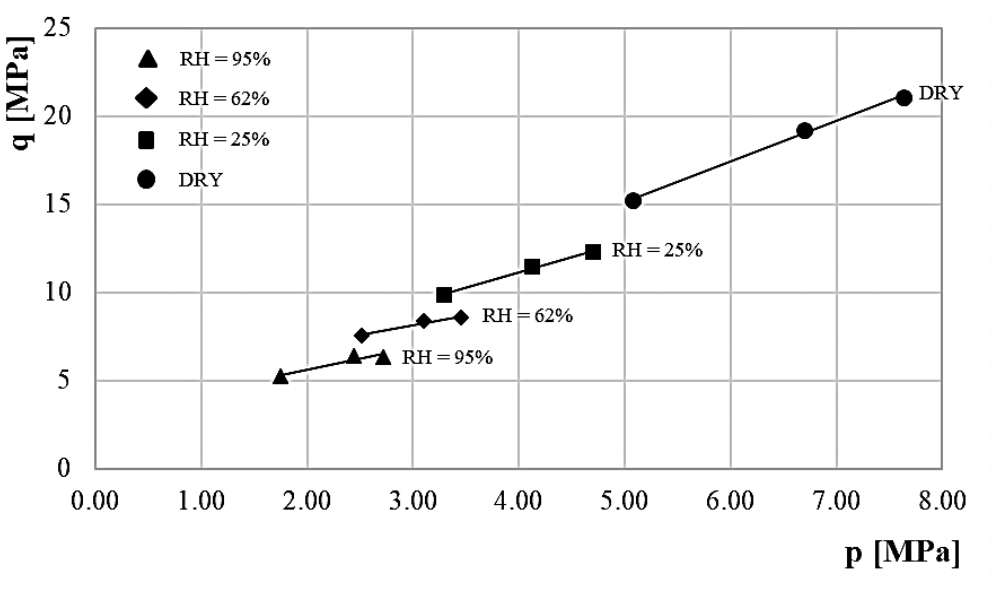

Figure 5.11: Strength envelopes of hyper-compacted earth mix 1 at different humidity levels.

Table 5.3: Strength parameters of hyper-compacted earth mix 1 at different humidity levels.

	M [-]	**φ [°]**	**C [MPa]**	**c [MPa]**
Dry	2.31	56.6	3.53	2.31
RH = 25 %	1.74	42.3	4.20	2.20
RH = 62 %	1.12	28.2	4.77	2.28
RH = 95 %	1.24	30.8	3.15	1.52

Figure 5.12 shows the variation of the Young's modulus E with confining pressure σ at all four humidity levels. Recall that the Young's modulus is here measured as the initial slope of the stress-strain curve, i.e. over the relatively small strain range when the material response is reasonably linear. Inspection of Figure 5.12 indicates that the Young's modulus decreases with increasing ambient humidity as a consequence of the growing degree of saturation of the material. The confining pressure exhibits a marked influence on Young's modulus only for the samples tested in dry conditions while the effect is almost negligible in all other cases.

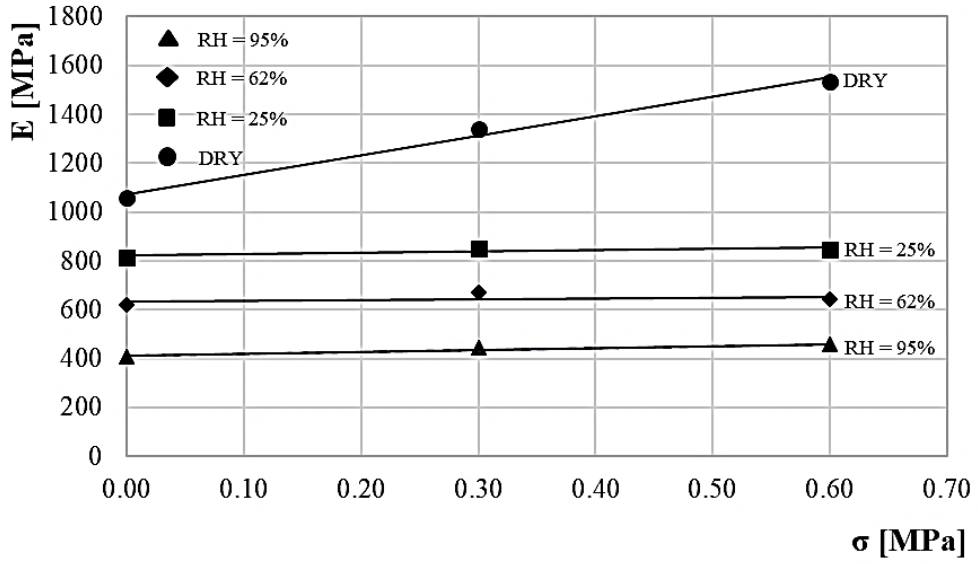

Figure 5.12: Stiffness envelopes of hyper-compacted earth mix 1 at different humidity levels.

Similar plots and tables are presented in the following part of this section for the hyper-compacted earth mix 3 and for the Proctor compacted earth mix 1 (Figures 5.13, 5.14, 5.15 and 5.16; Tables 5.4 and 5.5).

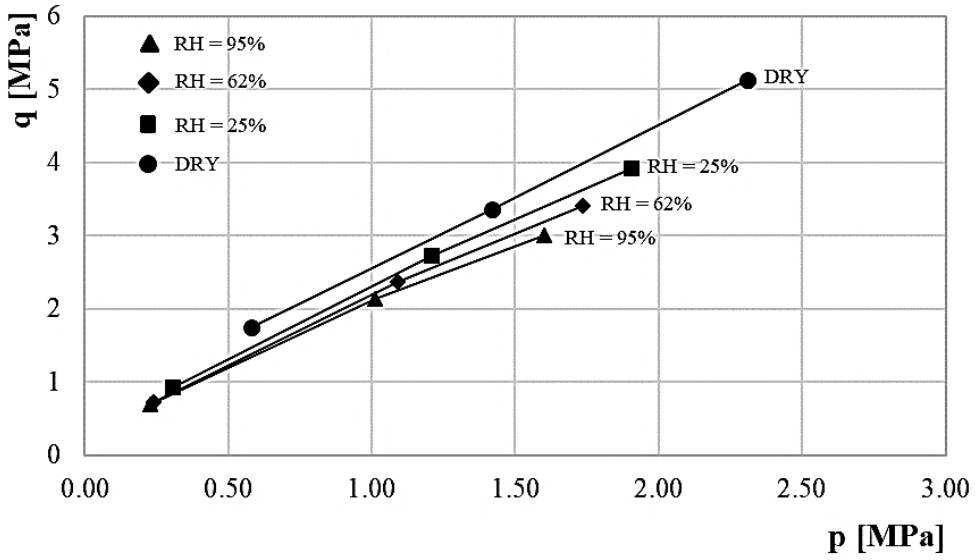

Figure 5.13: Strength envelopes of hyper-compacted earth mix 3 at different humidity levels.

Table 5.4: Strength parameters of hyper-compacted earth mix 3 at different humidity levels.

	M [-]	**φ [°]**	**C [MPa]**	**c [MPa]**
Dry	1.96	47.4	0.60	0.33
RH = 25 %	1.88	45.7	0.38	0.21
RH = 62 %	1.80	43.9	0.32	0.18
RH = 95 %	1.70	41.4	0.34	0.17

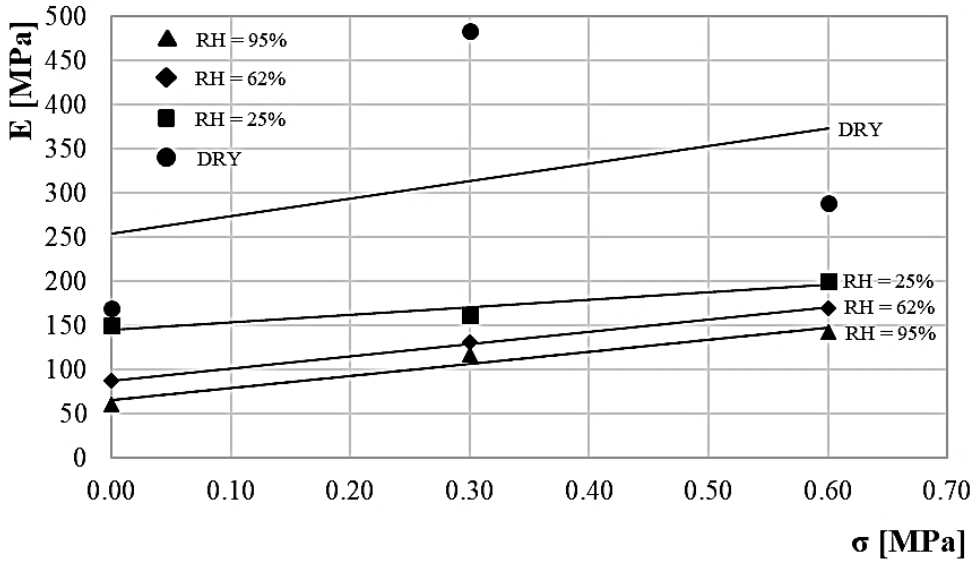

Figure 5.14: Stiffness envelopes of hyper-compacted earth mix 3 at different humidity levels.

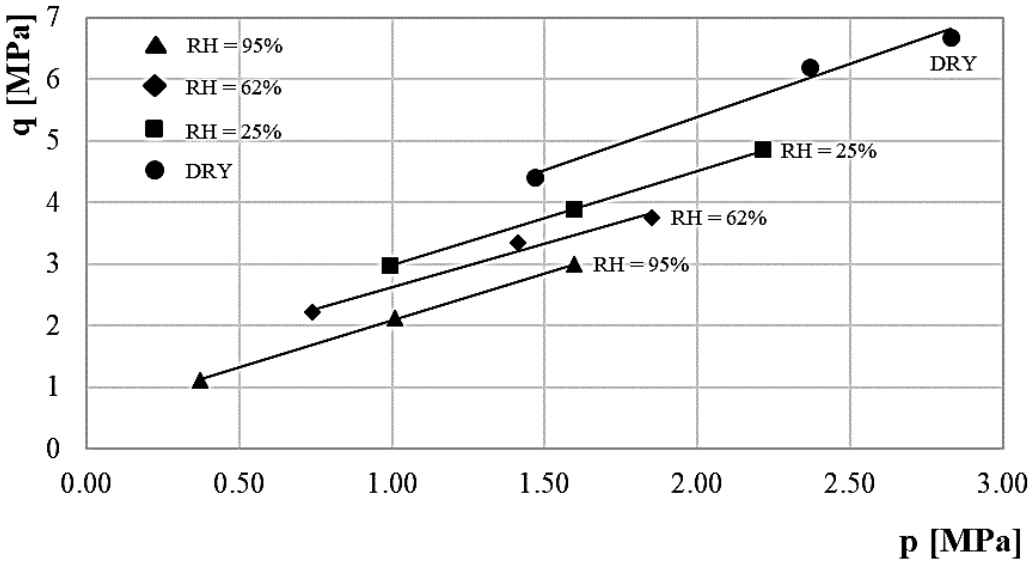

Figure 5.15: Strength envelopes of Proctor compacted earth mix 1 at different humidity levels.

Table 5.5: Strength parameters of Proctor compacted earth mix 1 at different humidity levels.

	M [-]	**φ [°]**	**C [MPa]**	**c [MPa]**
Dry	1.72	41.9	1.94	1.01
RH = 25 %	1.53	37.5	1.46	0.73
RH = 62 %	1.41	34.9	1.22	0.60
RH = 95 %	1.53	37.6	0.56	0.29

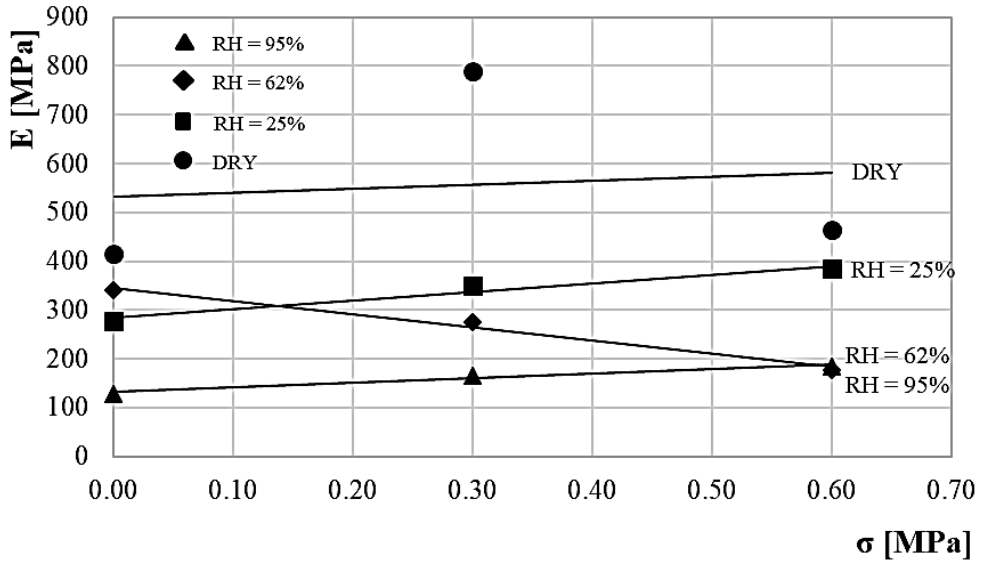

Figure 5.16: Stiffness envelopes of Proctor compacted earth mix 1 at different humidity levels.

Raw earth is characterised by the presence of meniscus water bridges between particles, which generate capillary bonding and increase the overall strength and stiffness of the material. The above results have shown that the mechanical characteristics of compacted earth tend to improve as ambient humidity reduces and, hence, degree of saturation decreases leading to an increase in number of inter-particle capillary menisci. At the same time, the the ability of the material to undergo significant plastic deformation before failure (i.e. ductility of the material) decreases as the material becomes drier.

The oven-dried samples exhibit the highest levels of strength and stiffness in apparent contradiction with the fact that, in this case, capillary menisci should ostensibly be absent and mechanical properties should therefore be poor. A truly dry material is a material saturated by air, which is conceptually no different from a material saturated by water, and should therefore obey the principle of effective stress. The expectation is that strength and stiffness should peak somewhere between fully dry and saturated conditions when the bonding action of capillary menisci should be most intense. As mentioned, a possible explanation of this apparent inconsistency may reside in the fact that the water content of the oven-dried samples is not zero, as commonly assumed, and that a small quantity of adsorbed and capillary water is still present, thus generating a suction inside the material. To further explore this aspect, additional tests must be performed on water saturated samples to compare the results with those for oven-dried samples presented in this paper.

Inspection of Figure 5.16 presents a decrease of the Young's modulus with increasing the confining pressure for Proctor compacted samples at the relative humiddity of 62 %. This result is counterintutive and might be consequence of an experimental error.

Figures 5.17 and 5.18 compare the stress-strain curves from triaxial tests performed at different confining pressures on the hyper-compacted samples of earth mix 1 and 3 under dry conditions and at a relative humidity of 95 %, respectively. These two humidity levels have been chosen because they correspond to the extremes of the range investigated in the present work and can therefore be used to infer the behaviour at intermediate humidity levels. Inspection of Figures 5.17 and 5.18 confirms the higher strength of earth mix 1 compared to earth mix 3, which is due to the diferrent particle grading and density of the two materials as previously discussed. In addition to this, inspection of Figures 5.17 and 5.18 indicates that the higher strength of earth mix 1 corresponds to a more fragile behaviour, which is rather undesirable as it favours the occurrence of abrupt failure mechanisms.

Figure 5.19 presents the ensemble of values of peak strength against the corresponding values of mean stress measured at different confining pressures and humidity levels on the hyper-compacted samples of earth mix 1 and 3. These results confirm that strength increases with growing material densification through compaction to high pressures. Nevertheless, material density is not the only important factor and particle grading has an equally important effect on the mechanical behaviour.

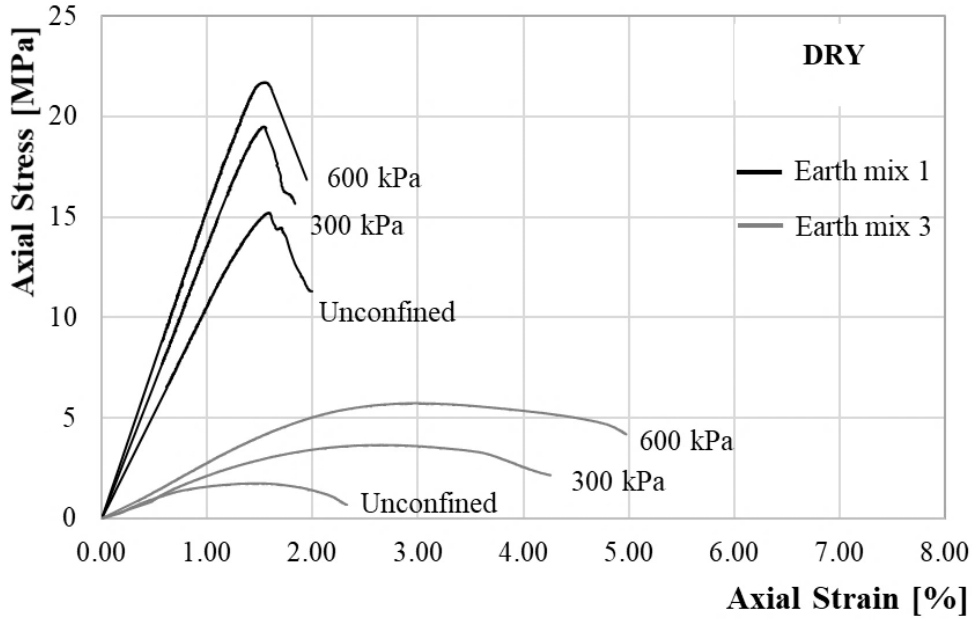

Figure 5.17: Comparison of results from triaxial tests on hyper-compacted earth mixes 1 and 3 under dry conditions.

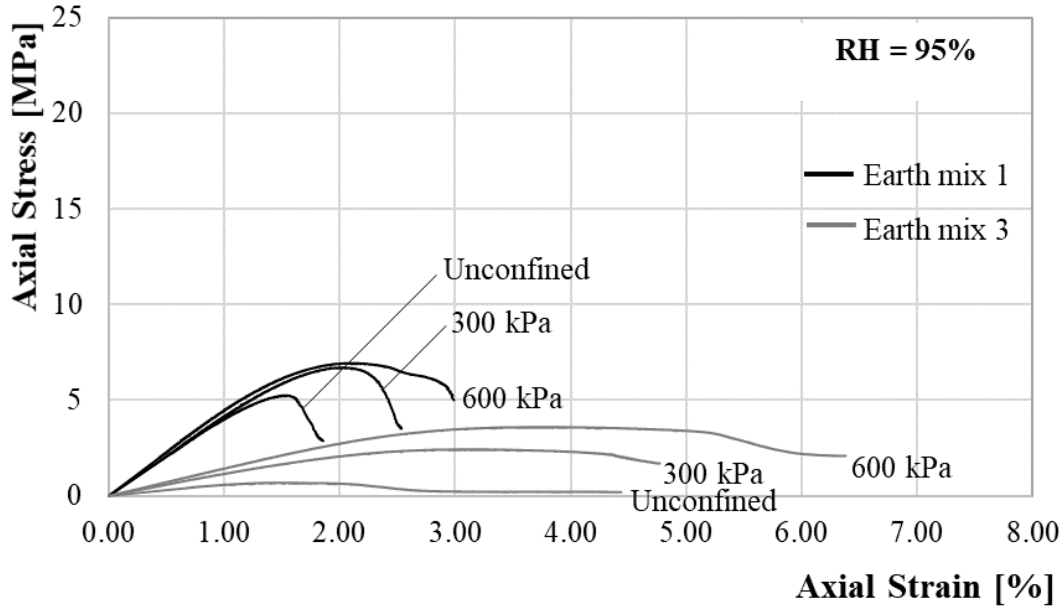

Figure 5.18: Comparison of results from triaxial tests on hyper-compacted earth mixes 1 and 3 at a relative humidity of 95 %.

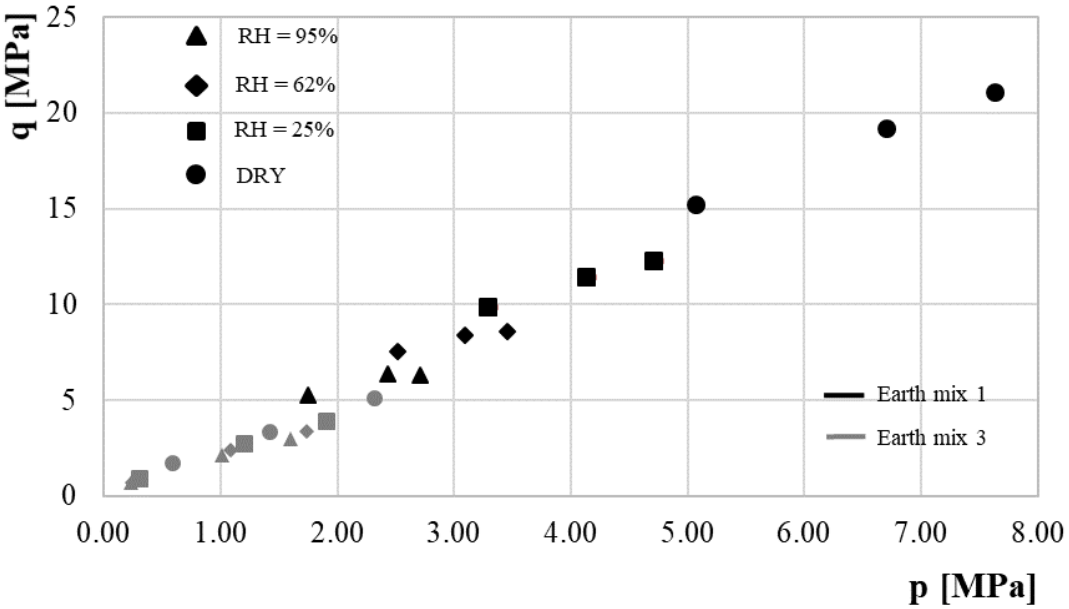

Figure 5.19: Values of peak strength measured at different confining pressures and humidity levels on hyper-compacted earth mixes 1 and 3.

In the same way, Figures 5.20 and 5.21 compare the stress-strain curves from the triaxial tests performed at different confining pressures on the hyper-compacted and Proctor compacted samples under dry conditions and at a relative humidity of 95 %, respectively. As expected, the hyper-compacted samples of earth mix 1 exhibit a higher strength than the Proctor compacted samples of the same material. This is because the former samples are

considerably denser than the latter ones due to the different compaction method. In spite of their relative mechanical weakness, the Proctor compacted samples were cosiderably more ductile (ability of the structure to accommodate the occurrence of potential settlements without incurring in abrupt failure) than the hyper-compacted samples. In this respect, a fine and well-graded earth mix can exhibit markedly larger values of strength and stiffness than a coarse and poorly-graded earth mix at similar levels of material density.

Figure 5.22 presents the ensemble of values of peak strength against the corresponding values of mean stress measured at different confining pressures and humidity levels on the hyper-compacted and Proctor compacted samples of earth mix 1. Inspection of Figure 5.22 confirm that, for the same earth mix, the strength increases with growing material densification through compaction at higher pressures.

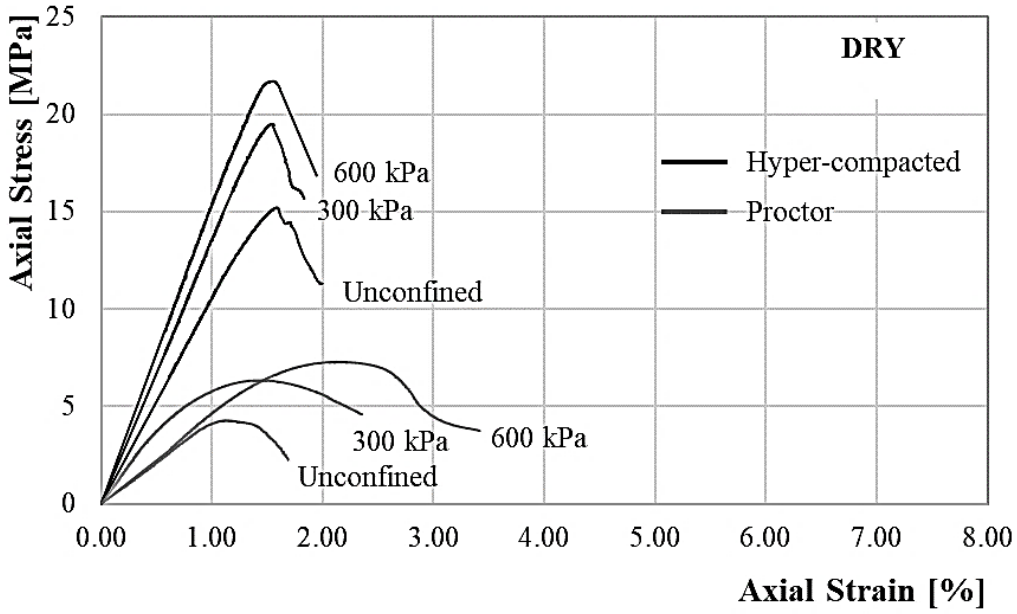

Figure 5.20: Comparison of results from triaxial tests on hyper-compacted and Proctor compacted samples of earth mix 1 under dry conditions.

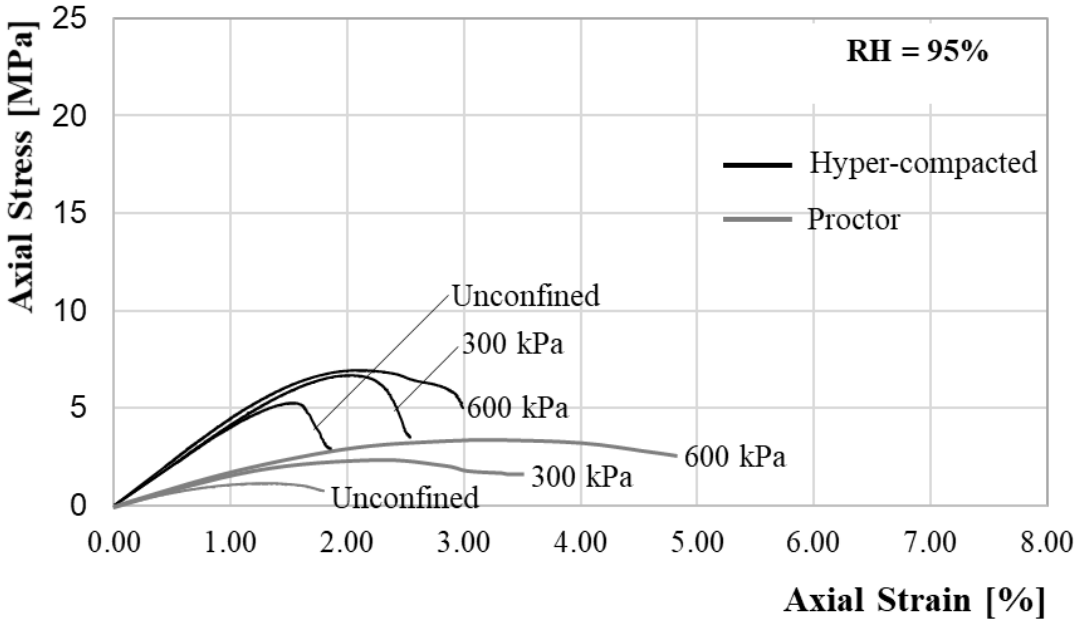

Figure 5.21: Comparison of results from triaxial tests on hyper-compacted and Proctor compacted samples of earth mix 1 at a relative humidity of 95 %.

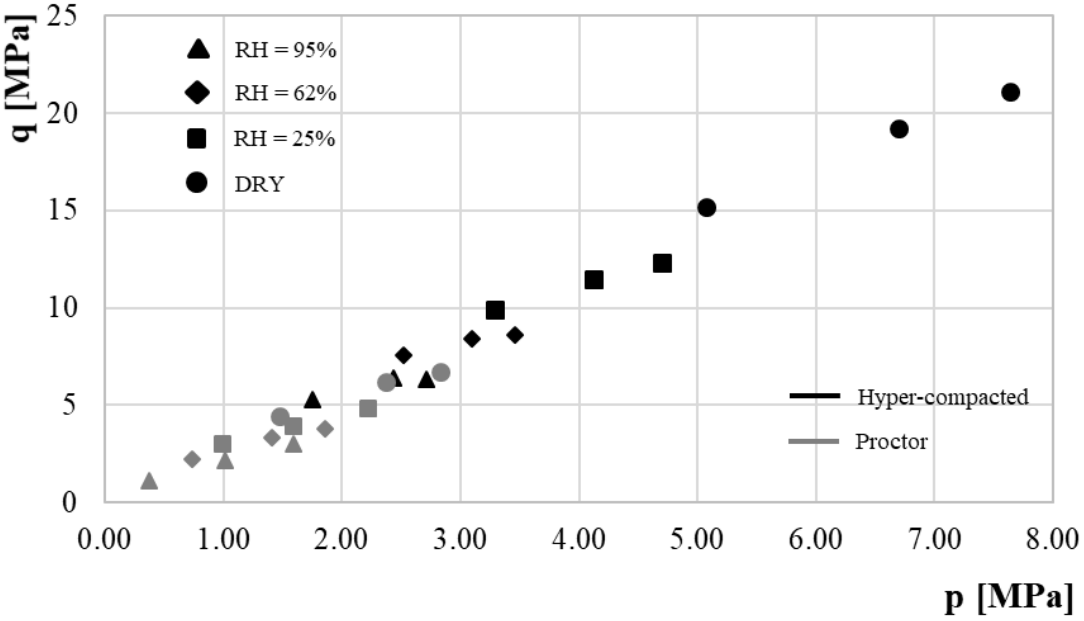

Figure 5.22: Values of peak strength measured at different confining pressures and humidity levels on hyper-compacted and Proctor compacted samples of earth mix 1.

5.2. Moisture buffering capacity

This section presents the results from a series of laboratory tests performed in the present work to investigate the hygroscopic behaviour of the same hyper-compacted earth mixes previously subjected to mechanical tests. The hygroscopic behaviour was investigated

through the measurement of the MBV (Moisture Buffering Value) of the material as discussed Section 2.3.

Hyper-compacted cylindrical samples with 50 mm diameter and 100 mm height were exposed to step cycles of relative humidity, between 53 % and 75 %, under a constant temperature of 23 °C inside the climatic chamber shown in Figure 5.23 (CLIMATS Type EX2221HA). Each of the two humidity levels was maintained for 12 hours while the sample mass was recorded every two hours. This experimental procedure is consistent with the norm ISO 24353 (2008) for the characterisation of the hygro-thermal behaviour of building materials exposed to cyclic variations of relative humidity over a daily period of time.

Each cylindrical sample was placed in the upright position inside an aluminium foil pan so that only the top and lateral surfaces were directly exposed to the atmosphere inside the climatic chamber. Therefore, the total area of the exposed surface was about 0.018 m^2, which is higher than the minimum value of 0.010 m^2 required by the norm ISO 24353 (2008). To confirm the repeatability of measurements, three replicate samples of the same material were tested, with the final MBV being calculated as the average of these three different measurements.

Figure 5.23: Climatic chamber CLIMATS Type EX2221-HA.

Before the start of the tests, all samples were equalised at a temperature of 23 °C and a relative humidity of 53 %. Equalisation was assumed to be complete when the mass of the sample changed less than 0.1 % over at least one week, which took generally a period of two weeks. After equalisation, the samples were exposed to the cyclic changes of relative humidity as previously described. Distinct MBVs were calculated during the moisture uptake and release stages of the consecutive cycles according to the following equation:

$$\mathrm{MBV} = \frac{\Delta m}{S\,\Delta\%RH} \tag{5.7}$$

where Δm is the absolute value of the sample mass variation (in grams), S is the exposed surface (in square meters) and $\Delta\%RH$ is the imposed relative humidity change (in percentage). The values of Δm measured at the end of a moisture uptake stage (i.e. at the end of the exposure to the high humidity level) provide the "MBV uptake" while the values of Δm measured at the end of a moisture release stage (i.e. at the end of the exposure to the low humidity level) provide the "MBV release". To take into account the change of sample dimensions caused by swelling of the earth, the exposed surface was calculated from the averages of three height measurements and three diameter measurements taken at the beginning of the test (i.e. at T = 23 °C and RH = 53 %) and at the end of each humidity increase step (i.e. at T = 23 °C and RH = 75 %). This assures that the small variations of sample dimensions, owed to swelling upon wetting at the high humidity level, are taken into account.

Figure 5.24 shows that the MBV is higher during moisture uptake than during moisture release for all three hyper-compacted earth mixes. This difference, however, reduces as the number of cycles increases and the material converges towards steady state. Steady state is conventionally defined as the occurrence of three consecutive "stable" cycles where moisture uptake at a humidity of 75 % is approximately equal to moisture release at a humidity of 53 %. In general, five cycles were sufficient to achieve steady state.

Results from MBV tests are also often presented in the form of moisture adsorption curves, which record the hygroscopic behaviour of the material throughout the cyclic variation of relative humidity. At any given time, the moisture adsorption is defined as the ratio between the variation of sample mass during a cycle (i.e. the difference between the current and initial masses of the sample) and the area of the exposed surface.

Figure 5.25 shows the moisture adsorption variation during the five relative humidity cycles imposed to the hyper-compacted samples of all three different earth mixes. Note that each curve is the average of the measurements from three samples for each earth mix. Inspection

of Figure 5.25 confirms that, for all samples, the MBVs differ during moisture uptake and release for the first two cycles due to the hysteretic behaviour of the soil. However, starting from the third cycle, the hygroscopic behaviour becomes virtually reversible with the moisture uptake becoming equal to the release, which is referred to as a stable cycle.

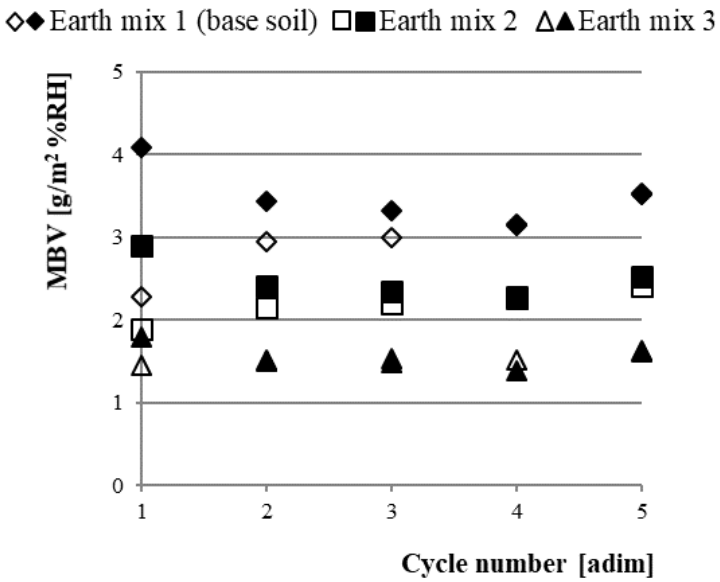

Figure 5.24: MBVs during moisture uptake and release in subsequent humidity cycles. Solid markers indicate MBV uptake while hollow markers indicate MBV release.

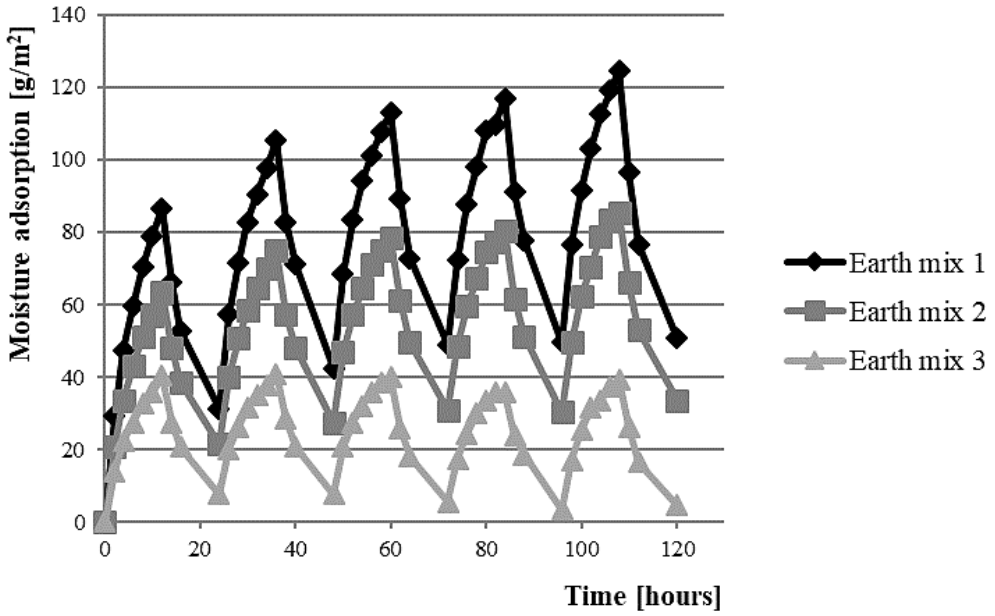

Figure 5.25: Moisture adsorption curves of the hyper-compacted samples of earth mixes 1, 2 and 3.

Figure 5.26 shows the moisture adsorption curves corresponding to the last stable cycles of the three earth mixes, when hygroscopic behaviour is virtually reversible with the moisture uptake approximately equal to the moisture release.

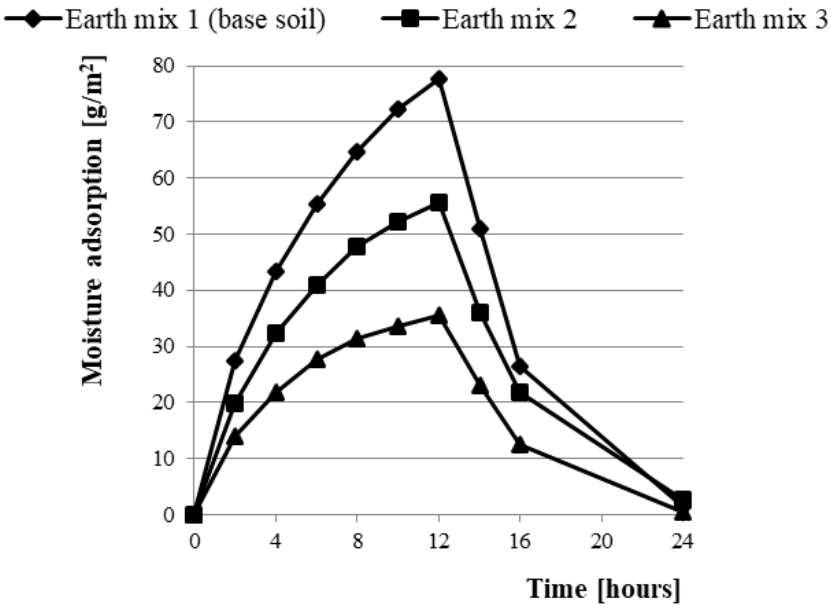

Figure 5.26: Moisture adsorption curves during last stable cycle.

The final MBV of the material is conventionally measured under steady state conditions and is calculated as the average of the uptake and release MBVs of the last three stable cycles. The final MBVs measured in the present work are summarised in Table 5.6, which shows that earth mix 1 exhibits a higher moisture buffering capacity than earth mixes 2 and 3. This is due to the presence of a larger fine fraction in earth mix 1 compared to earth mixes 2 and 3, which then means that earth mix 1 is capable of retaining more water than earth mixes 2 and 3. In particular, the MBV increases in an almost linear fashion with growing clay content (see Table 5.6) achieving a level that is twice higher for earth mix 1 compared to earth mix 3. Similar experimental observations were made for different earth materials by Jaquin et al. (2008) and Beckett and Augarde (2012).

Table 5.6: MBVs under steady state conditions.

Sample ID	**Clay content [%]**	**MBV [g/m²%RH]**
Earth mix 1 (base soil)	≈ 32	3.28
Earth mix 2	≈ 20	2.34
Earth mix 3	≈ 10	1.53

Figure 5.27 compares the MBVs measured in the present work against the MBVs measured by McGregor et al. (2014) on both unstabilised and stabilised earthen samples. The testing

procedure adopted by McGregor et al. (2014) (i.e. the levels and durations of the relative humidity steps) is identical to that adopted in the present work. Inspection of Figure 5.27 indicates that the earth mix 1 tested in the present study exhibits a moisture buffering capacity that is comparable with that of the unstabilised earth tested by McGregor et al. (2014). Also, the MBV of the hyper-compacted earth mix1 is about 1.5 times higher than the MBV measured by McGregor et al. (2014) on stabilised earth materials. The moisture buffering capacity of the materials tested in the present work decreases markedly with decreasing clay content in earth mixes 2 and 3, dropping to levels that are similar to those of the stabilised earth materials tested by McGregor et al. (2014).

The hygroscopic behaviour measured at the scale of cylindrical samples is here assumed to be representative of the behaviour at the scale of real bricks. This assumption is corroborated by experimental evidence from Bruno (2016), who confirmed that the measured MBV is independent of the modalities of application of the humidity load and the direction of vapour flow across the sample.

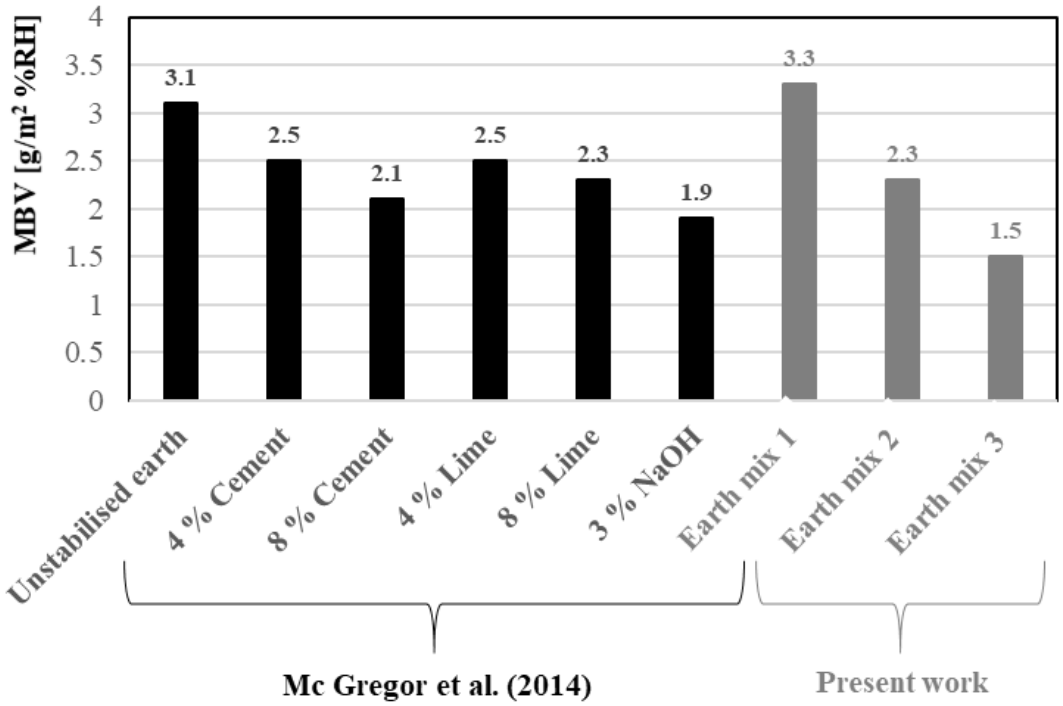

Figure5.27: Comparison of MBVs measured in the present work and in the work by McGregor et al. (2014).

5.3. Water durability properties

The hydrophilic nature of many soils enhances the moisture buffering capacity of the material but it is also responsible of the propensity to water erosion, and hence of the limited durability, of raw earth (see Section 2.4).

This section presents the results from different types of durability tests conducted to investigate the resistance of unstabilised earth to water erosion. Durability tests were undertaken according to the German norm "Earth blocks - Terms and definitions, requirements, test methods" DIN 18945 (2013), which describes the performance of immersion and suction tests. Drip tests were performed in accordance with the norm NZS 4298 (1998). Both suction and drip tests were accomplished at the scale of brick samples meanwhile immersion tests were performed at the scale of small cylindrical samples to avoid waste of material. All samples were hyper-compacted at the optimum water content as described in Section 4.2.2.

5.3.1. Immersion tests

Durability against water erosion was assessed by means of immersion tests on cylindrical hyper-compacted samples of 50 mm diameter and 50 mm height according to the standard experimental protocol described in the German norm DIN 18945 (2013). Before testing, all samples were equalised at the laboratory atmosphere, i.e. at a temperature of 20 ± 5 °C and a relative humidity of 40 ± 5 %, until the sample mass changed less than 0.1 % over at least one week, which took generally a period of three weeks. After equalisation, the sample was weighed to record its initial mass m_i and subsequently immersed in water for ten minutes. The sample was then removed from water and equalised again to the laboratory atmosphere in order to attain the same moisture content as before immersion. After equalisation, the final mass m_f was recorded and introduced, together with the initial mass m_i, in the following equation to calculate the percentage mass loss $\%\Delta m$ experienced by the sample during immersion:

$$\%\Delta m = \frac{m_i - m_f}{m_i} \times 100 \tag{5.8}$$

Table 5.7 summarises the results from all tests, which indicate that the hydrophilic nature of the three earth mixes has a clearly negative impact on water durability. All samples showed marked mass losses and exhibited numerous cracks after water immersion. Nevertheless, Table 5.7 shows that the finer and better-graded earth mix 1 exhibits a relatively small mass loss of only 13 % compared to 30 % for earth mix 2 and the complete dissolution of the sample in water for earth mix 3. Once again, these disparities might be attributed to the different densities of the samples but also to the distinct particle size distribution of the three earth mixes.

Table 5.7: Percentage of mass loss during immersion tests.

Sample ID	%Δm [%]
Earth mix 1 (base soil)	≈13
Earth mix 2	≈30
Earth mix 3	Complete dissolution after 4'30''

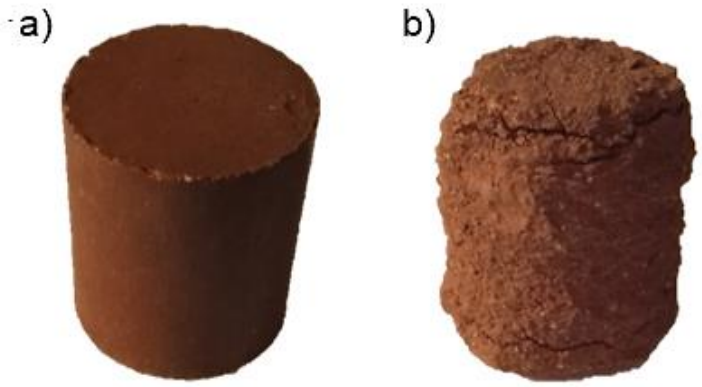

Figure 5.28: Hyper-compacted earth mix 1 before (a) and after (b) immersion in water for ten minutes.

Figure 5.28 shows two pictures of the hyper-compacted earth mix 1 taken before (a) and after (b) immersion in water. These pictures clearly indicate that immersion in water produces a marked erosion of the sample surface even for the relatively durable earth mix 1. This deterioration is also expected to negatively affect the strength and stiffness of the material, though this particular aspect has not been evaluated in the present work but will form part of future research.

5.3.2. Suction tests

Suction tests are performed to investigate the durability of compressed earth bricks when exposed to a temporary excess of water. This may be caused, for example, by the accumulation of water between the frame and the earthen infill of exterior timber frame walls or by capillary rise from the foundation soils into the building walls.

Bricks were hyper-compacted according to the fabricated method proposed by Bruno (2016) and described in Section 4.2.2. In particular, bricks of each earth mix were hyper-compacted at the optimum water content as determined on small cylindrical samples. After fabrication, the bricks were equalised under constant hygro-thermal conditions (i.e. T = 20 ± 5 °C and RH = 50 ± 5 %) for three weeks, which was long enough to attain a constant mass over time. In particular, three bricks were tested for each hyper-compacted earth mix to assess the repeatability of the experimental results.

A conventional fired brick with an absorbent cloth on top was placed at the bottom of a plastic container, which was partially filled with water (Figure 5.29). The level of the water into the container was maintained at 1 mm - 5 mm below the upper edge of the fired brick. The hyper-compacted earth brick was then placed over the absorbent cloth, which marked the start of the suction test. During the test, water was progressively absorbed by the earth brick through the cloth and the fired brick underneath. As adsorption progressed, it was necessary to top up the water level inside the container to keep it constant. According to the norm DIN 18945 (2013), samples were visually assessed after 30 min, 3 h and 24 h from the beginning of the test to detect cracks and permanent deformations owed to swelling.

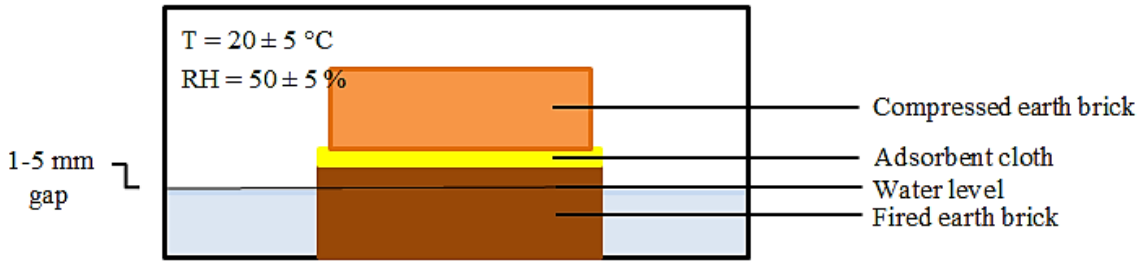

Figure 5.29: Suction test set-up.

Figure 5.30 shows the results of the suction tests performed on one of three bricks tested for each earth mix.

The results were very similar for the other two bricks of each earth mix and are therefore not included in Figure 5.30. As expected, earth mix 3 exhibited the weakest response to water adsorption with cracks and irreversible deformations already visible after 30 minutes from the beginning of the test. Bricks representative of earth mix 1 and earth mix 2 exhibited instead greater durability as confirmed by the fact that cracks only appeared after 3 hours after the beginning of the test. According to the norm DIN 18945 (2013), all earth bricks tested in the present work are only suitable for dry applications and cannot be exposed to running water.

Earth mix 1 (3 h)

Earth mix 2 (3 h)

Earth mix 3 (30 min)

Figure 5.30: Results for suction tests performed on hyper-compacted earth mixes 1, 2 and 3.

5.3.3. Drip tests

Drip tests were performed on hyper-compacted bricks of each earth mix, which were manufactured as described in Section 4.2.2. As before, the bricks were manufactured at their respective optimum water contents, which were previously determined at the scale of small cylindrical samples (see Section 4.2.2). Before testing, the bricks were equalised under constant hygro-thermal conditions (i.e. T = 20 ± 5 °C and RH = 50 ± 5 %) for three weeks to attain a constant mass over time.

The test procedure consisted in dripping 100 ml of water for up to 60 min from a height of 400 mm on the largest face of the brick. The surface of the brick was kept at an inclination of $\theta = 27$ °, as shown in Figure 5.31. The norm NZS 4298 (1998) requires the measurement of the final erosion depth at the impact point after 60 min but, in this work, the erosion depths were also noted at intermediate times of 15 min, 30 min and 45 min. The depth of erosion was recorded by using a Vernier calliper with a depth gauge having a precision of 0.02 mm. According to the norm NZS 4298 (1998), if the depth of erosion is less than 5 mm, the earthen material is deemed to have successfully passed the erosion test.

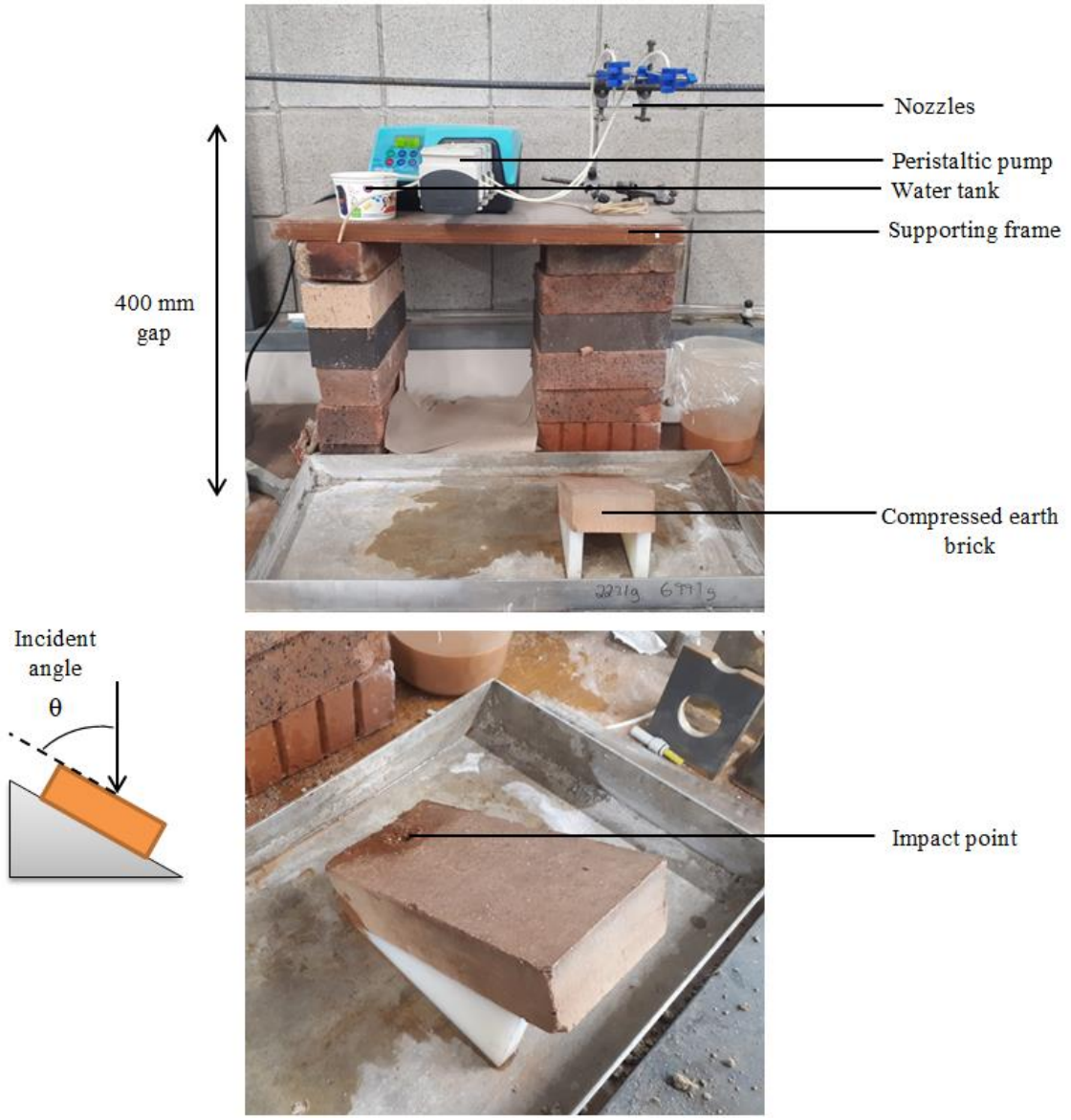

Figure 5.31: Drip test set-up.

Table 5.8 presents the final erosion depth measured after 60 min for each earth mix as the average of three test replicates. Inspection of Table 5.8 indicates that the samples of earth mix 2 and earth mix 3 failed to pass the test as they exhibited an erosion depth that is greater than the admissible limit. In the case of earth mix 1, the brick exhibited an erosion depth that is less than 5 mm, so this material successfully passed the durability test.

The erosion rates for the three earth mixes are presented in Figure 5.32. For earth mixes 2 and 3, the rates of erosion are higher than that for earth mix 1, which may be due to the higher amount of sand contained in the former earth mixes compared to the latter one.

The time required to achieve the maximum admissible erosion depth of 5 mm was also calculated for each earth mix by means of graphic extrapolation. Earth mix 3 requires about

30 minutes, earth mix 2 requires about 40 minutes, while earth mix 1 requires about 60 minutes.

Table 5.8: Final erosion depths of hyper-compacted bricks of earth mixes 1, 2 and 3.

Sample ID	Erosion depth after 60 min [mm]
Earth mix 1	4.38
Earth mix 2	8.96
Earth mix 3	10.52

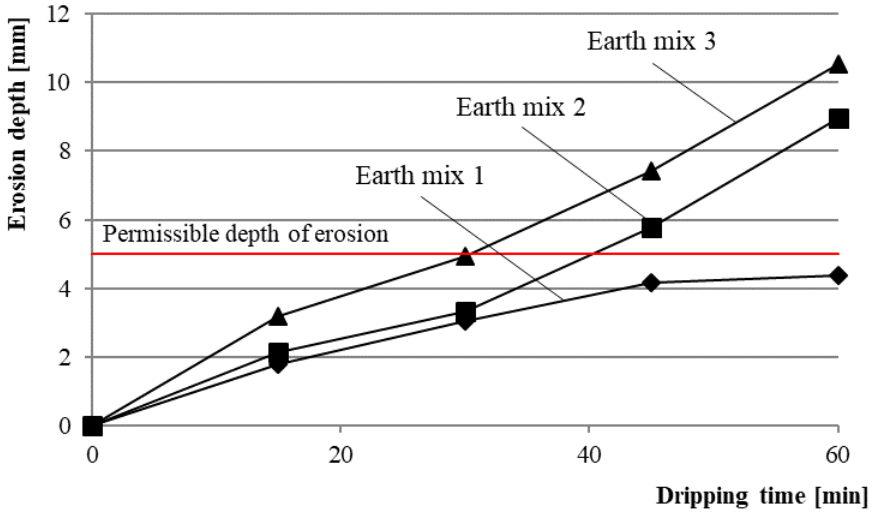

Figure 5.32: Depth of erosion versus time for hyper-compacted bricks of earth mixes 1, 2 and 3.

Consistent with the results from previous strength tests, inspection of Figure 5.32 indicates that an higher clay content enhances the bonding between soil particles and therefore improves the durability of the material. However, even for earth mix 1, the results from the durability tests are relatively poor, especially those from immersion and suction tests, which mandates the use of stabilisation for all earth mixes tested in the present work.

5.3.4. Bricks classification

The norm DIN 18945 (2013) adopts a classification of compressed earth bricks based on their resistance to natural weathering and their suitability for different applications (see Table 5.9).

Table 5.9: Classes of compressed earth bricks (DIN 18945, 2013).

Applications	Class
External wall exposed to natural weathering	Ia
Coated external wall exposed to natural weathering	Ib
External wall not exposed to natural weathering – Internal wall	II
Dry applications	III

Next, Table 5.10 presents the classification of the hyper-compacted bricks tested in the present work according to the norm DIN 18945 (2013) on the basis of immersion and suction test results. Note that, in Table 5.10, the results from the immersion tests on cylindrical samples are considered to be representative of the material behaviour at the brick scale.

Comparison of Tables 5.9 and 5.10 indicates that the hyper-compacted bricks of earth mix 1 may be used for the construction of external walls not exposed to natural weathering or for the construction of internal walls. Conversely, the hyper-compacted bricks of earth mixes 2 and 3 can only be used for dry applications where exposition to water is not envisaged during the entire service life of the structure. This is also consistent with previous test results, which have shown that earth mix 1 is the strongest and stiffest material with highest moisture buffering capacity (see Section 5.1 and 5.2).

Table 5.10: Classification of the hyper-compacted bricks tested in the present work (DIN 18945, 2013).

Sample ID	Immersion test	Suction test
Earth mix 1	II	Ib
Earth mix 2	III	Ib
Earth mix 3	III	III

Note that the classification of Table 5.10 is only partial because, to be complete, it should also include the results from contact tests (DIN 18945, 2013) that have not been performed in the present work. Previous studies have demonstrated that the different durability tests prescribed by the norm DIN 18945 (2013) may sometimes produce contradictory results. This is particularly important in the context of the present investigation because bricks are classified in accordance to the worst observed performance and the contact test represents the most severe assessment of material durability in the presence of water.

Results of drip tests were analysed in relation to the Erodability Index E_r (see Section 2.4) in accordance with the norm NZS 4298 (1998). Table 5.11 shows the classification of the

hyper-compacted bricks of all three earth mixes on the basis of their respective depths of pitting, at the impact point, after 60 minutes from the beginning of the drip test.

In conclusion, all bricks tested in the present work exhibit more or less unfavourable characteristics in terms of water durability and are therefore not suitable for direct exposure to natural weathering. The above results therefore demonstrate the urgency of further investigation about the use of sustainable stabilisation methods for improving the durability of earth materials while preserving their advantageous mechanical and moisture buffering properties.

Table 5.11: Erodability Index E_r classification of the hyper-compacted bricks tested in the present work (NZS 4298, 1998).

Sample ID	**Erodability Index [E_r]**	**Rating**
Earth mix 1	2	Slightly erosive
Earth mix 2	3	Erosive
Earth mix 3	4	Very erosive

5.4. Conclusions and final remarks

The main outcomes of the work presented in this chapter can be summarised as follows:

- The compressive strength and stiffness of compacted raw earth increase with growing density, though this increase is far from linear also because of a marked influence of earth grading on material behaviour;
- Besides the density, the particle size distribution and the clay content play a very important role in governing the mechanical performance of earth materials. A well-graded particle distribution and a higher amount of clay enhance capillary bonding between the earth particles providing higher levels of strength and stiffness;
- For classic geotechnical materials, it is well known that stiffness and strength reduce as saturation increases and pore suction decreases. The results from the present work are therefore consistent with unsaturated soil mechanics theories as they have shown that the mechanical characteristics of hyper-compacted earth improve as ambient humidity reduces and degree of saturation decreases. The decay of mechanical characteristics with increasing ambient humidity suggests that potential variations of moisture content inside the earth should be carefully considered during the design, construction and service life of buildings;

- Finer and well-graded earth mixes are characterised by a large moisture buffering capacity, with MBVs that are significantly larger than those of coarse and poorly-graded earth mixes. The MBV of the finest and best-graded earth mix tested in the present work is about 1.5 times higher than that measured on stabilised compacted earth samples by McGregor et al. (2014);
- Results from immersion, suction and drip tests have confirmed the relatively poor water durability of unstabilised earth and have led to the conclusion that all earth materials tested in the present work cannot be exposed to natural weathering without suitable stabilisation. It has, however, also been demonstrated that the utilisation of a fine and well-graded earth mix, with a clay content of about 30 %, can already reduce the vulnerability to water erosion by a significant amount. This improvement, albeit insufficient for mainstream building applications, reduces the need of stabilisation and the associated negative impact on the hygro-mechanical and environmental performance of the material;
- In most building applications, the durability of raw earth against water erosion must be improved by means of suitable stabilisation. It is, however, important that the chosen stabilisation method does not impact negatively on the advantageous mechanical and moisture buffering properties of raw earth;
- Results generally indicate that fine and well-graded earth mixes produce a better overall material performance than coarse and poorly-graded earth mixes regardless of the compaction level. Soil selection should therefore be carefully taken into account during the design of masonry structures.

6. Bio-stabilisation of raw earth using Enzymatic Induced Calcite Precipitation (EICP)

Chapter 3 has discussed the principles of calcite precipitation as a method for the stabilisation of earth building materials. Precipitation of calcite is a relatively straightforward chemical process, which is controlled by four key factors: a) the concentration of reagents, b) the temperature of the solution, c) the pH of the solution and d) the availability of nucleation sites. In particular, the present chapter investigates the factors that influence the kinetics of urea hydrolysis as the concentration of urea and calcium chloride. The objective is to optimise the catalysing effect of the urease enzyme and therefore to maximise the precipitation of calcite.

The optimised EICP method is then applied to the stabilisation of compressed earth to assess the improvement of material characteristics. In particular, a large series of experiments is performed on stabilised earth samples including immersion tests to measure durability to water, unconfined compression tests to measure strength/stiffness and moisture buffering tests to measure water storage capacity.

6.1. Factors affecting EICP efficiency: concentration of reagents

Samples of crude soybeans extract containing different equimolar concentrations of urea and calcium chloride were prepared inside test-tubes. The activity of the urease enzyme was detected, for each concentration level, by measuring the pH and the electrical conductivity of the solution using an acidity meter and ion-selective electrodes, respectively. Measurements of pH are useful because the release of ammonia during the hydrolysis of urea produces an increase of pH (see Section 3.2). The differences of pH between distinct samples can, however, be very small and a frequent calibration of the acidity meter is therefore required to minimise errors.

The amount of precipitated calcite was subsequently measured by weighing the solid material recovered after filtration of the test-tubes content. This allowed the identification of the optimal equimolar concentrations of urea and calcium chloride leading to the largest amount of calcite precipitation.

Finally, the mineralogical composition of the precipitated material was identified by means of X-Ray Diffraction (XRD) analysis.

6.1.1. Test-tube experiments

Twelve test-tubes with a capacity of 40 ml were filled with fresh liquid soybeans extract obtained by following the procedure described in Section 4.3.1. The soybeans extract was then mixed with twelve different equimolar concentrations of urea and calcium chloride, namely 0.010 mol/L, 0.025 mol/L, 0.050 mol/L, 0.10 mol/L, 0.50 mol/L, 1.00 mol/L, 1.50 mol/L, 2.00 mol/L, 2.50 mol/L, 3.00 mol/L, 3.50 mol/L and 4.00 mol/L. Urea was added to the extract immediately after centrifugation of the soybeans (see Section 4.3.3) while calcium chloride was added after 24 hours. Figure 6.1 shows the values of electrical conductivity and pH recorded one hour after the addition of urea, at different concentrations, to the soybeans extract.

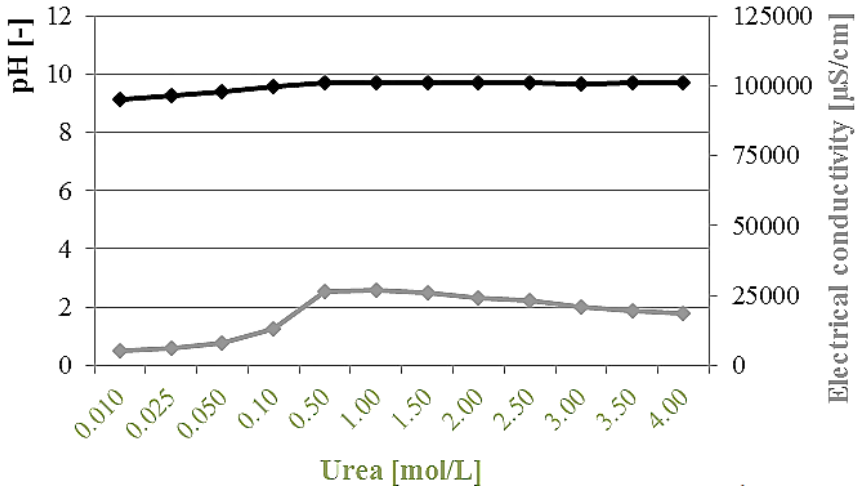

Figure 6.1: Measurements of pH and electrical conductivity taken one hour after adding urea to the liquid soybean extract (urea concentration varying from 0.010 mol/L to 4 mol/L).

Inspection of Figure 6.1 indicates that, regardless of the concentration of the added urea, the pH of the solution increases to about 10 from the initial value of 6 before addition of the urea. This marked increase of pH confirms the occurrence of urea hydrolysis triggered by the enzymatic activity. The alkaline environment generated by the production of ammonia and the consequent release of carbon dioxide are indeed the key precursors of calcite precipitation (Castanier et al., 1999). The initial electrical conductivity of the pure soybeans extract was equal to about 2400 µS/cm. After addition of urea, this value increases to a different level depending on the chosen concentration as shown in Figure 6.1. The variation of electrical conductivity suggests that the rate of hydrolysis increases with growing concentration of urea until a maximum is attained, after which the rate of hydrolysis decreases. This result may be explained by urease inhibition at high concentrations of reaction products (Nemati and Voordouw, 2003).

Figure 6.2 shows measurements taken 24 hours after the introduction of urea and indicates a marked increase in electrical conductivity. This suggests an enduring activity of the enzyme over time (though the pH remains approximately unchanged) and means that urea is hydrolysed at a relatively slow pace, so that sufficient time must be allowed for the reaction to occur. Figure 6.3 compares the enzyme activity, detected through electrical conductivity measurements, after 1 and 24 hours from the addition of urea to the liquid soybeans extract. The maximum value of electrical conductivity changes from about 27000 µS/cm after 1 hour to about 100000 µS/cm after 24 hours from the addition of urea.

After 24 hours from the addition of urea, equimolar concentrations of calcium chloride were introduced in each test-tube. Figure 6.4 shows the measurements of pH taken 1 hour after the addition of calcium chloride, which indicate a significant reduction of pH back to the initial level of the pure soybeans extract.

Calcium chloride is a water-soluble ionic compound that releases heat as it dissolves. During dissolution, calcium hydroxide is formed and hydrogen ions are released causing the pH of the solution to reduce. Another way to think about it is that calcium chloride absorbs hydroxide and leaves free protons behind, making the solution more acidic.

After the addition of calcium chloride, calcium carbonate started to precipitate at the bottom of the test-tubes as it could be observed by visual inspection. After about 72 hours from the beginning of the reaction, an equilibrium is reached with no more material precipitating at the bottom of the test-tubes. Figure 6.5 shows the development of the chemical reaction into the test-tubes and the final amount of precipitated material after 72 hours from the addition of calcium chloride.

The amount of precipitated material was then measured as follows: (i) the solution was passed through filter paper to collect the material deposited at the bottom of the test-tubes; (ii) the collected material was placed inside a small pan and oven-dried at 40° C for 3 days, after which the pan and its content were weighed; (iii) the amount of precipitated calcium carbonate was obtained as the difference between the weight from step (ii) and the weight of the clean pan. Figure 6.6 shows the collection of the precipitated material by using a vacuum system that facilitates percolation of the test-tubes content across the filter paper while Figure 6.7 shows the collected material after drying in an oven at 40 °C for 3 days.

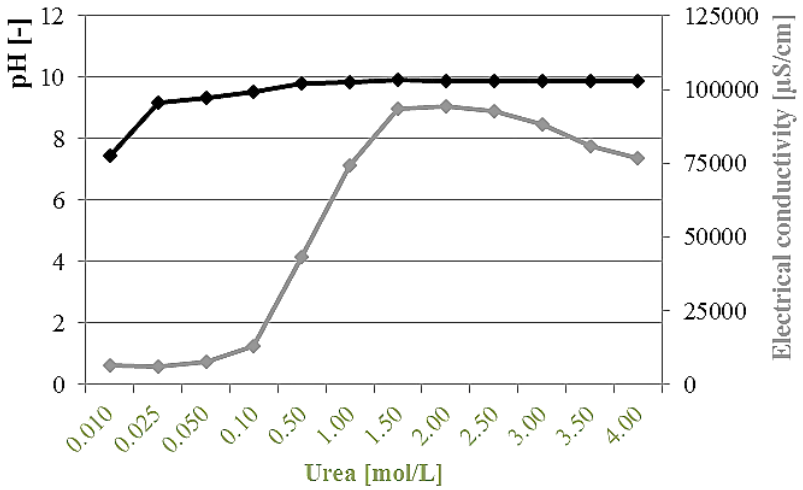

Figure 6.2: Measurements of pH and electrical conductivity taken 24 hours after adding urea to the crude soybeans extract (urea concentration varying from 0.010 mol/L to 4 mol/L).

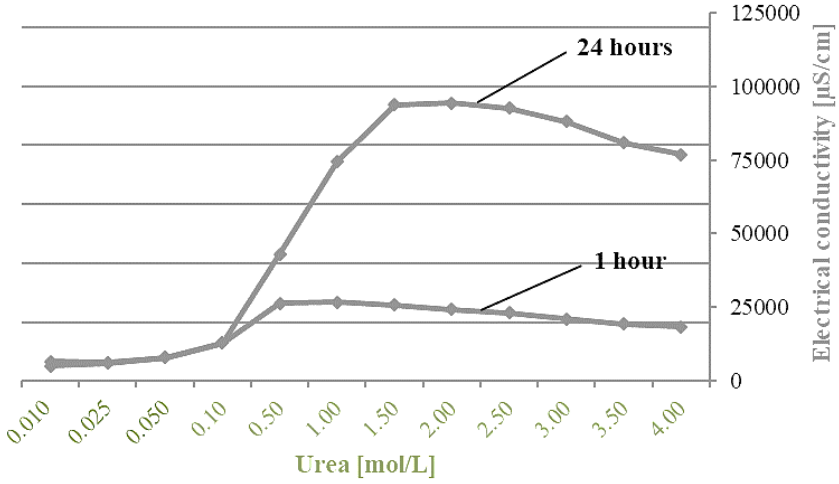

Figure 6.3: Measurements of electrical conductivity taken 1 and 24 hours after adding urea to the crude soybeans extract (urea concentration varying from 0.010 mol/L to 4 mol/L).

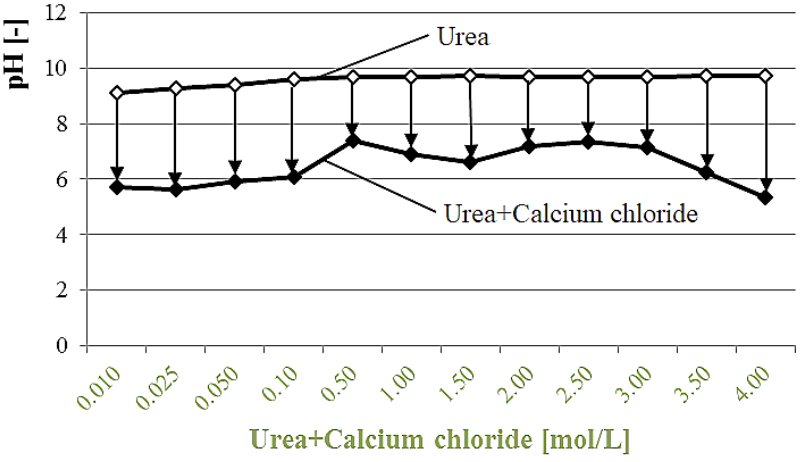

Figure 6.4: Reduction of pH after adding calcium chloride to the soybeans extract containing urea (equimolar urea and calcium chloride concentrations varying from 0.010 mol/L to 4 mol/L).

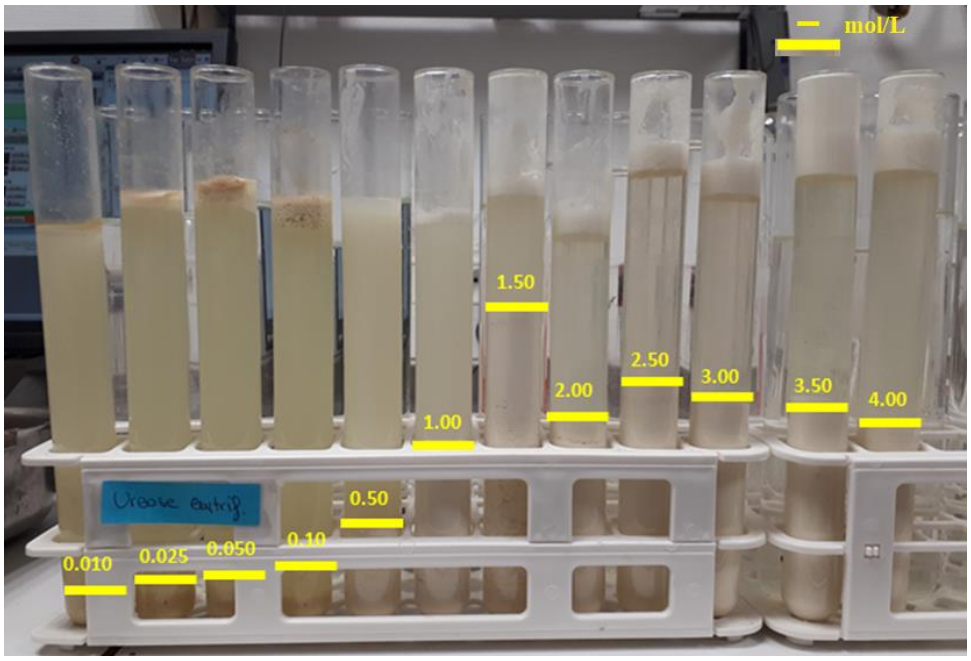

Figure 6.5: Visual examination of test-tubes after 72 hours from the addition of calcium chloride (equimolar urea and calcium chloride concentrations varying from 0.010 mol/L to 4 mol/L).

Figure 6.6: Collection of the precipitated material by using a vacuum system that facilitates percolation of the test-tubes content across the filter paper.

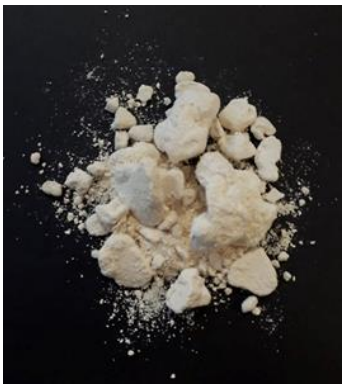

Figure 6.7: Precipitated calcium carbonate after being oven dried at 40 °C.

Each experiment was repeated three times to check the repeatability of results and the values herein reported are the averages of these three tests. The precipitation ratio (PR) is defined as the ratio between the actual mass of precipitated calcite $M^a_{CaCO_3}$ measured from the experiments and the theoretical mass of precipitated calcite $M^t_{CaCO_3}$ calculated from the chemical reactions shown in Chapter 3. The precipitation ratio is therefore defined by the following expression (Carmona et al., 2016):

$$PR(\%) = \frac{M^a_{CaCO_3}}{M^t_{CaCO_3}} \times 100 = \frac{M^a_{CaCO_3}}{C \times V \times M} \times 100 \quad (6.1)$$

where C is the concentration of the solution in mol/L, V is the solution volume in liters, and M is the molar mass of calcite (100.087 g/mol). Inspection of Figure 6.8 indicates that the precipitation ratio remains approximately equal to 100 % for increasing equimolar concentrations of urea and calcium chloride up to about 2.50 mol/L. Beyond this level, the precipitation ratio reduces below 100 % as the actual mass of precipitated calcite stays approximately constant while the theoretical mass continues to increase linearly with growing concentrations. This trend is consistent with the visual observation of the precipitated material inside test-tubes, which was largest for concentrations comprised between 1.50 mol/L and 2.50 mol/L. This result is also consistent with past applications of EICP to ground improvement, which have shown that this stabilisation technique becomes less effective if highly concentrated solutions of urea and calcium chloride are employed (e.g. Bull et al., 2014).

Inspection of Figure 6.8 indicates an optimal concentration of urea and calcium chloride equal to 2.50 mol/L. This concentration produces the largest precipitation of calcite and is therefore expected to generate the greatest degree of bonding between earth particles. Based on the above results, an equimolar concentration of urea and calcium chloride equal to 2.50 mol/L was used for the stabilisation of compressed earth in the following part of this work.

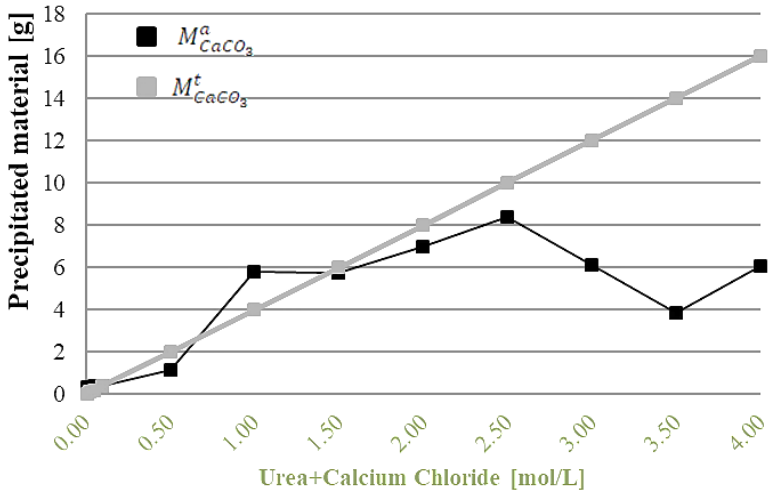

Figure 6.8: Theoretical ($\boldsymbol{M^t_{CaCO_3}}$) and actual ($\boldsymbol{M^a_{CaCO_3}}$) mass of precipitated calcite for equimolar concentrations of urea and calcium chloride from 0.010 mol/L to 4 mol/L (measured 72 hours after the addition of calcium chloride).

To further confirm that the precipitation reaction is catalysed by the urease enzyme present inside the soybeans extract, the same test-tube experiments were replicated by using, this time, distilled water instead of the soybeans extract. As expected, after 1 hour from the addition of urea to the distilled water, the pH and the electrical conductivity of the solution remained virtually unchanged and equal to the initial values of 8 and 20 µS/cm, respectively (Figure 6.9).

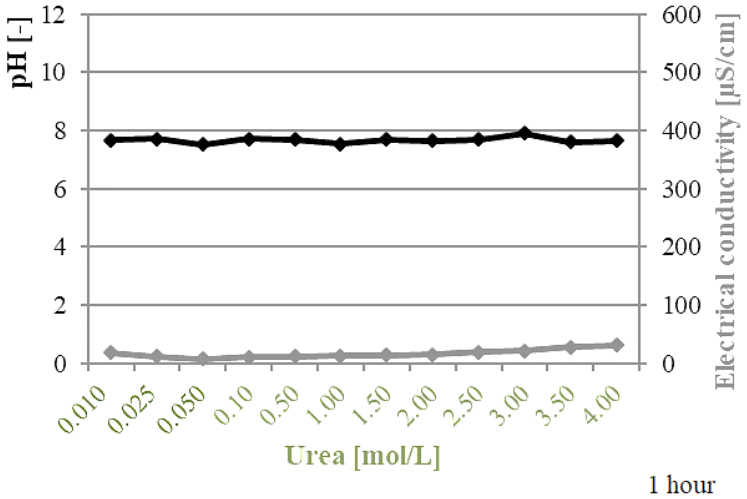

Figure 6.9: Measurements of pH and electrical conductivity taken 1 hour after adding urea to distilled water (urea concentration varying from 0.010 mol/L to 4 mol/L).

Figure 6.10 shows instead the measurements of pH taken after the addition of equimolar concentrations of calcium chloride (almost 24 hours after the addition of urea) to the distilled water already containing the urea. Unexpectedly, a raise in pH was recorded in this case, which was more marked for the test-tubes with higher reagents concentrations. An

explanation of this behaviour could be found in the spontaneous occurrence of the hydrolysis of urea in water, which however takes place at a much slower rate compared to the case where the urease enzyme is present as a catalyst.

The increase in pH after addition of both urea and calcium chloride (Figure 6.10) is consistent with the lack of calcite precipitation as confirmed by visual examination of test-tubes (Figure 6.11).

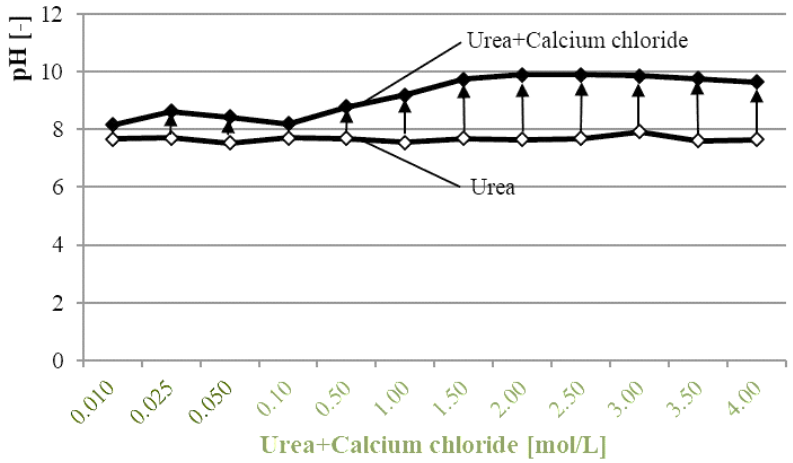

Figure 6.10: Increase of pH after adding calcium chloride to distilled water containing urea (equimolar urea and calcium chloride concentrations varying from 0.010 mol/L to 4 mol/L).

Figure 6.11: Visual examination of test-tubes after 72 hours from the addition of urea and calcium chloride in distilled water (equimolar urea and calcium chloride concentrations varying from 0.010 mol/L to 4 mol/L). No evidence of precipitation of calcium carbonate crystals.

The absence of urea hydrolisis is further corroborated by the measurements of electrical conductivity after 24 hours from the addition of urea in distilled water and before addition of calcium chloride (Figure 6.12). The highest value of electrical conductivity is about 25 µS/cm, which is only marginally higher than the level previously measured in distilled water and much lower than the value of 100000 µS/cm measured after adding urea to the soybeans extract. This result is consistent with the absence of ammonium ions produced by the hydrolisis of urea.

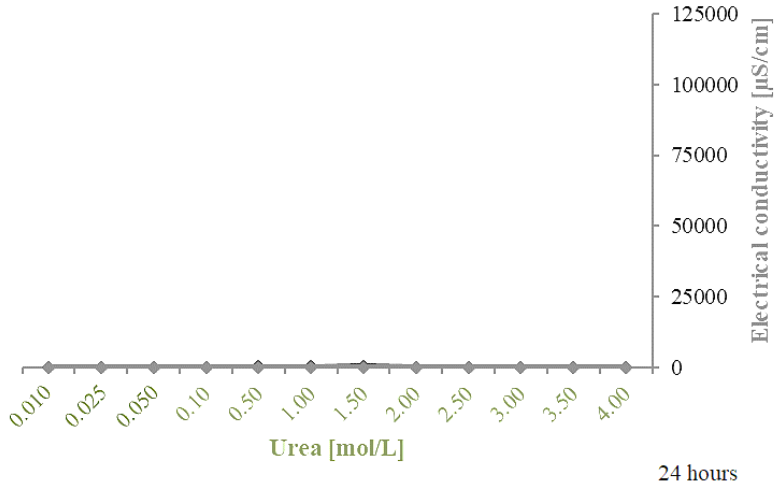

Figure 6.12: Measurements of electrical conductivity taken 24 hours after adding urea to distilled water (urea concentration varying from 0.010 mol/L to 4 mol/L).

Next, a modification was introduced to the previous experimental procedure by slightly modifying the source of urease enzyme. In this modified procedure, a fine soybeans powder, obtained by means of grinding, was used instead of a liquid soybean extract, obtained instead by means of centrifugation (see Section 4.3.4). This modification was introduced to investigate whether the efficiency of the catalyst effect of the urease enzyme could be improved by using directly a soybeans powder instead of a liquid extract.

Test-tubes were filled with distilled water to which the fine soybeans powder was subsequently added. A gram of soybeans powder was added for each 10 ml of distilled water, so that 4 grams of soybeans powder were added to each test-tube containing 40 ml of distilled water. This amount of soybeans powder was chosen in order to be consistent with the previous method where a liquid soybeans extract was instead used (see Section 4.3.1). Figure 6.13 shows the measurements of electrical conductivity taken after 1 and 24 hours from the addition of urea to the test-tubes containing already the mix of distilled water and fine soybeans powder. These measurements confirm that, similar to the case of the liquid extract,

the urease enzyme is also active inside the soybeans powder with a peak of efficiency recorded for a concentration of urea between 1.5 and 2.50 mol/L.

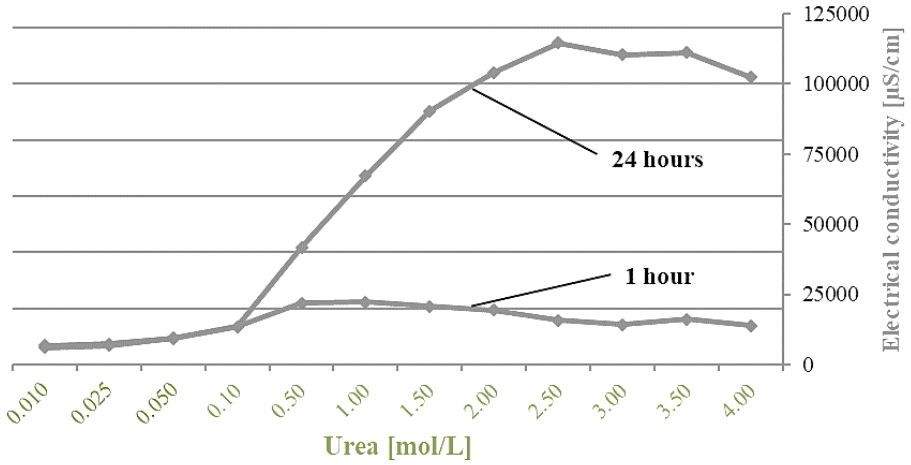

Figure 6.13: Measurements of electrical conductivity taken 1 and 24 hours after adding urea to distilled water plus soybeans powder (urea concentration varying from 0.010 mol/L to 4 mol/L).

Figure 6.14 compares the measuments of electrical conductivity taken 1 and 24 hours after the addition of urea for the two cases where the soybeans extract and the fine soybeans powder are respectively used

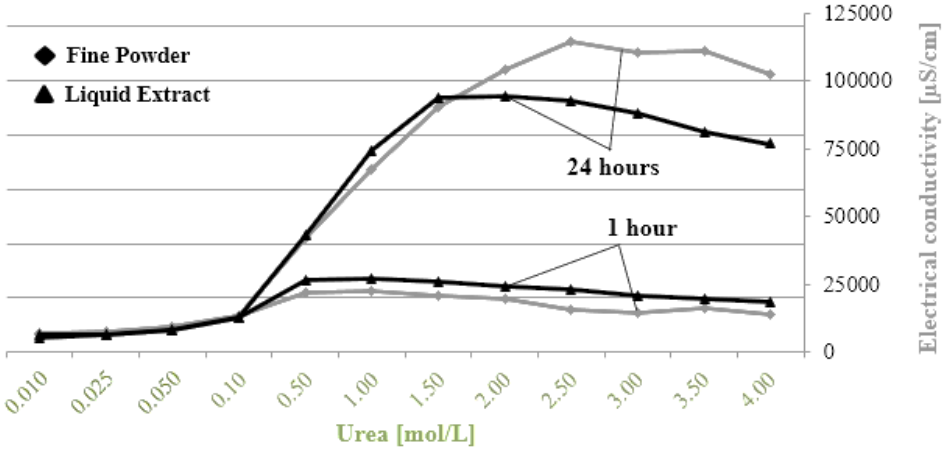

Figure 6.14: Comparison of electrical conductivity measurements taken 1 and 24 hours after adding urea to soybeans extract and distilled water plus fine soybeans powder, respectively (urea concentration varying from 0.010 mol/L to 4 mol/L).

Inspection of Figure 6.14 indicates that, after 24 hours from the addition of urea, the use of the soybeans powder leads to higher values of electrical conductivity compared to the soybeans extract with a peak level of about 125000 µS/cm. The higher efficiency of the soybeans powder compared to the liquid extract is particularly evident when higher concentrations of urea are employed. A negligible difference of electrical conductivity

between the two cases where the soybeans powder and the soybeans extract are respectively used is instead observed 1 hour after the addition of urea (Figure 6.14).

The subsequent addition of calcium chloride to the mix of distilled water and fine soybeans powder led to the rapid formation of a sticky yellow semi-liquid paste inside the test-tubes (Figure 6.15). The relatively high consistency of this paste did not allow the measurement of pH or the collection of precipitated calcium carbonate by means of filtration, unlike the case of the liquid soybeans extract.

Figure 6.15: Formation of a semi-liquid paste after addition of calcium chloride to test-tubes containing distilled water, soybeans powder and urea (urea/calcium chloride concentration of 2.50 mol/L).

6.1.2. X-ray Powder Diffraction (XRD)

X-ray Powder Diffraction (XRD) tests were performed on the precipitated material from the test-tubes, dried at the laboratory atmosphere and ground into a fine powder. The same procedure could not, however, be performed on the precipitated material from the test-tubes containing the soybeans powder. In this case, no collection of precipitated material was in fact possible due to the sticky consistency of the paste formed after addition of calcium chloride. XRD tests were performed directly on some samples of the paste and samples were distributed to form a layer with a flat surface inside a sample holder, which was subsequently introduced into the XRD machine (Figure 6.16).

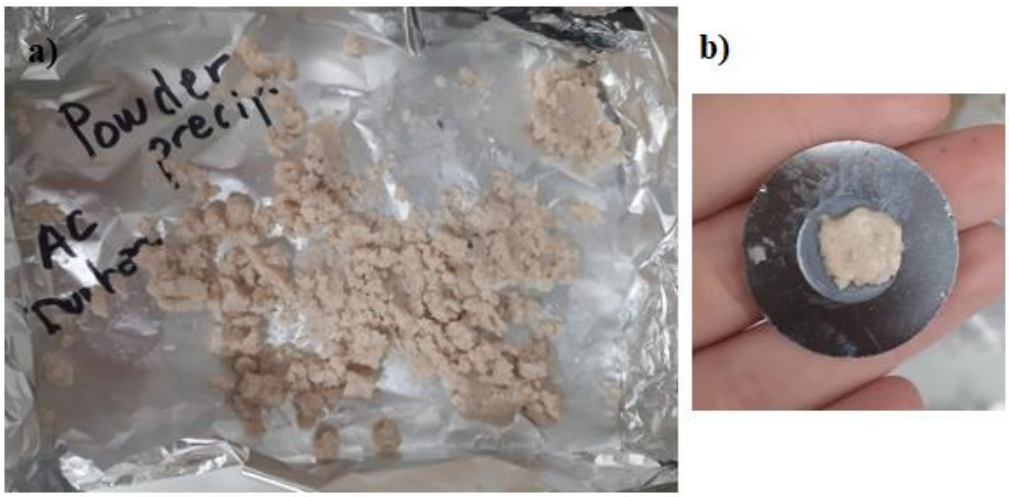

Figure 6.16: XRD analysis-Preparation of sample: sticky paste from test-tube containing distilled water, soybeans powder, urea and calcium chloride (urea/calcium chloride concentration of 2.50 mol/L) (a), distribution of the paste into the sample holder assuring a flat upper surface (b).

XRD analyses are based on the constructive interference of monochromatic X-rays and a crystalline sample (Figure 6.17). The X-rays generated by a cathode ray tube are filtered to produce a monochromatic radiation and are collimated to concentrate before being directed towards the sample. The interaction of the incident rays with the sample produces a constructive interference (and a diffracted ray) when conditions satisfy Bragg's Law

$$n\,\lambda = 2\,d\sin\theta \qquad (6.2)$$

That relates the wavelength of electromagnetic radiation λ to the diffraction angle θ and the lattice spacing in the crystalline sample d. A peak in intensity occurs when the mineral contains lattice planes with d-spacings appropriate to diffract X-rays at that value of θ. The intensity of diffracted X-rays is continuously recorded as the sample and detector rotate through their respective angles. Results are commonly presented as peak positions at 2θ and X-ray counts (intensity). The d-spacing of each peak is then obtained by solution of the Bragg equation for the appropriate value of λ.

Once all d-spacings have been determined, automated search/match routines compare the d-spacing of the tested sample to those of known materials. Because each mineral has a unique set of d-spacings, matching these d-spacings allows the identification of the sample. Files of d-spacings for hundreds of thousands inorganic compounds are available from the International Centre for Diffraction Data as the Powder Diffraction File.

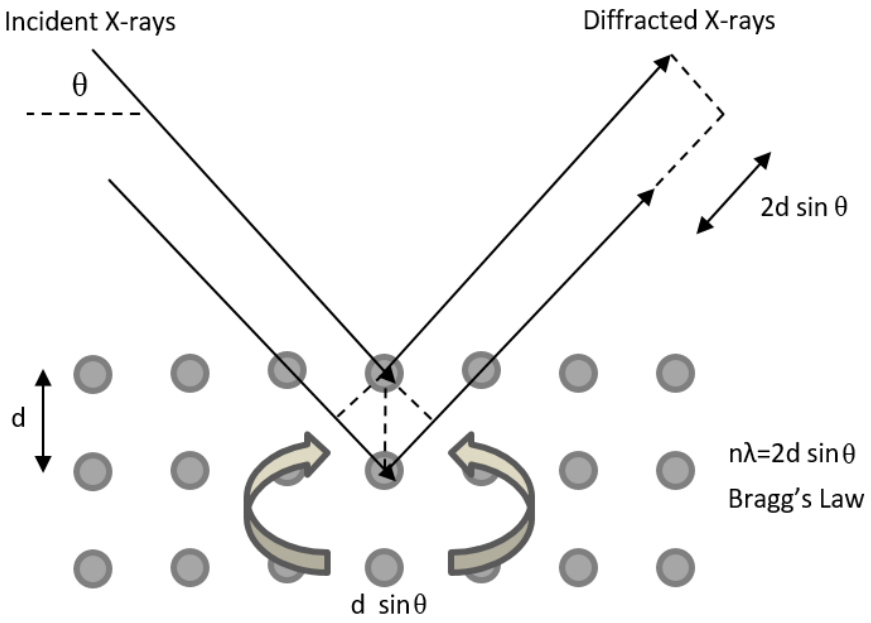

Figure 6.17: Principles of X-ray Diffraction.

Figure 6.18 shows the results of the XRD analysis performed on the material precipitated at the bottom of the test-tubes containing the soybeans extract mixed with urea and calcium chloride. The results confirmed that the mineralogy of the precipitated material comprises calcium carbonate in the form of calcite and vaterite. This provides further evidence of the occurrence of the stabilisation reactions. Calcite and vaterite, together with aragonite, are three polymorphs of calcium carbonate. Temperature has a significant impact on the specific calcium carbonate polymorph that is formed during the reaction. According to past evidence (Howie et al., 1992), the solubility of calcite in water increases with decreasing temperature. Also, the precipitation of calcium carbonate from dissolved calcium chloride produces calcite at temperatures below 35 °C while vaterite is predominantly formed along with calcite at higher temperatures.

Figure 6.19 presents results of the XRD analysis performed on the paste resulting from the mixture of distilled water, soybeans powder, urea and calcium chloride. Inspection of Figure 6.19 reveals the presence of calcium carbonate in the form of calcite and vaterite as already detected in the previous experiment. This result should, however, be taken with a degree of caution due to the organic nature of the tested material, which does not comply with the standard requirements of XRD analyses. Standard XRD analyses are in fact performed on inorganic crystalline materials because organic matter behaves as an amorphous phase, which does not give distinctive peaks as minerals do.

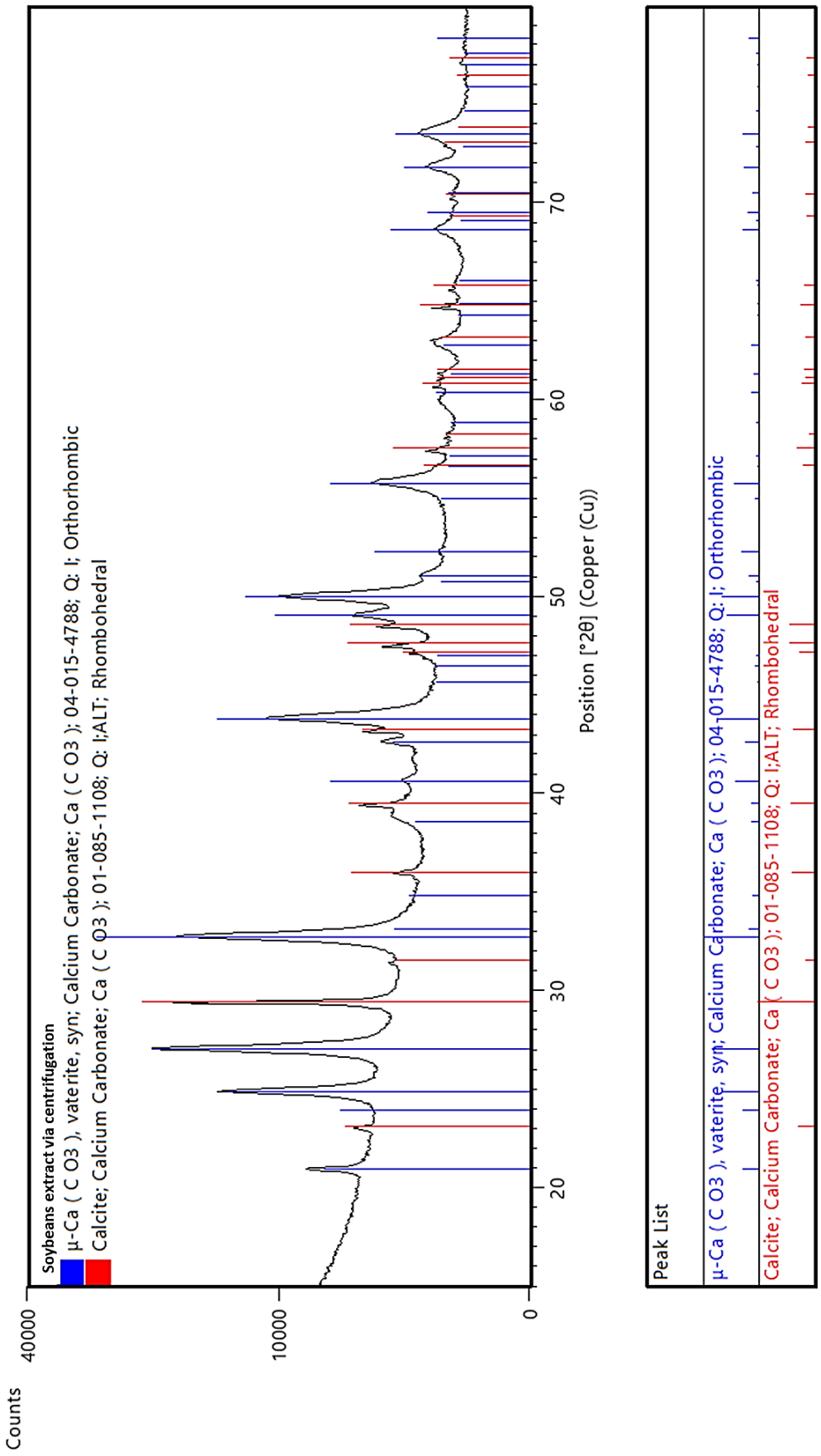

Figure 6.18: XRD analysis performed on the material precipitated at the bottom of a test-tube containing soybeans extract, urea and calcium chloride (urea/calcium chloride concentration of 2.50 mol/L).

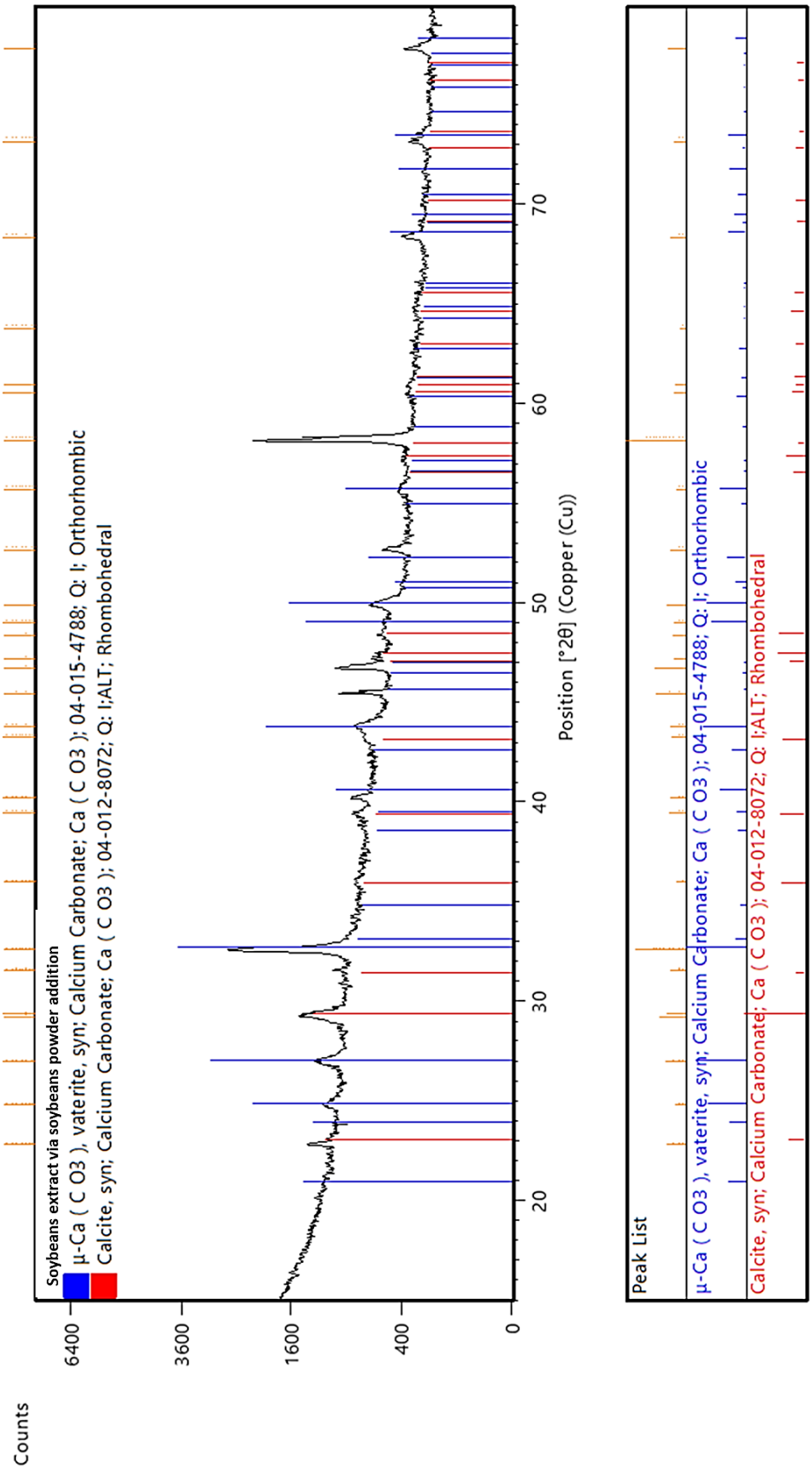

Figure 6.19: XRD analysis performed on a paste collected from a test-tube containing distilled water, soybeans powder, urea and calcium chloride (urea/calcium chloride concentration of 2.50 mol/L).

6.2. Soil stabilisation

In this section, the EICP method is applied for the stabilisation of earth mix 1. This is the earth mix with the best engineering properties and in particular, durability properties against water erosion according to the results presented in Chapter 5. Preliminary essays were made to assess the efficiency of different stabilisation protocols by comparing the results from water immersion tests, as prescribed by the norm DIN 18945 (2013). Based on this initial assessment, stabilised samples were prepared for further testing to measure the strength, stiffness and moisture buffering capacity of the material.

6.2.1. Preliminary essays

The main objective of this work is to improve the durability characteristics of compacted earth in the presence of excess water. For this reason, different stabilisation protocols were initially assessed by means of water immersion tests as described in the German norm DIN 18945 (2013).

Prior to performing the immersion tests, the stabilised samples were equalised at the laboratory atmosphere, corresponding to a temperature of 20 ± 5 °C and a relative humidity of 40 ± 5 %, until the soil mass changed less than 0.1 % over a period of at least one week. After equalisation, the initial mass m_i of each sample was recorded before proceeding with the immersion test as described in Section 5.3.1. The stabilised samples were individually submerged in water for ten minutes before being drained and equalised again under the laboratory atmosphere to attain the same moisture content as before immersion. The final sample mass m_f was then recorded and introduced, together with the initial mass m_i, in the following equation to calculate the percentage mass loss $\%\Delta m$ during immersion:

$$\%\Delta m = \frac{(m_i - m_f)}{m_i} \times 100 \quad (6.3)$$

Beside measuring the mass loss, a visual inspection of the sample was performed after each immersion test to detect the potential occurrence of swelling and/or cracking.

- **Essay 1**

Stabilised samples were prepared by hyper-compacting the earth into small cylindrical samples of 50 mm diameter and 50 mm height as described in Section 4.2.2. The samples were hyper-compacted at the optimum water content of 4.88 % but, instead of using distilled water as for the unstabilised samples, a cementing solution of soybeans extract, urea and calcium chloride was employed. The extract was prepared by wet centrifugation of soybeans

as described in Section 4.3.1. Urea and calcium chloride were then added to the extract at an equimolar concentration of 2.5 mol/L. This concentration produces the largest precipitation of calcium carbonate and is therefore expected to generate the highest degree of bonding between earth particles (see Section 6.1.1). Three replicates of each immersion test were performed to confirm the repeatability of the experimental procedure. The results presented here are therefore the averages of these three replicates.

Results from immersion tests indicate that the hyper-compacted stabilised samples lost about 12 % of their initial masses compared to 13 % for the hyper-compacted unstabilised samples (see Section 5.3.1). Figure 6.20 shows one of the three stabilised samples before (a) and after (b) immersion in water. Inspection of Figure 6.20 clearly indicates that water immersion produces a marked erosion of the sample surface with evidence of cracks and swelling.

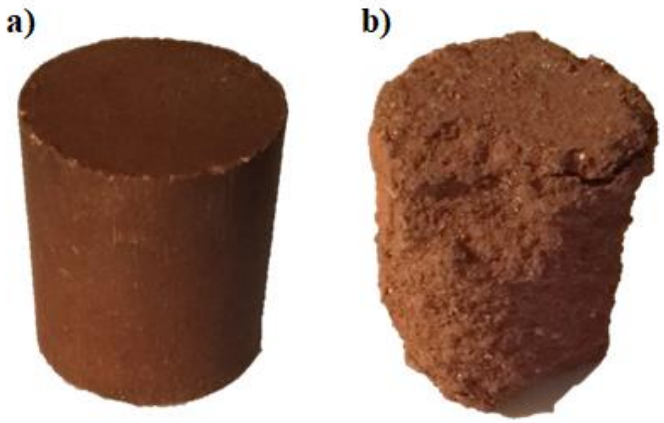

Figure 6.20: Hyper-compacted stabilised sample (urea/calcium chloride concentration of 2.50 mol/L) before (a) and after (b) immersion in water for 10 minutes.

The above results indicated that the addition of the cementing solution during hyper-compaction of the earth samples did not improve significantly the durability of the hyper-compacted material. An explanation of this result might be the relatively small amount of the cementing solution added to the soil, which is equal to the optimum water content of 4.88 % as previously explained. This small amount of the cementing solution may not induce sufficient precipitation of calcite crystals to achieve an adequate bonding of the earth particles.

- **Essay 2**

Stabilised samples were prepared by mixing 150 grams of dry earth with an amount of cementing solution equal to 80 % of the earth liquid limit (see Section 4.1.2). The cementing solution was prepared as previously described by dissolving equimolar concentrations (2.5

mol/L) of urea and calcium chloride into freshly centrifuged soybeans extract (see Section 4.3.1). The amount of the cementing solution added to the dry earth soil was in this essay considerably higher than the amount of cementing solution used in the previous essay 1. This was necessary to ensure a higher amount of calcite precipitation and hence a greater level of earth stabilisation.

The cementing solution was thoroughly mixed to the dry earth right after the addition of urea and calcium chloride, which resulted in the production of a slurry. To avoid the premature precipitations of calcite crystals in a loose soil, the slurry was immediately compacted. A manual compaction inside an oedometric ring was chosen to manufacture samples with a diameter of 60 mm and a height of 30 mm. For comparison, a set of unstabilised samples was also prepared in a similar way by replacing the cementing solution with distilled water.

Three replicates of each immersion test were performed after equalisation. The average results from these tests indicate that, following immersion in water, the unstabilised and stabilised samples lost 7 % and 2 % of their respective initial masses. The mass loss of the stabilised samples is therefore smaller than the mass loss of the unstabilised samples by a factor greater than three. Visual examination also highlighted that, unlike the unstabilised samples, the stabilised samples did not experience any cracking and swelling after immersion (Figure 6.21).

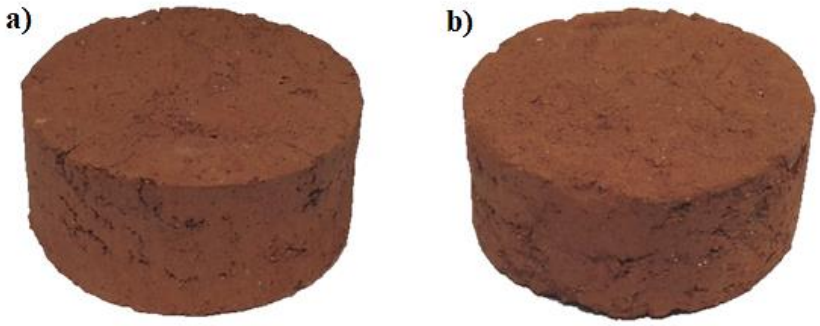

Figure 6.21: Slurry-stabilised sample with soybean extract (urea/calcium chloride concentration of 2.50 mol/L) before (a) and after immersion (b).

It is interesting to note that even the unstabilised samples exhibited a relatively small mass loss of only 7 %. The promising water durability of the unstabilised material can be explained by the manufacture of the samples from a wet earth paste, which results in a strong fabric orientation that seals the sample surface and reduces moisture infiltration (Maillard et al., 2014). Moreover, the high water content of these samples results in the development of strong consolidation pressures during equalisation due to the generation of elevated suctions, and hence high levels of effective stresses, inside the saturated material.

The durability of the unstabilised samples is further enhanced by the proposed stabilisation protocol thanks to the formation of calcite bonds between earth particles and to the occlusion of material pores by precipitated minerals, which contributes to reduce water permeability.

In particular, the improvement of the material due to the calcite precipitation was proven by an additional series of immersion tests that was performed by submerging the samples in water until their complete dissolution into loose soil particles. A set of three unstabilised and stabilised samples was tested and the results here presented are average values. In this case, the stabilised material withstanded water erosion for almost 5 hours before dissolution whereas the unstabilised material was completely dissolved after only 3 hours.

The above results indicate that the amount of the cementing product into the soil is a key factor affecting the efficiency of the proposed stabilisation method. The use of a larger amount of the cementing solution resulted in the precipitation of higher amounts of calcium carbonate and hence in a stronger bonding between earth particles together with a more effective occlusion of the earth pores.

Despite essay 2 revealed interesting promising results in term of durability against water erosion, the protocol was dropped. In fact, the earth mix in the form of a wet slurry and high content of the cementing solution (as for distilled water) were not compatible with the fabrication of hyper-compacted samples which saturation could be reached with much lower water contents.

- **Essay 3**

In the third essay, unstabilised samples were hyper-compacted at the optimum water content as described in Section 4.2.2. After equalisation, the external surface of the samples was sprayed with the cementing solution made of soybeans extract plus urea and calcium chloride in equimolar concentrations of 2.5 mol/L. The soybeans extract was prepared by means of wet centrifugation as described in Section 4.3.3.

The external surface treatment consisted in spraying the surface of the sample with small amounts of cementing solution over a given period of time. The total amount of cementing solution sprayed on the surface was equal to the 80 % of the liquid limit w_L of the earth making up the sample (see Section 4.1.2). In particular, the treatment was distributed in five applications over a period of five days to avoid cracking or swelling of the material following adsorption of the liquid. This was particularly important because, when the surface was sprayed at once with the whole amount of cementing solution, the sample experienced widespread cracking and swelling (Figure 6.22).

Figure 6.22: Formation of cracks after spraying the whole amount of cementing solution (equal to 80 % w_L) on the sample surface in a single application.

After treatment, the samples were equalised again to the laboratory atmosphere before being tested to water immersion. Immersion tests were repeated for a set of five samples and the following results were confirmed to be repeatable. During the immersion tests, all the samples exhibited waterproofing properties as the surface treatment resulted in the formation of an external waterproof coat. After some time, between 2 and 4 minutes depending on the uniformity and efficiency of the surface treatment, all the samples started to disintegrate rapidly with water filtrating across the material from cracks on the sample surface.

- **Essay 4**

Stabilised samples were prepared by mixing 100 grams of dry earth, 50 grams of fine soybeans powder (see Section 4.3.4) and an amount of distilled water equal to 80 % of the w_L of the earth (see Section 4.1.2). Equimolar concentrations (2.5 mol/L) of urea and calcium chloride were dissolved into distilled water before the solution was added to the mix of dry earth and soybeans powder.

Therefore, in this case, the soybeans powder is used as a source of urease enzyme instead of the liquid soybeans extract in essays 1 and 2. Similar to essay 2, a relatively large amount of distilled water was added to the mix of dry earth and soybeans powder to ensure an adequate precipitation of calcium carbonate across the entire sample mass and hence a good level of cementation among the earth particles. The resulting slurry was compacted by hand inside an oedometric ring to make a sample with a diameter of 60 mm and a height of 30 mm. As for essay 2, no time was waited between the preparation of the slurry and the subsequent compaction to avoid the premature precipitation of calcite crystals.

After preparation, the stabilised samples were equalised at the laboratory atmosphere as previously described. The immersion test was then repeated three times on similar samples to confirm the good repeatability of the experimental procedure. The average mass loss exhibited by the stabilised samples after immersion in water was only 1 % (Figure 6.23) with no evidence of cracking or swelling. This is the best result from all four durability essays, which suggests that the use of the fine soybeans powder enhances the activity of the urease enzyme as already observed in test-tubes experiments (see Section 6.1.1). The formation of a sticky paste made of earth and soybeans powder might also result in the development of a bio-film that fills the material voids and surrounds the earth particles, thus limiting the occurrence of water erosion.

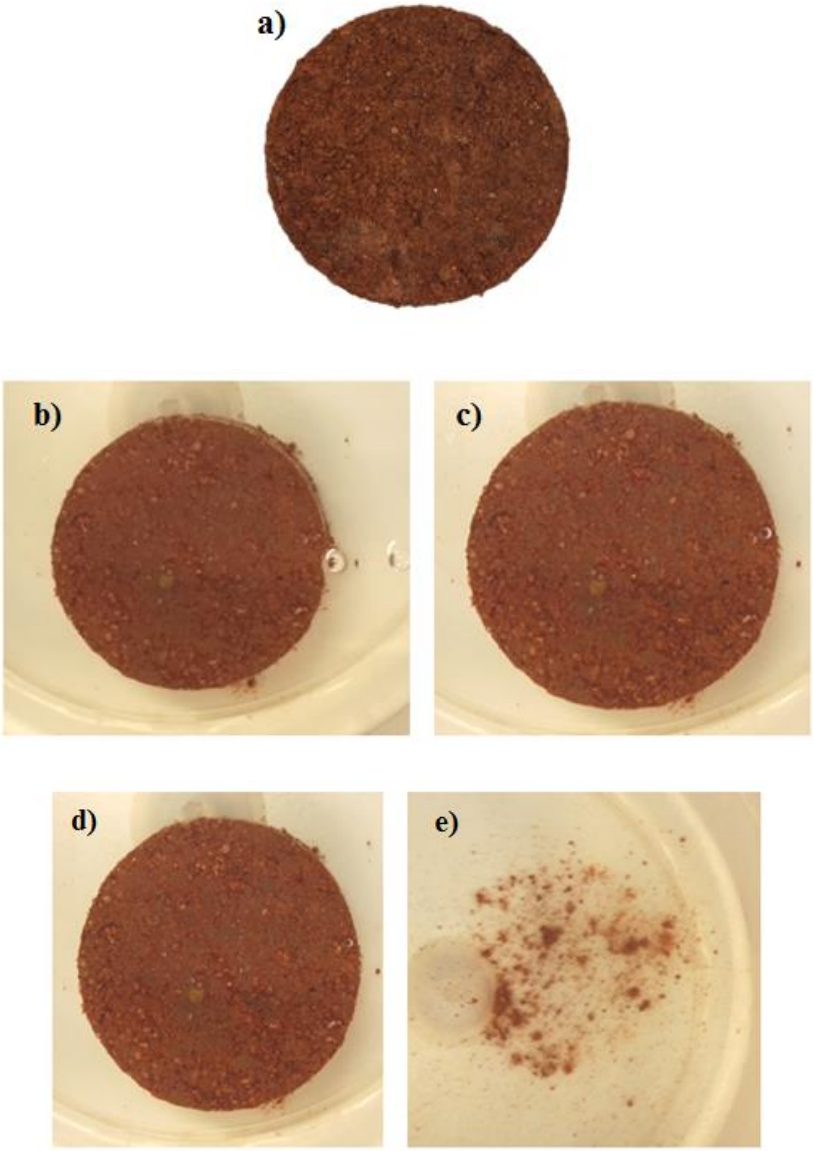

Figure 6.23: Slurry-stabilised sample with soybeans powder (urea/calcium chloride concentration of 2.50 mol/L) before (a) and during immersion at 3 minutes (b), 6 minutes (c) and 9 minutes (d). The mass loss after ten minutes of immersion in water was equal to 1 % (e).

Measures must be taken to prevent the growth of mould on the surface of the samples after exposure to water (Figure 6.24a). In fact, mould spores are present everywhere, in both outdoor and indoor air, and starts to grow when the right conditions in term of oxygen availability, temperature and relative humidity are created. Based on recent experimental data from studies about construction materials, the minimum relative humidity for mould growth (germination) is about 80 % (Riordan, 2016). In this work, the growth of mould after immersion was prevented by ensuring an adequate ventilation of the air surrounding the samples in order to reduce the humidity below the limit for mould growth. It was also found that drying the samples in an oven at a temperature of 105 °C prevented the occurrence of future germination (Figure 6.24b).

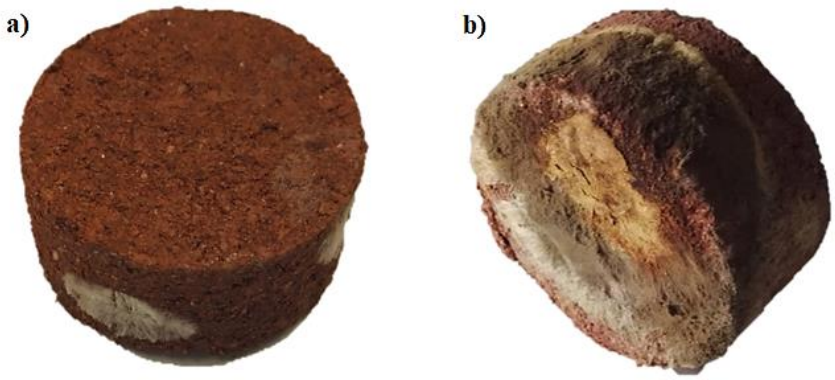

Figure 6.24: Growth of mould on the surface of slurry-stabilised sample with soybeans powder after exposure to moisture (a). Further mould growth was prevented by oven drying the sample at 105 °C (b).

6.2.2. Hygro-mechanical investigation of stabilised earth

Previous tests indicated that the use of soybeans powder enhances the activity of the urease enzyme resulting in higher levels of calcite precipitation and hence a larger degree of bonding between earth particles. A large amount of soybeans powder may result, however, in the appearance of mould efflorescence on the sample surface due to the elevated organic content of the material. Conversely, samples stabilised using the liquid soybeans extract do not exhibit mould growth but have a lower level of stabilisation due to a less effective degree of inter-particle bonding.

Based on the results from these initial tests, three different methods of stabilisation were selected for further hygro-mechanical characterisation. Two of these methods made use of either soybeans powder or liquid soybeans extract as a source of urease enzyme. The third method combined instead both these ingredients with the objective of reaping their

respective advantages while limiting their disadvantages. The following three different stabilisation methods were therefore selected:

- stabilisation using liquid soybeans extract as a source of urease enzyme (referred as SC);
- stabilisation using a fine soybeans powder as a source of urease enzyme (referred as SP);
- stabilisation using liquid soybeans extract + fine soybeans powder as a source of urease enzyme (referred ad SCP).

Table 6.1 and Figure 6.25 summary the composition of the cementing mixture added to the dry earth for each of the above three stabilisation methods.

Table 6.1: Composition of cementing mixture added to the dry earth for SC, SP and SCP stabilisation methods.

Stabilisation method ID	**Liquid soybeans extract**	**Fine soybeans powder**	**Distilled water**	**Reagents (2.50 mol/L urea/calcium chloride)**
SC	×	-	-	×
SP	-	×	×	×
SCP	×	×	×	×

A detailed hygro-mechanical laboratory investigation was performed on compacted samples of earth mix 1, which were stabilised according to the three methods shown in Table 6.1 and Figure 6.25. The concentrations of urea and calcium chloride (added to the soybeans extract for the SC and SCP methods or to distilled water for the SP method) were equal to the optimal value of 2.50 mol/L (see Section 6.1.1). For the SP and SCP methods, the amount of soybeans powder was equal to 1/12 of the total dry sample mass. This relatively little amount of soybeans powder was chosen, after some preliminary tests, to limit the growth of mould on the sample surface during exposure to water. A set of unstabilised samples, made of dry earth and distilled water, were also prepared for comparison by following the same manufacturing procedure.

Figure 6.25: Composition of cementing mixture added to the dry earth for SC, SP and SCP stabilisation methods.

Cylindrical earth samples of 50 mm diameter and 100 mm height were statically compacted at a water content of 12.4 % and a dry density of 1.97 g/cm^3. These values of water content and dry density are the standard Proctor optimum values, which were previously measured from a series of compaction tests performed on earth mix 1. Standard Proctor provides an intermediate level of compaction compared to hyper-compaction and hand compaction, which are the two sample manufacturing methods considered until now in this chapter. The choice of standard Proctor compaction was made to overcome the limitations of both hyper-compaction and hand compaction methods while preserving most of their respective advantages. In particular, the optimum water content used to manufacture Proctor standard samples is between the optimum water contents used for hyper-compacted and slurry-made samples. Similarly, dry density is bigger for Proctor compacted samples than for hand compacted samples. This means that a sufficient amount of cementing solution could be introduced in the Proctor compacted samples to ensure an adequate level of stabilisation, which was not the case for the hyper-compacted samples. At the same time, Proctor compacted samples were sufficiently dense for building applications, which was not the case for hand compacted samples.

The sample manufacturing procedure was as follows: (i) the dry earth was passed through a 2 mm mesh sieve to remove the largest particles; (ii) the dry earth was mixed with the relevant cementing solution in an amount equal to the standard Proctor optimum water content; (iii) the moist soil was statically compacted in 10 layers to attain the Proctor optimum dry density (an immediate compaction after mixing was necessary to prevent the premature precipitation of calcium carbonate crystals); (iv) the surface of each layer was lightly scarified before compaction of the subsequent layer; (v) after preparation, the samples were equalised under controlled humidity (50 ± 5 %) and temperature (20 ± 5 ºC) until the sample mass changed less than 0.1 % over at least one week.

6.2.2.1. X-ray Powder Diffraction (XRD) on stabilised earth

Five grams of each sample were ground into a fine powder and air dried at the laboratory environment before performing a XRD analysis. Results from the XRD analyses revealed the presence, in all samples, of kaolinite, microcline intermediate, muscovite, quartz and calcium carbonate in the form of calcite (Figures 6.26, 6.27 and 6.28). Calcite was identified in all samples, both unstabilised and stabilised, though a quantitative analysis indicated an amount of calcite of about 2 % for the unstabilised samples compared to about 8 % for the samples stabilised via the SP method.

The XRD analysis of the stabilised earth did not reveal the presence of calcium carbonate in the form of vaterite, which was different from what was observed in test-tubes experiments (see Section 6.1.2). The lack of vaterite could be explained by the temperature of the earth mix during compaction which, below 35 °C, only allows precipitation of calcium carbonate in the form of calcite.

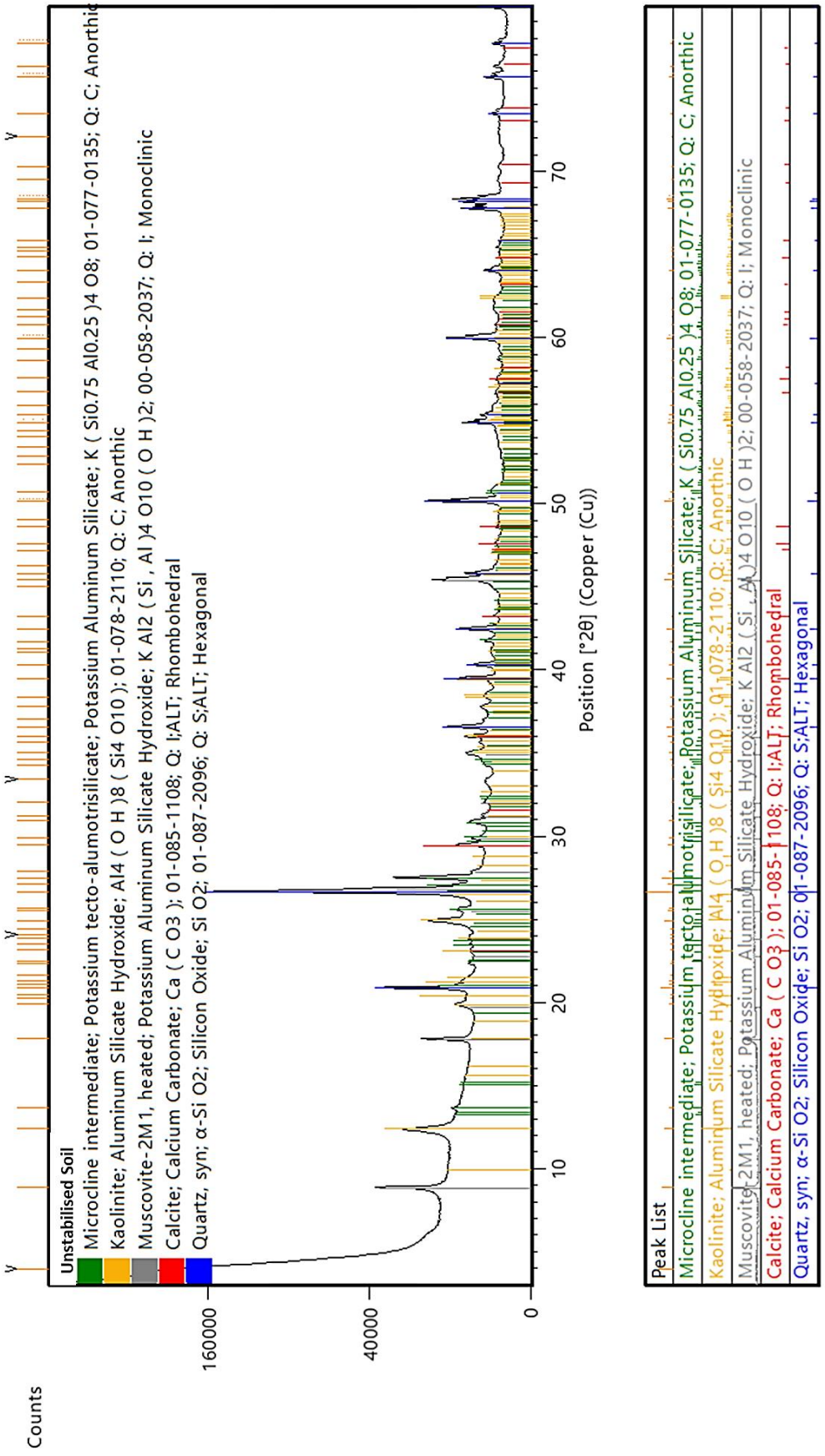

Figure 6.26: XRD analysis on unstabilised sample.

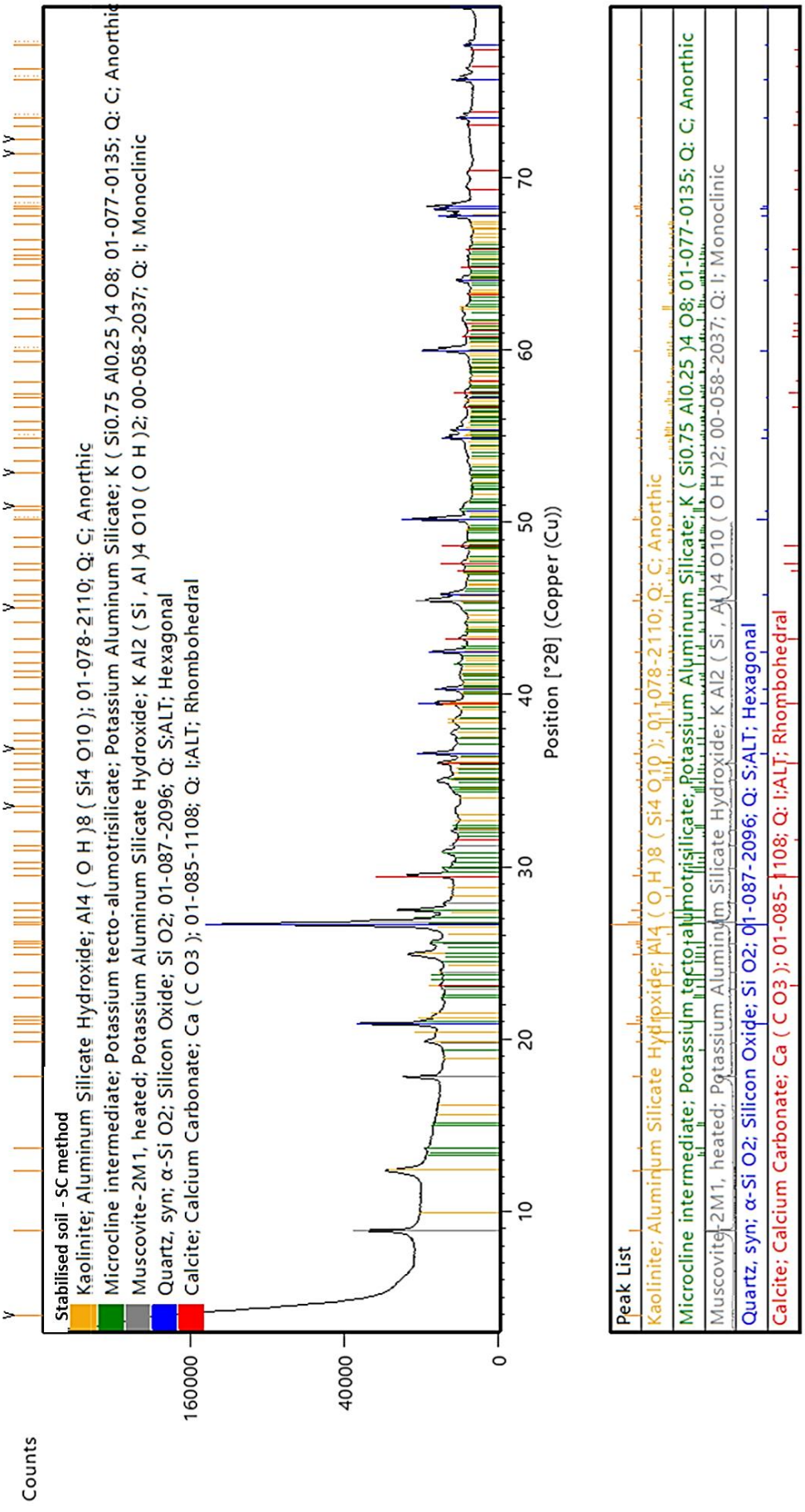

Figure 6.27: XRD analysis performed on SC stabilised sample.

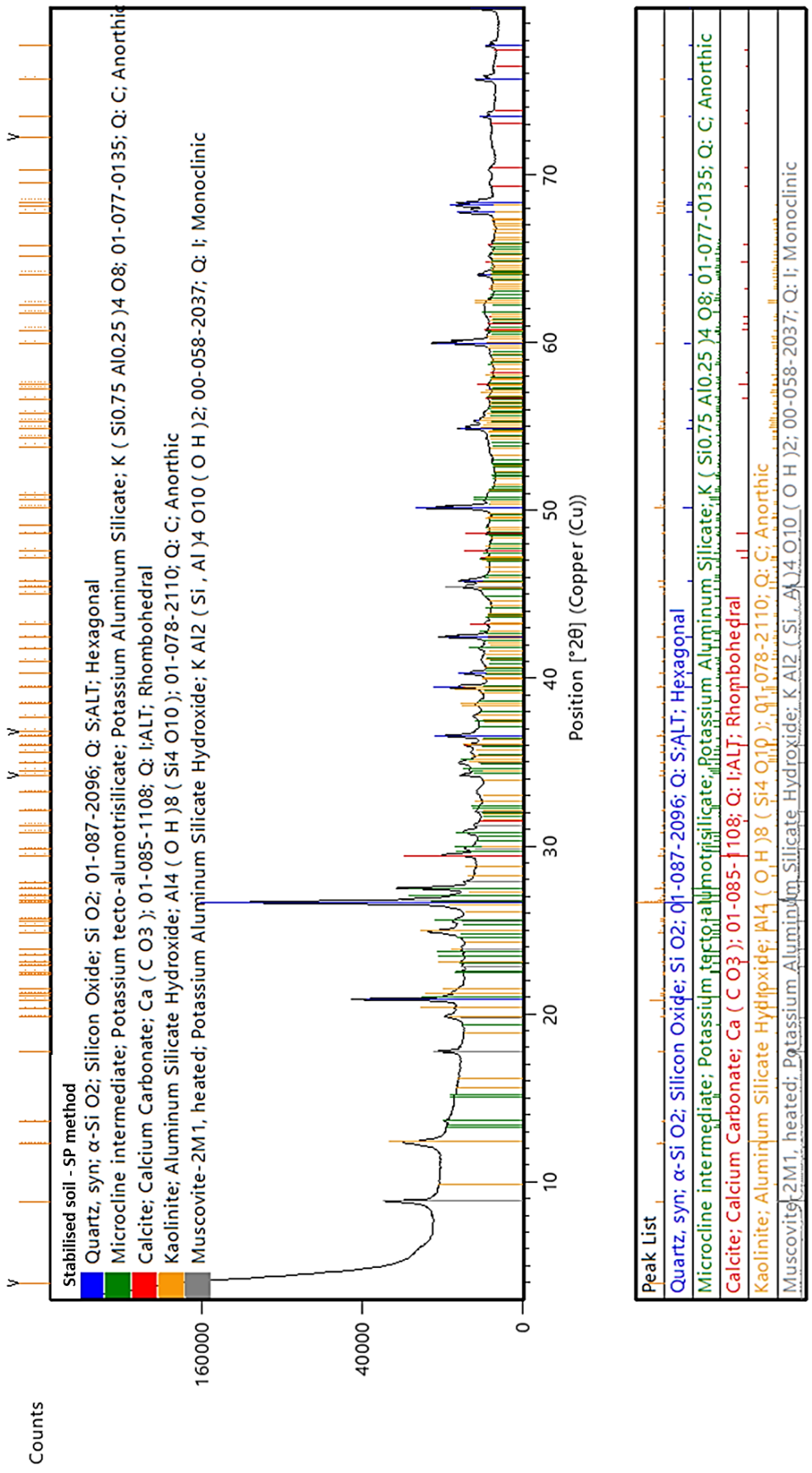

Figure 6.28: XRD analysis on SP stabilised sample.

6.2.2.2. Compressive strength and Young's modulus

After equalisation, all samples were subjected to unconfined compression using a Shimadzu universal testing machine with a loading capacity of 300 kN which is located at Durham University (UK). Load and displacement were automatically recorded by means of the TRAPEZIUM LITE X Software. A constant axial displacement rate of 0.001 mm/s was chosen for consistency with the previous tests on unstabilised hyper-compacted earth samples. Three samples were tested for each stabilisation method to confirm the repeatability of measurements. The final compressive strength and Young's modulus were then calculated as the average of these three measurements.

Figure 6.29 shows the peak values of compressive strength for each stabilisation method together with compressive strength of the unstabilised material. Inspection of Figure 6.29 indicates that compressive strength varies according to the chosen stabilisation method with the lowest, intermediate and highest levels of strength recorded for the SC, SP and SCP stabilised samples, respectively. Interestingly, only the SCP stabilisation method, which is a combination of the SC and SP methods, generated a level of strength, which is higher than that of the unstabilised samples. In particular, the use of the soybeans extract as the only source of urease enzyme (SC stabilisation method) negatively affected the mechanical properties of the material with a level of compressive strength that is twofold lower than that of the unstabilised samples. This result is in apparent contradictions with the observations made during test-tube experiments (see Section 6.1.1), when the precipitation of calcite crystals was clearly successful in a solution of soybeans extract, urea and calcium chloride. Conversely, the use of soybeans powder as the only source of urease enzyme like in the SP method produced a level of strength that is equivalent to that of the unstabilised material.

The visual examination of SP and SCP stabilised samples highlighted the formation of a crystallised white covering on the external surface of the samples. This observation provides further evidence of the greater efficiency of the stabilisation process when soybeans powder is used as a source of urease enzyme, either alone or in combination with the soybeans extract.

The Young's modulus was simply measured as the slope of the tangent to the stress-strain curves over the stress range where the material response is reasonably linear as previously explained in Section 5.1.2. Figure 6.30 shows the measured values of Young's modulus for all unstabilised and stabilised earth samples. Similar to compressive strength, the Young's modulus varies according to the chosen stabilisation method with the highest, intermediate

and lowest levels of stiffness recorded for the SCP, SP and SC stabilised samples, respectively. Moreover, all three stabilisation methods appear to have a detrimental effect on stiffness resulting in lower values of Young's modulus compared to the unstabilised material.

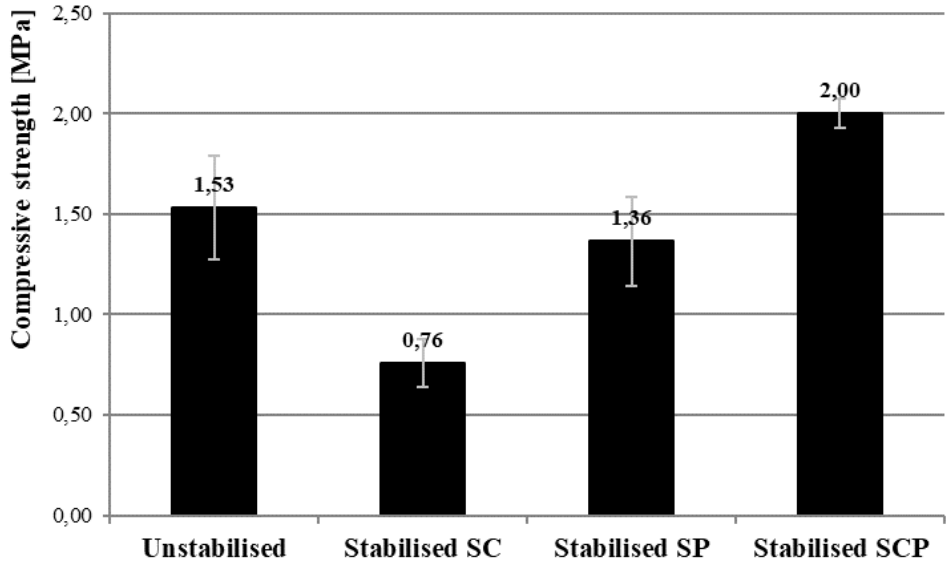

Figure 6.29: Compressive strength measured from unconfined compression tests on unstabilised, SC stabilised, SP stabilised and SCP stabilised samples.

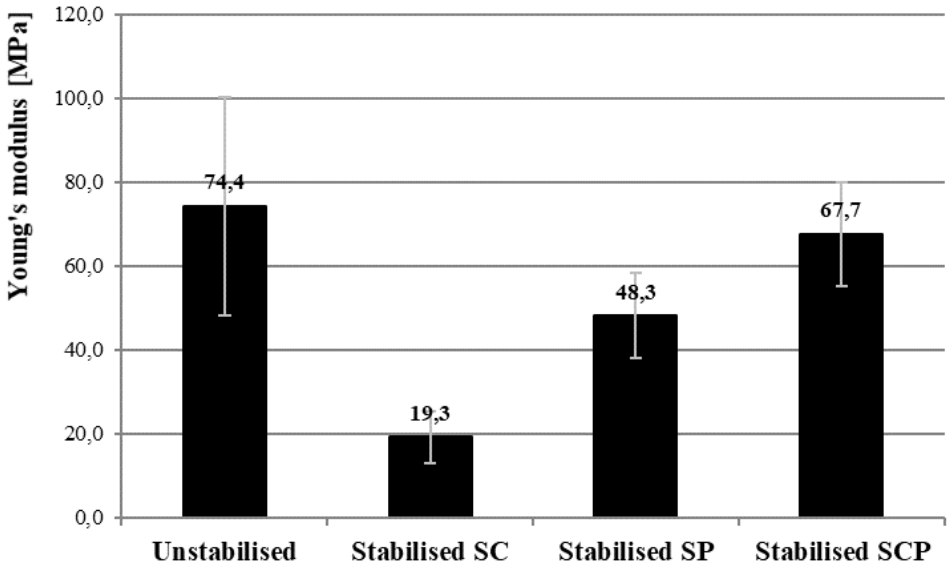

Figure 6.30: Young's modulus measured from unconfined compression tests on unstabilised, SC stabilised, SP stabilised and SCP stabilised samples.

6.2.2.3. Moisture buffering capacity

The hygroscopic behaviour of unstabilised and stabilised earth samples was experimentally assessed through the measurement of their moisture buffering values (MBV) following the same procedure described in see Section 5.2.

Figure 6.31 shows the variation of both the MBV uptake (measured under an imposed humidity of 75 %) and the MBV release (measured under an imposed humidity of 53 %) over consecutive humidity cycles for all tested samples. As expected, the MBVs of the uptake and release stages tend to converge towards the same steady state value as the number of cycles increases. In general, five cycles were sufficient to attain steady state conditions for all materials.

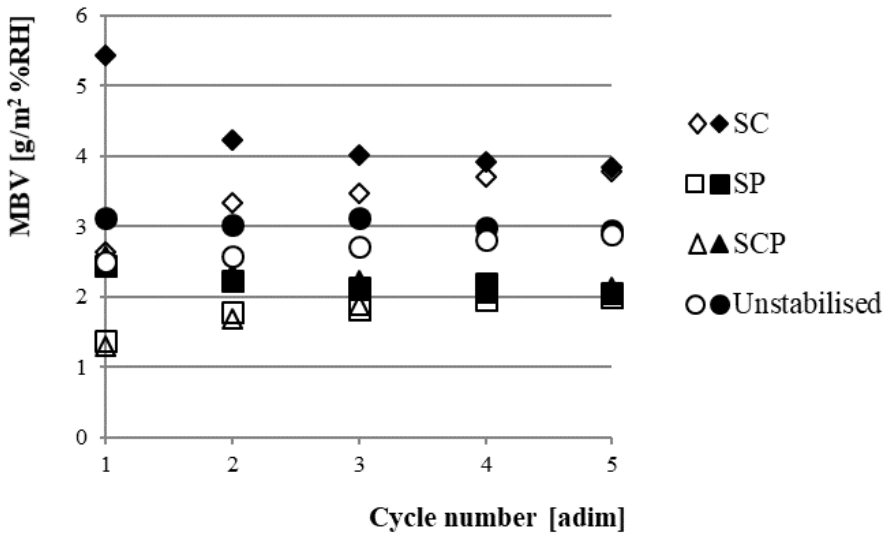

Figure 6.31: MBVs measured during the uptake and release stages of subsequent humidity cycles on unstabilised, SC stabilised, SP stabilised and SCP stabilised samples. Solid markers indicate the MBV uptake while hollow markers indicate the MBV release.

The final MBVs of the different materials were measured under steady state conditions and were calculated as the averages of the uptake and release values of the last three stable cycles measured on three replicates of each sample (Table 6.2). Inspection of Table 6.2 indicates that the moisture buffering capacity of the unstabilised material is reduced if the earth is subjected to SP and SCP stabilisation. Note that, in both these stabilisation methods, soybeans powder is employed as a source of urease enzyme. An explanation of this result is proposed later when the results of water immersion tests are presented. Yet, even for the SP and SCP stabilised samples, the MBV value remains larger than 2, which indicates relatively good hygroscopic properties.

Interestingly, the highest moisture buffering capacity is recorded when the earth is stabilised by means of soybeans extract, urea and calcium chloride (SC stabilisation). The use of the soybeans extract boosts the ability of the earth to adsorb/release moisture as demonstrated by a very high MBV close to 4, which is even greater than the MBV of the unstabilised earth.

Table 6.2: MBVs of unstabilised, SC stabilised, SP stabilised and SCP stabilised samples.

Sample ID	**MBV [g/m^2%RH]**
Unstabilised soil	2.91
SC	3.79
SP	2.03
SCP	2.07

6.2.2.4. Water durability properties

Water immersion tests were performed to evaluate the durability of the different samples against water erosion in accordance with German norm DIN 18945 (2013) as previously described (see Section 5.3.1).

Each test was performed in three replicates to evaluate the repeatability of the experimental procedure and the averages results of these three replicates are presented in the following. During immersion, the unstabilised samples lost about 42 % of their initial mass, which reduced to about 13 % when SC stabilisation was employed. An even better result was obtained in the two cases of SP and SCP stabilisation, when only 1 % of the initial sample mass was lost. A significant improvement of water durability is therefore achieved by using the proposed enzymatic stabilisation treatment, especially when the soybeans powder is used as a source of urease enzyme. The lower mass loss experienced by the stabilised samples is explained by the formation of calcite bonds between earth particles and by the partial occlusion of material voids with a consequent reduction of water permeability. Figure 6.32 compares the images of the samples taken before and after immersion for all stabilisation methods.

Figure 6.33 shows the images of two fragments of a SC stabilised sample and a SP stabilised sample, respectively, taken with a 4K digital KEYENCE microscope. In particular, the presence of organic ramifications occluding the material voids can be observed in the case of the SP stabilised sample. The presence of such ramifications could explain the hydrophobic behaviour of this material during immersion tests but also the relatively low MBV (see Section 6.2.2). This is consistent with previous results, which have showed that stabilisation by means of soybeans powder produces a strong reduction of the moisture

buffering capacity of the material compared to the case where the material is either unstabilised or stabilised with a soybeans extract.

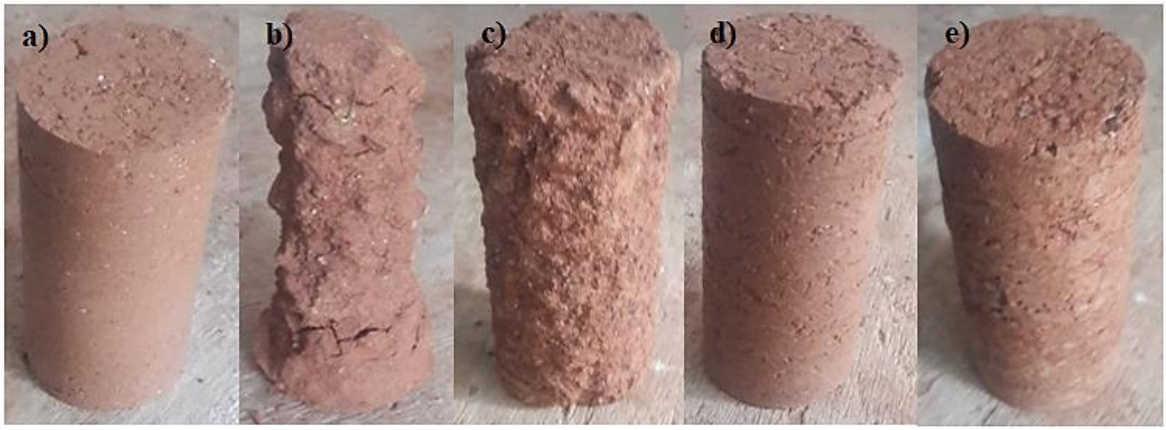

Figure 6.32: Reference sample before immersion (a); unstabilised sample after immersion exhibiting a mass loss of 42 % (b); SC stabilised sample after immersion exhibiting a mass loss of 13 % (c); SP stabilised sample after immersion exhibiting a mass loss of 1 % (d); SCP stabilised sample after immersion exhibiting a mass loss of 1 % (e).

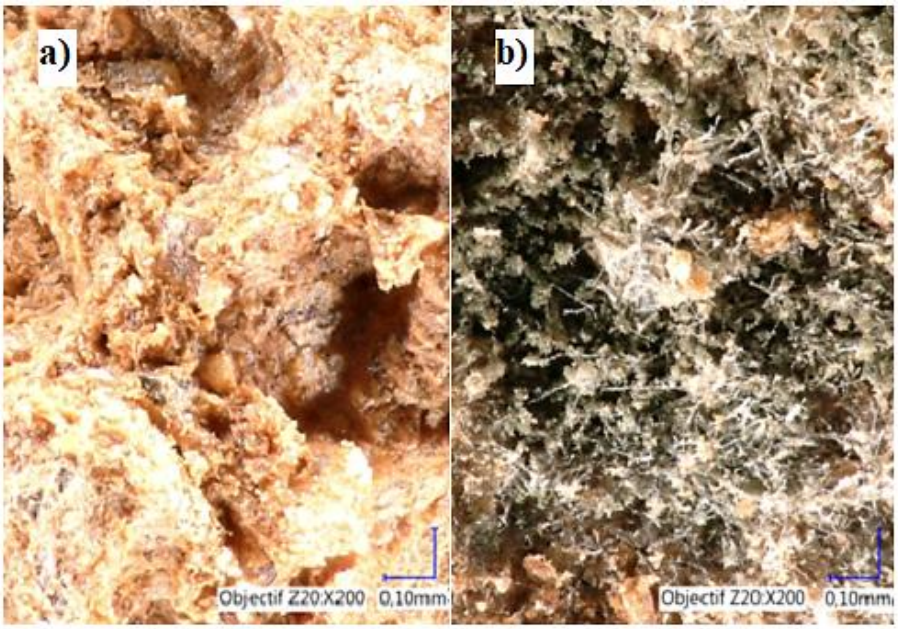

Figure 6.33: Digital microscope images of SC stabilised samples (a) and SP stabilised samples (b).

The combination of soybeans extract and soybeans powder as a source of urease enzyme promisingly improved the durability of the material against water erosion to levels that are acceptable for engineering applications. Nevertheless, further investigation is necessary to understand the nature of the interaction between the earth particles and the soybeans powder and, in particular, the consequences that the presence of organic matter as soybeans might induce on the long-term hygro-mechanical performance of the material.

6.3. Conclusions and final remarks

The present chapter has discussed the use of the urease enzyme to catalyse the hydrolysis of urea for earth stabilisation. The hydrolysis of urea leads to the production of carbonate ions, which react with dissolved calcium ions resulting in the precipitation of calcium carbonate (e.g., calcite). Calcium carbonate precipitation cements the earth particles together and occludes material pores, thus improving the mechanical characteristics of the material while reducing water permeability. This stabilisation method is commonly referred to as Enzyme Induced Calcite Precipitation (EICP).

The main outcomes of this chapter are summarised as follows:

- Test-tube experiments highlighted that the concentration of urea and calcium chloride plays an important role in the activity of the urease enzyme and on the amount of precipitated calcite. In particular, measurements of pH, electrical conductivity and precipitation ratio have indicated that the optimum concentration of urea and calcium chloride, leading to the largest precipitation of calcite, is equal to 2.5 mol/L.
- The addition of a fine soybeans powder to distilled water is an effective alternative to the use of soybeans extract. Both methods provided a good source of urease enzyme and lead to the production of carbonate ions as a result of urea hydrolysis. Measurements of electrical conductivity highlighted that the urease enzyme activity is slightly increased when the soybeans powder is used instead of the soybeans extract. This increase of activity is particularly noticeable in the presence of high urea concentrations. Note that, when the soybeans powder was used, the addition of calcium chloride turned the cementing solution into a paste-like fluid.
- Results of XRD analyses performed on the material precipitated at the bottom of the test-tubes containing soybeans extract, urea and calcium chloride confirmed the presence of calcium carbonate crystals in the form of calcite and vaterite. This result provides further evidence of the successful occurrence of the stabilisation reactions. Similar results were obtained from the XRD analyses performed on the paste-like fluid obtained after mixing soybeans powder, distilled water, urea and calcium chloride inside test-tubes. In this case, however, the XRD results need to be taken with a degree of caution due to the high organic content of the tested material, which does not comply with the standard requirements of XRD analyses.
- Results of XRD analyses performed on stabilised earth samples revealed the presence of minerals like kaolinite, microcline intermediate, muscovite, quartz and calcium

carbonate in the form of calcite. A quantitative analysis detected an amount of calcite of about 2 % in the unstabilised samples and about 8 % in the samples stabilised with soybeans powder, distilled water, urea and calcium chloride.

- Results of unconfined compression tests indicate that the compressive strength changes according to the chosen stabilisation method with the highest level of strength obtained for the case when the soybeans powder and the soybeans extract are used together. Interestingly, the other two stabilisation methods result in lower strength levels in comparison to the unstabilised material.
- Unstabilised earth has an excellent capacity to buffer moisture and hence exhibits an high hygro-thermal inertia. This capacity was not significantly changed by the stabilisation methods tested in the present work. The MBV tends to reduce slightly when the soybeans powder is employed during stabilisation while it tends to increase slightly when the soybeans extract is used.
- The water durability of both unstabilised and stabilised earth was assessed by performing immersion tests according to the norm DIN 18945 (2013). Stabilised samples exhibited improved durability against water erosion compared to unstabilised samples. Results from preliminary immersion tests indicated that the unstabilised samples lost about 42 % of their initial mass. The mass loss reduced to 1 % in the case of the samples stabilised with a combination of soybeans extract and soybeans powder. This level of erosion is adequate for the exposition of the material to natural weathering as indicated by the norm DIN 18945 (2013). Digital microscope images showed the presence of organic ramifications on the surface of the earth samples treated with soybeans powder. This explains the hydrophobic behaviour of this material during immersion tests but also the reduction of the moisture buffering capacity compared to the unstabilised earth.

7. Conclusions

This thesis investigated the hygro-mechanical properties of compacted earth for construction applications as an alternative to conventional energy-intensive building materials. One of the objectives of the present work is the improvement of the durability of compacted earth against water erosion. This objective is here achieved by adopting a novel stabilisation method, which reduces environmental impact while preserving the advantageous hygroscopic properties of compacted earth. The proposed stabilisation method is based on Enzymatic Induced Calcite Precipitation (EICP), which exploits the action of the urease enzyme to catalyse the hydrolysis of urea. One of the main points of originality of the work consists in the utilisation of crude plant-derived urease enzyme instead of pure reagent grade products, which reduces financial and environmental costs. This chapter summarises the main outcomes of this research and advances some recommendations for future work.

7.1. Materials and methods

The base soil used in the present work was provided by the brickwork factory Bouisset from the region of Toulouse (France). The grain size distribution and index properties of the soil correspond to those of a well graded silty clay of low plasticity. The predominantly kaolinitic clay fraction makes this soil suitable for earth construction because of its relativity low specific surface (10 m^2/g) and the consequently small swelling/shrinkage behaviour upon wetting/drying (Section 4.1.1 and 4.1.2).

The base soil was blended with different proportions of silica sand to obtain three distinct earth mixes with different clay contents spanning the entire admissible range for the manufacture of compressed earth bricks as suggested by AFNOR (2001); CRATerre-EAG (1998) and MOPT (1992). Despite grading differences, all earth mixes are consistent with existing construction guidelines (Section 4.1.3).

In order to increase dry density, and hence stiffness and strength, some of the earth samples tested in the present work were ”hyper-compacted” to a very large pressure of 100 MPa (Section 4.2.2). The hyper-compaction curve was defined to determine the optimal water content that allow attaining the highest level dry density for each earth mix (Section 4.2.2). The hyper-compaction of the three earth mixes at their respective optimum water contents produced very dense materials with a porosity between 13% and 14%, which is considerably lower than the porosity of standard Proctor compacted samples. The hyper-compaction method was employed for manufacturing both small cylindrical samples and full scale bricks

(Section 4.2.2).

The stabilisation method requires three main ingredients that are the urease enzyme, the urea and a calcium salt. The present research proposed an effective and economical procedure for obtaining the urease enzyme from the centrifugation of soybeans, which contain such enzyme (Section 4.3.1) The two other chemical reagents, urea ($CO(NH_2)_2$) and calcium chloride ($CaCl_2$), were purchased from chemicals suppliers.

Laboratory investigation indicated that only a freshly centrifuged soybeans extract could catalyse the hydrolysis of urea and hence the precipitation of calcite crystals (Section 4.3.3). An alternative, albeit similar, stabilisation method was also explored by using a soybeans powder, instead of a liquid soybeans extract, as a source of the urease enzyme (Section 4.3.4).

Unconfined compression tests were performed to measure the strength and stiffness of the compacted earth by using a constant axial displacement rate of 0.001 mm/s. All tests were performed on cylindrical samples with an aspect ratio of two to limit the radial confinement caused by friction between the sample extremities and the press plates during axial compression (Section 5.1).

Tests were also performed to investigate the variation of the mechanical properties of the compacted earth when exposed to fluctuations of ambient humidity. Samples were equalised inside a climatic chamber at a constant temperature of 25 °C and at different levels of relative humidity, namely 25 %, 62 %, 95 %. An additional set of samples was dried inside an oven for three days at a temperature of 105 °C to test the behaviour of the material under dry conditions. After equalisation, the samples were subjected to triaxial compression under three different levels of radial stress equal to 0 kPa, 300 kPa and 600 kPa with a constant axial displacement rate of 0.06 mm/min while the back pressure line was open to atmosphere. Results were subsequently processed to determine the variation of both stiffness and peak strength with confining pressure at each humidity level.

The hygroscopic behaviour was investigated through the measurement of the MBV (moisture buffering value) of the material (Section 5.2). Cylindrical samples were exposed to step cycles of relative humidity, between 75 % and 53 %, under a constant temperature of 23 °C inside a climatic chamber. Each humidity level was maintained for 12 hours while the sample mass was recorded every two hours. This experimental procedure is consistent with the norm ISO 24353 (2008) for the characterisation of the hygro-thermal behaviour of

building materials exposed to cyclic variations of relative humidity over a daily period of time.

Immersion and suction tests were undertaken according to the German norm "Earth blocks - Terms and definitions, requirements, test methods" DIN 18945 (2013) to explore the durability of the material against water erosion. Furthermore, drip tests were performed in accordance with the norm NZS 4298 (1998). Both suction and drip tests were undertaken at the scale of brick samples meanwhile immersion tests were performed at the scale of small cylindrical samples. Before testing, all samples were equalised at the laboratory atmosphere, i.e. at a temperature of 23 °C and a relative humidity of 40 ± 5 %.

7.2. Results and discussion

One of the objectives of the present work was to determine the influence of particle size distribution on the hygro-mechanical and durability characteristics of hyper-compacted unstabilised earth at the scale of small cylindrical samples (Chapter 5). Results showed that particle size distribution and clay content play a very important role in governing the hygro-mechanical performance of earth materials. Fine and well-graded earth mixes enhance capillary bonding between earth particles providing not only higher levels of strength and stiffness but also a larger moisture buffering capacity. Moreover, the utilisation of a fine and well-graded earth mix, with a clay content of about 30 %, can reduce vulnerability to water erosion by a significant amount. Nevertheless, results from immersion, suction and drip tests indicate that all earth materials tested in the present work cannot be directly exposed to natural weathering unless suitable stabilisation techniques are adopted.

Consistently with unsaturated soil mechanics theories, the mechanical characteristics of hyper-compacted earth improve as ambient humidity reduces and degree of saturation decreases. Hyper-compaction largely improves the mechanical performance of compacted earth but a marked increase in ambient humidity can still produce a considerable reduction of strength. This sensitivity of mechanical characteristics to ambient humidity means that variations of moisture content should be carefully considered during design, construction and service life of earth buildings.

The key factors influencing the kinetics of urea hydrolysis were initially investigated to better understand the fundamental processes of the adopted EICP stabilisation method. Test-tube experiments highlighted that the concentration of urea and calcium chloride play an important role in the activity of the urease enzyme and that an optimum concentration of 2.5 mol/L leads to the largest precipitation of calcite (Section 6.1.1). Moreover, a mix of a fine

soybeans powder and distilled water constitutes an effective alternative to the soybeans extract. Indeed, both the soybeans powder and the soybeans extract provide a good source of urease enzyme and lead to the production of carbonate ions as a result of urea hydrolysis. XRD analyses provided further evidence of the successful occurrence of the stabilisation reactions confirming the presence of calcium carbonate crystals in the form of calcite and vaterite in both cases (Section 6.1.2.).

Results of unconfined compression tests indicated that the compressive strength and stiffness changes depending on the chosen stabilisation method with the best mechanical performance obtained for the case when the soybeans powder and the soybeans extract are used together. The excellent capacity of unstabilised earth to buffer moisture was not significantly changed by stabilisation. In particular, the MBV reduced when the soybeans powder was employed while it increased when the soybeans extract was used. Results from immersion tests demonstrated that stabilised samples exhibit a higher resistance against water erosion compared to unstabilised samples. The unstabilised samples lost about 42 % of their initial mass, though the mass loss reduced to 1 % for the samples stabilised with a combination of soybeans extract and soybeans powder. This level of erosion is adequate for exposition to natural weathering as indicated by the norm DIN 18945 (2013). Digital microscope images showed the presence of organic ramifications on the surface of the earth samples treated with soybeans powder, which might explain the hydrophobic behaviour of this material during immersion tests but also the reduction of the moisture buffering capacity compared to the unstabilised earth.

7.3. Recommendations for future work

Based on the results of the present research, the following points require further investigation and might be the object of future studies:

- Future works could extend the application of the EICP stabilisation method to hyper-compacted earth by investigating the influence of the stabilisation procedure on the hygro-mechanical and durability properties of highly densified earth.
- Further investigation can be undertaken to assess whether the activity of the enzyme can be preserved for a longer time by sealing and/or freezing the fresh crude soybeans extract prior to use.
- Further experiments are also necessary to understand the nature of the interaction between the earth particles and the soybeans powder. In particular, these experiments

should clarify the consequences of the presence of organic matter on the long-term hygro-mechanical performance of the material.

- Additional tests could investigate the mechanical and hygroscopic behaviour of a masonry assembly by extending the present research from the small sample scale to the wall scale. In particular, future studies could focus on the effect of EICP stabilisation on the thermal and hydraulic transport properties of earth walls.
- A life cycle assessment of earth structures should also be performed to quantify the environmental impact of the proposed construction technique. This life cycle assessment must also take into account the presence of organic matter into the building material.

References

Achal, V., Mukherjee, A., Basu, P. C., Reddy, M. S. (2009). Strain improvement of Sporosarcina pasteurii for enhanced urease and calcite production. J Ind Microbiol Biotechnol, 36, 981–988.

Achal, V., & Pan, X. (2014). Influence of calcium sources on microbially induced calcium carbonate precipitation by Bacillus sp. CR2. Appl Biochem Biotechnol, 173, 307–317.

ADEME (2013). Consommation d'énergie dans les bâtiments – chiffres clés 2013. http://reseaux-chaleur.cerema.fr/consommation-denergie-dans-les-batiments-chiffrescles-2013.

AFNOR (1991). NF P 94-054 Soils: investigation and testing – Determination of particle density- Pycnometer method.

AFNOR (1992). NF P 94-057 Soils: investigation and testing – Granulometric analysis – Hydrometer method.

AFNOR (1993). NF P 94-051 Soils: Investigation and testing – Determination of Atterberg's limits – Liquid limit test using Casagrande apparatus – Plastic limit test on rolled thread.

AFNOR (1995). XP P 94-041 Soils: investigation and testing – Granulometric description – Wet sieving method.

AFNOR (2001). XP P13-901 Compressed earth blocks for walls and partitions: definitions – Specifications – Test methods – Delivery acceptance conditions.

Alexandra, S. (2006). Architecture and earth construction in Piaui: Research, characterization and analysis (Doctoral dissertation, Master thesis, Federal University of Piauí, Brasil).

Al Qabany, A., & Soga, K. (2013). Effect of chemical treatment used in MICP on engineering properties of cemented soils. Géotechnique, 63(4), 331.

Al-Thawadi, S., & Cord-Ruwisch, R. (2012). Calcium carbonate crystals formation by ureolytic bacteria isolated from Australian soil and sludge. J. Adv. Sci. Eng. Res, 2(1), 12-26.

Amin, M., Zomorodian, S. M. A., O'Kelly, B. C. (2017). Reducing the hydraulic erosion of sand using microbial-induced carbonate precipitation. Proceedings of the Institution of Civil Engineers—Ground Improvement, 170(2), 112–122. https://doi.org/10.1680/ jgrim.16.00028.

Arasan, S., Akbulut, S., & Hasiloglu, A. S. (2011). Effect of particle size and shape on the grain-size distribution using Image analysis. International journal of civil and structural engineering, 1(4), 968-985.

Arias, J. L., & Fernández, M. S. (2008). Polysaccharides and proteoglycans in calcium carbonate-based biomineralization. Chemical Reviews, 108(11), 4475-4482.

Arrigoni, A., Pelosato, R., Melia, P., Ruggieri, G., Sabbadini, S., & Dotelli, G. (2017). Life cycle assessment of natural building materials: the role of carbonation, mixture components and transport in the environmental impacts of hempcrete blocks. Journal of Cleaner Production, 149, 1051-1061.

Arundel, A. V., Sterling, E. M., Biggin, J. H., & Sterling, T. D. (1986). Indirect health effects of relative humidity in indoor environments. Environmental health perspectives, 65, 351-361.

ASTM D2487-00 (2000). Standard Classification of Soils for Engineering Purposes (Unified Soil Classification System). American Society for Testing and Materials International.

ASTM D559-03 (2012). Standard Test Methods for Wetting and Drying Compacted Soil-Cement Mixtures. American Society for Testing and Materials International.

ASTM D2166 (2013). Standard Test Method for Unconfined Compressive Strength of Cohesive Soil. American Society for Testing and Materials International.

Attom, M. F. (1997). The effect of compactive energy level on some soil properties. Applied Clay Science, 12 (1), 61-72.

Bao, R., Li, J., Li, L., Cutright, T.J., Chen, L., Zhu, J., et al. (2017). In: Bio-inspired bridge scour countermeasures: Streamlining and biocementation. International conference of transportation infrastructure and materials.

Barkay, T., & Schaefer, J. (2001). Metal and radionuclide bioremediation: issues, considerations and potentials. Current opinion in microbiology, 4(3), 318-323.

Beckett, C. T. S., & Augarde, C. E. (2012). The effect of humidity and temperature on the compressive strength of rammed earth. In Proceedings of 2nd European Conference on Unsaturated Soils, 287-292.

Ben Chekroun, K., Rodriguez-Navarro, C., Gonzalez-Munoz, M. T., Arias, J.M., Cultrone, G., Rodriguez-Gallego, M. (2004). Precipitation and growth morphology of calcium carbonate induced by Myxococcus xanthus: implications for recognition of bacterial carbonates. J Sediment Res, 74, 868–876.

Bergland, M. (1986). Rammed-earth portfolio. Fine Homebuilding, 34, 35-39.

Bossink, B. A. G., & Brouwers, H. J. H. (1996). Construction waste: quantification and source evaluation. Journal of construction engineering and management, 122(1), 55-60.

Brundtland, G. H. (1987). Brundtland report. Our common future. Comissão Mundial.

Bruno, A. W., Gallipoli, D., Perlot, C., & Mendes, J. (2016). Effect of very high compaction pressures on the physical and mechanical properties of earthen materials. In E3S web of conferences, 9, 14004. EDP Sciences.

Bruno, A. W. (2016). Hygro-mechanical characterisation of hypercompacted earth for sustainable construction. PhD Thesis, Université de Pau et des Pays de l'Adour, France.

Bruno, A. W., Gallipoli, D., Perlot, C., & Mendes, J. (2017a). Mechanical behaviour of hypercompacted earth for building construction. Materials and Structures, 50(2), 160.

Bruno, A. W., Gallipoli, D., Perlot, C., & Mendes, J. (2017b). Effect of stabilisation on mechanical properties, moisture buffering and water durability of hypercompacted earth. Construction and Building Materials, 149, 733-740.

BS 1377-2 (1990). Methods of test for soils for civil engineering purposes. Classification tests, British Standards.

BS 3921 (1985). Specification for clay bricks.

Bui, Q. B., Morel, J. C., Reddy, B. V., & Ghayad, W. (2009). Durability of rammed earth walls exposed for 20 years to natural weathering. Building and Environment, 44(5), 912-919.

Bui, Q. B., Morel, J. C., Hans, S., Meunier, N. (2009). Compression behaviour of nonindustrial materials in civil engineering by three scale experiments: the case of rammed earth. Materials and Structures, 42(8), 1101-1116.

Bui, Q. B., Morel, J. C., Hans, S., & Walker, P. (2014). Effect of moisture content on the mechanical characteristics of rammed earth. Construction and Building materials, 54, 163-169.

Carmona, J. P., Oliveira, P. J. V., & Lemos, L. J. (2016). Biostabilization of a sandy soil using enzymatic calcium carbonate precipitation. Procedia engineering, 143, 1301-1308.

Castanier, S., Le Métayer-Levrel, G., & Perthuisot, J. P. (1999). Ca-carbonates precipitation and limestone genesis-the micro-biogeologist point of view. Sedimentary geology, 126(1-4), 9-23.

Chen, L., Shen, Y., Xie, A., Huang, B., Jia, R., Guo, R., Tang, W. (2009). Bacteria-mediated synthesis of metal carbonate minerals with unusual morphologies and structures. Crys Growth Des, 9, 743–754.

Cheng, L., Cord-Ruwisch, R., Shahin, M. A. (2013). Cementation of sand soil by microbially induced calcite precipitation at various degrees of saturation. Canadian Geotechnical Journal, 50(1), 81–90. https://doi.org/10.1139/cgj-2012-0023.

Cheng, L., Cord-Ruwisch, R. (2014). Upscaling effects of soil improvement by microbially induced calcite precipitation by surface percolation. Geomicrobiology Journal, 31(5), 396–406. https://doi.org/10.1080/01490451.2013.836579.

Cheng, L., & Shahin, M. A. (2016). Urease active bioslurry: a novel soil improvement approach based on microbially induced carbonate precipitation. Canadian Geotechnical Journal, 53(9), 1376-1385.

Choi, S., Wu, S., Chu, J. (2016). Biocementation for sand using an eggshell as calcium source. Journal of Geotechnical and Geoenvironmental Engineering, 142(10), 2–5. https://doi.org/10.1061/(ASCE)GT.1943-5606.0001534.

Cid, J., Mazarrón, F. R. & Cañas, I. (2011), Las normativas de construcción con tierra en el mundo, Informes de la Construcción, 63, 159–169.

Cid-Falceto, J., Mazarrón, F. R., & Cañas, I. (2012). Assessment of compressed earth blocks made in Spain: International durability tests. Construction and Building Materials, 37, 738-745.

CRATerre-EAG (1998). CDI, Compressed earth blocks: Standards – Technology series No.11. Brussels: CDI.

Cuthbert, M. O., Riley, M. S., Handley-Sidhu, S., Renshaw, J. C., Tobler, D. J., Phoenix, V. R., Mackay, R. (2012). Controls on the rate of ureolysis and the morphology of carbonate precipitated by S. pasteurii biofilms and limits due to bacterial encapsulation. Ecol Eng, 41, 3240.

Dayton, L. (1991). Saving mud monuments, New Scientist, 38-42.

Dawson, A. (2012). Alternative and recycled materials for earth construction. In Modern Earth Buildings, 172-203. Woodhead Publishing.

Deboucha, S., & Hashim, R. (2011). A review on bricks and stabilized compressed earth blocks. Scientific Research and Essays, 6(3), 499-506.

DeJong, J. T., Fritzges, M. B., & Nüsslein, K. (2006). Microbially induced cementation to control sand response to undrained shear. Journal of Geotechnical and Geoenvironmental Engineering, 132(11), 1381-1392.

DeJong, J. T., Mortensen, B. M., Martinez, B. C., Nelson, D. C. (2010) Bio-mediated soil improvement. Ecol Eng, 36, 197–210.

Delgado, M. C. J., & Guerrero, I. C. (2007). The selection of soils for unstabilised earth building: A normative review. Construction and building materials, 21(2), 237-251.

De Muynck, W., De Belie, N., & Verstraete, W. (2010). Microbial carbonate precipitation in construction materials: a review. Ecological Engineering, 36(2), 118-136.

De Yoreo, J. J., Vekilov, P. G. (2003). Principles of crystal nucleation and growth. Rev Mineral Geochem, 54, 57–93.

Dhami, N. K., Reddy, M. S., Mukherjee, A. (2013a). Biomineralization of calcium carbonates and their engineered applications: a review. Front Microbiol, 4, 1–13.

Dhami, N. K., Reddy, M. S., Mukherjee, A. (2013b). Biomineralization of calcium carbonate polymorphs by the bacterial strains isolated from calcareous sites. J Microbiol Biotechnol, 23, 707–714.

Dhami, N. K., Reddy, M. S., & Mukherjee, A. (2013c). Bacillus megaterium mediated mineralization of calcium carbonate as biogenic surface treatment of green building materials. World Journal of Microbiology and Biotechnology, 29(12), 2397-2406.

Dhami, N. K., Reddy, M. S., Mukherjee, A. (2014). Synergistic role of bacterial urease and carbonic anhydrase in carbonate mineralization. Appl Biochem Biotechnol, 172, 2552–2561.

Dhami, N. K., & Mukherjee, A. (2015). Can we benefit from the microbes present in rammed earth?. Rammed Earth Construction: Cutting-Edge Research on Traditional and Modern Rammed Earth, 89.

Dilrukshi, R. A. N., & Kawasaki, S. (2016). Plant-derived urease induced sand cementation used in geotechnical engineering applications. In International Conference on Geomechanics, Geo-Energy and Geo-Resources-IC3G, 28-29.

DIN 18945 (2013). Earth blocks - Terms and definitions, requirements, test methods.

Dupraz, S., Menez, B., Gouze, P., Leprovost, R., Benezeth, P., Pokrovsky, O. S., Guyot, F. (2009). Experimental approach of CO_2 biomineralization in deep saline aquifers. Chem Geol, 265, 54–62.

Easton, D. (1996). The Rammed Earth House. Chelsea Green Publications Company.

EEA (2010). The European environment state and outlook 2010. Material resources and waste. European Environment Agency, Copenaghen.

Elert, K., Sebastián, E., Valverde, I., & Rodriguez-Navarro, C. (2008). Alkaline treatment of clay minerals from the Alhambra Formation: Implications for the conservation of earthen architecture. Applied Clay Science, 39(3-4), 122-132.

Elert, K., Pardo, E. S., & Rodriguez-Navarro, C. (2015). Alkaline activation as an alternative method for the consolidation of earthen architecture. Journal of Cultural Heritage, 16(4), 461-469.

El Mountassir, G., Lunn, R.J., Moir, H., MacLachlan, E. (2014). Hydrodynamic coupling in microbially mediated fracture mineralization: Formation of self-organized groundwater flow channels. Water Resources Research, 50(1), 1–16. https://doi.org/10.1002/ 2013WR013578.

Favre, N., Christ, M. L., Pierre, A. C. (2009). Biocatalytic capture of CO_2 with carbonic anhydrase and its transformation to solid carbonate. J Mol Catal B Enzym, 60, 163–170.

Fernández, R., Cuevas, J., Sánchez, L., de la Villa, R. V., & Leguey, S. (2006). Reactivity of the cement–bentonite interface with alkaline solutions using transport cells. Applied Geochemistry, 21(6), 977-992.

Ferrer, M. R., Quevedo-Sarmiento, J., Bejar, V., Delgado, R., Ramos-Cormenzana, A., Rivadeneyra, M. A. (1988). Calcium carbonate formation by Deleya halophila: effect on salt concentration and incubation temperature. Geomicrobiol J, 6, 49-57.

Ferris, F.G., Stehmeier, L.G., Kantzas, A., Mourits, F.M., (1996). Bacteriogenic mineral plugging. Journal of Canadian Petroleum Technology 35 (8) 56-61. https://doi.org/10. 2118/96-08-06.

Fisher, R. A. (1926). On the capillary forces in an ideal soil; correction of formulae given by WB Haines. The Journal of Agricultural Science, 16(3), 492-505.

Frencham, G. J. (1982). The performance of earth buildings. Deakin University, Geelong.

Gallipoli, D., Bruno, A. W., Perlot, C., & Mendes, J. (2017). A geotechnical perspective of raw earth building. Acta Geotechnica, 12(3), 463-478.

Ganendra, G., De Muynck, W., Ho, A., Arvaniti, E. C., Hosseinkhani, B., Ramos, J. A., Rahier, H., Boon, N. (2014). Formate oxidationdriven calcium carbonate precipitation by Methylocystis parvus OBBP. Appl Environ Microbiol, 80, 4659-4667.

Gaucher, E. C., & Blanc, P. (2006). Cement/clay interactions–a review: experiments, natural analogues, and modeling. Waste Management, 26(7), 776-788.

Gebauer, D., Gunawidjaja, P. N., Peter Ko, J. Y., Bacsik, Z., Aziz, B., Liu, L., Hu, Y., Bergstrom, L., Tai, C. W., Sham, T. K., Eden, M., Hedin, N. (2010). Proto-calcite and proto-vaterite in amorphous calcium carbonates. Angew Chem Int Ed, 49, 8889–8891.

Gerendás, J., Zhu, Z., & Sattelmacher, B. (1998). Influence of N and Ni supply on nitrogen metabolism and urease activity in rice (Oryza sativa L.). Journal of Experimental Botany, 49(326), 1545-1554.

Gomez, M. G., Martinez, B. C., DeJong, J. T., Hunt, C. E., De Vlaming, L. A., Major, D. W., et al. (2015). Field-scale bio-cementation tests to improve sands. Proceedings of the Institution of Civil Engineers-Ground Improvement, 168, 1–11. https://doi.org/10.1680/ grim.13.00052.

González, M. J., & Navarro, J. G. (2006). Assessment of the decrease of CO_2 emissions in the construction field through the selection of materials: Practical case study of three houses of low environmental impact. Building and environment, 41(7), 902-909.

Gorospe, C. M., Han, S. H., Kim, S. G., Park, J. Y., Kang, C. H., Jeong, J. H., So, J. S. (2013). Effects of different calcium salts on calcium carbonate crystal formation by Sporosarcina pasteurii KCTC 3558. Biotechnol Bioproc Eng, 18, 903–908.

Hamdan, N., & Kavazanjian Jr, E. (2016). Enzyme-induced carbonate mineral precipitation for fugitive dust control. Géotechnique, 66(7), 546-555.

Hammes, F., & Verstraete, W. (2002). Key roles of pH and calcium metabolism in microbial carbonate precipitation. Reviews in environmental science and biotechnology, 1(1), 3-7.

Hammes, F., Boon, N., de Villiers, J., Verstraete, W., Siciliano, S. D. (2003). Strain-specific ureolytic microbial calcium carbonate precipitation. Appl Environ Microbiol, 69, 4901–4909.

Harkes, M. P., Van Paassen, L. A., Booster, J. L., Whiffin, V. S., & van Loosdrecht, M. C. (2010). Fixation and distribution of bacterial activity in sand to induce carbonate precipitation for ground reinforcement. Ecological Engineering, 36(2), 112-117.

Heathcote, K. A. (1995). Durability of earthwall buildings. Construction and building materials, *9*(3), 185-189.

Heathcote, K., & Jankulovski, E. (1993). Relationship between moisture content and strength of soilcrete blocks: Results of experimental investigation into relationship between moisture content and compressive strength of cement-stabilized soilcrete blocks. Building research and information, 21(2), 103-108.

Houben, H., & Guillaud, H. (1994). Earth construction. A comprehensive guide.

Houben, H. & Guillaud, H. (1996). Earth construction - A comprehensive guide. Second Edition. Intermediate Technology Publications. London, UK.

Howie, R. A., Zussman, J., & Deer, W. (1992). An introduction to rock-forming minerals. Longman.

Hua, B., Deng, B., Thornton, E. C., Yang, J., Amonette, J. E. (2007). Incorporation of chromate into calcium carbonate structure during coprecipitation. Water Air Soil Pollut, 179, 381–390.

ISO 24353 (2008). Hygrothermal performance of building materials and products determination of moisture adsorption/desorption properties in response to humidity variation. Geneva, Switzerland: International Organization for Standardization.

Jaquin, P. A., Augarde, C. E., & Legrand, L. (2008). Unsaturated characteristics of rammed earth. In First European Conference on Unsaturated Soils, 417-422.

Jaquin, P. A., Augarde, C. E., Gallipoli, D., & Toll, D. G. (2009). The strength of unstabilised rammed earth materials. Géotechnique, 59(5), 487-490.

Jayasinghe, C., & Kamaladasa, N. (2007). Compressive strength characteristics of cement stabilized rammed earth walls. Construction and Building Materials, 21(11), 1971-1976.

Karnland, O., Olsson, S., Nilsson, U., & Sellin, P. (2007). Experimentally determined swelling pressures and geochemical interactions of compacted Wyoming bentonite with highly alkaline solutions. Physics and Chemistry of the Earth, Parts A/B/C, 32(1-7), 275-286.

Kawaguchi, T., & Decho, A. W. (2002). A laboratory investigation of cyanobacterial extracellular polymeric secretions (EPS) in influencing $CaCO_3$ polymorphism. Journal of Crystal Growth, 240(1-2), 230-235.

Keable, J. (1996). Rammed earth structures: a code of practice. Intermediate Technology.

Kebao, R., Kagi, D., & building Protection, T. D. (2012). Integral admixtures and surface treatments for modern earth buildings. Modern Earth Buildings: Materials, Engineering, Constructions and Applications, 256.

Keefe, L. (2012). Earth building: methods and materials, repair and conservation. Routledge.

Kile, D. E., Eberl, D. D., Hoch, A. R., & Reddy, M. M. (2000). An assessment of calcite crystal growth mechanisms based on crystal size distributions. Geochimica et Cosmochimica Acta, 64(17), 2937-2950.

Kouakou, C. H., & Morel, J. C. (2009). Strength and elasto-plastic properties of nonindustrial building materials manufactured with clay as a natural binder. Applied Clay Science, 44(1), 27-34.

Kwan, A. K. H., Mora, C. F., Chan, H. C. (1999). Particle shape analysis of coarse aggregate using digital image processing. Cement and Concrete Research 29, 1403–1410.

Lauchnor, E. G., Schultz, L. N., Bugni, S., Mitchell, A. C., Cunningham, A. B., Gerlach, R. (2013). Bacterially induced calcium carbonate precipitation and strontium coprecipitation in a porous media flow system. Environ Sci Technol, 47, 1557–1564.

Li, M., Cheng, X., Guo, H. (2013). Heavy metal removal by biomineralization of urease producing bacteria isolated from soil. Int Biodeter Biodegr, 76, 81–85.

Likos, W. J., & Lu, N. (2004). Hysteresis of capillary stress in unsaturated granular soil. Journal of Engineering mechanics, 130(6), 646-655.

Little, B., & Morton, T. (2001). Building with earth in Scotland: Innovative design and sustainability. Edinburgh: Scottish Executive Central Research Unit.

Loewenthal, R. E., Marais, G. V. R. (1978). Carbonate chemistry of aquatic systems: theory and application, Ann Arbor Science, 1. Ann Arbor

Lucas, R. (1918). Ueber das Zeitgesetz des kapillaren Aufstiegs von Flüssigkeiten. Colloid & Polymer Science, 23(1), 15-22.

Maillard, P., & Aubert, J. E. (2014). Effects of the anisotropy of extruded earth bricks on their hygrothermal properties. Construction and Building Materials, 63, 56-61.

Maniatidis, V., & Walker, P. (2003). A review of rammed earth construction. Innovation Project "Developing Rammed Earth for UK Housing", Natural Building Technology Group, Department of Architecture & Civil Engineering, University of Bath.

Martirena, F., Rodriguez-Rodriguez, Y., Callico, A., Gonzalez, R., Diaz, Y., Bracho, G., Alujas, A., Guerra de Leon, J. O. & Alvarado-Capó, Y (2014). Microorganism - based bioplasticizer for cementitious materials. Construction and Building Materials 60: 91–97.

McConnaughey, T. A., Burdett, J., Whelan, J. F., & Paull, C. K. (1997). Carbon isotopes in biological carbonates: respiration and photosynthesis. Geochimica et Cosmochimica Acta, 61(3), 611-622.

McGregor, F., Heath, A., Fodde, E., & Shea, A. (2014). Conditions affecting the moisture buffering measurement performed on compressed earth blocks. Building and Environment, 75, 11-18.

McHenry, P. G. (1989). Adobe and rammed earth buildings: design and construction. University of Arizona Press.

Minke, G. (2000). Earth construction handbook: the building material earth in modern architecture.

Minto, J. M., MacLachlan, E., El Mountassir, G., & Lunn, R. J. (2016). Rock fracture grouting with microbially induced carbonate precipitation. Water Resources Research, 52(11), 8827-8844.

Mitchell, J. K., & Soga, K. (2005). Fundamentals of soil behavior. Hoboken, NJ: John Wiley & Sons, 3.

Mitchell, J. K., & Santamarina, J. C. (2005). Biological considerations in geotechnical engineering. Journal of geotechnical and geoenvironmental engineering, 131(10), 1222-1233.

Mitchell, A. C., & Ferris, F. G. (2005). The coprecipitation of Sr into calcite precipitates induced by bacterial ureolysis in artificial groundwater: temperature and kinetics dependence. Geochim Gosmochim Acta, 69, 4199–4210.

Mobley, H. L., & Hausinger, R. P. (1989). Microbial ureases: significance, regulation, and molecular characterization. Microbiology and Molecular Biology Reviews, 53(1), 85-108.

Mobley, H. L., Island, M. D., & Hausinger, R. P. (1995). Molecular biology of microbial ureases. Microbiol. Mol. Biol. Rev., 59(3), 451-480.

MOPT (1992). Bases Para el Diseño y Construcción con Tapial. Madrid, Spain: Centro de Publicaciones, Secretaría General Técnica, Ministerio de Obras Públicas y Transportes.

Mora, C. F., Kwan, A. K. H. (2000). Sphericity, Shape Factor, and Convexity Measurement of Coarse Aggregate for Concrete Using Digital Image Processing. Cement and Concrete Research, 30(3), 351-358.

Morales, L., Romero, E., Jommi, C., Garzón, E., & Giménez, A. (2015). Feasibility of a soft biological improvement of natural soils used in compacted linear earth construction. Acta Geotechnica, 10(1), 157-171.

Morel, J. C., Pkla, A., & Walker, P. (2007). Compressive strength testing of compressed earth blocks. Construction and Building Materials, 21(2), 303-309.

Morton, T., Stevenson, F., Taylor, B. and Charlton Smith, N. (2005). Low Cost Earth Brick Construction. Fife, Scotland, UK: Arc, Chartered Architects.

Morton, T. (2008). Earth masonry. Design and Construction Guidelines.

Nam, I. H., Chon, C. M., Jung, K. Y., Choi, S. G., Choi, H., & Park, S. S. (2015). Calcite precipitation by ureolytic plant (Canavalia ensiformis) extracts as effective biomaterials. KSCE Journal of Civil Engineering, 19(6), 1620-1625.

Nemati, M., & Voordouw, G. (2003). Modification of porous media permeability, using calcium carbonate produced enzymatically in situ. Enzyme and Microbial Technology, *33*(5), 635-642.

Nemati, M., Greene, E. A., & Voordouw, G. (2005). Permeability profile modification using bacterially formed calcium carbonate: comparison with enzymic option. Process Biochemistry, 40(2), 925-933.

Ng, W. S., Lee, M. L., & Hii, S. L. (2012). An overview of the factors affecting microbial-induced calcite precipitation and its potential application in soil improvement. World Academy of Science, Engineering and Technology, 62, 723-729.

Norton, J. (1997). Building with Earth. A handbook. Second Edition. Intermediate Technology Publications, London, UK.

NZS 4297 (1998). Engineering Design of Earth Buildings. Wellington: Standards New Zealand

NZS 4298 (1998). Materials and Workmanship For Earth Buildings. Wellington: Standards New Zealand.

NZS 4299 (1998). Earth Buildings Not Requiring Specific Design. Wellington: Standards New Zealand.

Okwadha, G. D., & Li, J. (2010). "Optimum conditions for microbial carbonate precipitation." Chemosphere, 81(9), 1143–1148.

Olivier, M., & Mesbah, A. (1986). Le matériau terre: Essai de compactage statique pour la fabrication de briques de terre compressées. Bull Liaison Labo P et, 146.

Pacheco-Torgal, F., & Jalali, S. (2012). Earth construction: Lessons from the past for future eco-efficient construction. Construction and building materials, 29, 512-519.

Park, S. J., Park, Y. M., Chun, W. Y., Kim, W. J., Ghim, S. Y. (2010). Calcite-forming bacteria for compressive strength improvement in mortar. J Microbiol Biotechnol, 20, 782–788.

Park, S. S., Choi, S. G., & Nam, I. H. (2014). Effect of plant-induced calcite precipitation on the strength of sand. Journal of Materials in Civil Engineering, 26(8), 06014017.

Pettit NM, Smith ARJ, Freedman RB, Burns RG (1976) Soil urease: Activity, stability and kinetic properties. Soil Biol Biochem 8:479-484.

Phillips, A. J., Gerlach, R., Lauchnor, E., Mitchell, A. C., Cunningham, A. B., & Spangler, L. (2013). Engineered applications of ureolytic biomineralization: a review. Biofouling, 29(6), 715-733.

Polacco, J. C., & Holland, M. A. (1993). Roles of urease in plant cells. In International review of cytology, 145, 65-103. Academic Press.

Price, C. A., & Doehne, E. (2011). Stone conservation: an overview of current research. Getty publications.

Ramachandran, S. K., Ramakrishnan, V., Bang, S. S. (2001). Remediation of concrete using micro-organisms. ACI Materials Journal, 98(1), 3–9. https://doi.org/10.14359/10154.

Reddy, B. V., & Kumar, P. P. (2010). Embodied energy in cement stabilised rammed earth walls. Energy and Buildings, 42(3), 380-385.

Rode, C., Peuhkuri, R. H., Mortensen, L. H., Hansen, K. K., Time, B., Gustavsen, A., & Harderup, L. E. (2005). Moisture buffering of building materials.

Rowshanbakht, K., Khamehchiyan, M., Sajedi, R. H., Nikudel, M. R. (2016). Effect of injected bacterial suspension volume and relative density on carbonate precipitation resulting from microbial treatment. Ecological Engineering, 89, 49–55. https://doi.org/10. 1016/j.ecoleng.2016.01.010.

Salifu, E., MacLachlan, E., Iyer, K. R., Knapp, C. W., Tarantino, A. (2016). Application of microbially induced calcite precipitation in erosion mitigation and stabilisation of sandy soil foreshore slopes: A preliminary investigation. Engineering Geology, 201, 96–105. https://doi.org/10.1016/j.enggeo.2015.12.027.

Sanchez-Navas A, Martin-Algarra A, Rivadeneyra MA, Melchor S, Martin-Ramos JD (2009) Crystal-growth behavior in Ca– Mg carbonate bacterial spherulites. Cryst Growth Des 9:2690–2699

Sarada D, Choonia HS, Sarode DD, Lele SS (2009) Biocalcification by Bacillus pasteurii urease: a novel application. J Ind Microbiol Biotechnol 36:1111–1115.

Schäfer, A., Harms, H., Zehnder, A.J.B., (1998). Bacterial accumulation at the air-water interface. Environmental Science and Technology 32 (23), 3704–3712 https://doi.org/ 10.1021/ es980191u.

Schroeder, H. (2016). Sustainable building with earth (Vol. 582). Basel, Switzerland: Springer.

Schultz, L., Betsey, P., Mitchell, A.C., Cunningham, A.B. and Gerlach, R. (2011) Imaging Biologically Induced Mineralisation in Fully Hydrated Flow Systems, Microscopy Today, 19(5), 12-15. https://doi.org/10.1017/S1551929511000848.

Seed, H. B., Wookward, R. J., & Lundgren, R. (1964). Clay mineralogical aspects of the Atterberg limits. Journal of Soil Mechanics & Foundations Div, 90(Proc. Paper 3983).

Sharma, A., & Ramkrishnan, R. (2016). Study on effect of microbial induced calcite precipitates on strength of fine grained soils. Perspectives in Science, 8, 198-202.

Shen, Q., Wang, L., Huang, Y., Sun, J., Wang, H., Zhou, Y., Wang, D. (2006). Oriented aggregation and novel phase transforma- tion of vaterite controlled by the synergistic effect of calcium dodecyl sulfate and n-pentanol. J Phys Chem B, 110, 23148–23153.

Silver, S., Toth, K., Scribner, H. (1975). Facilitated transport of calcium by cells and subcellular membranes of Bacillus subtilis and Escherichia coli. J. Bacteriol. 122, 880–885.

Sirko, A., & Brodzik, R. (2000). Plant ureases: roles and regulation. Acta Biochimica Polonica, 47(4), 1189-1195.

Skempton, A. W. (1953). The colloidal activity of clays. Selected Papers on Soil Mechanics, 106-118.

Spanos, N., Koutsoukos, P. G. (1998). The transformation of vaterite to calcite: effect of the conditions of the solution in contact with the mineral phase. J Crystal Growth, 191, 783–790.

Stitt, M. (1999). Nitrate regulation of metabolism and growth. Current opinion in plant biology, 2(3), 178-186.

Stocks-Fischer, S., Galinat, J. K., & Bang, S. S. (1999). Microbiological precipitation of $CaCO_3$. Soil Biology and Biochemistry, 31(11), 1563-1571.

Tai, C. Y., & Chen, F. B. (1998). Polymorphism of $CaCO_3$ precipitated in a constant-composition environment. AIChE J, 44, 1790–1798.

TERCRUSO (2013). Caractérisation des briques de terre crue de Midi-Pyrénées, (http://www.cercad.fr/IMG/pdf/tercruso±rapport_final_lmdc2013-04-r120.pdf).

Terzis, D., & Laloui, L. (2017). On the application of microbially induced calcite precipitation for soils: a multiscale study. In Advances in Laboratory Testing and Modelling of Soils and Shales, 388-394. Springer, Cham.

Terzis, D., & Laloui, L. (2018). 3-D micro-architecture and mechanical response of soil cemented via microbial-induced calcite precipitation. Scientific Reports, 8(1), 1416. https://doi.org/10.1038/s41598-018-19895-w.

Thompson, J. B., & Ferris, F. G. (1990). Cyanobacterial precipitation of gypsum, calcite, and magnesite from natural alkaline lake water. Geology, 18(10), 995-998.

Thormark, C. (2006). The effect of material choice on the total energy need and recycling potential of a building. Building and environment, 41(8), 1019-1026.

Tobler, D. J., MacLachlan, E., Phoenix, V. R. (2012). Microbially mediated plugging of porous media and the impact of differing injection strategies. Ecological Engineering, 42, 270–278. https://doi.org/10.1016/j.ecoleng.2012.02.027.

Tourney, J., Ngwenya, B. T. (2009). Bacterial extracellular polymeric substances (EPS) mediate $CaCO_3$ morphology and polymorphism. Chem Geol, 262, 138–146.

van Paassen, L. A., Pieron, M., Mulder, A., van der Linden, T. J. M., van Loosdrecht, M. C. M., Ngan-Tillard, D. J. M. (2009). In: Vrkljan (Ed.), Strength and deformation of biologically cemented sandstone. Proceedings of the ISRM regional conference EUROCK 2009-rock engineering in difficult ground conditions-soft rocks and karst. Taylor & Francis Group, Dubrovnik, Croatia, 405–410.

Van Paassen, L. A., Ghose, R., van der Linden, T. J. M., van der Star, W. R. L., van Loosdrecht, M. C. M. (2010). Quantifying biomediated ground improvement by ureolysis: Large-scale biogrout experiment. Journal of Geotechnical and Geoenvironmental Engineering, 136, 1721–1728. https://doi.org/10.1061/(ASCE)GT. 1943-5606.0000382.

Von Wirén, N., Gazzarrini, S., Gojon, A., & Frommer, W. B. (2000). The molecular physiology of ammonium uptake and retrieval. Current opinion in plant biology, 3(3), 254-261.

Walker, P. (2000). Strength and durability testing of earth blocks. In Proceedings of the 6th international seminar on Structural Masonry for developing countries, 110-118.

Walker, P., Keable, R., Martin, J., Maniatidis, V. (2005). Rammed earth-Design and construction guidelines, BRE Bookshop.

Wargocki, P., Wyon, D. P., Baik, Y. K., Clausen, G., & Fanger, P. O. (1999). Perceived air quality, sick building syndrome (SBS) symptoms and productivity in an office with two different pollution loads. Indoor air, 9(3), 165-179.

Warthmann, R., Van Lith, Y., Vasconcelos, C., McKenzie, J. A., & Karpoff, A. M. (2000). Bacterially induced dolomite precipitation in anoxic culture experiments. Geology, 28(12), 1091-1094.

Washburn, E. W. (1921). The dynamics of capillary flow. Physical review, 17(3), 273.

Wei, H., Shen, Q., Zhao, Y., Wang, D., Xu, D. (2003). Influence of polyvinylpyrrolidone on the precipitation of calcium carbonate and on the transformation of vaterite to calcite. J Cryst Growth, 250, 516–524.

Whiffin, V. S. (2004). Microbial $CaCO_3$ precipitation for the production of biocement (Doctoral dissertation, Murdoch University).

Whiffin, V. S., van Paassen, L. A., & Harkes, M. P. (2007). Microbial carbonate precipitation as a soil improvement technique. Geo-microbiology Journal, 24(5), 417-423.

Wu, F., Li, G., Li, H. N., & Jia, J. Q. (2013). Strength and stress–strain characteristics of traditional adobe block and masonry. Materials and structures, 46(9), 1449-1457.

Xu, X., Han, J. T., Kim, D. H., Cho, K. (2006). Two modes of transformation of amorphous calcium carbonate films in air. J Phys Chem B, 110, 2764–2770.